The kinetics of barium sulphate scale formation and inhibition in the bulk solution and on surfaces

Ogbemi Bukuaghangin

Submitted in accordance with the requirement for the degree of

Doctor of Philosophy

The University of Leeds

School of Mechanical Engineering

Leeds, UK

September, 2017

The candidate confirms that the work submitted is his own, except where work which has formed part of jointly-authored publications has been included. The contribution of the candidate and other co-author in published work from this thesis has been clearly indicated. The candidate confirms that appropriate credit has been given within the thesis where reference has been made to the work of others.

In the papers contributed to this thesis, the candidate (first author) carried out all the experiments, analysis and preparation of the manuscripts. All other authors contributed by proof reading and providing insight on the discussions.

Acknowledgments

My deepest gratitude goes to Professor Anne Neville and Dr Thibaut Charpentier for their supervision, understanding, encouragement and mentorship from the beginning stage to the last stage of this project. They asked the right questions to keep me thinking deeper; and they see the big pictures, as well as, the small details.

I would like to appreciate the Federal Republic of Nigeria and FAST research group for their financial support and technical contributions towards the success of this project. A special appreciation to Professor Lucky Akaruese and Hon. Daniel Reyenieju for their encouragement and counselling during my study.

I would like to appreciate every member of the Institute of functional surface (iFS) research group for keeping a friendly working environment, sharing of knowledge and contributions to the success of this project. A very special thanks to the administrative staff and technicians of iFS research group for their involvement and contributions: Ron, Michael, Jordan, Andrew, and Fiona just to mention a few. I would also like to particularly thank every member of the scale research group for sharing their knowledge and advice.

A special appreciation goes to my parents, siblings, and friends who came alongside with me and prayed me through the entire process of my research; most especially during the dark times when I wonder why I ever thought could write anything that would make sense. These four years would have been different without their encouragement, endless love and support.

Those that I have mentioned here and so many more unrecognised, may the Lord continue to shower blessings upon each and every one of you.

Abstract

The deposition and subsequent growth of inorganic scale on completion equipment is a major problem in the oil and gas industry. Several studies have been conducted on the kinetics of both bulk precipitation and surface deposition of barium sulphate. These studies were often conducted in a closed system and measurements were taken off-line and in this study, a flow cell was designed to study both kinetic processes *in-situ* and in an open system. The set-up allows real-time analysis of a metallic sample by following various scaling parameters such as surface coverage, number and size of crystals formed on the scaling surface. The experimental results were fitted to a diffusion-controlled model to study the mechanism of the surface crystallisation process.

The kinetics and mechanisms of barium sulphate bulk precipitation and surface deposition with the absence and presence of scale inhibitors (diethylene triamine penta methylene phosphonic Acid (DETMP), VinylSulphonate Acrylic acid co-polymer (VS-Co) and poly-phosphino carboxylic acid (PPCA)) were studied. The influence of saturation ratio, flow rate, pre-scaled surface and interval injection on the surface inhibition performance of PPCA scale inhibitor was studied. In addition, the formation of barium sulphate in a multiphase environment was investigated.

The results showed that the deposition of barium sulphate on a metallic steel could occur simply by heterogeneous nucleation and grow and not always by the adhesion of pre-precipitated crystals from the bulk solution. It also revealed the strong effect of saturation ratio and temperature on the nucleation mechanism of barium sulphate deposition on surfaces.

In terms of preventing surface growth by the application of scale inhibitor, the study showed that scale inhibitor could act as a promoter of the crystallization process rather than hindering the crystal growth. Furthermore, the study highlights the importance of starting the chemical treatment as early as

possible to limit the pre-existing layer of scale which can considerably disrupt the efficiency of scale inhibitors.

It was found from the study that pre-existing layers of crystals can act as active sites for nucleation and further growth of crystals. The results also show the significance of taking into account the injection of scale inhibitor from the control valve into a process line; inappropriate injection could affect the prevention of scale during continuous injection.

The study demonstrated that the presence of oil droplets can influence the deposition of barium sulphate on surfaces. This suggests in choosing an anti-scaling surface to prevent scale formation, tests should be conducted to evaluate the performance of the surfaces both in an aqueous environment and multiphase environment.

Table of contents

List of figures

List of tables

Publications

Journal paper

Bukuaghangin, Ogbemi, Olujide Sanni, Nikil Kapur, Michael Huggan, Anne Neville, and Thibaut Charpentier. "Kinetics study of barium sulphate surface scaling and inhibition with a once-through flow system." *Journal of Petroleum Science and Engineering* 147 (2016): 699-706.

Conference proceedings

Bukuaghangin, Ogbemi, Olujide Sanni, Anne Neville, and Thibaut Charpentier. "A Kinetic Study of Barium Sulphate Formation in Presence of Scale Inhibitor in a Flowing System." In *Proceedings of a meeting held 6-10 March 2016, Vancouver, Canada*, vol. 5, pp. 3398-3411. NACE International, 2016.

Sanni, Olujide, Ogbemi Bukuaghangin, Thibaut Charpentier, Nikil Kapur, and Anne Neville. "Using a real-time visualisation technique for the assessment of surface scale kinetics and mechanisms of inhibition." In *SPE International Oilfield Scale Conference and Exhibition*. Society of Petroleum Engineers, 2016.

Bukuaghangin, Ogbemi, Anne Neville, and Thibaut VJ Charpentier. "Scale Formation in Multiphase Conditions." In *Proceedings of the Oil Field Chemistry Symposium, Gielo*. 2015.

Nomenclature

Terms	Definition	Units
γ	Free surface energy	$J.m^{-2}$
σ	Interfacial energy	$J.m^{-2}$
N_o	Number of particles	
ρ	Density	g/m^3
k_{spx}	Solubility product	
T	Temperature	K
N_A	Avogadro number	mol^{-1}
R	Gas constant	$mol^{-1}.K^{-1}$
G	Overalls excess free energy	$K.J^{-1}.mol^{-1}$
ΔG_S	Volume free energy	$K.J^{-1}.mol^{-1}$
ΔG_V	Surface excess free energy	$K.J^{-1}.mol^{-1}$
r	Equivalent radius of the crystals	m
r_c	Critical radius	m
J	Nucleation rate	Number of nuclei/$s.m^3$
K	Constant	
N	Number of crystals	
M	Mass of solid deposit	G
A(t)	Surface area of crystals	m^2
K_c	Crystal growth constant	
C	Solute concentration	mol^{-1}

Terms	Definition	Units
Re	Reynolds number	
N_o	Active nucleation sites	
γ_L	Liquid surface tension	$N.m^{-1}$
γ_{SL}	Solid/liquid interfacial free energy	$N.m^{-1}$
γS	Solid surface free energy	$N.m^{-1}$
T	Time	s
S(t)	Surface coverage	%
$S_{ext}(t)$	Extended surface coverage	%
t_{ind}	Induction time	s
T_r	Relaxation time	s
T_n	Period of nucleation	s
F	Shape ratio	
Ø	Wetting angle	°
θ	Incident angle	°
C(t)	Ba^{2+} concentration at sampling time	ppm
$C_b(t)$	Ba^{2+} concentration in the blank solution	ppm
C_O	control sample Ba^{2+} concentration at time, t = 0	ppm

Abbreviations

Abbreviation	Definition
SR	Saturation Ratio
SI	Saturation Index
PPCA	Poly-phosphino carboxylic acid
DETPMP	Diethylene triamine penta methylene phosphonic Acid
VS-Co	VinylSulphonate Acrylic acid co-polymer
FAU	Formazin Attenuation Units
RCE	Rotating Cylinder Electrode
PVS	Polyvinyl sulphonate
SEM	Scanning electron microscopy
ICP-AES	Inductively Coupled Plasma - Atomic Emission Spectroscopy
XRD	X-Ray Diffraction
PBTC	2-Phosphono-butane-1, 2, 4-tricarboxylic acid
MIC	Minimum Inhibitor Concentration
EDX	Energy Dispersive X-ray analysis system
FW	Formation water
SW	Sea water

Chapter 1 Introduction

Crude oil and gas for decades have been a major source of energy used in the world. The emergence of new technologies, increase in both population and standard of living, has led to the continual increase in demand for energy. According to the United State Energy International Administration (EIA), it is estimated that the energy consumption would increase by 57% from 2004 to 2030 as shown in Figure 1-1[1].

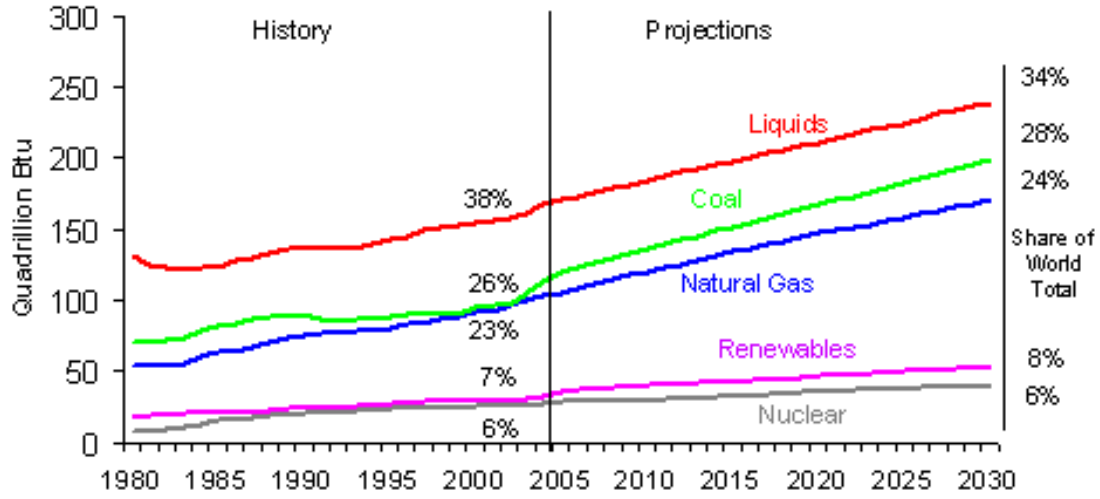

Figure 1-1: World market fuel used fuel types [1]

The high demand of energy in the world has led to the exploitation and production of more oil reservoirs. As the reservoirs mature (*i.e.* reservoir initial pressure decline), various techniques (such as water injection and steam injection) are used to increase the pressure of these reservoirs to increase oil production. The major challenges faced by using these techniques are corrosion, bio-fouling and mineral scale deposition [2]. This research focuses mainly on mineral scale formation both in the bulk solution and on the surfaces.

1.1 Oil and gas formation and production

Oil and gas are formed from the remains of organisms that are decayed in the sedimentary rock alongside with the minerals of the rock. When these rocks are buried by overlying sediment, the organic matter decomposes and converts to oil and natural gas through bacterial processes coupled with high temperature and pressure [3, 4]. Furthermore, the oil and gas along with water migrate from the rock into adjacent porous reservoir rock (which is usually sandstones, limestone's, or dolomites) [5]. The movement continues until they meet an impermeable rock. Due to the difference in density, gas is found at the top followed by oil and water; an oil reservoir is presented in Figure 1-2 showing the different layers formed by gas, oil and water.

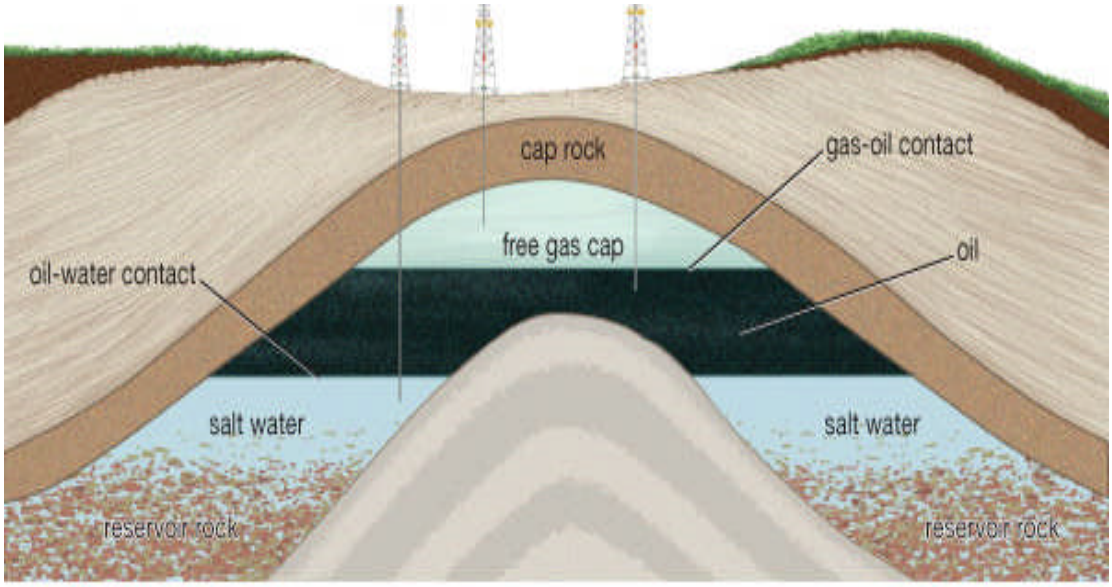

Figure 1-2: An illustration of oil reservoir [6]

After the oil exploration and drilling process has been achieved, during the production stage of oil and gas, there are three different recovery techniques used; primary, secondary and tertiary recovery techniques [7, 8]. In the primary recovery technique oil is forced to the surface by the reservoir pressure, and pumps could be used when the pressure reduces. The primary recovery techniques account for 10% of oil production [8]. When the reservoir matures and if there is no aquifer water to replace the producing oil, water or gas is been injected into the reservoir to increase the pressure, this technique

is known as *secondary recovery*; it results in the recovery of 20-40 % of the reservoir's original oil in place. Figure 1-3 gives a vivid explanation of secondary recovery techniques.

Lastly, tertiary recovery techniques (otherwise known as enhanced oil recovery) involve the injection of steam, solvent or bacterial and detergent to improve the oil recovery; these techniques account for 30-70 % of reservoir original oil in place. One of the drawbacks for the use of the last two techniques is that it could lead to the precipitating of solid (scale). The types of scales formed in the oil and gas industry will be discussed in the next section.

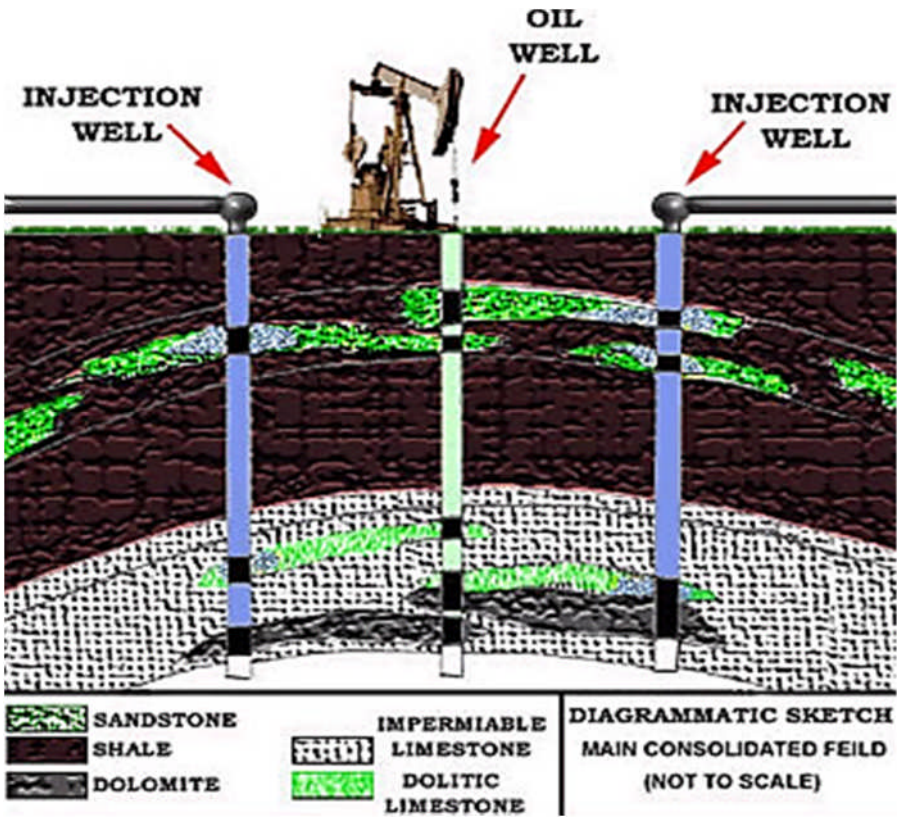

Figure 1-3: Secondary recovery techniques

1.2 Scale formation and the economic impact in the oil industry

Oilfield scales are inorganic deposits that form due to the precipitation of solid from brines that are present in the reservoir and production system. They have

been seen over the years as the major cause of formation damage either in injection or production [9, 10]. In addition, it influences equipment wear and corrosion, restricts flow and causes a reduction in heat exchanger efficiency. This leads to an increase in maintenance costs, emergency shutdown, reduction in production and production–equipment failures; thus increasing the operational and production costs. Scales are usually formed in perforation and tubes; mostly where the temperature and/or pressure are very low [11]. They could be formed during secondary recovery when sea water is used to increase the pressure in the reservoir; knowing that formation water contains cations (Ba^{2+}, Ca^{2+}, Sr^{2+}) and sea water contains SO_4^{2-} ions. When these two incompatible waters are mixed, it leads to changes in the supersaturation of the mixture, thereby leading to precipitation of scales [12]. In addition, they may also occur when brine evaporates due to high temperature/pressure (HT/HP) gas wells (i.e. when high-temperature steam comes in contact with brine increasing its solubility, which results in precipitation) [13].

The economic impact of scale formation in oilfield operation is very crucial, considering that millions of dollars have been spent in the mitigation and removal of scale during production [14]. Moreover, it is estimated that the global cost of scale is about USD 1.4 billion every year; Figure 1-4 shows the percentage of money spent on scale all over the world. In the future, it is expected that the cost of scale will increase since more oil reservoir would be mature and would require secondary recovery to increase production. Common scales formed in oil and gas production are gypsum, calcite, barite, iron carbonate and sulphide [10].

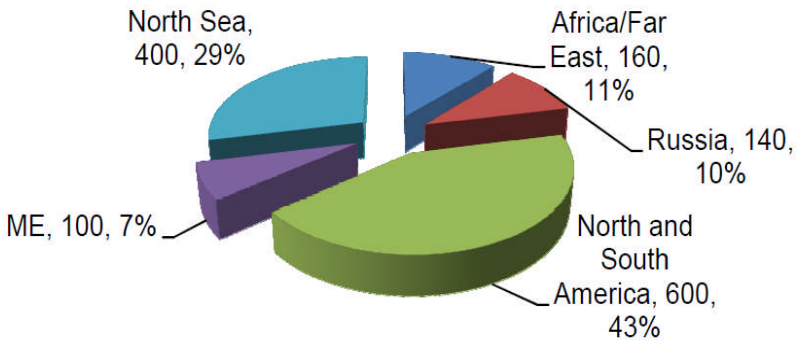

Figure 1-4: Global cost of scale [13]

The most common scale formed in the oil and gas industries are calcium carbonate ($CaCO_3$) and barium sulphate ($BaSO_4$). Although $BaSO_4$ is rarely formed when compared with other sulphate scales, it is particularly tenacious and resistant to acid treatment. It is therefore of paramount importance to understand the mechanism and kinetics of barium sulphate formation in order to accurately predict its occurrence. In preventing mineral scale fouling, there are various techniques used [15-19]. A recent study by Charpentier *et al*. [20] shows the prospective of using novel coating for the prevention of mineral scale fouling. In this work, infused porous surfaces were used to reduce the deposition of calcium carbonate. Nevertheless, the most popular approach for mitigating barium sulphate is generally through the use chemical scale inhibitors. These chemicals tend to reduce the driving force for crystallization and successive growth of crystals by disrupting the thermodynamic stability of growing nuclei and/or by blocking the active sites of crystals, thus preventing further growth [21-23]. The performance of scale inhibitors in oilfield operations is the foremost concern of field operators. Information is needed to make efficient decisions that ensure the control and prevention of scale. These decisions are based on evaluating the performance of scale inhibitors under various environmental conditions such as temperature, pH, hydrodynamic conditions and brine composition.

Although an extensive body of literature is available for bulk precipitation reactions [24-28]; only limited numbers focus on evaluation of surface studies focusing on fouling mechanisms and crystals growth at solid interfaces. Studies have shown that the mechanisms and kinetics controlling bulk and surface deposition are different [29-31]. If wrongly applied common chemical inhibitors such as a Polyphosphinocarboxylic acid (PPCA) can reduce bulk precipitation while at the same time enhance surface deposition [32-35].

A study by Morizot and Neville [35] illustrated the difference of inhibition mechanisms of PPCA on barite scale both in bulk precipitation and surface deposition. The results from this research showed that when 25ppm of PPCA was applied, bulk scaling was greatly reduced; but enhanced surface deposition occurred. A similar study by Graham *et al.* [32-34] showed that using inhibitor concentration below the Minimum Inhibitor Concentration (MIC,

from standard bulk jar test determination) reduced bulk precipitation, but enhanced surface scaling. These studies mentioned were carried out in a closed system (i.e. brines are recirculated) and as such the saturation ratio was decreasing as a function of time.

In addition, oil and gas field operations rarely take place in single phase conditions, they are usually more complex due to the presence of multiphase environment (oil/water mixtures). However, to date, very limited research has been conducted in an oil phase conditions. Hence, there is a need for test to be carried out in the multiphase environment to mimic more realistic oilfield condition, by so doing, reducing the inconsistencies between laboratory test and what is observed in the oilfield.

1.3 Aims and objectives

The aim of this study is to develop a better understanding of the kinetics of barium sulphate formation and inhibition. The precise objectives of the thesis are described as follows:

- Understanding the kinetics of barium sulphate formation both in bulk and on metallic surface: To investigate the relationship between bulk precipitation and surface deposition of barium sulphate in a flowing system. Furthermore, understanding the nucleation mechanism of barium sulphate on a metallic surface at different thermodynamic conditions. Knowledge gained from this research will improve the understanding of scale formation in oil and gas production facilities.

- Investigate the effect of scale inhibitor on the growth of barium sulphate: To evaluate the different mechanisms of three scale inhibitors on the growth of barium sulphate crystals on surfaces. In addition, understanding factors that could affect surface scale inhibition. This information would help improve the use to scale inhibitor during application.

- Investigate scale formation in a multiphase environment: Developing an understanding of surface fouling of barium sulphate using different surfaces and scale inhibitors, both in an aqueous and oil phase environment. Information achieved from this investigation would help reduce the gap between laboratory test and real oilfield conditions.

1.4 Thesis outline

The thesis is structured as follows:

Chapter one. This chapter presents a brief overview of scale formation in the oil and gas industry, the economic impact of scale formation and the objective of this work.

Chapter two: This chapter gives a review of scaling process fundamentals, scaling control/prevention and factors that affect scale inhibition**.**

Chapter three: This chapter describes the various experimental procedures and materials used in achieving the project objectives.

Chapter four: In this chapter, results regarding the kinetics of bulk precipitation and surface deposition of barium sulphate with and without the presence of scale inhibitors are presented.

Chapter five: In this chapter, result of factors that could influence the efficiency of scale inhibitor are presented.

Chapter six: This chapter presents scale formation results conducted in multiphase conditions.

Chapter Seven: In the chapter, results presented in chapter 4 to chapter 6 are analysed and discussed.

Chapter Eight: The key conclusions obtained from this study are presented in this chapter.

Chapter Nine: This chapter provides the suggested future work for this study.

Chapter 2 Theory and literature review of scale formation and inhibition

The formation of inorganic scales coupled with the production of hydrocarbon has been a major concern in oilfield operations. These mineral scale deposits result in the reduction of production regardless of where they are formed. Deposits formed in the reservoir block the formation matrix, restricting fluid flow leading to formation damage. Scale mineral formed in the production facilities will block pipes causing several operational problems [13, 36, 37]. However, scale can act as suppression of corrosion, on the contrary when these scales contain defects, voids and cracks, they can lead to enhanced localized corrosion [38]. The common oilfield scales are shown in Table 2-1, relating to their solubility in acid and primary variables that affect their solubility [39]. They include calcium carbonate ($CaCO_3$), iron carbonate ($FeCO_3$), iron sulphide (FeS), barium sulphate ($BaSO_4$), strontium sulphate ($SrSO_4$), calcium sulphate ($CaSO_4$). There are three basic mechanisms by which scales could be formed in the oil and gas industry [40, 41]:

1. Increase in temperature and/or in pressure drop of a brine, which reduces the solubility of the salt in the solution.

2. Mixing of two incompatible brines (i.e. formation water and injection water).

3. Evaporation of brine resulting in an increase of the salt concentration above the solubility limit.

Historically, the most common mineral scales formed in the oil and gas industry are the calcium carbonate and barium sulphate. Calcium carbonate is formed due to the presence of bicarbonate ions and calcium ions found in production water, which is precipitated due to the reduction in pressure during production. The change of condition allows the release of carbon dioxide from

the solution resulting to increase in pH of the solution and the precipitation of calcium carbonate scale; this is shown in Equation 2-1.

$$Ca^{2+}_{(aq)} + 2HCO_3^-{}_{(aq)} \leftrightarrow CaCO_{3\,(S)} \downarrow + CO_{2\,(g)} + H_2O_{(l)} \quad \text{2-1}$$

Barium sulphate occurs due to the mixing of formation water that is highly rich in barium cations and injection seawater that is enriched with sulphate anions. The formation of barium sulphate is very troublesome since scales formed are insoluble in most fluids and cannot be dissolved by acid, making it difficult to be removed once it is formed and deposited during oilfield operations, most especially in the reservoir.

$$Ba^{2+}{}_{(aq)} + SO_4^{2-}{}_{(aq)} \leftrightarrow BaSO_4{}_{(S)} \quad \text{2-2}$$

Table 2-1: Type of scale formed in the oil and gas industry

Name	Chemical Formula	Primary Variables	Acid Solubility
Calcium Carbonate	$CaC0_3$	Partial pressure of $C0_2$, temperature, TDS	Yes
Calcium Sulphate: **Gypsum**	$CaSO_4.2H_20$ $CaSO_4.1/2H_20$ $CaSO_4$	Partial pressure of $C0_2$, temperature, TDS	No
Barium Sulphate	$BaSO_4$	Temperature, pressure	No
Strontium Sulphate	$SrSO_4$	TDS	No
Iron Compounds: **Ferrous Carbonate** **Ferrous Sulphide**	$FeCO_3$ FeS	Corrosion, dissolved gases, pH	Yes

Barium sulphate could be formed at any point in the production system depending on where the formation and seawater mix. Figure 2-1 shows

possible case locations of where barium sulphate could be formed throughout the flow path of water during production [42].

1. At the surface facility where incompatible water mixed;
2. When injected water start to mix with reservoir formation water;
3. Down-hole the formation where the injection water displace the reservoir water;
4. Location in the reservoir where the mixed injection water and formation water are about to reach the producing well;
5. Location down-hole the reservoir where the mixed water is in the range of producing well;
6. The connection of branched zone where each branch produce different water;
7. At the manifold of producing zone where water is produced from different block within the same producing zone;
8. Topside of side facilities where produced fluids are mixed from different production zones to separate the oil and gas from water or in pipelines that do transports produced fluids to onshore processing facilities;
9. Discarding well where the produced water is injected for final disposal.

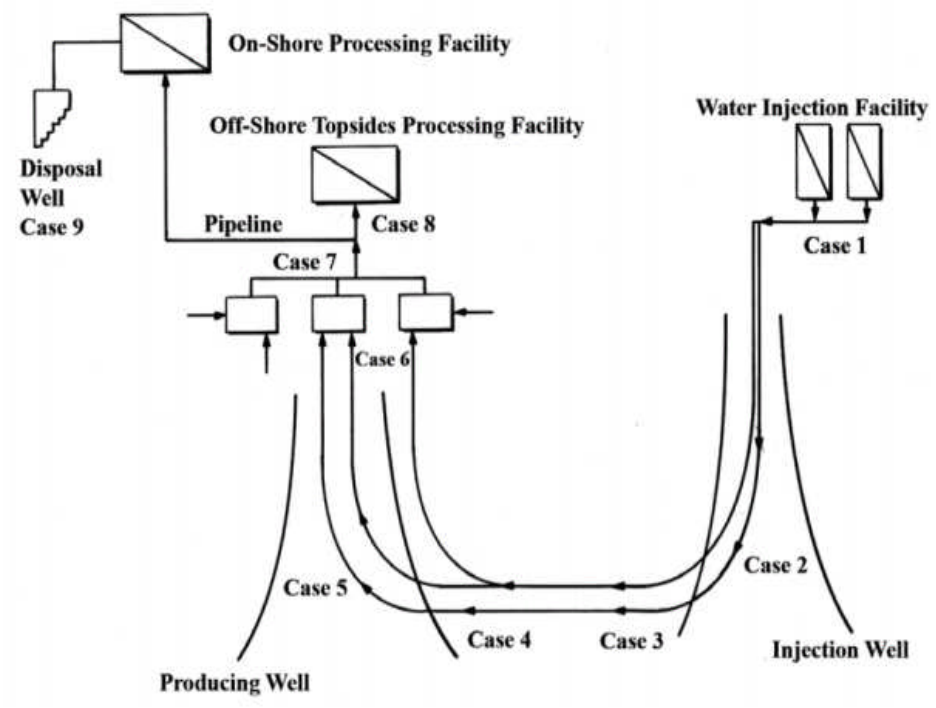

Figure 2-1: Possible location of barium sulphate scale deposit [43]

Precipitation of barium sulphate can only occur when the solution concentration has exceeded its solubility; when the solution has attained supersaturation, then after nucleation and crystal growth takes place which is illustrated in Figure 2-2. The next three sections explain in details the various kinetic processes in precipitation.

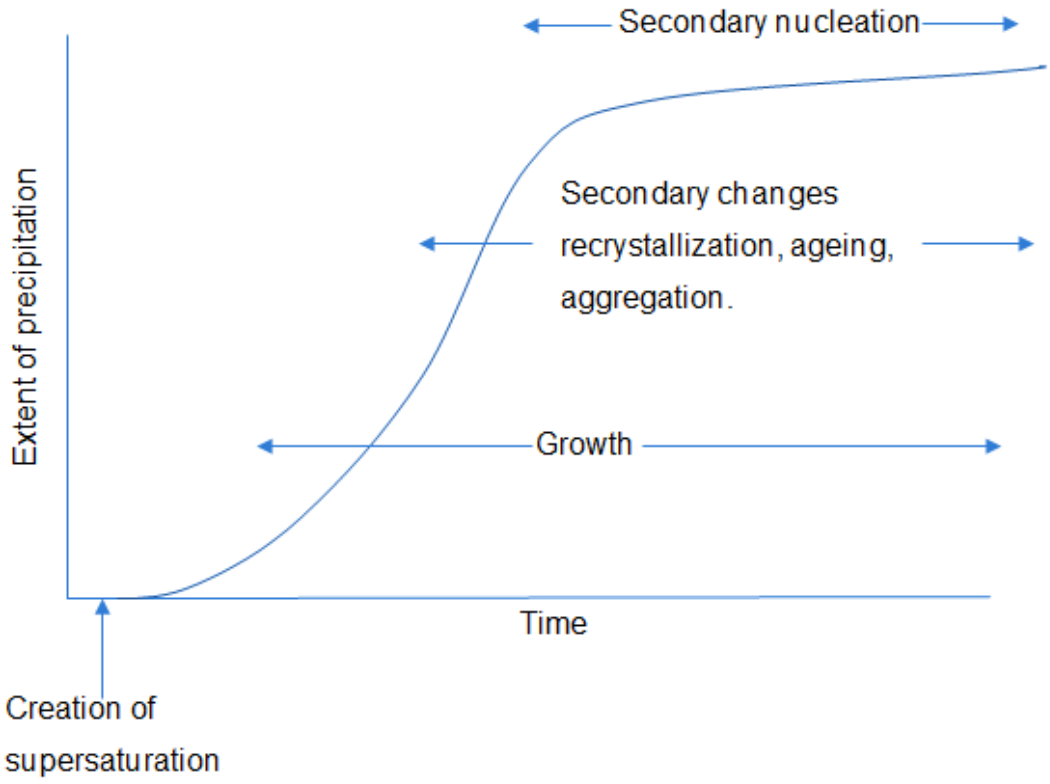

Figure 2-2: Kinetic processes involved in precipitation [43]

2.1 Supersaturation

From a thermodynamic point of view, precipitation usually takes place when the solubility of mineral salt is exceeded. This condition normally occurs when the solution is been supersaturated [44]. Therefore, supersaturation is the primary cause of the formation of scales in a solution. The extent of supersaturation can be expressed in term of supersaturation index (SI), which corresponds to the logarithm of saturation ratio (SR); mathematically saturation ratio can be expressed:

$$SR = \frac{IAP}{k_{PSX}} \quad 2\text{-}3$$

Where IAP is the ion activity product and K_{psx} is the solubility product for mineral salt [45]. Although the saturation index can be used to estimate the scaling tendency of any scale; a limitation of the saturation index is that it does not give information about the interaction of ionic species and information about the precipitation kinetics [44]. Below shows the three tendencies for the scale to form, from a thermodynamic point of view:

SR < 1 Undersaturated solution: there is no tendency of scale to form and the scale is likely to dissolve.

SR = 1 Equilibrium solution: both scale formation and dissolution rate occurs at the same rate. This implies that scale will not be formed in the solution.

SR > 1: Supersaturation solution: implies that scale is likely to occur, which is thermodynamically possible.

The saturation of a solution is a key factor for crystallization in the bulk solution and in seeded crystals. This is shown in Figure 2-3 representing the crystallization potential under different kinds of solution. From Figure 2-3 which is divided into three major zones: Undersaturated, saturated and supersaturated. The undersaturated region corresponds to the area under the solubility curve, solution conditions are undersaturated with respect to the macromolecule, spontaneous homogeneous nucleation would unable to occur and crystals placed in the solution will dissolve.

The next region (saturated) is measured experimentally and is represented by the two-dimension solubility curve. Alongside the saturation, spontaneous homogeneous nucleation would not take place and any crystals added to the solution will not dissolve or increase in size. The last region can be further divided into three regions (metastable supersaturation, liable supersaturation and precipitation zone). The metastable supersaturation occurs when the spontaneous homogeneous nucleation does not take place in a reasonable length of time but the crystal will continue to grow in the solution. The liable supersaturation represents the region where spontaneous homogeneous

nucleation could occur and the crystal added to the solution will grow. Further, this region is not appropriate for seeding when compared to the metastable region; and the crystal added to the region can shock the solution, resulting in excessive nucleation [46].

Finally, precipitation zone is an area that is always supersaturated with respect to crystal growth. The crystallization of barium sulphate occurs like other crystallisation processes, which consist of three stages: induction, nucleation and growth. These three different stages are explained in the next four sections below.

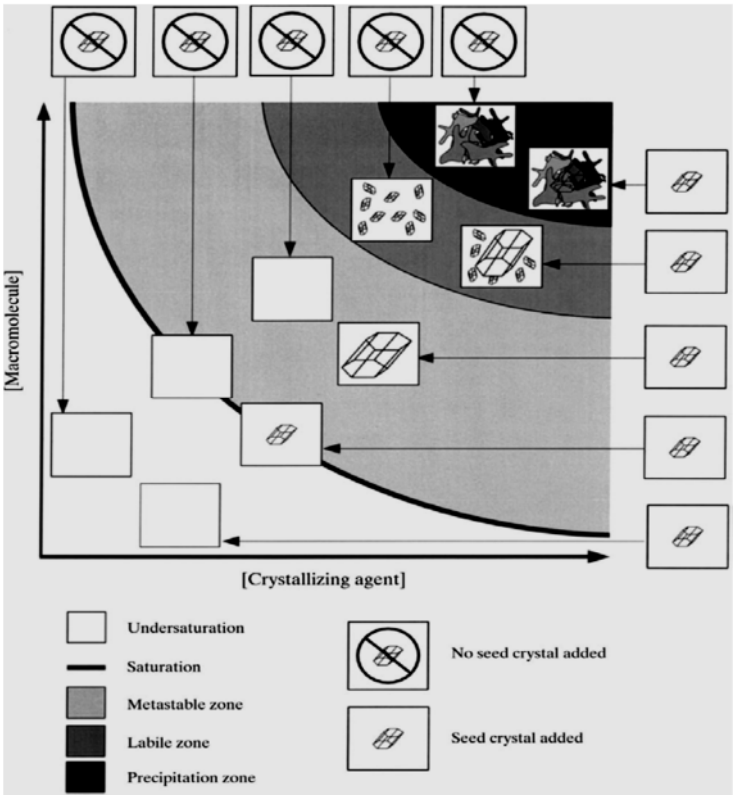

Figure 2-3: A two-dimensional representation of the three major saturation zones:[45]

2.2 Induction time

Induction time is the time elapsed from creation of supersaturation of a system to the first appearance of secondary solid phase (critical nuclei). It is a function of the supersaturation and the temperature of the solution. The induction time could be determined by the change in concentration or conductivity,

turbidimetrically and visually depending on the physical property being followed [43]. The induction time is the total sum of the time needed to reach steady-state nucleation (t_{tr}), the time necessary for the crystal to grow to a visible size (t_g) and the time for critical nuclei to be formed (t_i) as shown in the equation 2.2[43].

$$t_{ind} = t_{tr} + t_i + t_g \qquad 2\text{-}4$$

It can be related to the nucleation rate when the nucleation time is greater than the growth time. It is assumed that the induction time is inversely proportional to the nucleation rate as expressed below [43, 47]:

$$\boldsymbol{t_{ind} \propto J^{-1}} \qquad 2\text{-}5$$

2.3 Nucleation

Nucleation is the process of formation of stable nuclei after the solution has attained supersaturation and induction time. This process occurs at a very high-supersaturated region. Nucleation can either be primary or secondary as illustrated in Figure 2-4: Primary nucleation results in the absence of crystalline surface, while secondary nucleation result from the presence of the crystalline surfaces [48], both nucleation processes are explained in the next subsection.

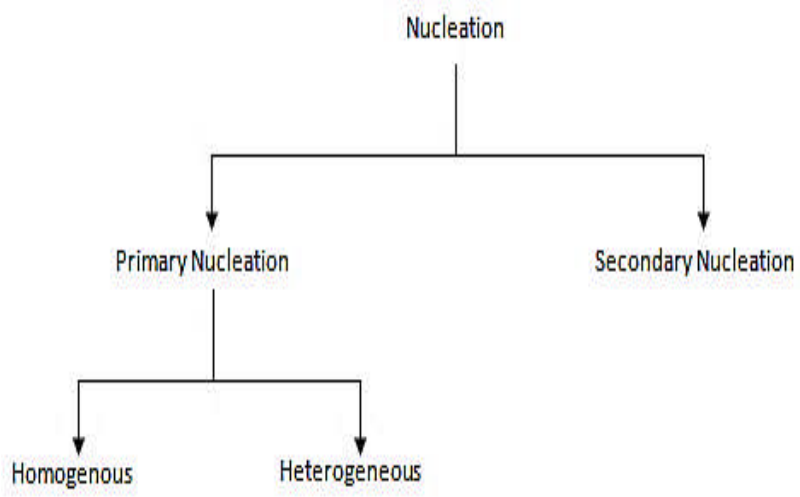

Figure 2-4: Types of nucleation [48]

2.3.1 Primary nucleation

Primary nucleation occurs when the solution has attained very high saturation. When it occurs in the absence of foreign crystal/particles in the solution is called homogeneous nucleation. On the other hand, when it occurs with the presence of a foreign particle in the solution or due to the roughness of a substrate it is known as heterogeneous nucleation. The Figure 2-5 gives a pictorial illustration of both nucleation processes.

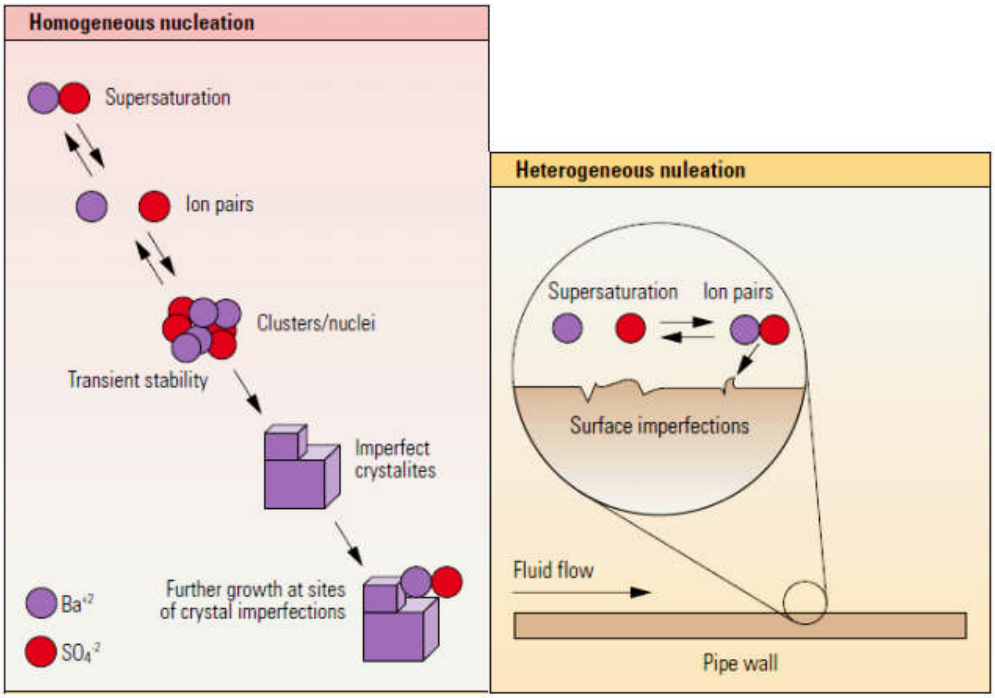

Figure 2-5: Process of primary nucleation [35]

2.3.1.1 Homogeneous Nucleation

Nucleation occurs when ions start to pair by electrostatic interaction to reach a critical size. Classical nucleation theory based on vapour condensation is one of the most famous starting points to explain this process. The nucleation is initiated when there is excess free energy available in the system, resulting from the supersaturation of the system [49]. The excess of the free energy

variation during a homogeneous nucleation process is described in Equation 2.8

$$\Delta G = \Delta G_s + \Delta G_v = 4\pi r^2\gamma + \frac{4}{3}\pi r^3 \Delta G_v \quad \text{2-6}$$

Where ΔG is the total for the excess free energy between the solute in the solution and the small spherical particle of radius (r), ΔG_v (volume free energy) is the excess free energy between the very large particle and the solute in the solution. And ΔG_s is the excess free energy between the surface of the particle and the bulk of the particle. The graphical representation of the equation is shown in Figure 2-6, the role of both the volume and surface free energy charge. The net free energy change increases with the increase of the particle size to attain a maximum size known as $\Delta G_{(crit)}$ [49, 50]. The $\Delta G_{(crit)}$ must be attained for the formation of stable particle, which relates to the critical size of the nuclei. This implies that particle formed below the critical radius cannot be able to grow and it will re-dissolve into the system.

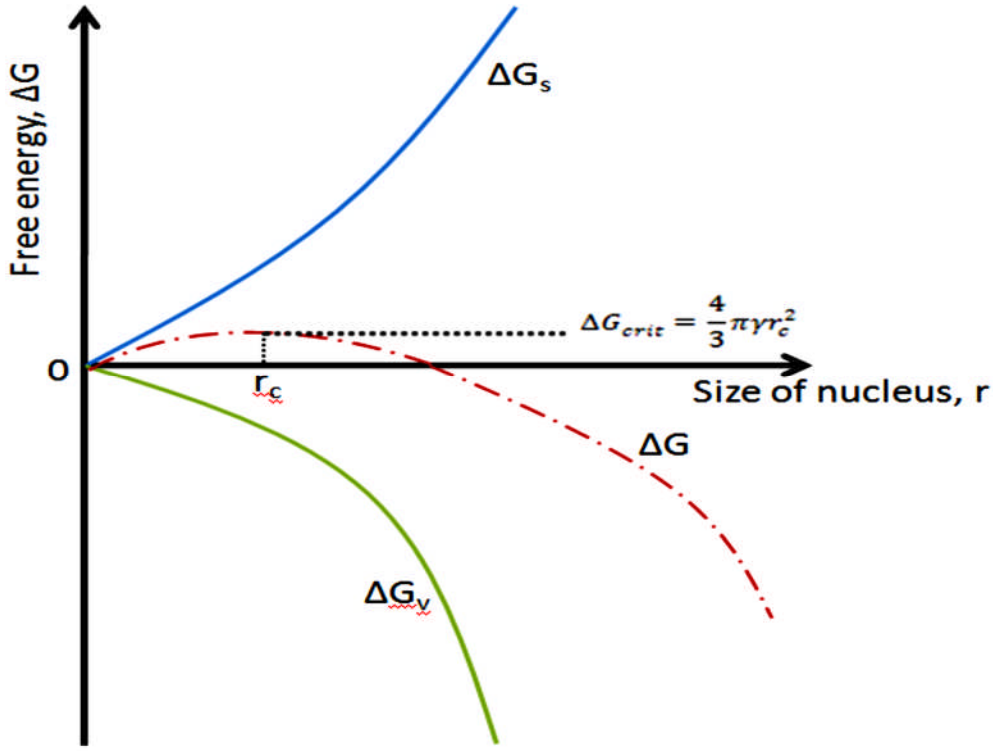

Figure 2-6: Free energy diagram for nucleation and critical radius

The critical radius can be evaluated by differentiating equation 2.6 with respect to r:

$$\frac{d\Delta G}{dr} = 8\pi r\sigma + 4\pi r^2 \Delta G_v = 0 \qquad 2\text{-}7$$

$$r_c = \frac{-2\sigma}{\Delta G_v} \qquad 2\text{-}8$$

Therefore the free energy change $\Delta G_{(crit)}$ can be calculated by substituting ΔG_v from equation into the equation.

$$\Delta G_{crit} = \frac{4\pi\sigma r_c}{3} \qquad 2\text{-}9$$

The cluster growth is governed by Gibbs-Thompson equation

$$In\ \frac{c}{c^{cric}} = In\ S = \frac{2\sigma v}{kTr} \qquad 2\text{-}10$$

Where c is the concentration of the cluster size r. substituting for r_c in equation

$$\Delta G_{crit} = \frac{4\pi\sigma r_c}{3(kTIn\ S)^2} \qquad 2\text{-}11$$

The rate of nucleation, which is the number of nuclei formed per unit time per unit volume, can be expressed using Arrhenius type as:

$$J = Bexp\left[\frac{-\Delta G_{crit}}{kT}\right] \qquad 2\text{-}12$$

Substituting $\Delta G_{(crit)}$ from equation 2.11

$$J = Bexp\left[\frac{-16\pi\sigma^3 V^2}{3k^3T^3(In\ S)^2}\right] \qquad 2\text{-}13$$

Where T denotes the temperature, V the molecular volume, *k* Boltzmann constant, *B* constant and will vary depending on the order of the reaction, σ is interfacial tension and S is the saturation ratio.

2.3.1.2 Heterogeneous Nucleation

The presence of foreign particle and surface can induce nucleation at very low supersaturation. This type of nucleation is known as heterogeneous

nucleation. It requires a lower energy when compared with homogeneous nucleation; since the foreign particle and surface allows the adsorption of crystal material and lowers the critical free energy of the system [51]. Furthermore, the rate at which the free energy decrease depends on the wetting angle of the solid phase:

$$\Delta G_{hom} = \emptyset \Delta G_{het} \qquad 2\text{-}14$$

$$\emptyset = \frac{1}{4}(2 + \cos\theta)(1 - \cos\theta)^2 \qquad 2\text{-}15$$

Ø denotes wetting angle and θ is contact angle between the crystalline deposit and the foreign solid surface.

2.3.2 Secondary nucleation

Secondary nucleation results from the parent crystals present in the supersaturated solution. Due to the presence of the parent crystal which has a catalytic effect on the nucleation process, a lower supersaturation is needed when compared to primary nucleation (both homogeneous and heterogeneous nucleation) [50]. The mechanism of secondary nucleation can is divided into two cases: Catalytic mechanism which involves the sweeping away of solute aggregate from the adsorption layer on the crystal surface and generation of nuclei in the supersaturated solution. Breaking mechanism involves the formation of fine particles by reduction in size. The breaking mechanism can occur via abrasion, attrition and fracture [52]. Abrasion is the removal of a tiny particle from a growing crystal; attrition involves the disintegration of a parent particle into two different parts, while fracture denotes the fragmentation of crystals into two or more similar pieces.

In a similar research conducted by Daudely *et al*. [53], they distinguished the mechanism of secondary nucleation into two: Surface breeding which relates to surface structure during the growth of nuclei, while mechanical breeding mechanism denote from crystalline material being removed by mechanical action exerted on the parent crystal [53, 54]. The mechanisms are shown in Figure 2-7.

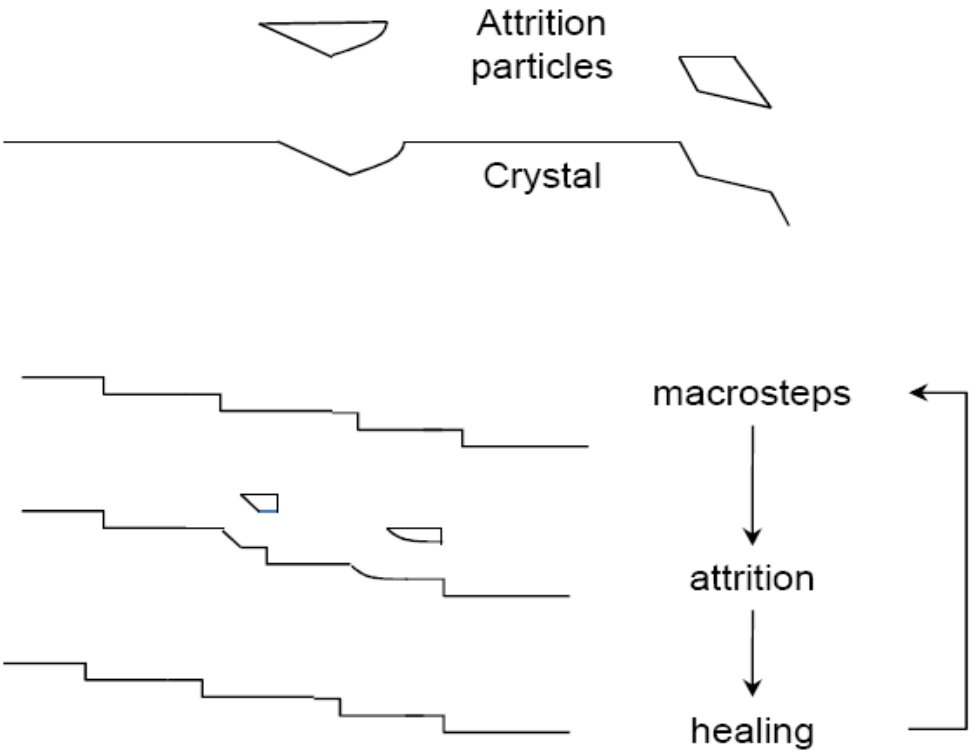

Figure 2-7: Visualisation of the difference between the mechanical breeding and the surface breeding mechanism [54]

2.4 Crystal growth

As discussed in the previous section, after nucleation process, the next stage involves the growth of particle (nuclei) into larger particle by the addition of the molecule from the supersaturated solution. This process is known as *crystal growth*, and alongside with nucleation determines the final particle size and distribution of the system [51]. The mechanism of crystal growth is described by three theories: Surface energy, adsorption layer theory, and screw dislocation theory, which are explained in next subsections.

2.4.1 Surface energy theory

The surface energy theories are based on the thermodynamic equilibrium state proposed by Gibbs. It was postulated that growth of crystal is similar to an isolated droplet of fluid; which implies that in equilibrium, crystals will be

stable when their surface free energy is in minimum for a given volume [49]. Curie calculates the end forms and shapes of crystal in equilibrium with a solution or vapour using Gibbs principle. In 1901 Wulff gave an extension of Currie's thoughts and relates the connection between surface free energy and growth rate of different faces [50]. Other researchers extended and modified this theory but the surface energy theories of crystals have not been generally acceptable based on the fact that the theory did not explain the effect of supersaturation and solution movement of the crystal growth rate [49, 50].

2.4.2 Adsorption layer theory

This theorem was developed by Kossel, Stranki and Volmer based on the role of surface and volume free energy changes associated with the formation of stable nuclei on the surface [49, 55]. In their study, they showed the role of homogeneities on the growth sites. A crystal surface consists of the surface site, ledge-kink site and ledge site, which is shown in Figure 2-8. In the surface site, the atom will be attached to the surface of the growing layer, while that of the ledge site molecule will be attached to both the growing step and surface. But ledge-kink site, the molecule will be attached to the three surfaces. Showing that binding energy is at maximum in the ledge-kink site when compared to that of the surface and ledge site. Hence, the molecule on the crystal surface will move to the ledge-kink site and get incorporated [49]. This process will continue until the whole layer is completed. Furthermore, the crystal growth continues in a layer-by-layer manner.

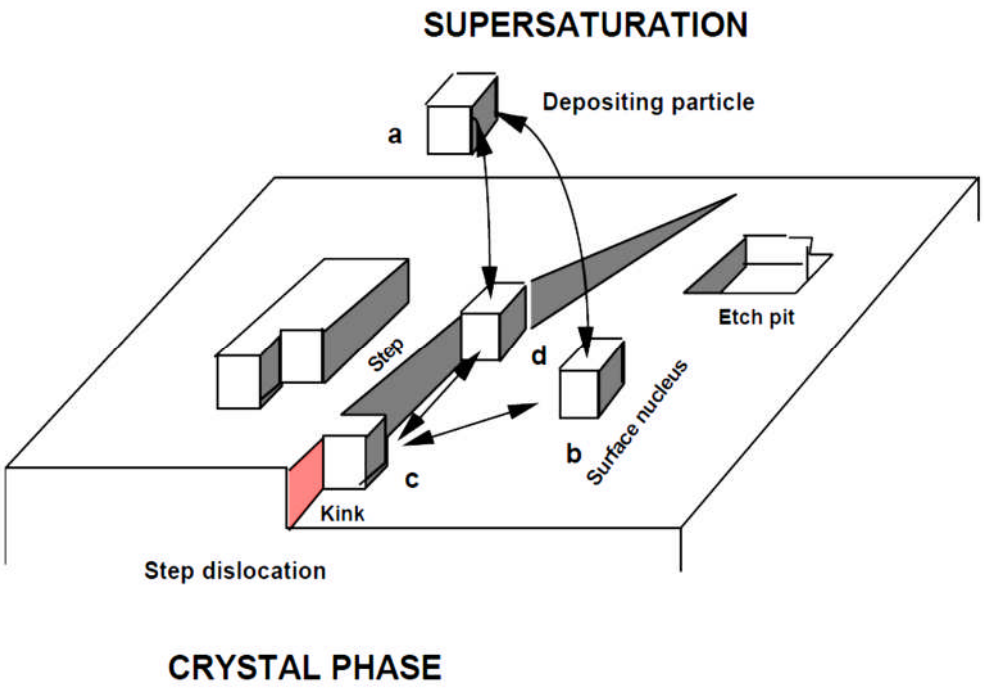

Figure 2-8: Representation of a crystal surface complete with defects [50]

2.4.3 Screw dislocation theory

One of the limitations of the previous theories discussed above was that they did not consider the growth of crystals at a low supersaturation and it is indecisively the reason that they consider the crystal growth rate as a continuous process, with the formation of critical size nucleus the rate-determining step. Frank was the first to propose a theory of crystal growth at low supersaturation and he suggested that dislocation (screw dislocation) in the crystal was the source of continuous creation of new steps, which can be spread across the surface of the crystal and promote crystal growth [49, 55]. This growth occurs by rotating of the steps around the dislocated point as shown in Figure 2-9.

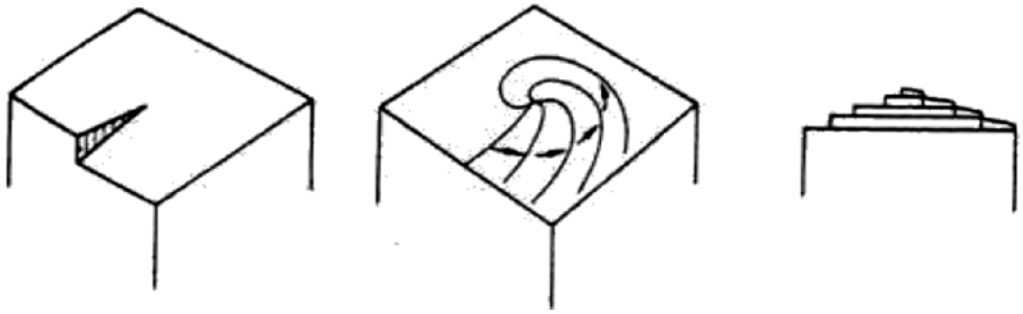

Figure 2-9: Diagram of screw dislocation mechanism [37]

2.5 Adhesion

As discussed previously, the problem faced by the oil and gas industries is the build-up of scale on surfaces. Adhesion is one of the mechanisms by which scale can be formed on surfaces. It can be defined as a phenomenon where two different bodies are held together by interfacial forces, such as valences forces and ions interlocking forces [56, 57]. There are several theories that could explain this phenomenon; the next subsection explains some of the theories.

2.5.1 Adhesion theories

The study of the mechanism of the adhesion is the major concern of most research; however, the interpretation of the mechanism is as complicated as the phenomenon itself [58]. Classical theories of adhesion have been developed to explain these mechanisms. For details regarding the theories, the various reviews could be consulted [56, 57].

In term of fouling process, the interaction between the fouling particle and surface is usually explained using the DLVO theory named after B. V. Derjaguin, L. D.,Landau, E. J. W. Verwey, and J. Th. G. Overbeek [59]. The reason is that fouling process could only occur with particulate materials of colloidal size with a dimension of ≤1μm; making the effect of gravitational force on the material negligible [60]. However, the larger particle would not be able to adhere to the surface, due to the effect of gravitational and hydrodynamic

force which is strong enough to remove them. The theory explains that the attractive forces between colloidal particles are as a result of *van der Waal* interaction [60]. Whereas when the particle is been immersed in a liquid, an electrostatic force is formed which is very repulsive.

In addition, a study by Oliveira [60] shows that van der Waal and electrostatic double–layer repulsion is not sufficient enough to explain the scaling process. Furthermore, the study shows that physiochemical factors play a major role in fouling; some practical findings that could help prevent or mitigate fouling were discussed [60]. Some of these factors that could affect scaling process are explained in section 2.7.

2.6 Barium sulphate

Barium sulphate exists as a white orthorhombic crystal or powder; they are also referred to as barite. It is moderately soft crystalline white opaque to transparent mineral as shown in Figure 2-10. Barium sulphate is formed by mixing of fluid containing Barium and sulphate ion in the sea floor.

$$Ba\,Cl_2 + Na_2SO_4 \rightarrow BaSO_4 \downarrow +2NaCl \qquad 2\text{-}16$$

Figure 2-10: Barium Sulphate mineral [61]

The mass composition of barium sulphate is 58.84% of barium, 13.74% of sulphur and 27.42% of oxygen; the chemical properties are summarized in Table 2-2.

Table 2-2: Chemical properties of barium sulphate [30]

Chemical formula	$BaSO_4$
Density	4.5g/cm^3
Solubility	2.33mg/l
Melting point	1580°C
Molecular Weight	233.38g/mol

2.7 Factors affecting scale formation

This section presents various factors that influence the formation of barium sulphate scale in the bulk precipitation and surface deposition.

2.7.1 Effect of temperature and pressure

The variation of temperature controls the scaling trend of barium sulphate, knowing that temperature is related to the supersaturation ratio of a system. The solubility of barium sulphate increases with respect to increase in temperature because the dissociation of $BaSO_4$ is an endothermic reaction [37, 39, 62, 63]; as shown in Figure 2-11. Subsequently, barium sulphate crystallization and adhesion will take place when the temperature of the system is reduced. Furthermore, the effect of temperature is more significant when evaluating the inhibition efficiency of chemical inhibitors.

The sulphate of barium, calcium and strontium are more soluble at high pressure. Consequently, barium sulphate will be precipitated when there is a reduction in pressure [39, 62]; nevertheless the effect of pressure in scaling tendency of $BaSO_4$ is less when compared to that of temperature. Moreover,

the influences of scaling tendency of $BaSO_4$ by pressure variation must occur with a synergistic effect of an increase in temperature.

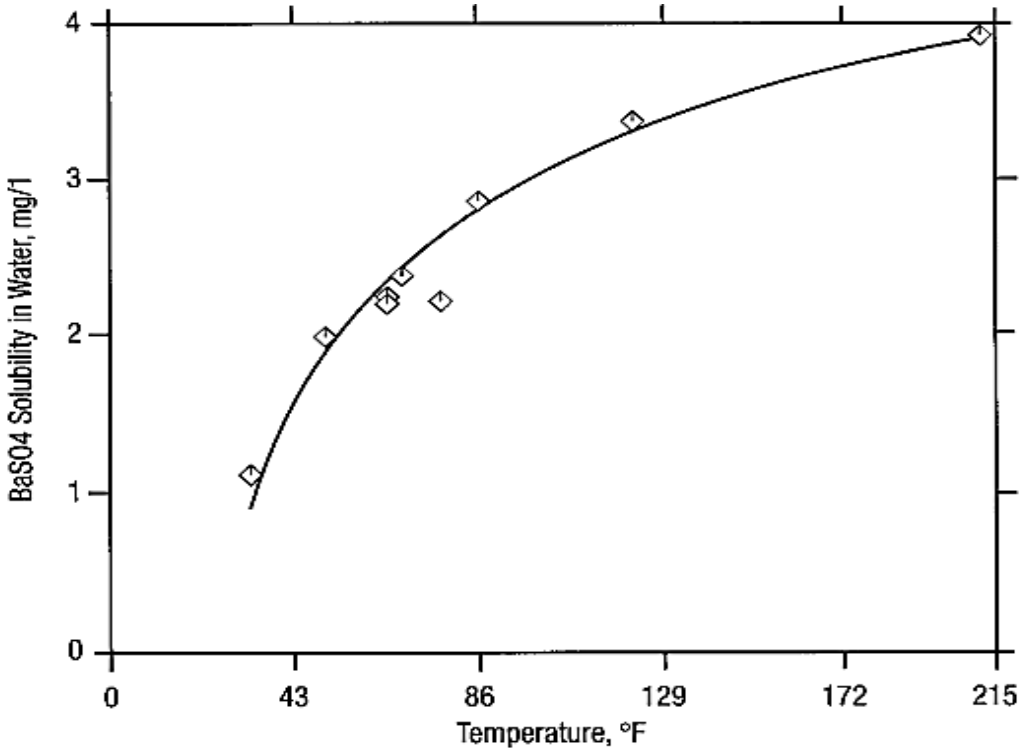

Figure 2-11: Barium sulphate solubility in water [49]

According to research performed by Dyer and Graham [11] to study the effect of temperature and pressure on oil scale formation of barium sulphate and calcium carbonate using dynamic tube blocking. The scaling tendency of barium sulphate scale increases with a decrease in temperature, while that of carbonate increase with an increase in temperature. Furthermore, the increase in pressure reduces the scaling tendency in both carbonate and sulphate scale. At lower pressure condition of 1.37×10^6 Pa, the rapid increase of differential pressure of 6.9×10^3 Pa was observed at higher pressures, indicating that at a lower pressure the scaling tendency increased.

2.7.2 Effect of saturation ratio

As discussed in section 2.1 saturation ratio is the thermodynamic driving force of scale formation. Todd and Yuan [12] showed the effect of supersaturation ratio of barium and strontium sulphate scale on formation damage. From their

study as shown in Figure 2-12, the crystal formed at high supersaturation ratio was larger than the ones formed at low supersaturation ratio. Also, in Figure 2-12 at higher supersaturation ratio 67% of initial permeability was lost in a short time of injection of the brine; while at lower saturation ratio <15% of the initial permeability was lost. This shows that the saturation ratio influences the scaling tendency, morphology and size of crystal formed.

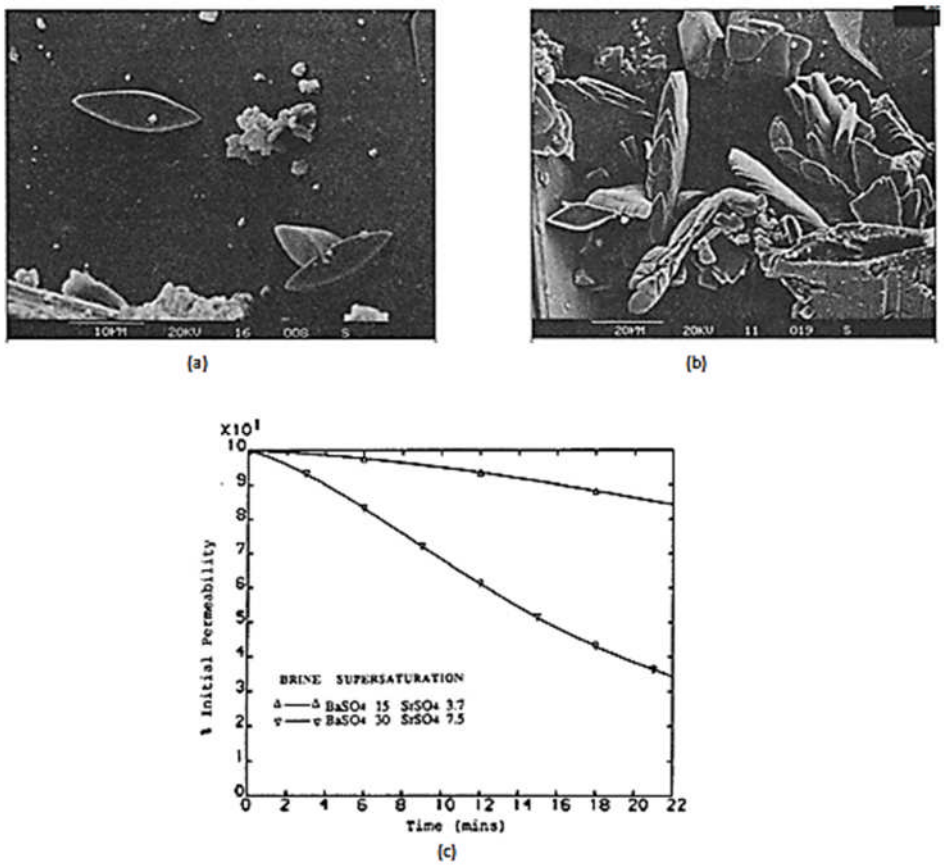

Figure 2-12: (a) Scale core with brine with $BaSO_4$ supersaturation of 15 and $SrSO_4$ of 3.7 (b) Scale core with brine with $BaSO_4$ supersaturation of 30 and $SrSO_4$ of 7.5 (c) Effect of supersaturation of $BaS0_4$ and $SrSO_4$ permeability decline [12]

2.7.3 Effect of solution pH

The pH is a measure of $[H^+]$, and range of pH is found to be generally between 4 and 7 in a different location in the oil plant [64]. Nevertheless, the solubility of barium compounds increases with respect to decrease in pH, the solubility of barium sulphate is unaffected by the variation of pH [62, 65]. This was

checked by using a Multiscale prediction software, by comparing the saturation ratio of North Sea Sea water (NSSW), formation water (FW) brine mixing at two different ratios (60/40 and 80/20) in pH range of between 5 and 9 at 95˚C [25]. The saturation ratio variation was less than 1 unit in both mixing ratios shown in Figure 2-13 and Figure 2-14. However, a study by Peyvandi *et al* [66], shows that the pH affects the morphology of $BaSO_4$. In addition, the effect of pH is more significant during the presence of chemical scale inhibitors.

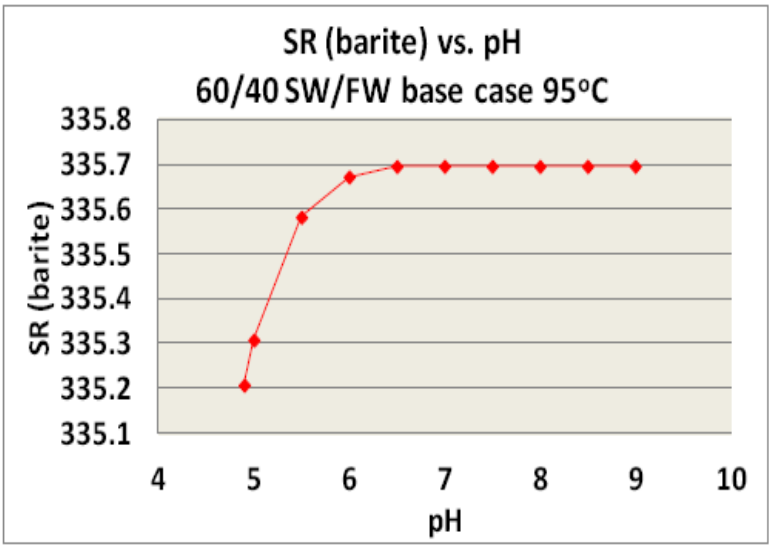

Figure 2-13: SR (barite) vs. pH, 60/40 NSSW/FW Base Case, 95˚C [25]

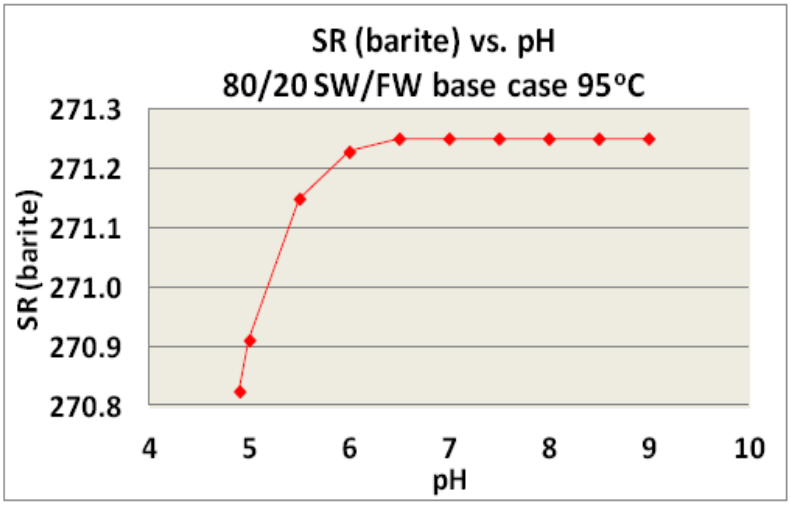

Figure 2-14: SR (barite) vs. pH, 80/20 NSSW/FW Base Case, 95˚C [25]

2.7.4 Effect of divalent cations

The divalent cations Ca^{2+}, Sr^{2+} and Mg^{2+} that are present in the formation water and seawater affect the nucleation and growth process of barium sulphate; although their concentration differs depending on origin source. The presence of calcium ions during the formation of barium sulphate results in co-crystallization of calcium in the barium sulphate lattice [67-69]. Also, it has been reported that about 6% of Ba^{2+} is substituted by calcium, as illustrated in Figure 2-15 [67]. This calcium ion inclusion tends to decrease the barium lattice parameter, which retards the lattice growth (i.e. increasing the solubility of barium sulphate in the solution) or makes the lattice growth easy for inhibition [67-70]. Similarly, the Sr^{2+} may also have the same effect as the Ca^{2+} [71], but the concentration of strontium ions in the formation water is very low; making the effect less important than that of Ca^{2+} [25, 72].

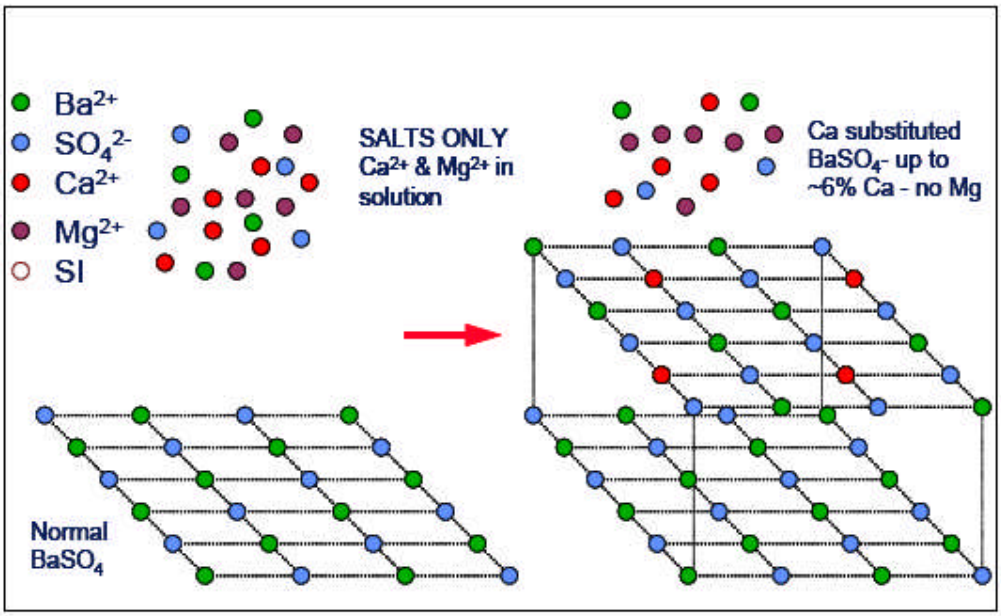

Figure 2-15: Schematic diagram illustrating Ca inclusion into the barite lattice [68]

2.7.5 Effect of Ionic Strength

The salt content of the brine plays a vital role in the scaling tendency of barium sulphate; since the barium sulphate solubility is strongly affected by the ionic

strength of the solution [39, 73]. Furthermore, the ionic strength is a function of the concentration of ions present in the solution. Consequently, an increase of sodium and chloride ions will increase the solubility of $BaSO_4$. On the contrary, a reduction of the ionic strength will increase the scaling tendency of barium sulphate [74]. For instance, an increase in NaCl concentration of the brine would increase the effect of temperature on the barium sulphate solubility. This explains why barium sulphate occurs in a hot well that produces high salinity brines [74].

2.8 Scale control strategy

Basically, there are five categories by which scale may be controlled during the production of oil and gas [19] (namely: fluid modification, flow modification, substrate modification, damage removal and chemical scale inhibitors).

2.8.1 Fluid modification

Generally, it is known that the formation of barium sulphate scale results from the scaling ions from formation water and seawater. An approach to reduce the barium sulphate scale is by partially removing the sulphate ions from the injection seawater by the use of desulphation plant [41, 75, 76]. This could reduce the sulphate content of the injection seawater from a range of 2700-3000ppm to range of 40-120ppm. Conversely, the use of aquifer water and re-injecting produced brine during production could also reduce the scaling tendency.

2.8.2 Flow modification

Since the formation of scale is as a result of precipitation of ions from water, scale could be mitigated by good well production strategy. For instance, choking back well that produce water that could lead to mixing of incompatible water. Furthermore, the separation of incompatible brine before they could mix to form sulphate scales if promising this could mitigate the mineral scale

formed during production. A drawback to this technique is that scale may form in pumps due to a reduction in pressure and increase in temperature, leading to failure in pumps [19].

2.8.3 Substrate modification

The use of modified surfaces has been shown to affect the kinetics and morphology of the fouling process [77, 78]. This technique has drawn various researchers to conduct studies in this area because of the role of these surfaces on the influence of the amount and kinetics of fouling [77]. Bio-fouling industry has taken more advantage of the application of this method to reduce or mitigate the marine biological species on surface [15]. In most of their research, the system that has lower surface energy is shown to reduce the induction time for heat transfer through the surface and lower the fouling adhesion [15, 77, 79]. In recent time, researchers in the inorganic fouling industry have also applied the use of modified surface due to some similarity with bio-fouling process [15].

Cheong *et al*. [15] studied the mechanism of calcium carbonate on polymer surfaces and stainless steel surfaces treated with commercially-available coatings, using stainless steel as the reference surface. The study shows that surface coating such as Tech 23, Tech 100 and DLC offer brilliant potential to mitigate the formation of calcium carbonate during the initial stage of scale formation as shown in Figure 2-16. In terms of the effect of surface energy relating to scaling process, although the surface coating followed the normal trend of lower surface energy, which implies lower scaling tendency; in the case of the polymer surface, it was found that the reverse was the case. A higher scaling tendency for lower surface energy surface was observed which is contrary to most research finding on the effect of surface energy on fouling (either inorganic or organic) as shown by the dotted line in Figure 2-17.

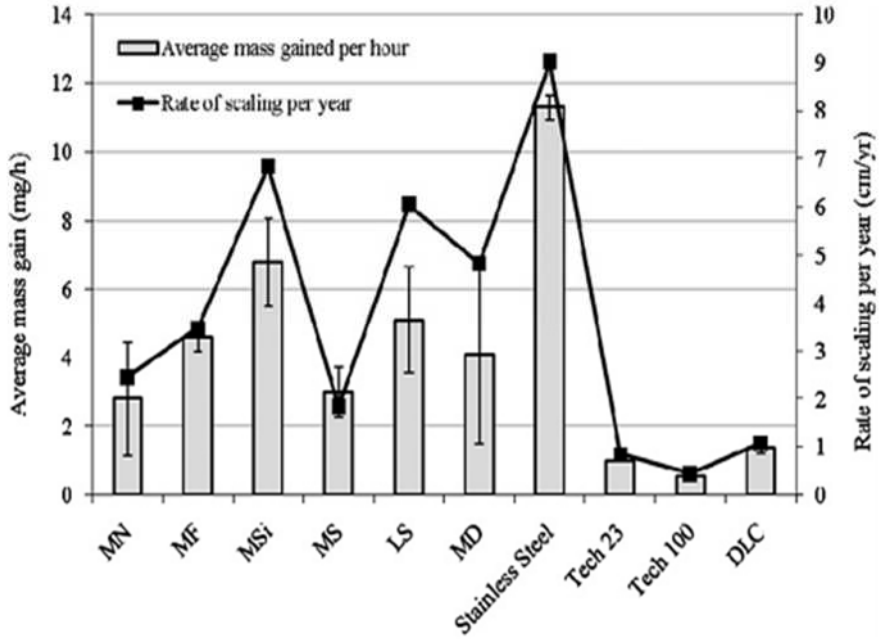

Figure 2-16: Result of 1hr deposition test at 1800 rpm to assess the scaling tendency of each test surface [15]

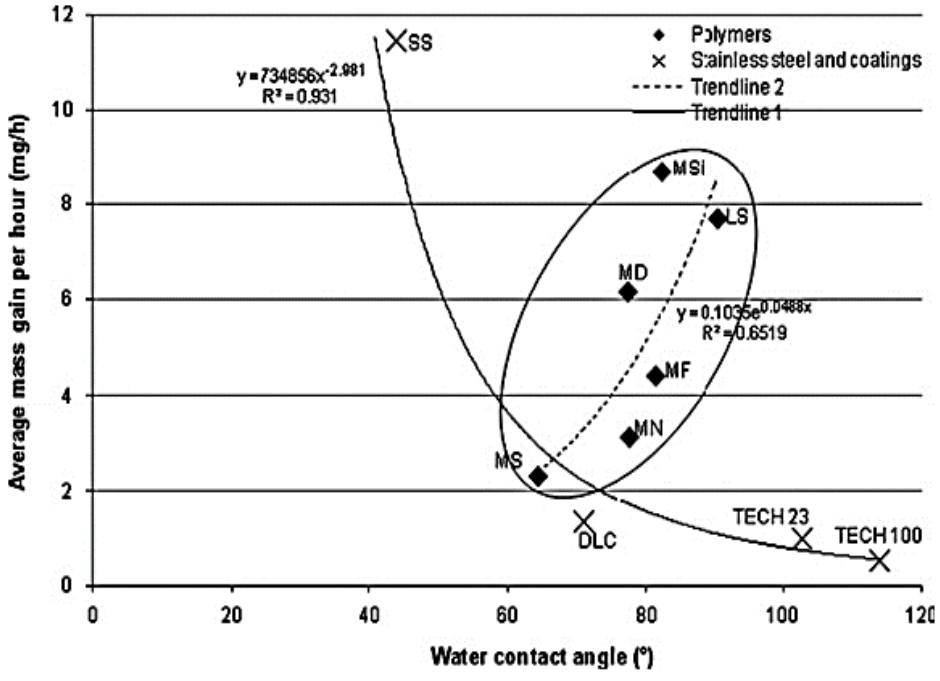

Figure 2-17: Mass gain (mg) vs water contact angle measurement (^{0}) [15]

Jaouhari *et al.* [80] studied the influence of nature and surface of three different substrates (gold, bronze and stainless steel) on deposition kinetics of calcium carbonate using an electrochemical method based on oxygen reduction. It was observed that gold scaled very quickly followed by bronze and stainless steel was the slowest. According to the researchers, they related the deposition partly as a result of the presence of oxide at the electrode surface, which blocks the calcium carbonate precipitation by slowing oxygen reduction. Furthermore, they concluded that substrate determines the nucleation rate and subsequently the polymorphs formed on it.

Charpentier *et al.* [81] investigated the ability of chemically and morphologically modified coatings in the prevention of mineral scaling conducted under laminar and turbulent dynamic conditions using a rotating cylinder electrode in a complex scaling environment. According to the authors, anti-fouling properties with coating F1, F4, SG3, 4 and 5 are the most promising in terms of mass gain reduction as shown in Figure 2-18. Also, it was found that material with lower surface energy with the presence of micro or nanometer scale texture, tends to scale more due to offering multitude nucleation site (heterogeneous surface nucleation) for scaling; thus facilitating the growth of crystals on the surface.

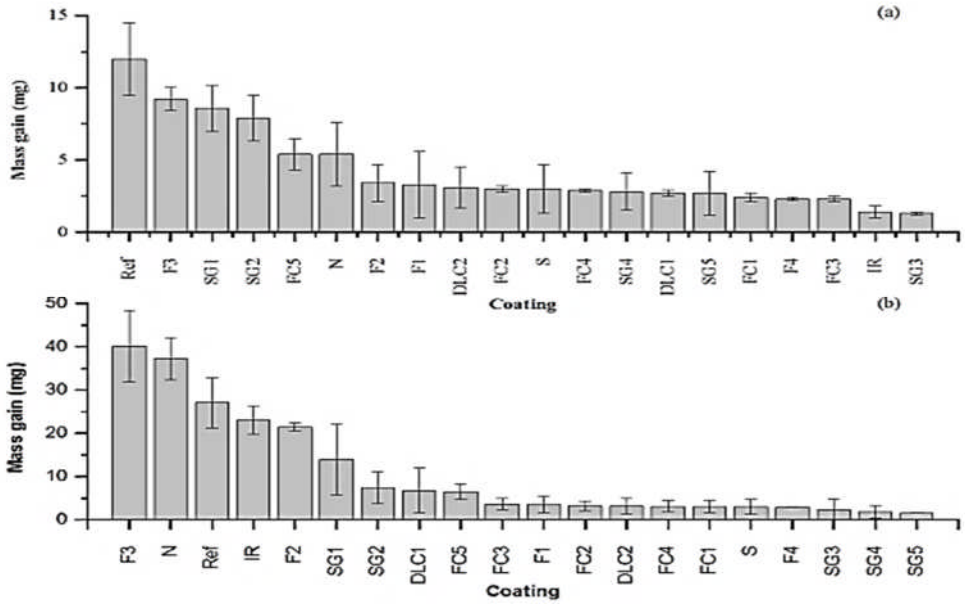

Figure 2-18: Mass gain surface 2 hours immersion in complex scaling brine (a): Laminar (b): Turbulent flow condition [81]

Eroini *et al.* [78] investigated the effect of different substrates (stainless steel, stainless steel pre-treated with (PPCA), Polytetrafluoroethylene (PTFE), Diamond-Like Carbon (DLC), ceramic and polymer coated stainless steels and an isotropic super-finished stainless steel surface) on the ability to reduce scaling of calcium carbonate. The study showed that super-finished surfaces have most efficiency in terms of preventing scaling, whereas polymer and ceramic coatings performed worse both before and after erosion as illustrated in Figure 2-19. Also, different morphologies of crystals were observed with the different surface, which occurs as a result of the shape of asperities on the surface.

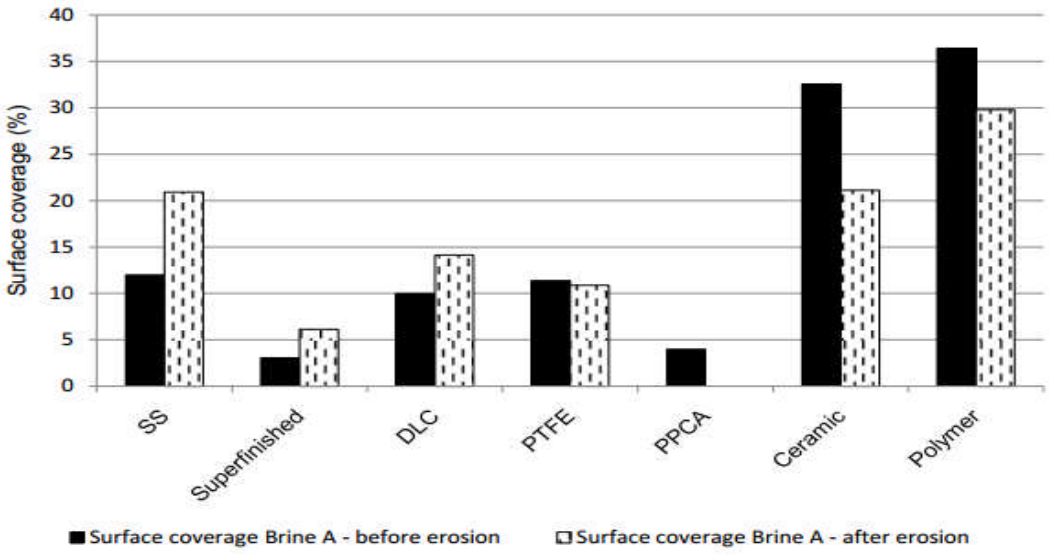

Figure 2-19: Surface coverage (%) formed from Brine A on the different surface before and after erosion [78]

In a research by MacAdam and Parsons [82], the effect of different materials (diamond-like carbon (DLC), PTFE, stainless steel (306a) and TiN3) and finishing on the deposition kinetics of calcium carbonate formation was investigated. It was observed that despite PTFE coating having the lowest surface free energy when compared to the other material; there was no reduction in scaling which is shown in Figure 2-20. While in the case of the DLC coating, it reduces the scale formation by 60%. Figure 2-21 shows the

effect of material roughness on scale rate; it could be seen that the scaling rate increases with increase in the level of roughness.

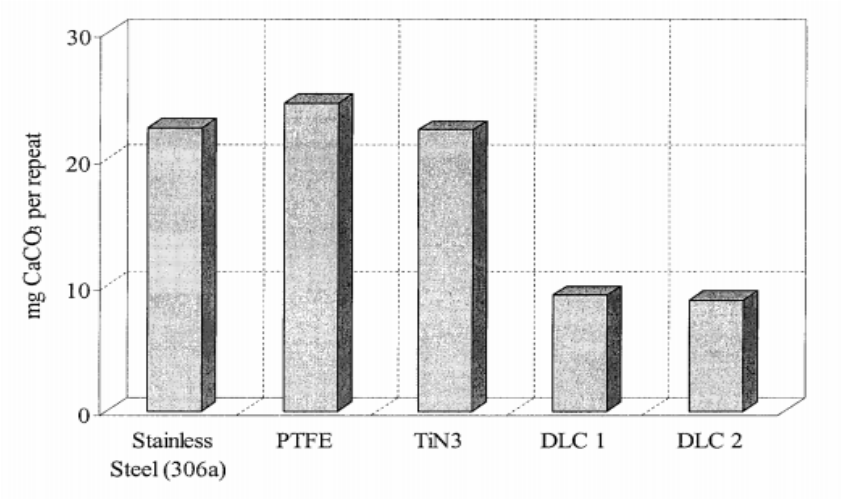

Figure 2-20. The effect of different coatings on $CaCO_3$ scaling rate (300 $mg.l^{-1}$ $CaCO_3$, 70^0C, 5 repeats) [82]

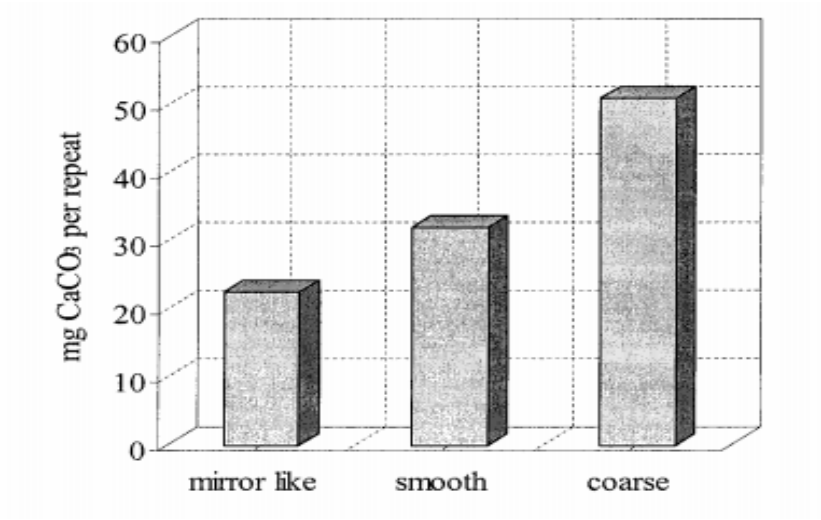

Figure 2-21. The effect of surface finish on $CaCO_3$ scaling rate (300 mg l^{-1} $CaCO_3$, 70˚C, 5 repeats) [82]

2.8.4 Damage removal

When the scale cannot be prevented during production, the scale needs to be removed. The scale can be removed chemically and mechanically or by the application of both methods when formed [48].

2.8.4.1 Chemical removal

In most cases, the use of chemical removal is preferable than mechanical removal since it is less expensive when compared to that of mechanical removal. This method involves the use of an acid such as hydrochloric acid for insoluble scales (calcium carbonate). But for barium sulphate which is soluble in acid, strong chelating agent such as an ethylene-diamine-tetra-acetic acid (EDTA) or diethylene-triamine-penta-acetic acid (DTPA) are normally used for their removal. The chelating agents are molecules that break up the scale by isolating and locking up metallic ions in solution within their closed ring-like structure [48]. A drawback to this method is that the effectiveness is affected by the surface to volume ratio of the scale.

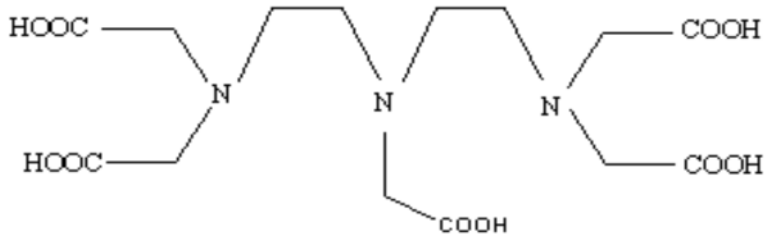

Figure 2-22: Diethylene-triamine-penta-acetic acid (DTPA) structure

2.8.4.2 Mechanical removal

They are different methods that could be applied to remove scale mechanically. They include explosive, milling, jet blasting just to mention a few. However, the various method applied depends on the type and location of scale formed. For instance, explosive and impact techniques are used for brittle scale, while jet blasting techniques are used to remove soft scale. A shortcoming of this technique is that it is expensive, difficult to perform and required to be repeated in a short period of time [83].

2.8.5 Chemical scale inhibitors

The most common and successful method used in the prevention of scales in the oil and gas industry is the use of scale inhibitors; when applied it prevents

the scale crystal from nucleating, growing and adhering to the solid surface. In the application of scale inhibitor for scale prevention and down-hole treatments in the oil and gas industry “squeeze treatment” is the desired method used [74, 84]. It involves the injection of scale inhibitors into the surrounding near-well reservoir, which is then further pushed into the reservoir by a brine over-flush; before the application of the main scale inhibitor, a pre-flush or spearhead is usually injected to prepare the rock surface for the scale inhibitor shown as illustrated in Figure 2-23. The well is then shut in for a particular time to allow the scale inhibitor to be phase separate or adsorb onto the rock. For a successfully squeeze treatment, it is required that the produced fluid contains a critical concentration needed to prevent scaling, which is also known as minimum inhibitor concentration (MIC). Therefore, the concentration of the inhibitor inside the wellbore has to be retained and maintained above the MIC, which then leaches slowly back into the produced-water protecting the well from scale damage.

In general, there are two retention mechanisms, which allow the scale inhibitor to be retained and released in the reservoir; precipitation and adsorption. The precipitation process is based on the formation of insoluble inhibitor/calcium salt in the formation pore space; which is achieved by adjusting the calcium ions concentration, inhibition concentration, pH and temperature [85]. On the other hand, the adsorption process occurs due to the van der Waals and electrostatic interaction between the inhibitor and formation minerals (rock); and the scale is absorbed from the solution to the formation minerals [85]. It is required that the chemical scale inhibitor provides long-term protection for the well formation and tubular. In addition, the scale should be compatible with the brine formation and relatively stable to thermal degradation under the well down-hole conditions.

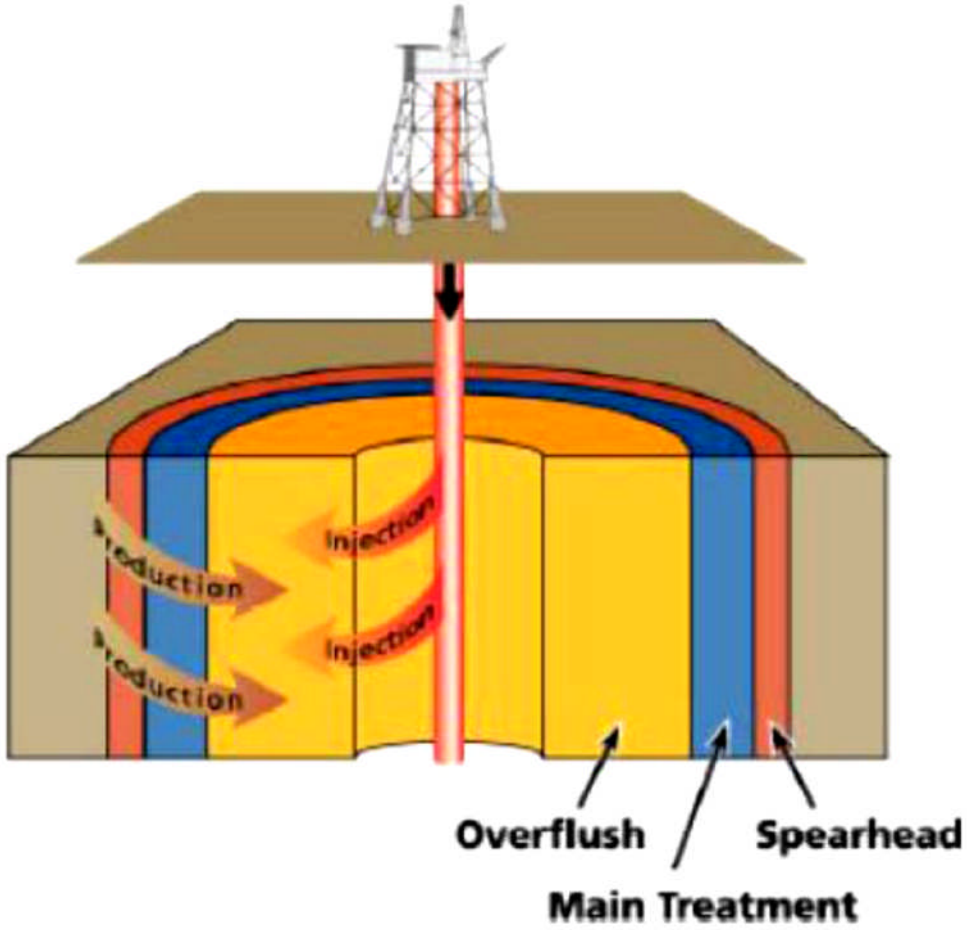

Figure 2-23: A schematic illustration of scale inhibitor squeeze treatment process [86]

2.9 Types of scale inhibitors

In the application of scale inhibitor in the oilfield, the main families of scale inhibitor are explained in this section.

2.9.1 Phosphonates

Phosphonates are substance that comprises of one or more group of C-PO $(OH)_2$. Their inhibition mechanism involves the prevention of crystal growth, making them less ineffective in the nucleation inhibition. Phosphonate scale inhibitors are widely used in the oil and gas industry due to high inhibition retention and high inhibitor efficiency [13, 14]; they are thermal/hydrolytically stable, making them very effective at a wide range of temperature down-hole

reservoir without breaking down into orthophosphate [87, 88]; their concentration in the formation water is easily detected [89]. Nevertheless, thermal ageing reduces their performance against sulphate scale [19].The widely used phosphonate is the diethylenetriamine penta methylphosphonic acid (DETPMP). Figure 2-24 shows the chemical structures of DETPMP.

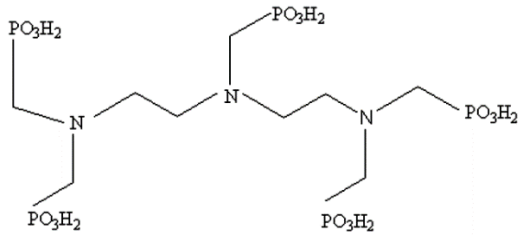

Figure 2-24: Diethylenetriamine penta methylphosphonic acid (DETPMP) structure

2.9.2 Polycarboxylic acid

Polycarboxylic acid is a generic name for compounds comprises of multiple carboxylic acid functional group (-COOH). The commonly used polycarboxylic acid used in the oil and gas industry is the polymalaic acid PMA and polyacrylate acid (PAA). The effectiveness of the polycarboxylic group depends on the relative molecular weight spacing and the number of carboxylic groups. On the reason that when they have same molecular weight, the more number of carboxyl on carbon chain and if the carboxyl group are gathered in high density. It reduces the freedom of adjacent carbon atom, which in turn increases the degree of association of alkaline-earth metal lattice; leading to increase in scale efficiency. In contrast, their efficiency is greatly affected by high temperature. Examples of polycarboxylic acid scale inhibitors are shown in Figure 2-25.

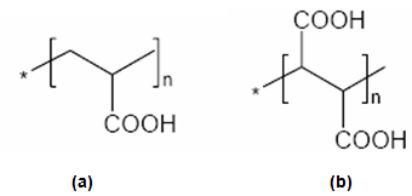

Figure 2-25: Structure of polymalaic acid (PMA) and polyacrylate acid (PAA)

2.9.3 Polyelectrolytes

These are polymers whose repeating unit produces an electrolyte group. Subsequently, the polymer contains at least one of the following groups: sulfonic acid (-SO_3H); ester (-COOR); carboxylic acid (-COOH), phosphonic acid (-PO_3H_2), acrylamide (-$CONH_2$). Due to the ability of this inhibitor having the properties of different groups, they could function as both for nucleation and crystal growth inhibition [90]. However, their efficiency is greatly affected by their molecular weight [28, 90]. Examples of polyelectrolytes are phosphonocarboxylic acid (POCA) and 2-Phosphono-butane-1, 2, 4-tricarboxylic acid (PBTC), Polyphosphinocarboxylic acid (PPCA), polyvinyl sulfonate and polyacrylic acid copolymer (PVS). The structures of each of the chemical inhibitors are shown in Figure 2-26.

The various chemical scale inhibitors have their different mechanism by which they function. The next section explains the various mechanisms exhibited by scale inhibitors.

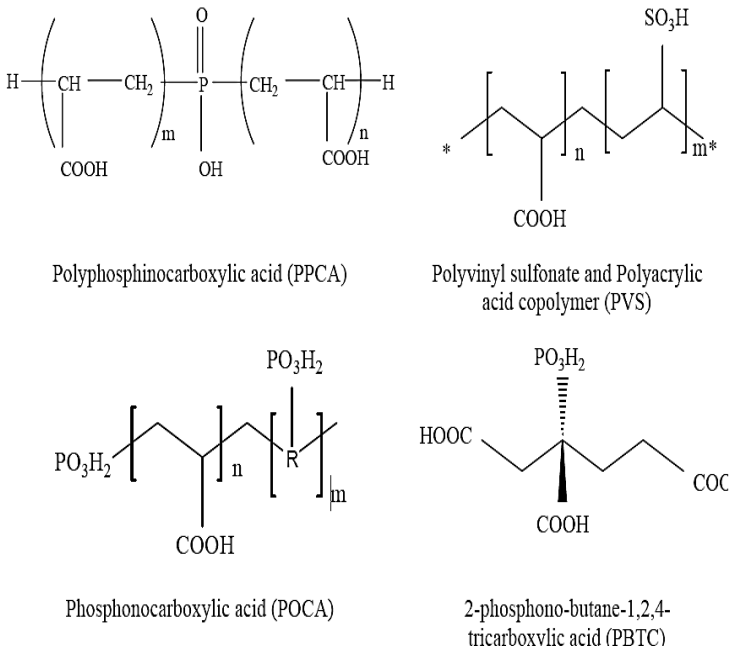

Figure 2-26: Schematic representation of polyelectrolytes used as scale inhibitors

2.10 Inhibition mechanism

As discussed in section 2.8.5 chemical scale inhibitors are the most cost-effective method for the prevention/mitigation of scale formation in the oil and gas industry. Each type of chemical inhibitor possesses its own mechanism by which it functions. Generally, they are three mechanism in which scale inhibitors typically works as illustrated in Figure 2-27.

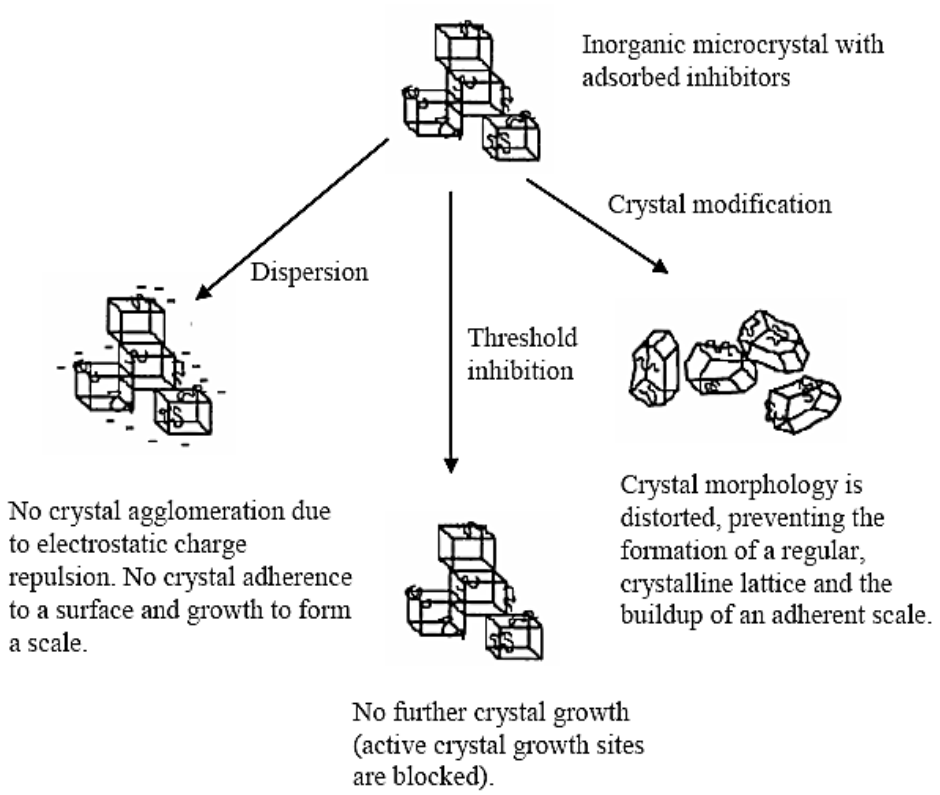

Figure 2-27: Three main inhibition mechanisms [38]

2.10.1 Threshold effect

This mechanism involves the prevention of crystal at the initial stage of nucleation. These chemicals tend to prevent the ion (Ba^{2+} and $S0_4^{2-}$) from aggregating together by promoting the formation of small crystals that act as a nucleation site but prevent crystal growth. Consequently, reducing the supersaturation of solution and preventing nucleation.

2.10.2 Crystal distortion/ modification

Crystal distortion involves the reduction of crystal growth by changing their morphology. This occurs by inhibitors being absorbed on the surface changing their properties. This tends to limit their sizes, preventing crystal agglomeration and surface deposition. Further, the modified shape usually has less contact forces to the surface, which can be swept away by the process flow.

2.10.3 Dispersion

Dispersion involves the prevention of microcrystal adsorption and agglomeration. This is achieved by inhibitors being absorbed onto the growing crystal, increasing the anionic on the crystal surface, by so doing increasing the electrostatic charge repulsion between crystals; resulting in the formation of a more stable dispersion of microcrystal.

2.11 Factor affecting inhibitor performance

In the application of scale inhibitors in the oilfield, the performance of scale inhibitors could be affected by two features: Structural and environmental features [91].

2.11.1 Structural features

The variation of chemicals could affect the scale inhibition performance. For instance, the presence of functional groups such as hydroxyl and sulphuric group is seen to enhance the inhibitor efficiency, while that of the hydrophobic group is seen to block the action of other functional groups in the scale inhibitor causing steric hindrance [92-95]. In addition, the location of functional group and the molecular weight distribution could also have a significant impact on the scale performance [92, 93]. According to Bromley *et al*. [96], it

was reported that the greatest inhibitors of barite growth occurs when the link between two sets of phosphonate group was greater than 6 Á and allow at least two of the four molecules to incorporated on the surface.

2.11.2 Environmental features

These features are associated with the change of environmental conditions in the reservoir and during the course of the squeeze treatment [11, 25, 85, 97, 98]; Some of these environmental changes are explained below.

2.11.3 Solution pH

It is generally understood that the scale inhibitor performance will be reduced below a certain pH level. This occurs for the reason that the efficiency of scale inhibitor depends on the functional groups being ionized in order to bind strongly with the scaling mineral lattice [91]. For illustration, phosphonate (DETPMP) and polyacrylate (PPCA) species are greatly affected by variation of pH because they are very weak; having less dissociated at low pH. In contrast, functional groups containing strong acid like sulphonic acid (-SO_3H) will completely dissociate to –SO_3: making them effective even at very low pH value [91]. In a study by Sorbie and Laing [67], they show the effect of variation of three inhibitors (DETPMP, PPCA and PVS). From Figure 2-28 and Figure 2-29, it is seen that both DETPMP and PPCA were unable to function at pH 2 since the performance of the inhibitor were low at 0.5 hours and 1 hour. On the contrary, the inhibitor performance of PVS was high at low pH level, with inhibition efficiency greater than 50%.

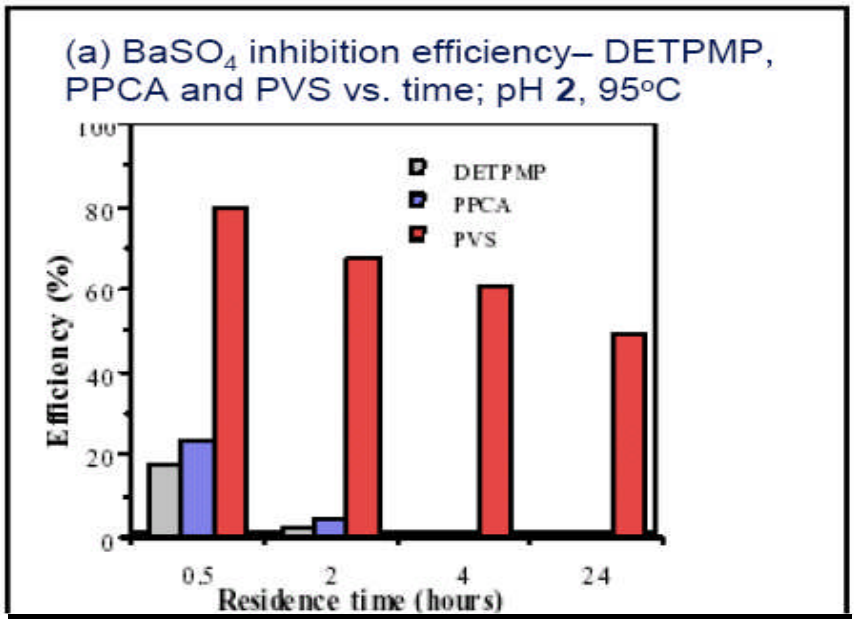

Figure 2-28: $BaSO_4$ inhibition efficiency at pH 2 for DETPMP, PPCA and PVS [68]

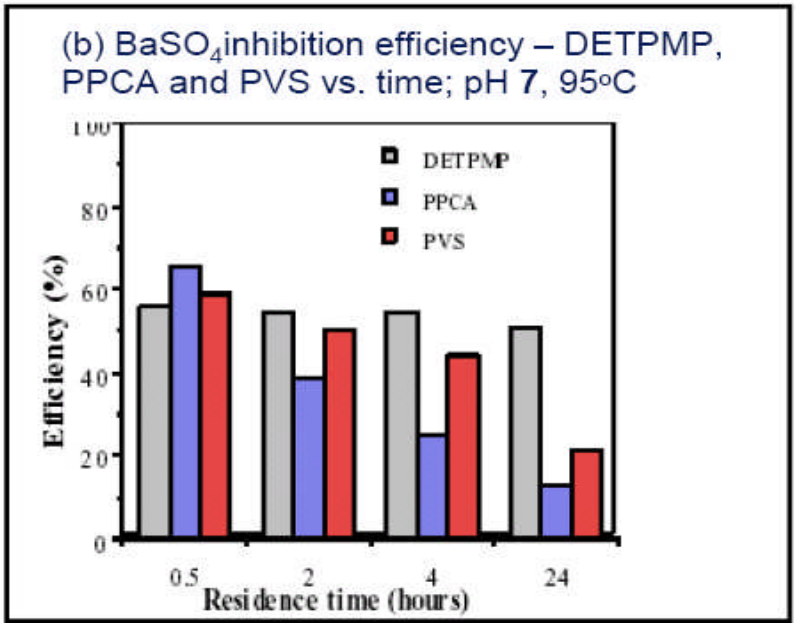

Figure 2-29: $BaSO_4$ inhibition efficiency at pH 7 for DETPMP, PPCA and PVS [68]

2.11.3.1 Temperature

The crystal inhibition is dominated by the thermodynamic properties of adsorption of inhibitors on the scale crystal (i.e. Free Energy (G_{ads})). On the other hand, free energy depends on the change in enthalpy and entropy as shown in the equation below.

$$\Delta G_{ads} = H_{ads} - T\Delta S_{ads} \quad 2\text{-}17$$

Therefore, it is anticipated that temperature will have a major impact on the effectiveness of an inhibitor. From literature, it was found that phosphonates are less effective at low temperature, whilst co-polymer and sulphonated polymer perform better at lower temperature [67, 99, 100]. The reason for phosphonate ability not to perform at a lower temperature is that since they function more as a crystal growth blocking and the barium sulphate supersaturation ratio is high at low temperature; it implies that more concentration of phosphonate will be needed to prevent scaling [99]. Conversely, the sulphonate polymer species have high performance at a lower temperature is because of reaction kinetics. At lower temperature barium sulphate saturation ratio is high, but the rate of formation is very low and knowing they function as nucleation inhibition it allows the inhibitor to act on scaling crystals [25, 67]. To emphasize this point, research carried out by Sorbie and Laing [67] identified the effect of temperature on inhibitors performance on three different inhibitors (DETPMP, PPCA, and PVS) using two scaling conditions (mild and severe). The study revealed that the performance of DETPMP was high at 95˚C, while that of PPCA and PVS were high at a low temperature of 5˚C and 50˚C as shown in Figure 2-30 and Figure 2-31.

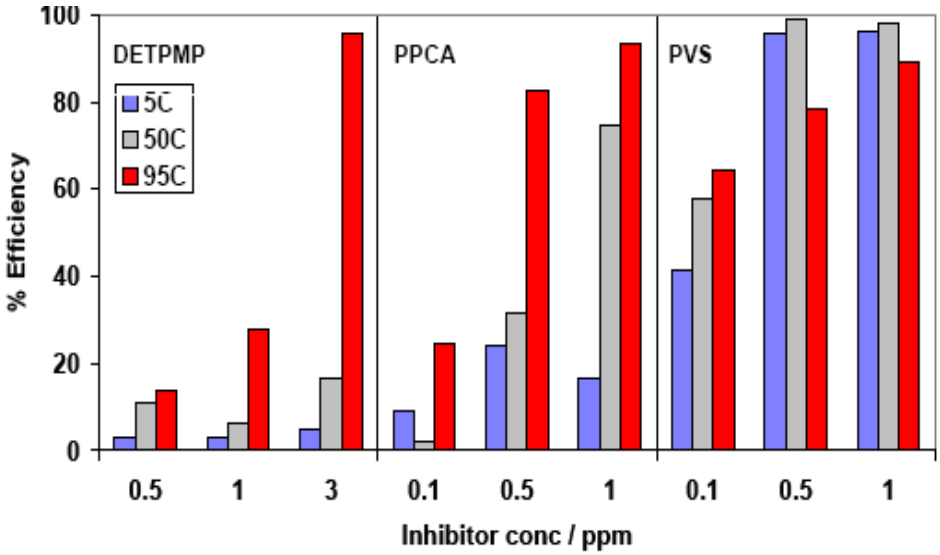

Figure 2-30: $BaSO_4$ inhibition efficiency of DETPMP, PVS and PPCA vs. Temp.; 50:50 Brent/SW brine mix after 22 hours [68]

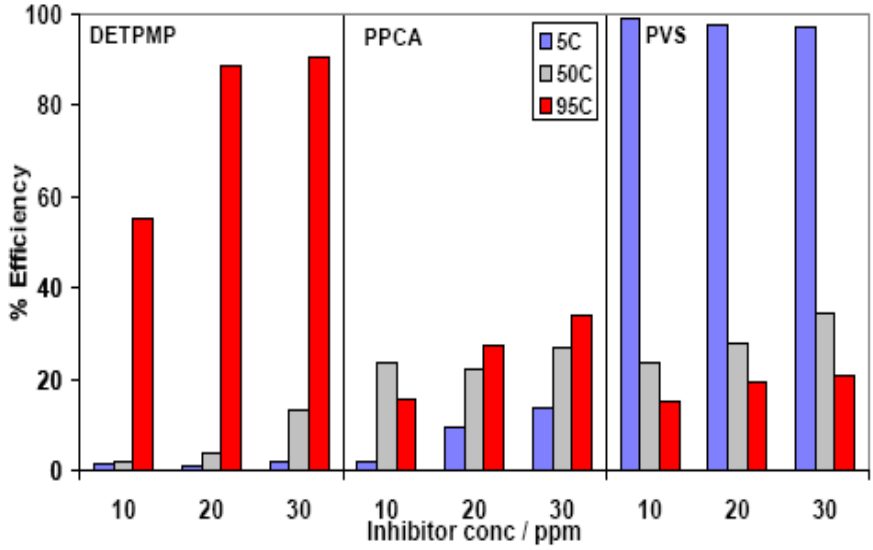

Figure 2-31: $BaSO_4$ inhibition efficiency of DETPMP, PVS and PPCA vs. Temp.; 50:50 Forties/SW brine mix after 22 hours [68]

2.11.3.2 Effect of Divalent Cation Concentration

The concentration of Ca^{2+} present in the injection and produced brine could affect the ability of scale inhibitor being retained in the formation through precipitation and adsorption [85]. This occurs through the influence of calcium

ions involved in the formation of surface/inhibitor complexes [21, 25, 26, 85, 97, 98]. Furthermore, the binding takes place by hydrogen bonding or calcium bridging between the surface or crystal and the functional group of the scale inhibitors depending on pH, temperature, and concentration of the inhibitors. In the presence of high concentration of calcium ions, phosphonate inhibitor tends to be very effective due to the formation of Ca^{2+}/ phosphonate complexes; on the other hand, polymers are not effective at a low concentration of calcium ions [67, 91]. Similarly, the presence of Mg^{2+} is known to poison scale inhibitors reducing their performance. Phosphonates are more affected by Mg^{2+} ion when compared to polymeric series. This reduction of the scale inhibitor occurs due to the fact that Mg^{2+}/inhibitor complexes are unable to be incorporated into the barite lattice unlike that of Ca^{2+}/inhibitor complexes as illustrated in Figure 2-32.

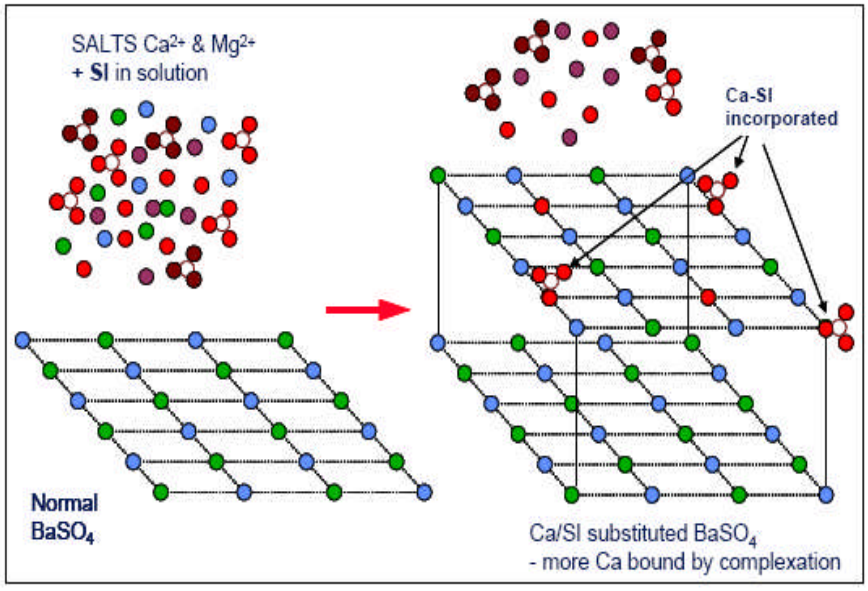

Figure 2-32: $BaSO_4$ growth with Ca-SI complex inclusion and Ca inclusion and no Mg-SI inclusion [68]

2.12 Bulk characterization

Conventionally, the study of scale formation has been focused on the bulk precipitation using static bulk jar test. The kinetics of scale formed in the bulk solution can be measured by the various techniques listed below:

2.12.1 Turbidity measurement

Turbidity is the measure of the degree of ‘cloudiness’ of a solution due to the presence of suspended particles in the solution. As the barium sulphate precipitate, the solution becomes cloudier. The turbidity meter measures the amount of light that is scattered by the suspended particles in the solution. Mavredaki [30] studied the kinetics of bulk phase during the initial stage of precipitation of barium sulphate in the presence and absence of scale inhibitors using a turbidity measurement. Tantayakom *et al*. [64], studied scale inhibition using a turbidity measurement; in their research, they found out that the critical supersaturation ratio increases with scale inhibitors concentration and solution pH, while it decreases with increase in elapsed time after mixing the precipitating solution.

2.12.2 Change in barium ion concentration

The change in concentration of barium ions in a solution due to precipitation of barium sulphate can be used to characterise the bulk precipitation process. The analysis of the concentration of barium ions in the solution after tests can be measured using an Inductively Coupled Plasma - Atomic Emission Spectroscopy (ICP-AES) [25, 101, 102]. Also, barium ion selective electrode can be used to measure the change in concentration of barium ions [103].

2.12.3 Conductivity measurement

Conductivity is the ability of a solution to carry electrical current. It is directly proportional to the ionic species and concentration present in solution. Hence, the concentration of barium ions can be measured with a conductivity meter. As the scaling process in the bulk solution occurs, the conductivity of the solution reduces. Jones *et al*. [69] used the conductivity techniques to monitor the effect of calcium ions on the precipitation of barium sulphate. In their study, they found that the solubility of barium sulphate was as a result of an increase in ionic strength of the solution. In another research by Jones *et al*. [104], they

studied the interaction of EDTA with barium sulphate by using conductivity measurement [104, 105].

2.13 Surface deposition characterization

In most research scale studies, the focus has been the precipitation processes in the bulk phase. Nevertheless, it has been reported that jar test does not correlate with plant information [106]. Also, studies have shown that the mechanisms and kinetics controlling bulk and surface deposition are different. During the last few decades focus has shifted to study the scaling on the metal substrate using various techniques. The next few paragraph below gives some techniques used in surface deposition studies.

Pina *et al*. [107] studied the effect of five different phosphonate scale inhibitors on barium sulphate (001) face using in-situ AFM techniques. In their research, they found that the techniques provided both quantitative and qualitative data about the inhibition growth of barium sulphate (001) face.

Teng *et al*. [108] investigated the kinetics of calcium carbonate growth rate using *in-situ* AFM techniques. From their studies, they observed that at low supersaturation, the growth is initiated solely by surface imperfections, while as the supersaturation increases the two-dimensional surface nucleation and crystal defects become dominate which is consistent with the prediction of classical BCF theories. Ruiz *et al*. [109] investigated the effect of copolymer inhibitor on barium sulphate precipitation using an *in-situ* AFM. From their study, AFM techniques show to be a good tool to investigate scale formation and inhibition.

Abdel-Aal *et al*. [110] investigated the scaling of calcium carbonate by combining Ca^{2+} ion measurements with QCM techniques. They found that the scaling process occurs mainly by direct growth of calcite on the surface of the metal at high supersaturation, while at low supersaturation ratio leaf-like vaterite is adhered to the surface. Also, they found that the rate and amount of scale formed were affected by the inclination angle of the surface to the solution and the stirring rate. Garcia *et al*. [111] investigated the efficiency of

three different scale inhibitors and the scaling process using the QCM. From their study, they concluded that the QCM was an effective tool to evaluate the scale formation and inhibition process.

Hennessy *et al*. [68] used an *in-situ* pressure flow cell to study the formation of barite under a non-ambient condition with Synchrotron X-Ray Diffraction. According to their investigation, the precipitation of barite was successfully monitored using realistic oilfield information. Moreover, they suggested that the technique will be useful for oilfield application to understand the effect of the scale-inhibition mechanism. Chen *et al.* [112] developed an *in-situ* cell to study the formation of calcium carbonate and effect of scale inhibitor (PPCA) on crystal growth by using synchrotron radiation wide-angle X-ray scattering (WAXS). It was found that scale deposition on the surface is divided into two phase (unstable and stable phase). In addition, it was reported that the inhibitor reduces surface deposition by suppressing calcite formation, resulting in vaterite-dominated scale.

In a study by Quddus and Allam [113], Rotating Cylinder Electrode (RCE) apparatus was used to determine the effect of fluid hydrodynamic on barite formation. According to their study, the scale deposition rate increased with respect to increase in the Reynolds number. And they further suggest since the hydrodynamic plays a role in scale formation process, it must be considered in any part of the scale management system.

A new method was developed by Euvrard *et al*. [114] in order to visualize and monitor the kinetics of calcium carbonate scale in real time, the set-up comprises of an electrochemical cell coupled with a video set-up. A schematic illustration of the flow cell is shown in Figure 2-33.The system was able to quantify in real time the morphometric characteristic of the crystal and also enable the continuous study of nucleation and growth of crystal.

In a similar research, Martinod *et al.* [105] studied the effect of a conventional phosphorus scale inhibitor (polyphosphinocarboxylic acid (PPCA) and two environmentally friendly inhibitors (polymaleic acid (PMA) and carboxymethyl inulin (CMI)) on calcium carbonate using an electrochemical cell, optical and measurement set-up. During the study, different mechanisms were observed,

which depended on when the inhibitors were applied during the crystallization process. PPCA and PMA tend to inhibit the growth of crystal, however PPCA had higher efficiency when compared to PMA. In contrast, CMI seems to have no significant effect on the kinetics of crystal regardless of when it been applied; Figure 2-34 gives a pictorial explanation of the effect of the three scale inhibitors.

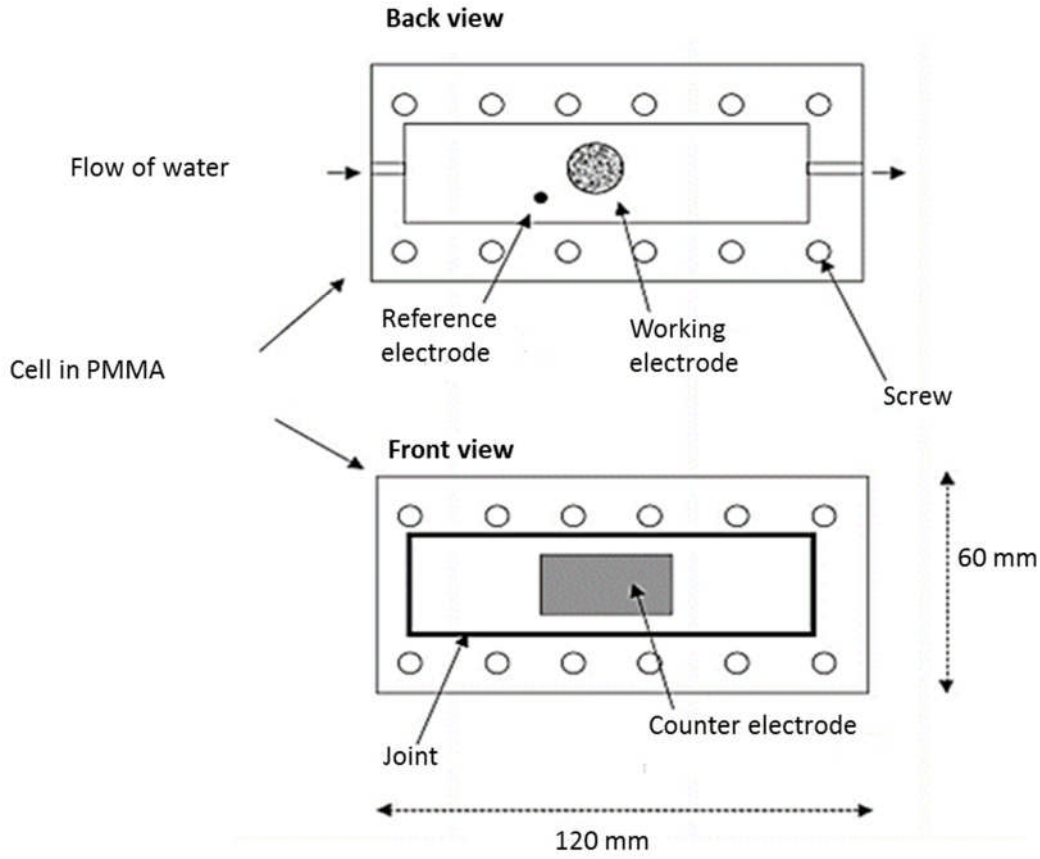

Figure 2-33: Electrochemical cell [101]

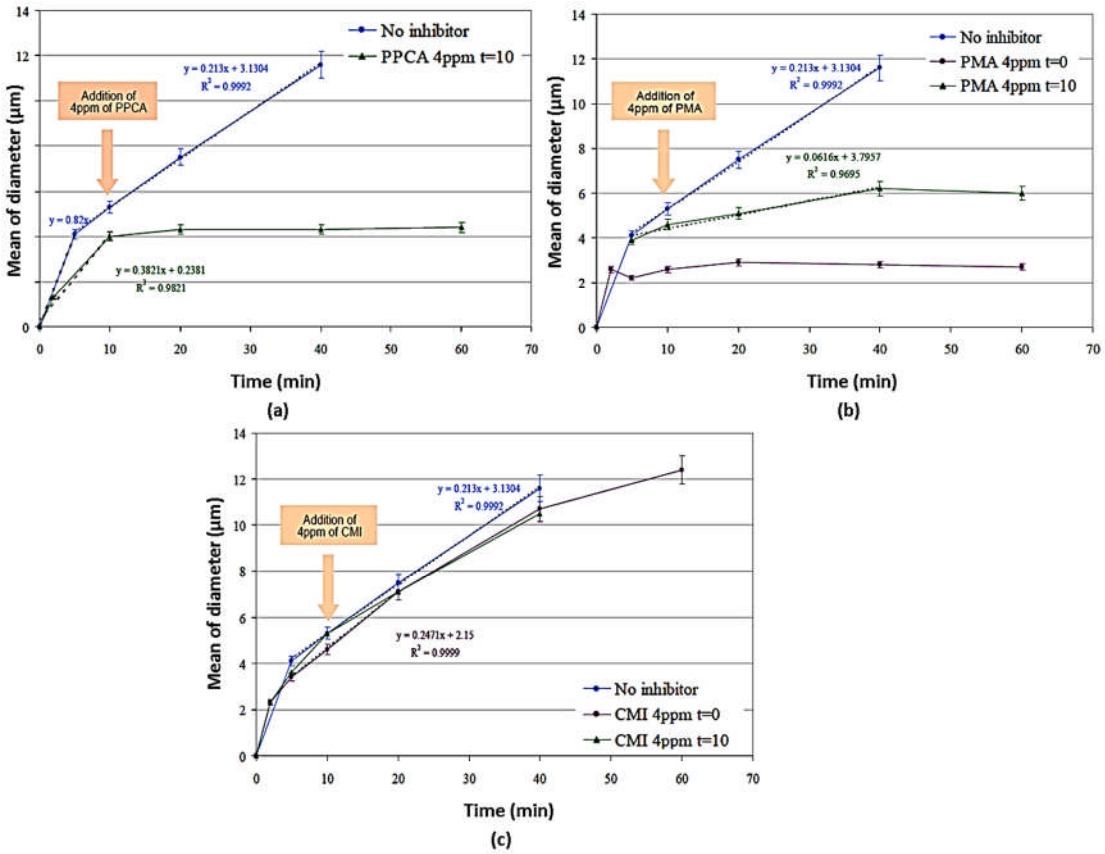

Figure 2-34: (a) Effect of 4ppm of PPCA on the mean diameter of the crystals of $CaCO_3$ nucleated and grown for 10 minutes in absence of inhibitors (b) Effect of 4ppm of PMA on the mean diameter of the crystals of $CaCO_3$ nucleated and grown for 10 minutes in absence of inhibitors (c) Effect of 4ppm of CMI on the mean diameter of the crystals of $CaCO_3$ nucleated and grown for 10 minutes in absence of inhibitors [101]

2.14 Bulk precipitation vs surface deposition kinetics

Ever since the application of scale inhibitors to prevent precipitation of scale, it has been assumed that scale chemical functions same way in the bulk solution and on surfaces of the substrate. As discussed in section 2.14, the studies of scale formation using traditional beaker/jar test do not give reliable information. Also, it has been shown that there are extensive dissimilarities between scaling rate estimated by predictive model (i.e. based on scaling indices and thermodynamic to predict precipitation tendency) and actual

deposition on the component surface. However, research on the relationship between the scale deposition on a solid surface and bulk precipitation has been carried out by few researchers [32, 101, 113, 115, 116].

Graham *et al*. [101] compared the efficiency of scale inhibitor (PPCA) in preventing bulk precipitation and surface deposition of $BaSO_4$ at different temperature (5°C, 50°C and 95°C) and inhibitor concentration (below and above MIC). From their investigation, they summarise their main findings with a schematic diagram shown in Figure 2-35. Regarding the inhibited experiment, they observed bulk precipitation and surface deposition was greatly reduced at a concentration above-MIC. Furthermore, at a concentration below-MIC bulk precipitation was reduced but enhanced surface deposition. It was postulated that the promotion of surface deposition (below-MIC), was due to low film coverage of the scale inhibitor on the metallic sample, as well as, a high concentration of barium ions in the bulk solution. In the uninhibited case, an opposite trend was observed. Low surface deposit of barium sulphate was formed on the metallic steel compared to bulk precipitation. This was attributed to high supersaturation of the brine, resulting in fast precipitate of barium sulphate in the bulk solution rather than depositing on the metallic surface.

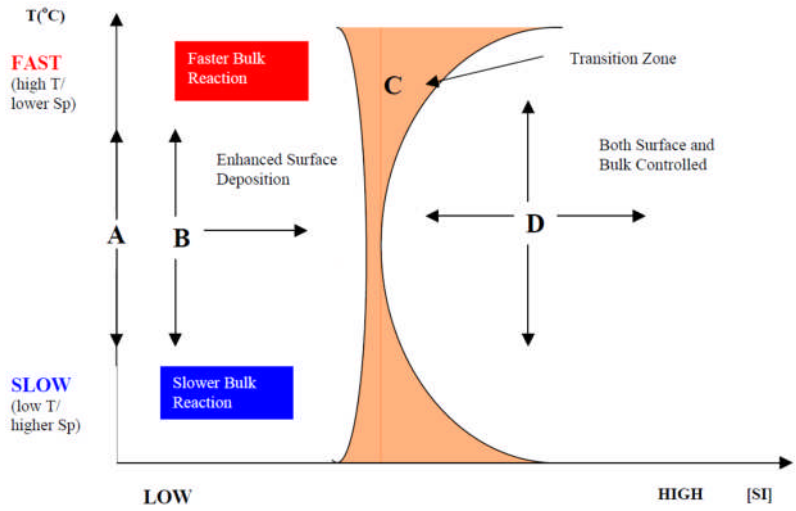

Figure 2-35: Schematic diagram illustrating the surface scaling and bulk precipitation according to inhibitor concentration and temperature

A study conducted by Chen *et al.* [29] to investigate the initial stages of bulk precipitation and surface deposition of calcium carbonate, using three different brine solutions having different saturation ratio. From their research, they were able to validate that the induction time for both bulk precipitation and surface deposition are different; surface deposition tends to occur sooner when compared to bulk precipitation at low supersaturation ratio. Also, in their studies the size of crystals formed in both processes was different. In the bulk solution, the size of the crystal was 5 micron, while that of the surface deposition was 10-20 micron shown in Figure 2-36. This confirmed that heterogeneous condition promotes crystal growth when related to the homogeneous condition.

In similar research by Mavredaki [30], the study of the initial stages of barium sulphate scale formation was investigated, using QCM for surface deposition measurement; while turbidity measurement was used to characterise the bulk solution. From the studies, when comparing the bulk precipitation and surface deposition, she found that the kinetics of surface precipitation was different from bulk phase. As shown in Figure 2-37 the mixture of B and C reached a plateau but the scaling activities on the surface still continue. In conclusion, from the two studies, it implies that both processes (bulk precipitation and surface deposition) have different kinetics.

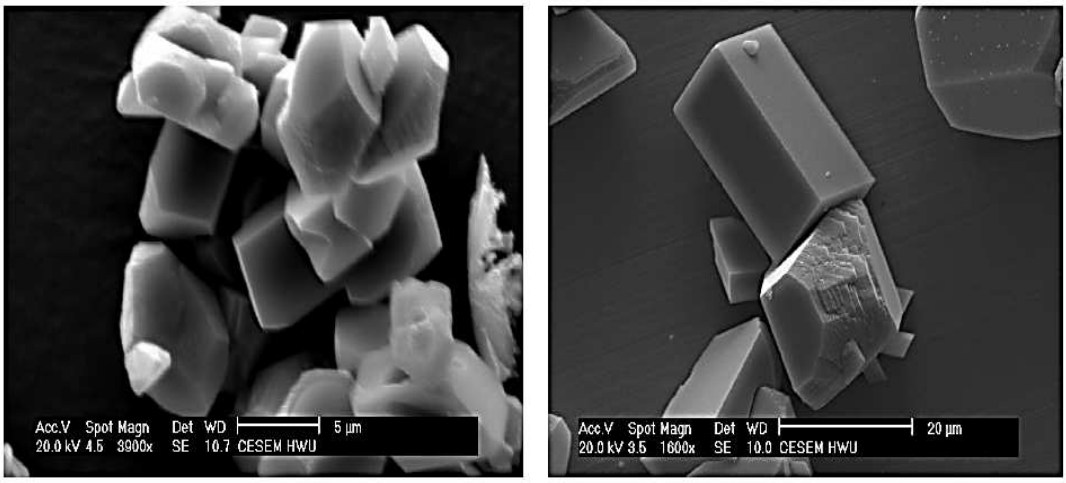

Figure 2-36 Comparison of morphology of bulk precipitate and surface deposit after 24 hours (a) bulk precipitate (b) surface deposit [25]

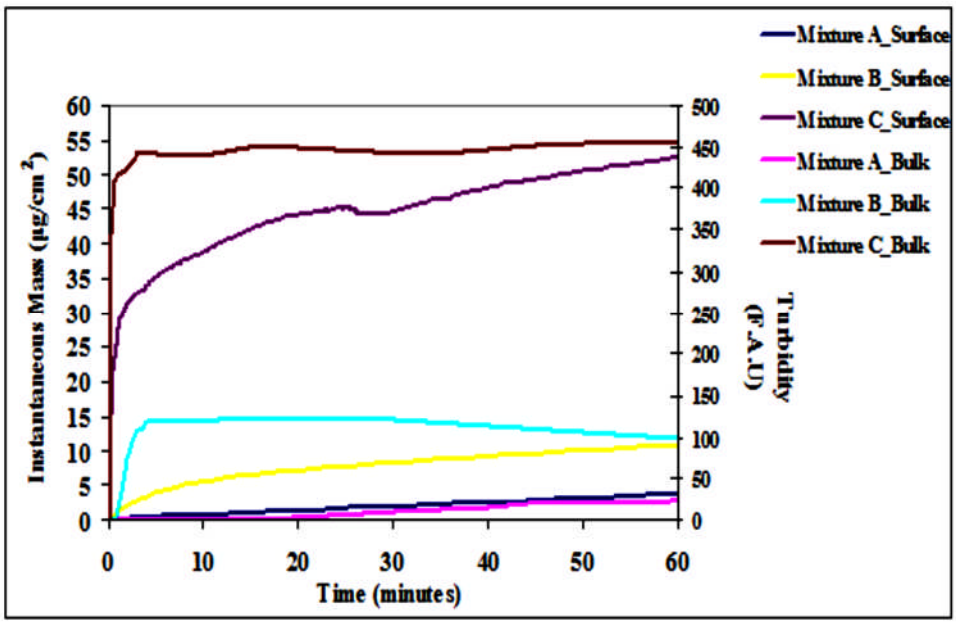

Figure 2-37 Surface and bulk measurements for the three different brines focusing on the lower scale measurements [91]

2.15 Summary of literature review

From the review presented in this chapter, it is clear that the mechanisms of barite scale formation are a complex and are affected by various factors. The most effective method to prevent the occurrence of barite scale in the oilfield is the application of chemical scale inhibitors. These scale inhibitors are generally used in squeeze treatments because of the various benefits mentioned during the review. Also, the determination of the scale inhibition mechanisms is challenging since scale inhibitors are being affected by various factors. The effects of these factors have been studied by various researchers considering only the bulk precipitation (primary homogeneous nucleation) rather than the surface deposition and growth (primary heterogeneous nucleation) [32, 38, 101]. On the contrary, studies have shown that the kinetics of both bulk precipitation and surface deposition are different [30]. Therefore, it is important for studies to be carried out to investigate these factors under more realistic simulated oilfield conditions in the laboratory: considering both the influence of both bulk precipitation and surface deposition.

In recent times, *in-situ* visualization methods have been used to study scale formation kinetics on surfaces; most studies have been carried out in a closed system [58, 117]. There is a serious limitation of this if the intention is to quantify the scale kinetics as a function of the saturation ratio seen by the surface. For this reason, *in-situ* visualization methods in an open system were developed and used to study the kinetics of barium sulphate scale and mechanism of scale inhibitor action on both bulk precipitation and surface deposition. This gives a more realistic simulation of the oil field processes when compared to a closed system.

In addition, in terms of preventing the formation of scale by using modified substrates, the use of these surfaces from the reviews has shown to significantly reduce the amount of scale formed. Furthermore, these studies were carried out in the aqueous phase, but oilfield operations barely occur in the aqueous phase. Surface scaling tests on multiphase environment have not been conducted. In this study of scaling tests were conducted both in the aqueous phase and multiphase environment.

This study is aimed at improving the understanding of the kinetics of barium sulphate precipitation in the bulk solution and deposition on the surface with and without the influence of scale inhibitors. Also, it will improve the understanding of how different conditions (such as flow rate, pre-scaled surface and saturation ratio) can affect the surface scale inhibition. Lastly, it will expand the knowledge of how the presence of oil phase could influence the surface scaling and inhibition of barium sulphate. The next chapter presents the experimental techniques and procedures that were used during the study.

Chapter 3 Methodology

3.1 Introduction

In order to understand the processes of bulk precipitation and surface deposition of barium sulphate and their interactions, several methodologies are required. In this chapter, the various test setups, experimental procedures and materials used to achieve the thesis objectives mentioned in chapter 1 are described. The schematic diagram in Figure 3-1 shows the structure of the chapter.

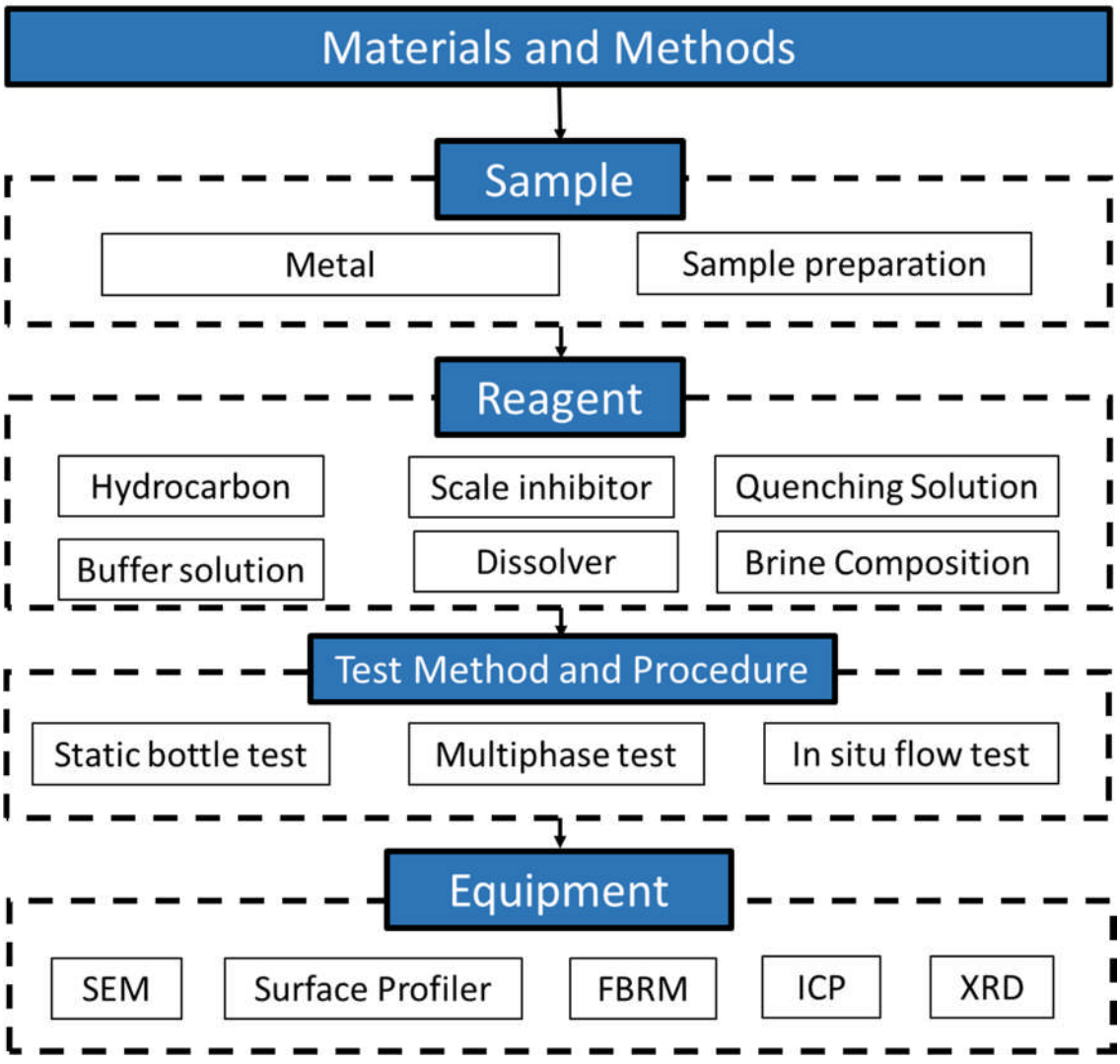

Figure 3-1: Outline of chapter 3

3.2 Metal sample

The substrate used for surface fouling is stainless steel UNS S31603. The composition of the stainless steel material is presented in Table 3-1. This material is chosen due to its high resistance to corrosion in a wide range of pH values.

Table 3-1: Composition of the stainless steel [118]

Composition	Percentage by weight
Carbon	0.030
Manganese	2.00
Silicon	0.75
Chromium	16.00-18.00
Nickel	10.00-14.00
Molybdenum	2.00-3.00
Phosphorus	0.045
Sulphur	0.030
Nitrogen	0.10
Iron	7.0

3.2.1 Sample preparation

Two different geometries of stainless steel samples were used during the project as shown in Figure 3-2. The first sample (hollow cylindrical sample) with a diameter (12 mm), which was used for to study surface scaling in multiphase condition did not require any preparation prior to the test. The second sample (10 mm diameter) required some preparation before the test. The sample preparation was divided into three steps (namely: grinding,

polishing and cleaning). First, the samples were mounted in epoxy resin. The next step which is grinding and polishing were carried out on the manual polishing machine (Buehler Beta Grid Polisher).

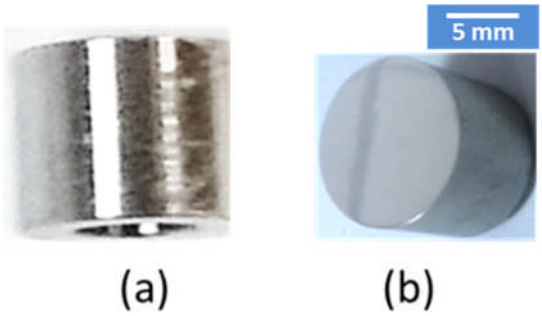

Figure 3-2: (a) Rotating cylinder electrode (RCE) sample (scale forms on the cylinder surface) (b) *In-situ* test sample (scale forms on the flat surface).

Grinding was performed using diamond bonded discs (MetPrep), while the polishing steps were done with polishing cloths (MicroCloth, Buehler) and diamond suspensions (3 µm). In the grinding process, the samples were wet-ground progressively using P300, P600 and P1200. During this process, samples are cleaned in between each step with deionized water then dried with compressed air. Final cleaning followed by rinsing with deionized water, acetone was used before and after each polishing step.

3.3 Reagents

3.3.1 Brine composition

The mixture of two incompatible brines provides the supersaturation conditions for the precipitation of barium sulphate formation. In this study, the North Sea seawater (NSSW) which is the source of sulphate ions (SO_4^{2-}) and Forties Formation Water (FW) which is the source of barium ions (Ba^{2+}) are used during the experiment. During the project, the brine composition was varied in each of the results chapters. The concentration of the salts was adjusted to reach a specific saturation ratio (SR). Hence, the exact brine

composition is given in the respective results chapters. The $BaSO_4$ saturation ratios (SR) for various ratios were predicted using Multiscale Software. Table 3-2 presents an overview of the inorganic salts used during the making of the brines.

Table 3-2: Inorganic salts for the brines

NSSW	FW
NaCl	NaCl
$CaCl_2.6H_2O$	$CaCl_2.6H_2O$
$MgCl_2.6H_2O$	$MgCl_2.6H_2O$
KCl	KCl
-	$BaCl_2.2H_2O$
-	$SrCl_2.6H_2O$
Na_2SO_4	-

3.3.2 Chemical inhibitors

Three scale inhibitors were selected to examine their performance on the surface deposition and bulk precipitation of barium sulphate on stainless steel. These scale inhibitors are commonly used in the oil and gas industries. The first applied was Diethylenediamine Penta MethylenePhosphonic Acid (DETPMP) with an active concentration of 45 % and molecular weight of 573 g/mol was supplied by Italmach chemicals. The second scale inhibitor used was VinylSulphonate Acrylic Acid Co-Polymer (VS-Co) with an active concentration of 60% was provided by Nalco Champion. Lastly, PolyPhosphinoCarboxylic Acid (PPCA) with an active concentration of 47 % and molecular weight of 3600 g/mol supplied by BWA was applied. The structures of each of the chemical inhibitors are presented in Figure 3-3 to Figure 3-5 respectively.

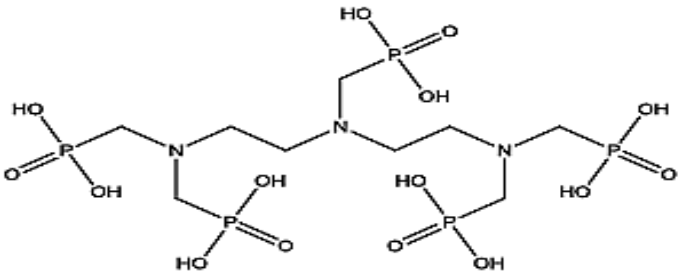

Figure 3-3: Chemical structure of DETPMP

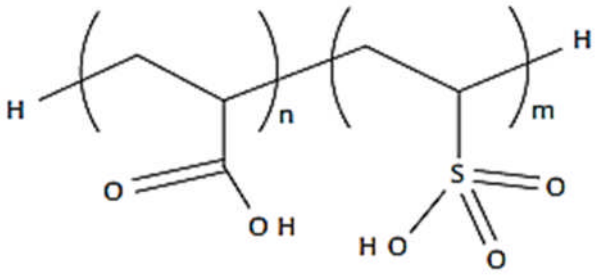

Figure 3-4: Chemical structure of VS-Co

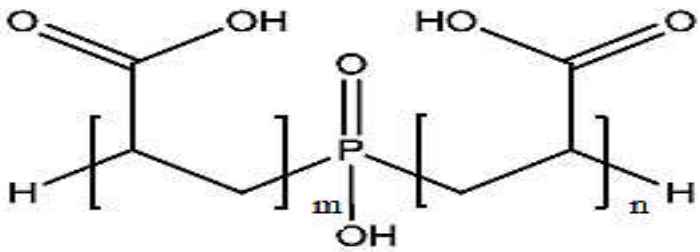

Figure 3-5: Chemical structure of PPCA

3.3.3 Buffer solution

A 10% v/v of a buffer solution was added to the brine solution to adjust the pH value of the solution to 5.5. The buffer solution was prepared by dissolving 34g of sodium acetate tri-hydrate and 1g of acetic acid in 250ml of distilled water.

3.3.4 Quenching solution

Quenching solution samples were used to stop further precipitating of scale during sampling. The solution consists of 1000 ppm of polyvinyl sulphonate (PVS) and 3000 ppm of potassium chloride (KCl) which is adjusted to pH 8-8.5 by dropping of 0.1N NaOH and/or 10% HCl.

3.3.5 Dissolver solution

In order to analyse the surface deposition of scale on the metallic steel, the sample was dissolved in a solution containing 25g of Ethylene-diamine-tetra-acetic acid (EDTA) and 25g of potassium hydroxide (KOH) in 500 ml of distilled water giving a pH of approximately 11.

3.3.6 Hydrocarbon

The hydrocarbon used in this study under multiphase conditions was Isopar M. It is a high-purity iso-paraffinic hydrocarbon having carbon number ranging from C_{11} to C_{16} and was supplied by VWR. The chemical properties of Isopar M are shown in Table 3-3.

Table 3-3: Chemical properties of Isopar M

Property	
Max. sulphur content (mg/kg)	1
Max. carbonyl content (mg/kg)	10
Max. aromatic content (mg/kg)	500
Density at 25 ºC (kg/dm3)	0.7771
Viscosity at 25 ºC (mPas)	2.08

3.4 Test set-up

In the course of this project, three different set-ups were used to study the kinetics of bulk precipitation, surface deposition and the performance of scale inhibitors. They are described below:

3.4.1 Static bulk jar tests

This test was used to determine the performance of scale inhibitor (SI) [119]. The experiment consists of scaling brines, which are mixed in 250 ml bottles. The $BaSO_4$ precipitation was then followed by measuring the concentration of barium as a function of time (t) and the efficiency of the inhibitor is calculated by using Equation 3-1;

$$I.E = 100\left[\frac{C(t) - C_b(t)}{C_0 - C_b(t)}\right] \quad \text{3-1}$$

Where,

C (t) = test sample Ba^{2+} concentration at sampling time, (ppm)

$C_b(t)$ = Ba^{2+} concentration in the blank solution (no scale inhibitor) and

C_O = control sample Ba^{2+} concentration at time, t = 0 (ppm).

When the scale inhibitor has an inhibition efficiency of above 95% at both 2 and 22 hours residence time, the concentration is referred to as the “minimum inhibitor concentration (MIC)”.

3.4.2 Rotating Cylinder Electrode (RCE)

The RCE set-up allows the study of the effect of flow condition on surface fouling. This set-up was used to perform a test on single and multiphase condition. The RCE consist of a rotating electrode module and a control unit

which allows perfect regulation of the rotating velocity. The electrode is made of insulating material with the metallic cylindrical stainless steel sample that revolves within the shaft.

The RCE electrode, temperature probe and an overhead stirrer are placed in a 2 L beaker as shown in Figure 3-6. The beaker is placed on a hot plate that is incorporated with a thermometer thermostat which ensures the solution temperature remains constant during the tests. Prior to the test, the temperature probe is placed inside a Hastelloy tube containing a heating fluid to prevent deposition of scale on the temperature probe; thus reducing possible errors during experiments.

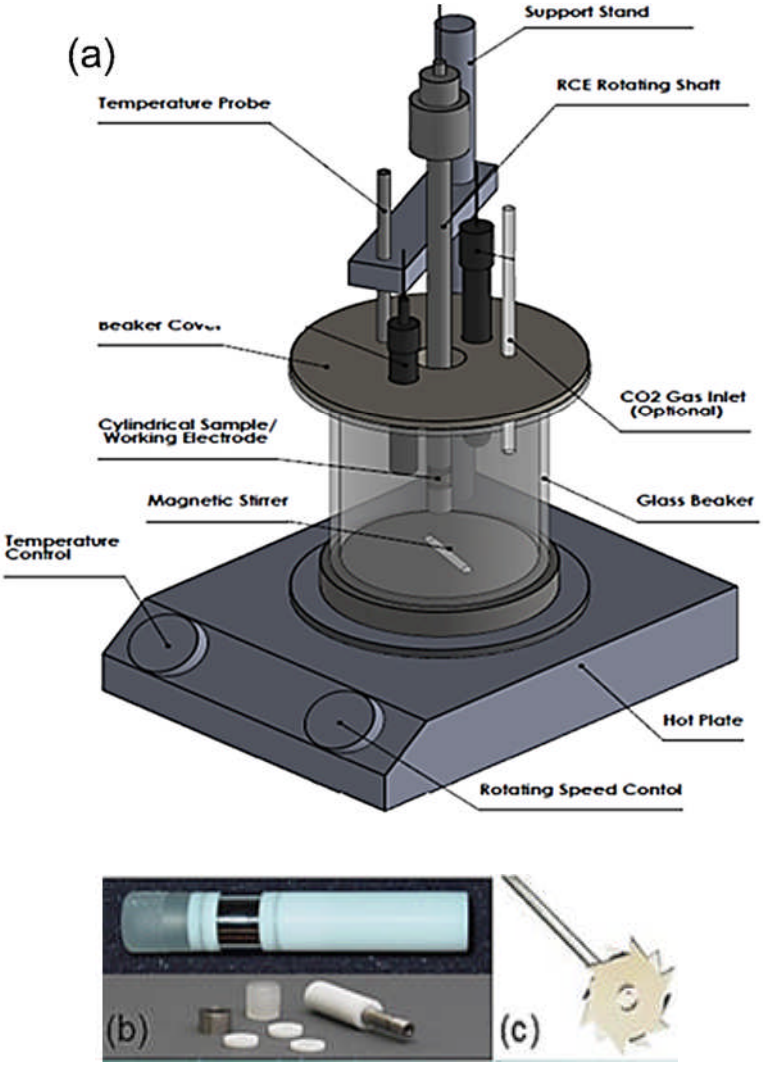

Figure 3-6: (a) Schematic diagram of rotating cylinder electrode (RCE) device (b) RCE electrode unit with metallic cylinder samples (c) stirrer

3.4.3 *In-situ* flow test

In the *in-situ* flow test, both surface deposition and bulk precipitation are studied under laminar conditions. The set-up includes an *in-situ* flow cell, pump, water bath, turbidity probe, camera, and conductivity meter as shown in Figure 3-7.

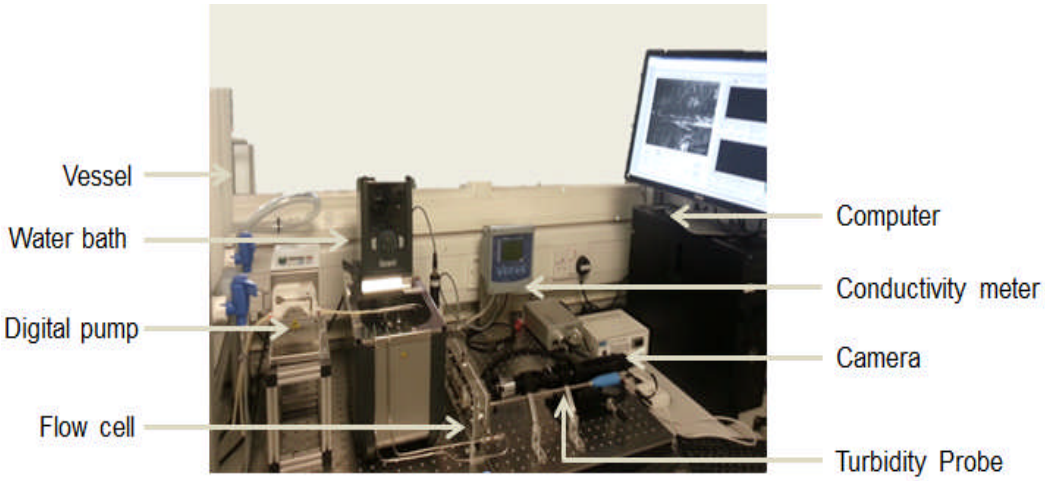

Figure 3-7: *In situ* flow cell set-up

A schematic illustration of the set-up is shown in Figure 3-8. The set-up allowed surface fouling and bulk precipitation to be assessed simultaneously. The design is inspired from the cell developed by Euvrard *et al.* [114]. In the initial setup the brines are recirculated (closed system), whereby the saturation ratio would decrease with time; therefore restricting kinetic studies to short periods of time. In this work, the set-up was adjusted to include a once-through flow system (open system) [120]. The flow cell was designed to work under atmospheric pressure and can be adjusted to allow experimental conditions (e.g. saturation ratio, inhibitor concentration) to be kept constant at the point where the imaging is done.

A more detailed geometry of the flow cell (cell volume of 15 ml) where the surface deposition occurs is shown in Figure 3-9. Prior to the design of the flow cell, a CFD modelling was conducted using COMSOL to evaluate the flow velocity across the cell. From Figure 3-10, results show that the flow in the cell is uniform and the maximum Reynold number for each of the flow rates used

during the test were laminar flow regimes as shown in Table 3-4. Also, it was observed that there was no recirculation in the flow cell. The flow regime of other two flow rates used are presented in Appendix A. The surface deposition was analysed using a camera (produced by Ximea) to allow real-time observation of surface fouling.

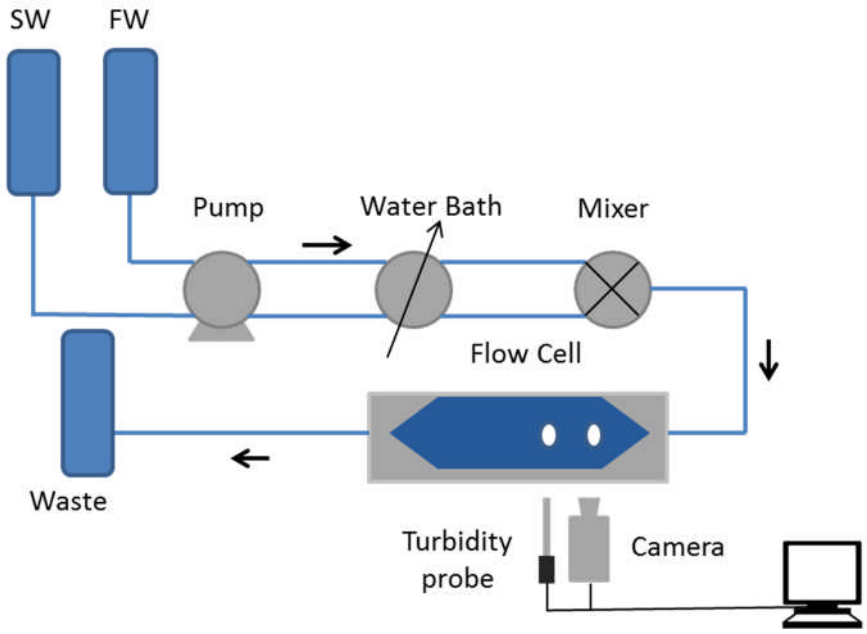

Figure 3-8: Schematic of experimental set-up

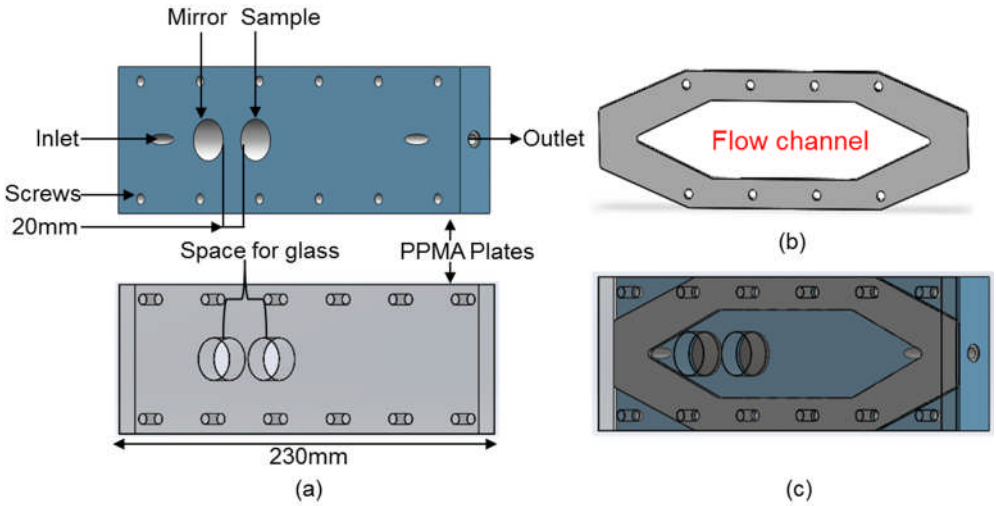

Figure 3-9: Flow cell consists of: (a) two PPMA plates and (b) a Teflon gasket with volume of 15 ml. (c) Assembly of the three different parts

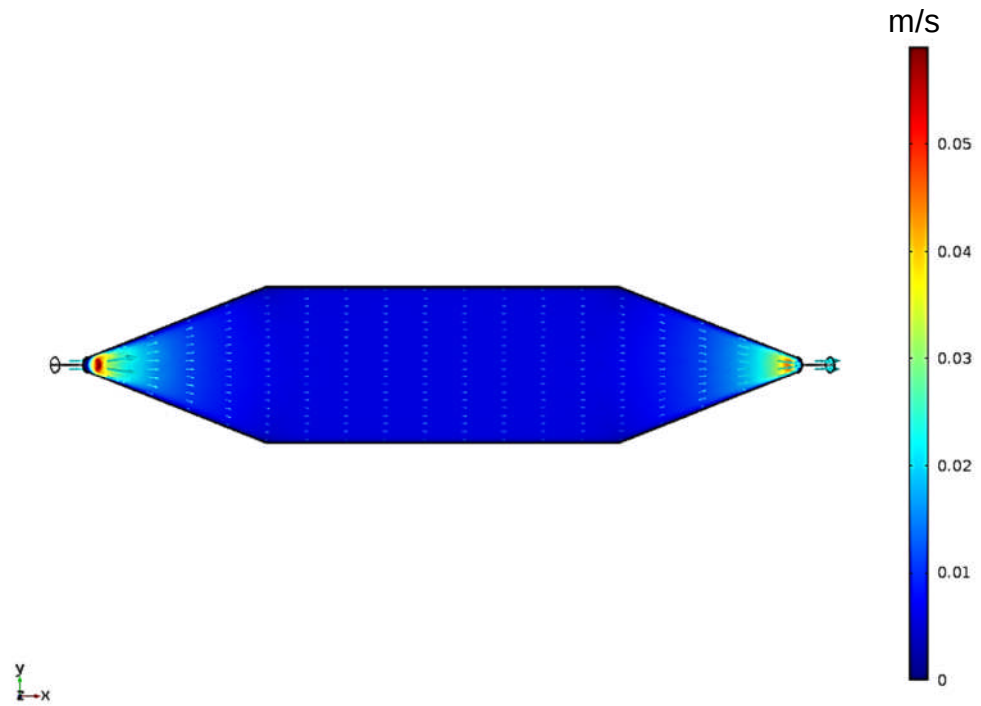

Figure 3-10: CFD modelling of flow channel showing the flow velocity of the cell (flow rate of 20ml/min).

Table 3-4: Hydrodynamic parameters

Flowrate (ml/min)	Flowrate (m/s)	Average velocity at centre m/s	Maximum Reynolds number
20	3.34×10^{-7}	0.0032	7
40	6.67×10^{-7}	0.0127	15
60	7.02×10^{-7}	0.0187	23

The images were processed to assess the number of particles and their size as well as the barium sulphate surface coverage. Similarly, real-time measurements of the bulk precipitation were performed using a turbidity probe. As the scaling process occurs, the solution becomes more turbid during the initial stages of precipitation of barium sulphate. The induction time and the kinetics of the reaction can be followed. Figure 3-11 shows a schematic illustration of a typical turbidity curve, showing the three regimes (namely: (a)

induction time, (b) crystal growth, and (c) further growth and agglomeration). The turbidity probe consists of a steel fibre optic probe placed in front of the flow cell. The turbidity probe consists of two optical fibres: the first optical fibre emitted light into the flow cell, while the second optical fibre transmits the responding scattered light reflected by the mirror place behind the flow channel as shown in Figure 3-12.

Bulk precipitation is detected when the light transmitted is reduced due to disruption of reflected light initiated by the formation of crystals in the bulk solution. The change in transmittance reading is recorded to a computer in voltage (ranging from 1 to 0 volts). In order to relate the voltage signal to turbidity value, a known turbidity standard (0, 50, 200, 400 and 800 FAU) produced by HACH were used for the calibration.

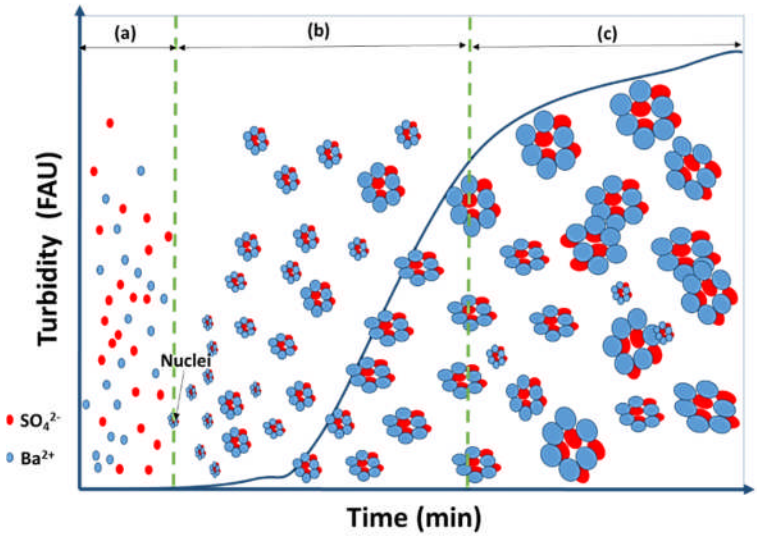

Figure 3-11: Schematic diagram illustrating turbidity curve

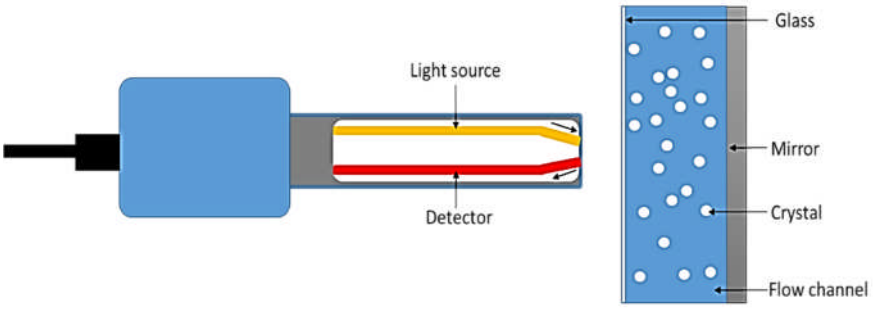

Figure 3-12: Schematic diagram of turbidity probe

3.5 Growth and nucleation model

A model developed by Beaunier *et al.* [121] which was further modified by Euvard *et al.* [114] and data generated by the *in-situ* flow visualization cell were used to determine whether the nucleation is either progressive or instantaneous. Progressive nucleation is the nucleation that occurs when the formation of new nuclei and the growth of crystal occurs currently. Instantaneous nucleation is described as a process where nuclei are formed at beginning of the crystallization process but remains constant afterwards. The model assumes that crystallization is controlled by diffusion. Also, it suggests that the unit area of the substrate has a finite number of nucleation actives sites N_0 (µm) and that all nucleation events are independent of each other. Thus, the probability of nucleation at time (t) depends on the number of free sites. For non-growing crystals, the number density of nuclei follows:

$$N(t) = N_0[1 - \exp(-At)] \qquad 3\text{-}2$$

Where A(s^{-1}) is the nucleation rate constant (conversion of a site into nucleus); in our approach, the density of active sites N_0 is the detected number of crystals. Two different cases exist according to the nucleation rate constant value:

- When $At \ll 1$, it implies progressive nucleation; N(t) is close to N_0At, the number of converted sites increases linearly with time.
- When $At \gg 1$, N(t) is close to N_0, which indicates that all active sites have generated nuclei in the very early stages of the process (instantaneous nucleation).

A drawback in the analysis of the data is the overlapping of crystals and the actual covered surface is S(t) is different from the extended surface area $S_{ext}(t)$ that would be covered by all the nuclei at time t without overlapping effects. The correlation between the S(t) and $S_{ext}(t)$:

$$S(t) = 1 - \exp(-S_{ext}(t)) \qquad 3\text{-}3$$

$$S_{ext}\,(t) = \left(\frac{MK_1}{\rho}\right).\,(\,t - \frac{1}{A} + \exp\frac{-At}{A}) \qquad 3\text{-}4$$

Where K_1 the lateral growth rate (mol/μm/s), ρ is the density of crystal (g/μm^3), A is the nucleation rate and M is the molar mass of $BaSO_4$ (233.38 g/mol).

From the equation the surface coverage S(t) is:

$$S(t) = 1 - \ exp\left(\frac{MK_1}{\rho}\right).\,(\,t - \frac{1}{A} + \exp\frac{-At}{A}) \qquad 3\text{-}5$$

For an extended time, S(t) is simplified as follows:

$$S(t) = 1 - \ exp\left(\frac{MK_1}{\rho}\right).\,(\,t - \frac{1}{A}) \qquad 3\text{-}6$$

For instantaneous nucleation:

$$S_{ext}(t) = \ -Ln\big(1 - S(t)\big) = \ \frac{MK_1N_0t}{\rho} \qquad 3\text{-}7$$

For progressive nucleation:

$$S_{ext}(t) = \ -Ln\big(1 - S(t)\big) = \ \frac{MK_1N_0t^2}{\rho} \qquad 3\text{-}8$$

The instantaneous nucleation $S_{ext}(t)$ is directly proportional to time, while for progressive nucleation $S_{ext}(t)$ is a linear function of t^2.

3.6 Test conditions

The test conditions for both *in-situ* test and RCE tests are shown in Table 3-5. The temperatures were chosen since the temperature varies in the oil industry from 50ºC in top surface facilities and 95ºC above in the reservoirs [34].

Table 3-5: Experimental conditions

Parameters	Conditions	
	In-situ test	RCE test
Pressure	Atmospheric	
Flow rate	20, 40 and 60 ml/min	Static
Duration of test	4 hours	
Mixing Ratio	50:50	10:90
Temperature	25°C and 50°C	80°C

3.7 Experimental procedures

3.7.1 Bulk jar test

The two brines NSSW and FW are prepared by dissolving the appropriate salt in distilled water and vacuum filtered separately through a 0.45µm membrane to remove any form of impurities or crystals. Also, the inhibitors are prepared by weighing and dissolving the scale inhibitors in distilled water to create a stock solution of 1000 ppm active SI. The stock solution of inhibitor is then added to the NSSW to give the required concentration.

The appropriate volume of NSSW/SI and FW are measured into separate bottles. To each of the brine, buffer solution is added to produce the required pH for the experiment. Both bottles are placed in the water bath and are heated up to the required temperature for 60 minutes. The two brines are mixed after 60 minutes and the tests are sampled (1 ml of solution) after 2 and 22 hours. The 1ml taken is added to a test tube containing 9 ml of quenching solution preventing further precipitation of $BaSO_4$.

3.7.2 Rotating Cylinder Electrode (RCE) test

The same methodology described in section 3.7.1 was followed during the brines (NSSW and FW) and SI preparation. In addition, Isopar M is added to the FW prior to the experiment and the overhead stirrer was set at 500 rpm throughout the experiment to maintain the emulsion.

The metal sample is placed in the beaker containing the FW/oil. Both vessels are placed in the hot plate are heated up to 80 ºC for 60 minutes. The NSSW/SI and FW/oil are mixed in a 2-litre vessel containing the metal sample. Figure 3-13 gives a schematic illustration of the experimental procedure. Scaling tests were carried out at oil-to-water (o/w) ratios of 0:100, 5:95, 20:80 and 50:50 by adding 0ml, 53ml, 250 ml and 1000ml of paraffinic oil in 1000ml of scaling brine. The metal sample is removed at the end of the experiment, cleaned with distilled water and placed in 10ml of EDTA solution to dissolve the scale deposit and analysed using ICP.

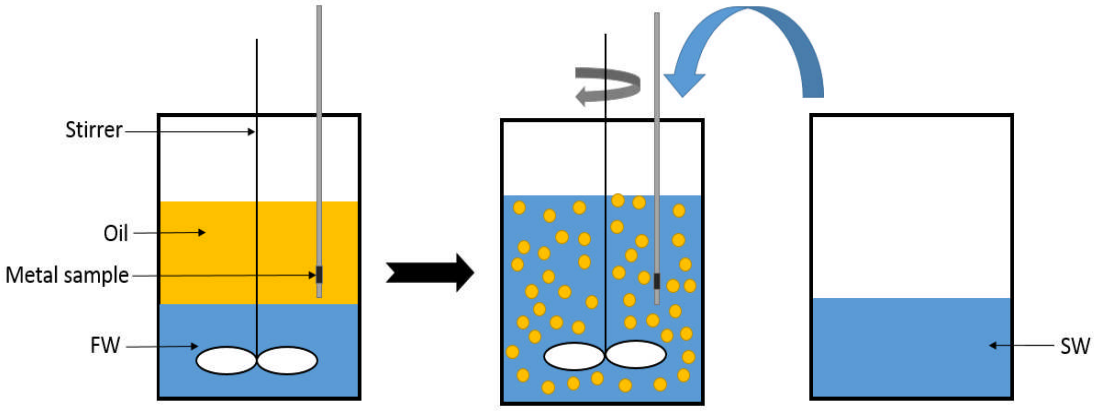

Figure 3-13: Schematic illustration of experimental procedure using RCE set-up

3.7.3 In- situ flow test

The similar methodology described in section 3.7.1 was followed during the brines (NSSW and FW) and SI preparation. Prior to the start of the experiment, the thermostatic bath is set to the desired operating temperature of the test. The two brine solutions are pumped from the vessel through the thermostatic

bath to heat them up to the desired experimental temperature, they are mixed in a tee chamber before entering the flow cell. In the flow cell, the camera takes images of the scale formed on the substrate every 5 minutes during the course of the experiment. The image is analysed by a software to assess number of particle, particle size and surface coverage formed on the surface. Furthermore, turbidity probe measures the turbidity of the solution.

3.7.3.1 Repeatability tests and analysis for surface crystallization

Preliminary tests were carried out to assess the precision and the repeatability of the *in-situ* flow techniques. Brine solution with SR=60 at 50°C was run through the *in-situ* flow cell at 20 ml/min for 4 hrs. The scaling test was repeated three times (R1, R2 and R3) using different stainless steel samples, under same experimental conditions. As stated previously, the images were captured every 5 minutes interval and analysed. Figure 3-14 presents the surface coverage with time, repeated three times for SR=60 using the *in-situ* flow rig and image analysis program. The repeatability results indicate that the techniques are suitable to study the surface crystallization process with high accuracy.

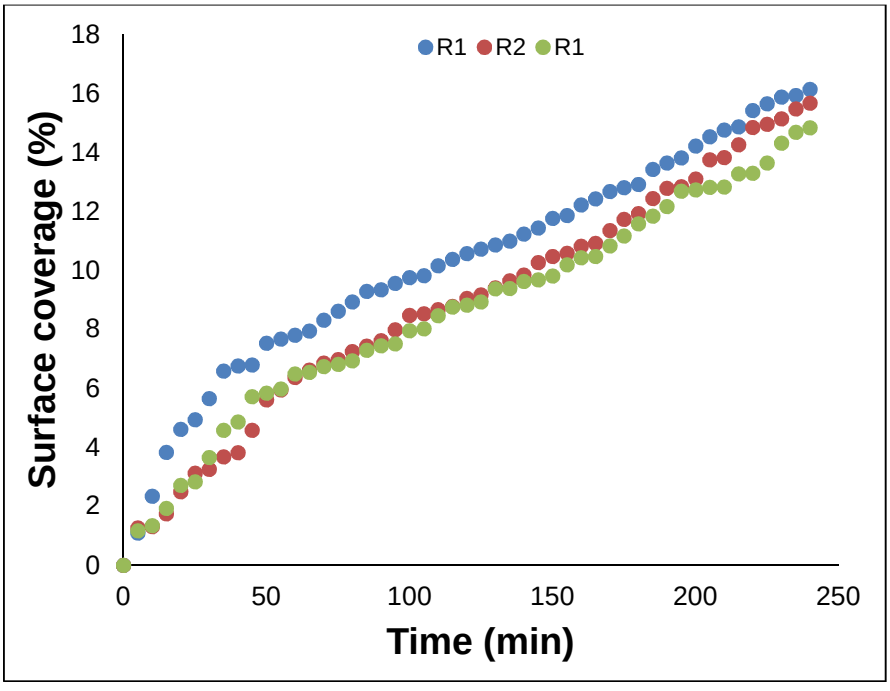

Figure 3-14: Repeatability test for surface coverage at SR = 60, T = 50°C

3.8 Equipment

3.8.1 Scanning Electron Microscopy (SEM) and Energy Dispersive X-ray analysis system (EDX)

The Scanning Electron microscope (SEM) Philips ® X130 is used after the deposition test to assess the morphology and size of the scale deposits formed on the metallic surface. Prior to the analyses, the metal is coated with 3 nm gold to make it conductive and when electrons strike the sample (with a high-energy beam of 10keV or 20keV); a variety of signal is generated and the detected signal is then converted into images.

In addition to the SEM, energy dispersive X-ray micro-analysis (EDX) is incorporated in the system. It is a powerful tool used to identify the elemental composition of sample surface down to their atomic level. Similarly to the SEM sample preparation for analysis, the sample is coated with gold to make it conductive. Therefore the surface is strike with the beam, and the surface emits an array of scattered signals (backscattered electrons, secondary electrons, characteristics X-rays and other photons) which is detected by a sensor and the composition of the assessed; Figure 3-15 shows an example of a SEM machine.

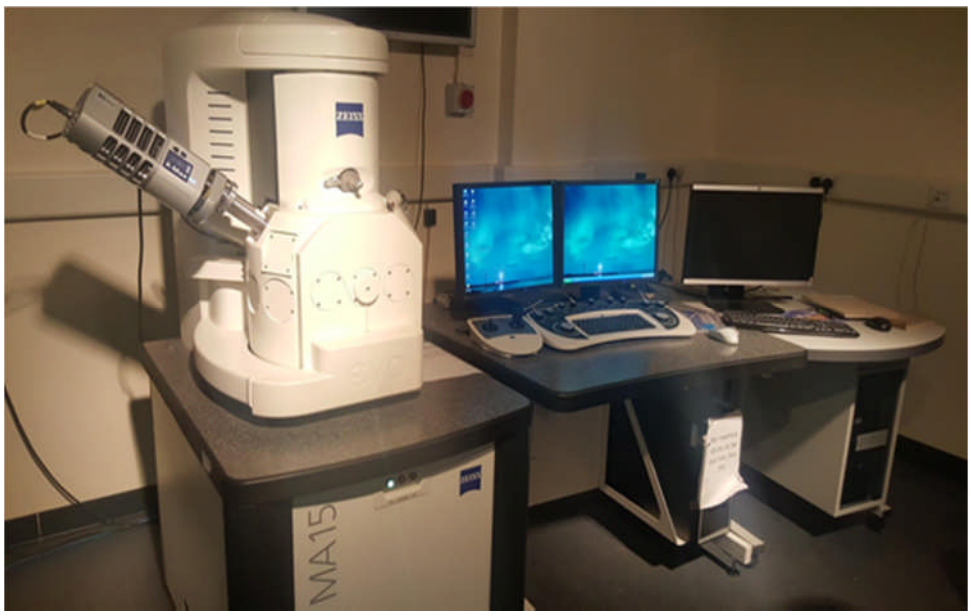

Figure 3-15: Scanning Electron Microscopy (SEM)

3.8.2 JY138 Ultrace model Inductively Coupled Plasma - Atomic Emission Spectroscopy (ICP-AES)

Measuring the barium ion concentration in the solution after sampling was performed using JY138 Ultrace model Inductively Coupled Plasma - Atomic Emission Spectroscopy (ICP-AES). The ICP-AES is a technique commonly used for element analysis. The technique involves using a plasma source to make a specific element emit light after which a spectrometer separates the light in a characterisation wavelength as shown in Figure 3-16. At the outset, the sample is converted to an aerosol by a nebulizer. At the core of the ICP sustains a temperature of 10000k, the aerosol tends to vaporise quickly due to the high temperature; thus the element are liberated as a free atom in their gaseous state.

Also, in the plasma additional energy is transferred to the atom and ion, promoting the excitation of the electron to higher energy level. And when the excited atoms and ions return to the ground state through the emission of photons, the wavelength of the photons are used to characterize the particular elements.

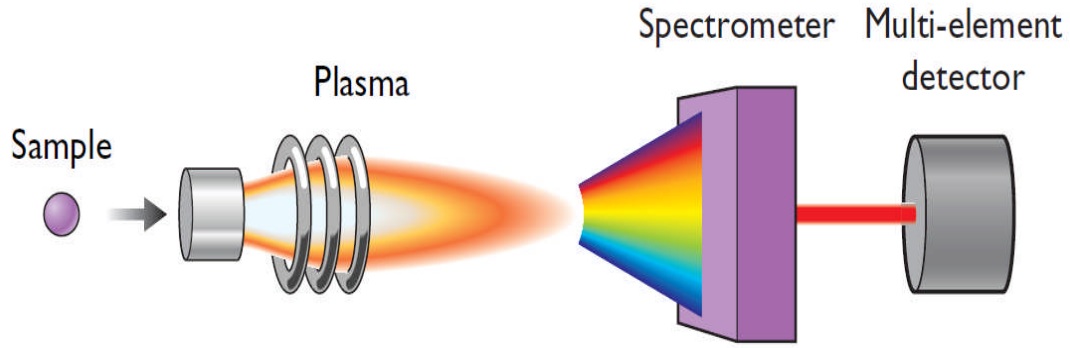

Figure 3-16: Schematic of an ICP-AES

3.8.3 Surface profilometer

A surface profilometer is a device used to measure the roughness of a surface. In this work, a Taylor Hobson surface profiler was used to measure

surface roughness of the substrate. The roughness of the substrate could be determined by measuring the deviation from a mean line representing the surface profile. A number of standard parameters are used to describe the surface roughness. Few of these parameters are explained below;

- **Average Roughness (R_a)**: is the average of individual height and depth from the mean line.

$$R_a = \frac{1}{lm}\int_0^{lm} |z(x)|\, dx \qquad 3\text{-}9$$

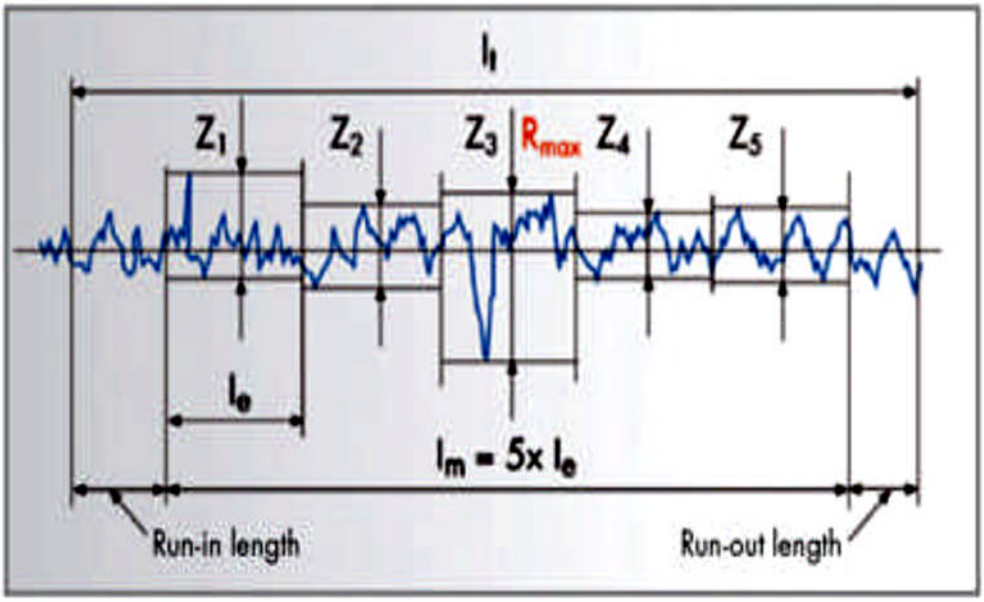

Figure 3-17. Evaluation of surface roughness profile

- **Skewness (R_{sk}):** is the measure of the symmetry of the profile about the mean line.

$$R_a = \frac{1}{R_q^3}\left(\frac{1}{l}\int_0^{l} |z^2(x)|\, dx\right) \qquad 3\text{-}10$$

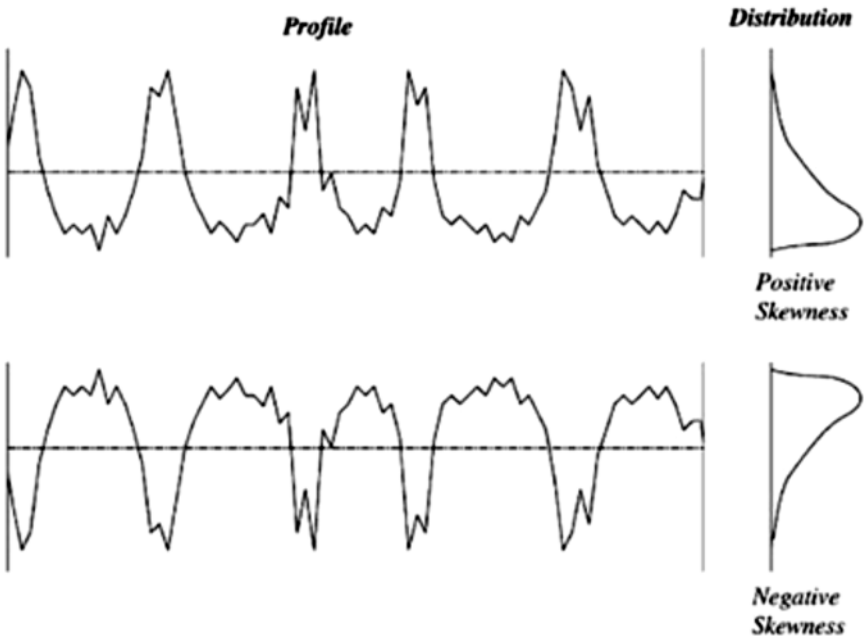

Figure 3-18. The distribution curve of surface skewness

3.8.4 Contact angle measurement

As discussed in chapter 2, the surface property (such as wettability) of a substrate tends to affect the surface deposition of scale. In order to characterise the surface affinity of the different surfaces with water and isopar M, contact angle measurement was used. The contact angle is defined as the angle formed by the intersection of a liquid-solid interface and the liquid-vapour interface as shown in Figure 3-19. For a perfect (smooth and chemically homogeneous) solid surface, the surface free energy can be evaluated by determining the contact angle measurement using Young's equation:

$$\gamma_S = \gamma_{SL} + \gamma_L \, Cos\, \theta \qquad 3\text{-}11$$

Where γ_S , γ_{SL} and γ_L represent the solid surface free energy (N/m), the solid-liquid interfacial tension (N/m), liquid surface tension (N/m), respectively, and θ is the contact angle (º).

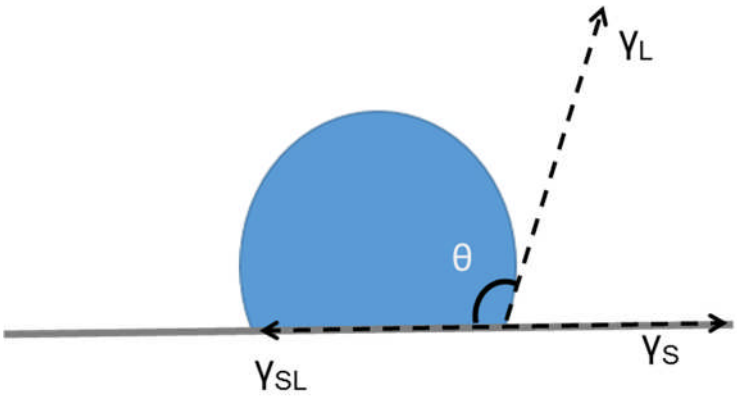

Figure 3-19: Definition of the contact angle formed at a solid surface

3.8.5 X-Ray Diffraction (XRD)

X-ray diffraction is a well-known surface analyses technique used to identify unknown crystalline materials (e.g. mineral, inorganic compounds, solid solution, clay). The goniometer which represents the mechanical assembly consists of three basic elements namely (X-ray tube, sample holder and an X-ray detector) as shown in Figure 3-20. This technique function by emitting x-ray with fixed wavelength to the sample and the intensity of the reflected radiation is recorded.

In this research, x-ray diffraction investigation of crystals on the metallic surface was performed using Philips PanAlytical X'pert PRO diffractometer. The PanAlytical X'pert X-ray generator was setup at a voltage of 40 kV and an intensity of 40 mA using a dual copper CuKα1+2 radiation with 10 X10 mm divergence slit. The diffraction pattern of the deposited scale on the stainless steel was collect at 2θ=20 º – 60 º at a 5 min -1 scanning rate. After each test, product identification was conducted using the Phillips X'Pert HighScore Plus program. The software helps to identify a compound by comparing with the diffraction pattern with of data banks available in the program. Prior to each product identification, the diffraction pattern was also treated using the HighScore Plus.

This chapter has discussed the materials, equipments and experimental procedures used in achieving the research objectives. The next three chapter

(chapter 4, chapter 5 and chapter 6) present the results obtained from the experiments conducted.

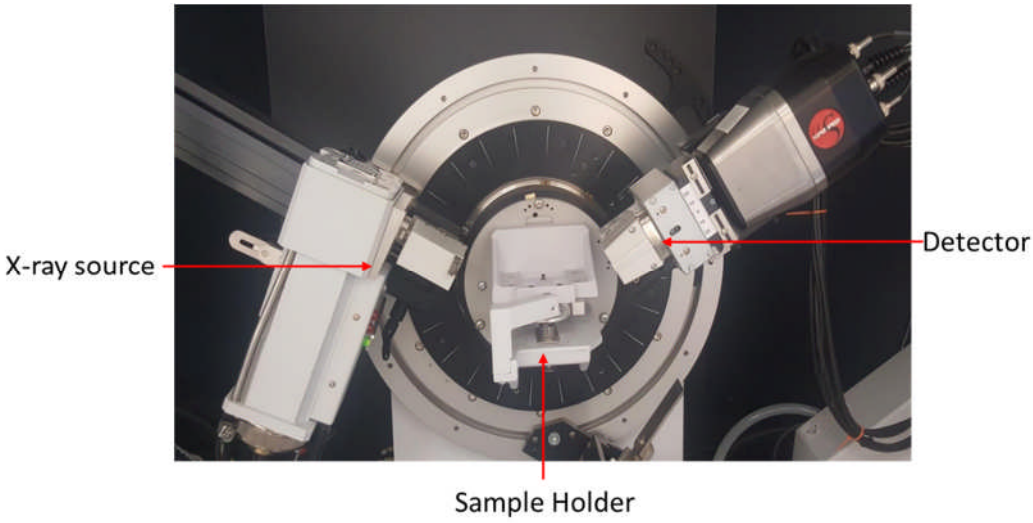

Figure 3-20: The part of a XRD Goniometer

Chapter 4 The kinetics of barium sulphate bulk precipitation and surface deposition

4.1 Introduction

In this chapter, surface crystallization and bulk precipitation of barium sulphate in the absence and presence of three scale inhibitors (Diethylene Triamine penta Methylene Phosphonic acid (DETMP), VinylSulphonate Acrylic acid co-polymer (VS-Co) and Poly-Phosphino Carboxylic Acid (PPCA) were studied using a once-through flow system. An optical technique was used to follow the nucleation and growth process of barium sulphate on a stainless steel *in-situ* and in real time. Conversely, a turbidity probe was used to assess crystals formed in the bulk solution. This technique allows the observation of the surface growth of crystals, thereby improving the understanding of scale inhibition mechanism on surface growth. The outline of this chapter is described in Figure 4-1

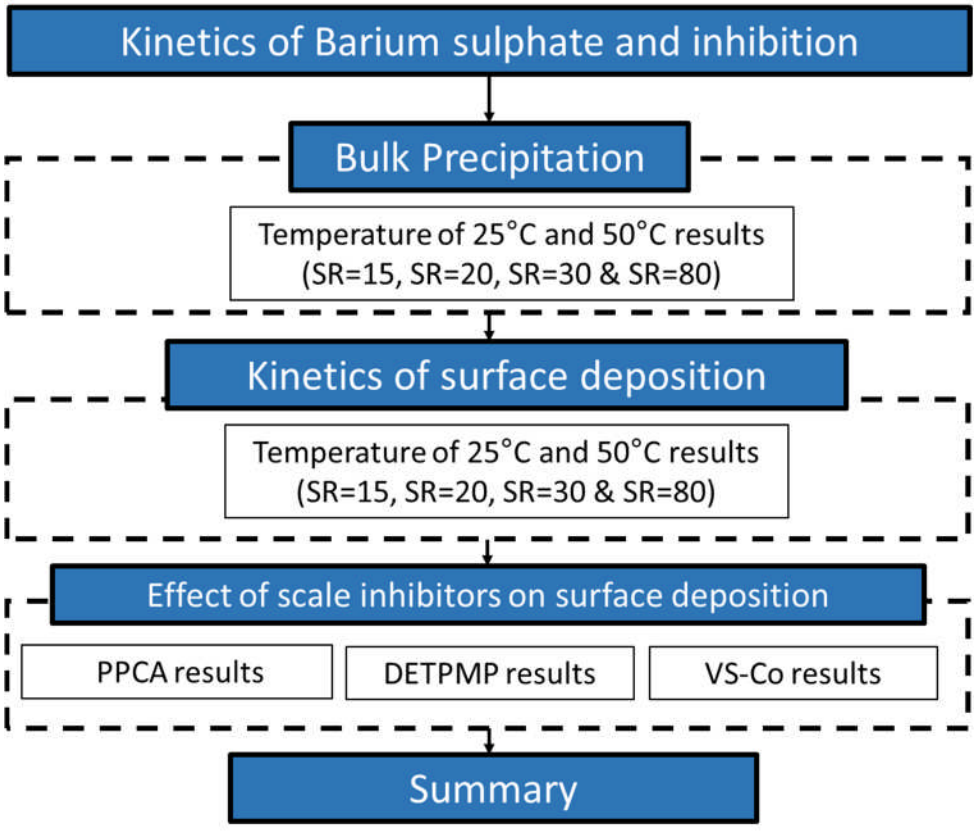

Figure 4-1: Outline of chapter

4.2 Brine composition

The supersaturation conditions necessary for the formation of barium sulphate scale were achieved by mixing two incompatible brines as explained in chapter 3. North sea seawater (NSSW) provided the source of anions (SO_4^{2-}) while Formation Water (FW) the source of cations (Ba^{2+}). The compositions of the brines used in this chapter are presented in Table 4-1 and Table 4-2; the brines were mixed in a 50:50 ratio at a temperature of 25°C and 50°C.

Table 4-1: Brine composition

Ion	Formula	Conc./ppm (NSSW)	Conc./ppm (FW)
Na	NaCl	10890	31275
Ca^{2+}	$CaCl_2.6H_2O$	428	2000
Mg^{2+}	$MgCl_2.6H_2O$	1366	739
K	KCl	460	654
Ba^{2+}	$BaCl_2.2H_2O$	0	See table 4-2
Sr^{2+}	$SrCl_2.6H_2O$	0	771
SO_4^{2-}	Na_2SO_4	See table 4-2	0

Table 4-2: SO_4^{2-} and Ba^{2+} concentrations in ppm

Temp	25˚C		50˚C	
SR	SO_4^{2-}	Ba^{2+}	SO_4^{2-}	Ba^{2+}
15	145	52	300	57
20	150	54	350	64
30	300	54	500	65
80	700	60	800	110

4.3 Bulk precipitation measurement of barium sulphate

In this section, the kinetics of bulk precipitation of barium sulphate with saturation ratios (15, 20, 30 and 80) at 25°C and 50°C are presented. In order to characterise the kinetics of the bulk phase, a turbidity probe was used to assess the precipitation of barium sulphate. The turbidity of the solution was measured in the flow cell next to the steel sample as previously explained in chapter 3. It is important in this study to understand whether when the flow passes the stainless steel coupon, there are any particles precipitated in the flow. As scaling progresses, the solution becomes more turbid during the initial stages of precipitation of barium sulphate. The induction time and the kinetics of the reaction can be measured as explained in section 3.4.3.

Figure 4-2 shows the turbidity measurement of barium sulphate precipitation over a period of 4 hours for the 4 different brines at 25ºC. The turbidity value was found to be 0 FAU which indicates that no bulk precipitation of barium sulphate occurred in the flow cell for the range of saturation ratios considered. $BaSO_4$ bulk precipitation was observed in the collection vessel but this occurred after the fluid had passed the working section of the flow cell. This implies that the induction time of the different brines used is greater than the residence time (*i.e.* time it takes for the fluid to pass through the flow cell).

Figure 4-3 shows the turbidity value measured for the four supersaturated brines at 50ºC. Although, the temperature was increased to 50ºC the turbidity value was still 0 FAU. As previously explained at 25ºC, the results indicate that no precipitation of barium sulphate was formed in the bulk solution for these set of brines during the test duration of 4 hours.

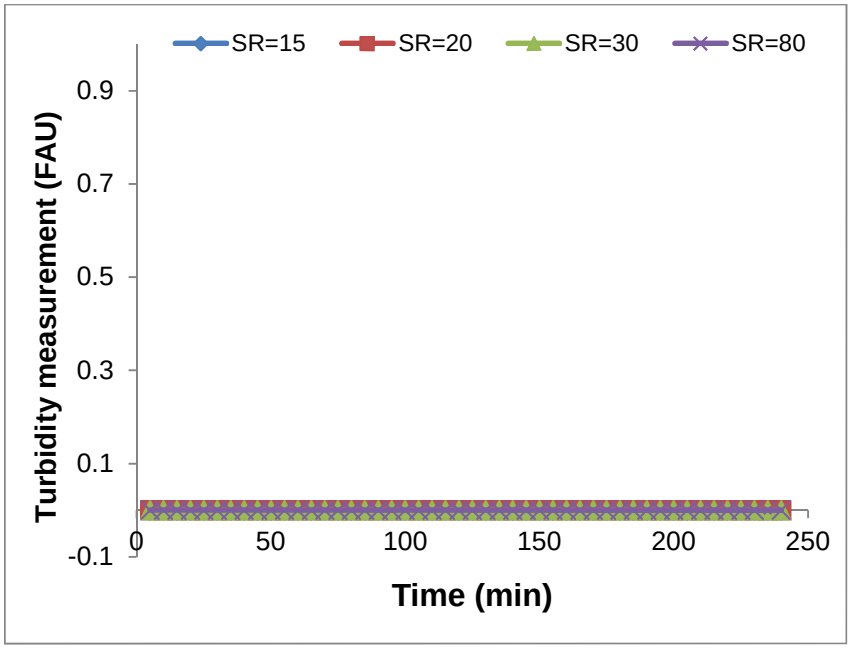

Figure 4-2: Turbidity measurement of different brines (SR 15, 20, 30 and 80) at 25ºC for 4 hours of experiment

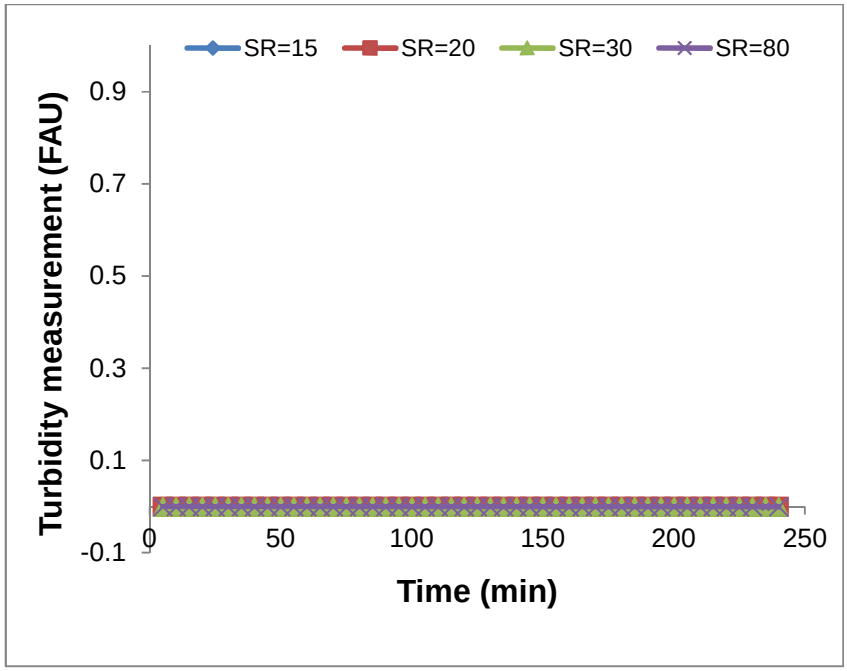

Figure 4-3: Turbidity measurement of different brines (SR 15, 20, 30 and 80) at 50ºC for 4 hours of experiment

4.4 Barium sulphate surface deposition kinetics study

This section focuses on the barium sulphate surface crystallization kinetics on a stainless steel surface. As explained in chapter 3, the barium sulphate surface deposition is assessed by using a camera which allows a real-time observation of surface scaling. Subsequently, the images captured were processed to assess the number of particles and their size as well as the barium sulphate surface coverage. The same conditions used for the bulk scaling measurement assessment were applied in the surface kinetics study.

4.4.1 Average size of crystals

Figure 4-4 shows the average size of barium sulphate crystals formed on the stainless steel surface for all brines at 25ºC after 4 hours. At SR 15, there were no crystals formed on the surface of the metal in the first 5 minutes of the test. Crystals were formed on the metallic surface between 5 -10 minutes after the start of the experiment. Also, the average size of crystals formed was fairly constant, which was due to slow growth of crystals and the formation of new nuclei on the metal surface. The same trend was observed at SR 20, although crystals were formed on the surface in the first 5 minutes of the experiment.

At SR=30, the average size of crystals increased for the first 15 minutes, but experience a slight decrease due to the formation of new nuclei. However, towards the end of the experiment it slightly increased. From the images captured as shown in Figure 4-8, it can be observed that the slight increase in the average size of crystals was attributed to the agglomeration of crystals on the metal surface. At SR=80, the average size of crystals was fluctuating for the first 15 minutes due to the surface growth of crystals and the formation of new crystal formed on the metallic surface. After 60 minutes, the average size increased linearly throughout the experiment reaching a maximum size of 76 μm^2. It can be assumed after 60 minutes, nucleation has stopped and only growth of crystals was observed.

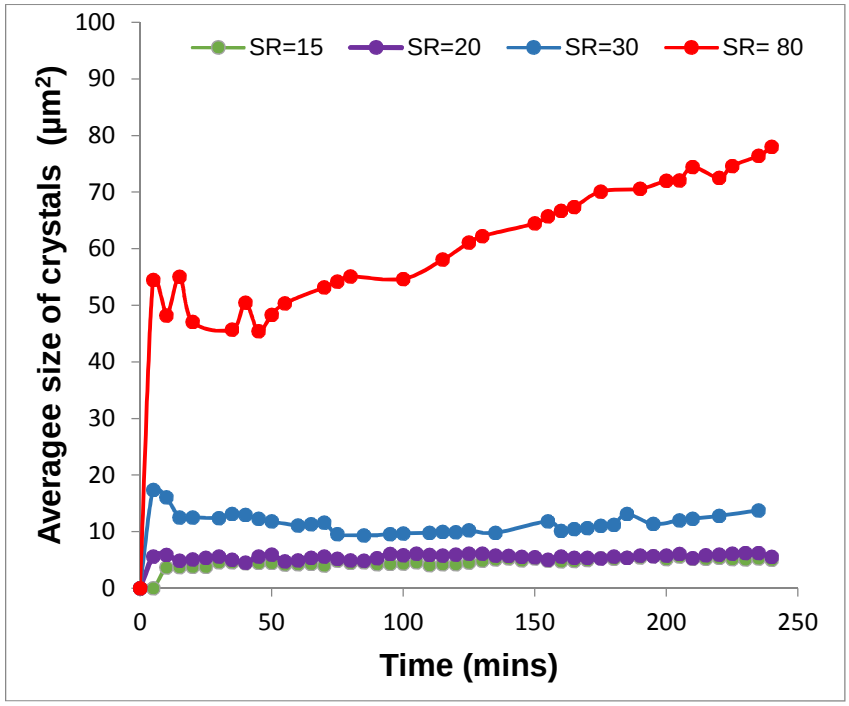

Figure 4-4: Average size of crystals formed on the stainless steel 25°C for a range of SR15, 20, 30 and 80

Figure 4-5 shows the average size of crystals formed on the metallic steel surface at 50ºC for the four different brines. At SR=15, there was no induction time, crystals were formed during the first 5 minutes on the surface unlike at a lower temperature (25ºC). However, the average size of particle was relatively constant throughout the experiment. At SR=20, the average size of crystals increase for the first 10 minutes, and then it slightly reduced due to the formation of new crystals. However, the average size of crystals start to increase slowly after 90 minutes and attained an average size of 50 μm^2 at the end of the experiment. For SR=30, a different trend was observed when the temperature was increased to 50ºC, the average size of crystals increased linearly through throughout the experiment. At SR=80, it shows a similar linear trend, however the growth of crystals was faster when compared to the same experiment run at 25ºC as expected.

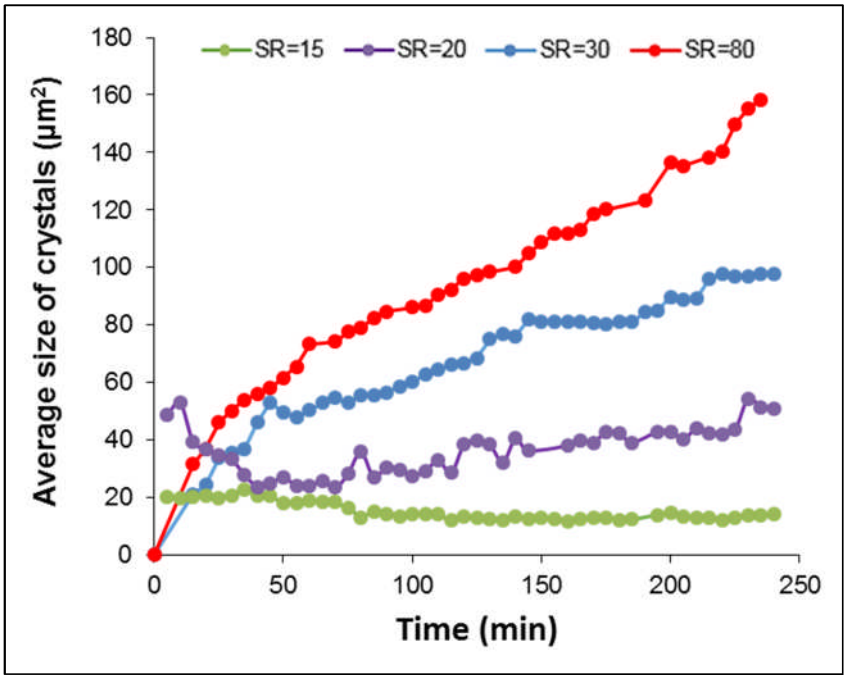

Figure 4-5: Average size of crystals formed on the stainless steel at 50°C for a range of SR15, 20, 30 and 80

4.4.2 Number of crystals

Figure 4-6 shows the number of crystals formed on the surface as a function of time for the different brines at 25ºC. Indeed, at lower saturation ratio (SR=15, 20 and 30) the number of crystals formed on the metallic surface increases throughout the test; but the rate of nuclei formation was faster with increase in the saturation ratio. At SR=80, the number of crystals increased rapidly in the first 75 mins, afterwards, the number of crystals reaches a plateau.

Figure 4-7 shows the number of crystals growing on the stainless steel surfaces as a function of time for the different brines at 50ºC. At lower saturation ratios (SR=15 and SR=20) the number of crystals growing on the surface increases throughout the experiment as observed for the same SR at 25ºC. However, at SR=30 a different trend was observed when the temperature was increased, the population of crystals reaches a plateau within an hour. Also, a different trend was observed when the temperature was increased for SR=80. From the result, it appears that there was a slight

reduction in the population of the crystals formed on the metal surface. This reduction was attributed to the agglomeration of crystals.

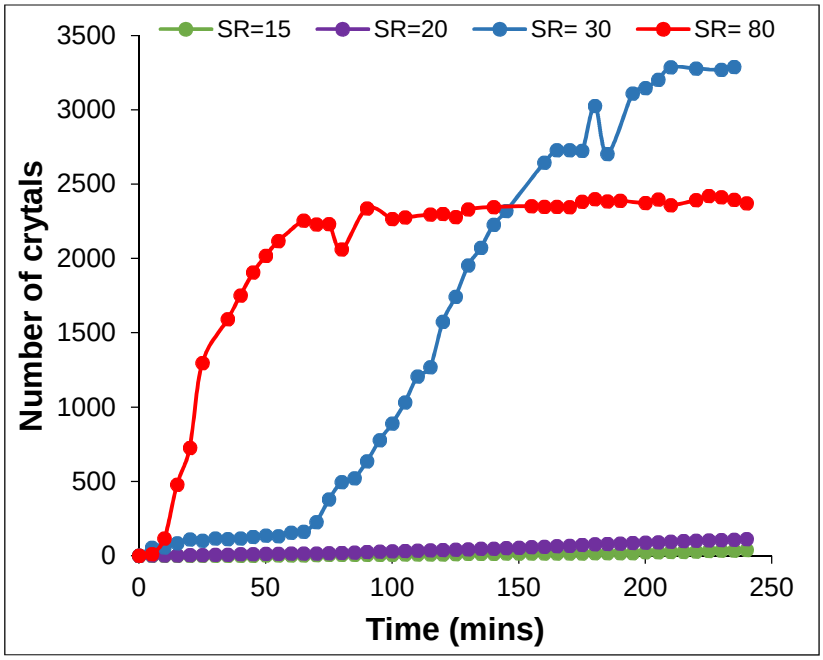

Figure 4-6: Number of crystals deposited on the stainless steel at 25°C for a range of SR15, 20, 30 and 80

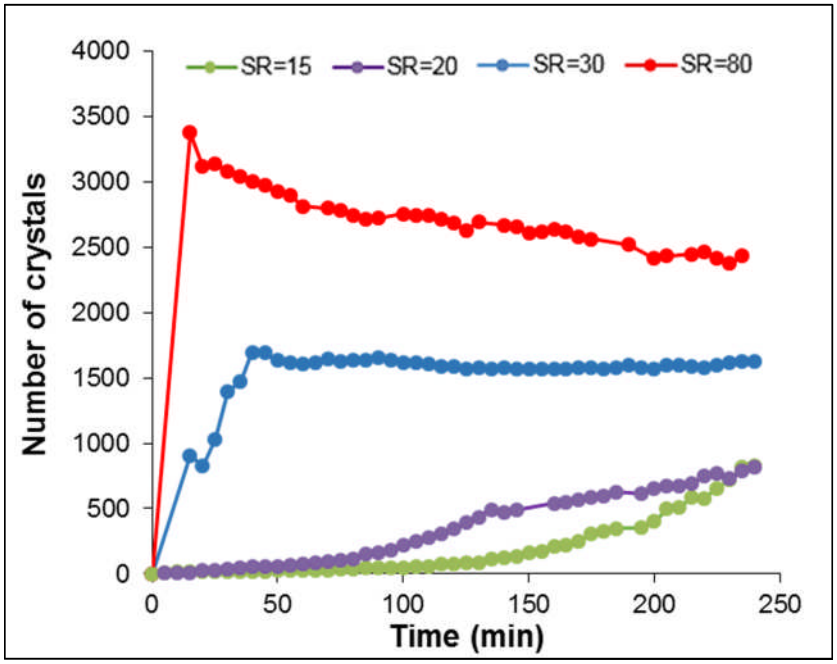

Figure 4-7: Number of crystals deposited on the stainless steel at 50°C for a range of SR15, 20, 30 and 80

4.4.3 Surface coverage

As expected the surface coverage increased as the SR was increased as shown in Figure 4-8 [122]. Figure 4-9 and Figure 4-10 presents the surface coverage of barium sulphate surface scaling of brines used at 25°C and 50°C. The surface coverage was higher for all brines at 50°C when compared to 25°C; most especially the brine with high SR. This can be seen by visual comparison of Figure 4-8 and Figure 4-11, it can be observed that the surface coverage of barium sulphate on the metallic samples for all brines at 50°C is higher when compared to 25°C. However, the factors controlling surface scaling changes, depending on the saturation ratio considered. For SR=15, no surface coverage was observed for the first 5 minutes of the experiment. From Figure 4-5 and Figure 4-7, it shows that the increase of the surface coverage was due to the formation of new nuclei on the surface of the stainless steel rather than an increase in the average size of crystals.

A similar trend was observed for SR=20 and SR=30, but the kinetics were faster due to an increase in the saturation ratio. A different trend was observed at SR=80, initially, the surface coverage increased quickly in the first 60 mins; due to the formation of new crystals. Afterwards, there was a slight increase of barium surface crystals on the metal surface. In this case, the slow increase of the surface coverage was predominantly caused by the growth of crystals.

Figure 4-10 shows the surface coverage of barium sulphate crystals deposited on the stainless steel surface for brine with SR 15, 20, 30 and 80 at 50°C. As explained previously, factors controlling the increase of the surface coverage depend on the saturation ratio considered. For SR of 30 and 80, the surface coverage was controlled by an increase in nucleation and subsequent growth of crystals. However, at a lower SR=15 and SR=20, the surface coverage was controlled by the constant formation of new nucleation sites.

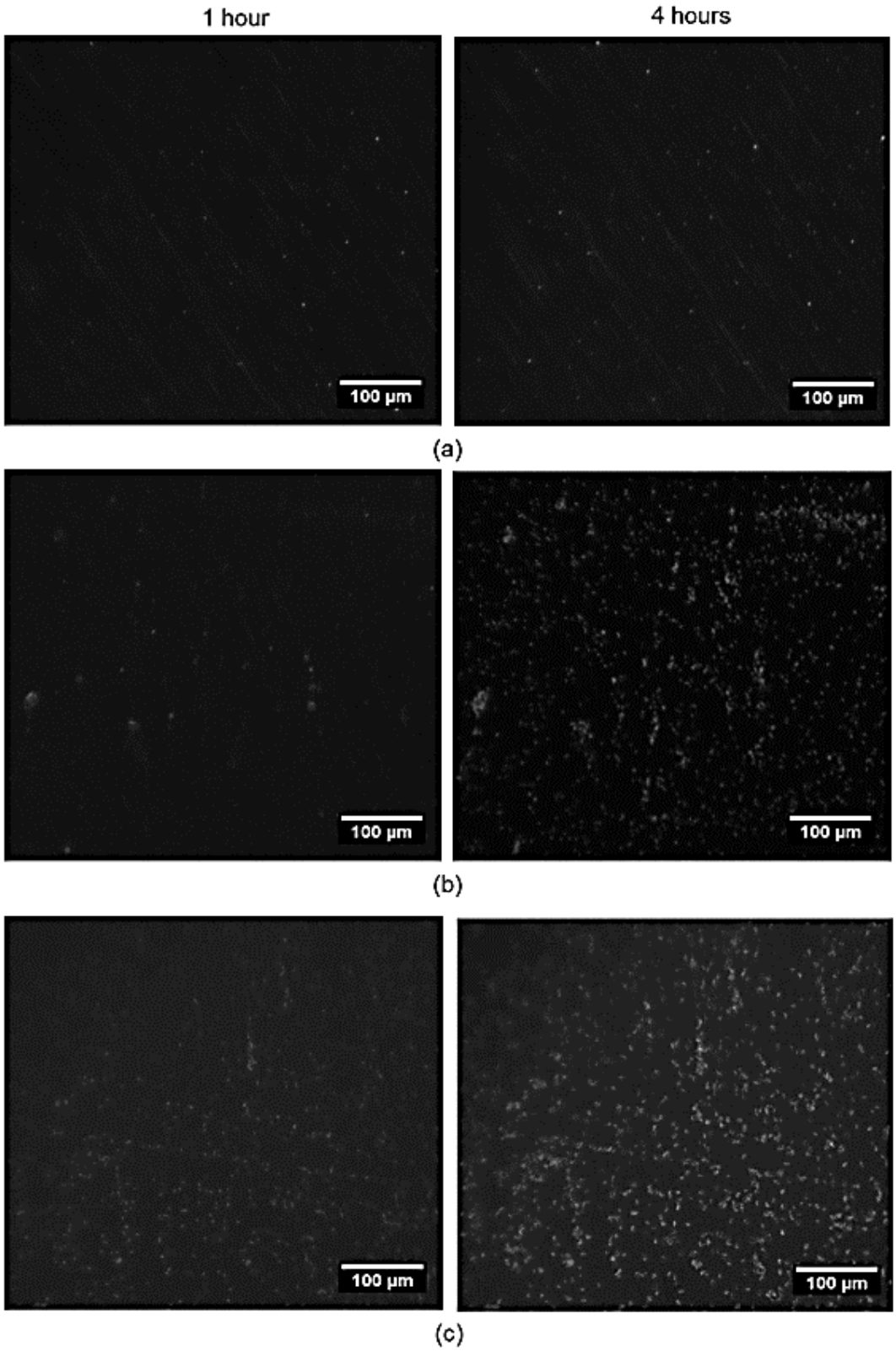

Figure 4-8: Images of $BaSO_4$ scale deposition on the stainless steel at 1 and 4 hours for brine with SR (a) 20, (b) 30 and (c) 80 at 25ºC

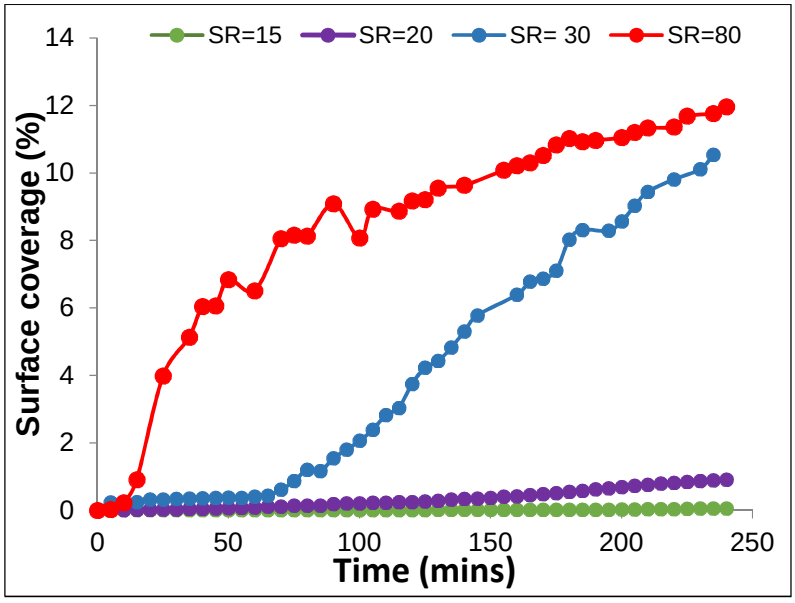

Figure 4-9: Surface coverage of $BaSO_4$ formed at 25°C for a range of SR15, 20, 30 and 80

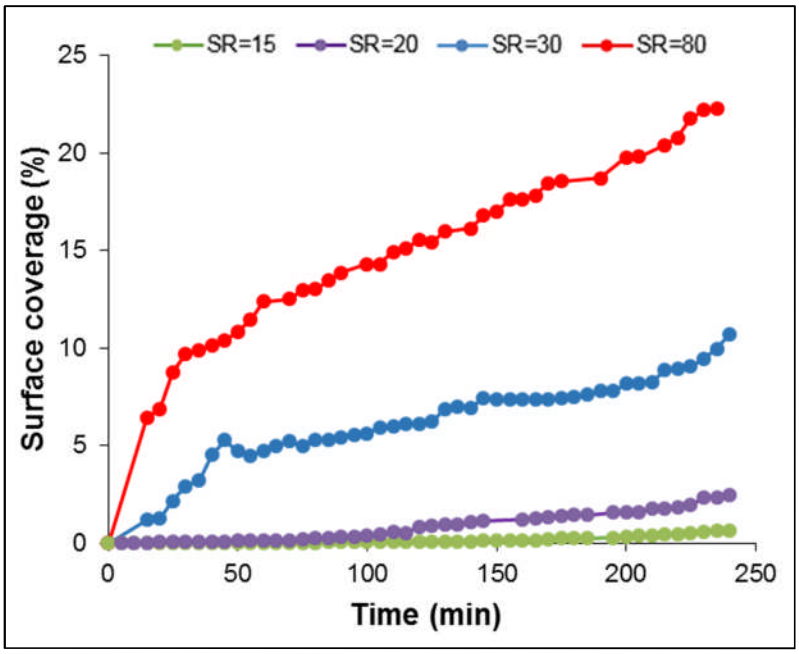

Figure 4-10: Surface coverage of $BaSO_4$ formed at 50°C for a range of SR15, 20, 30 and 80

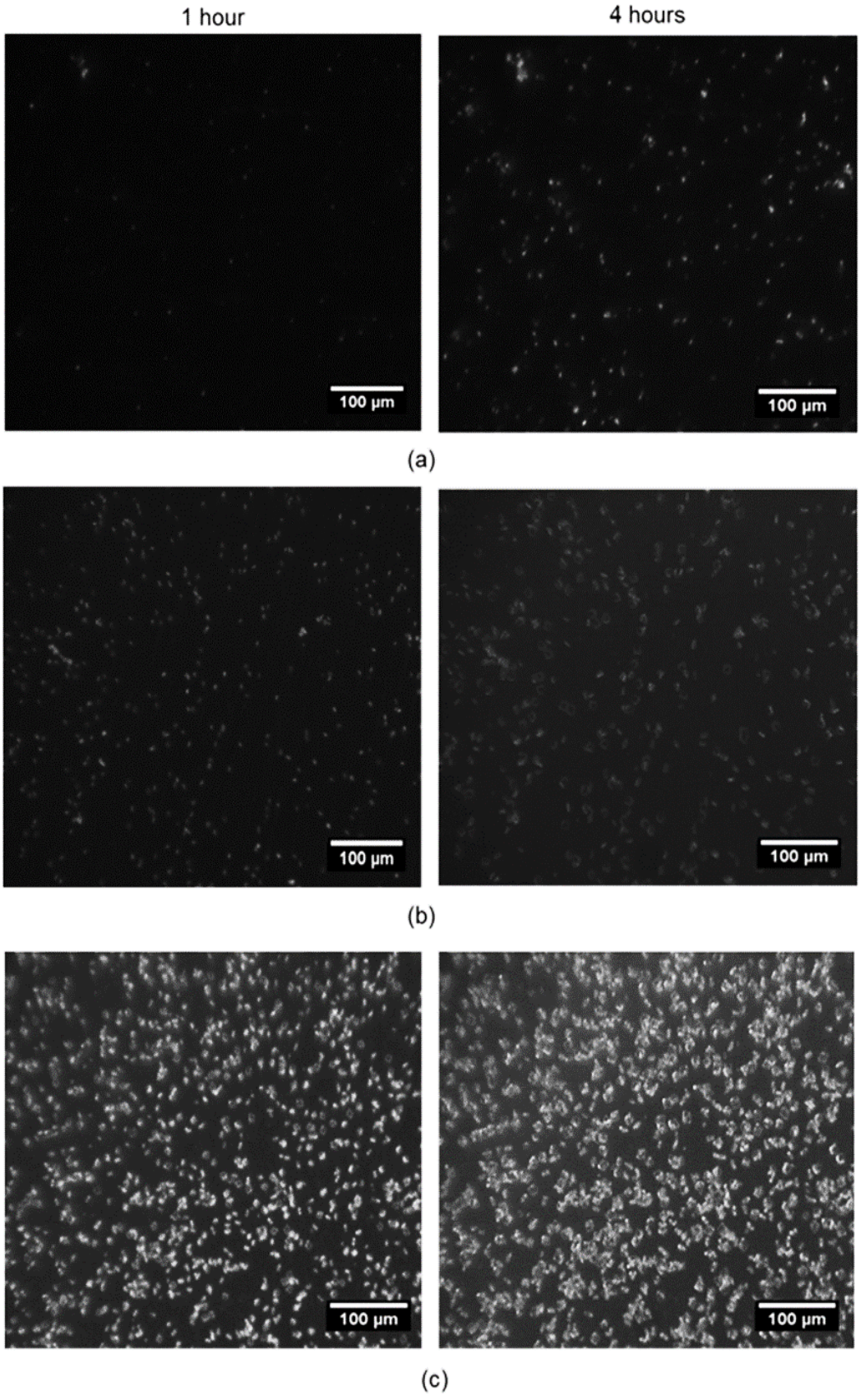

Figure 4-11: Images of $BaSO_4$ scale deposition at 1 and 4 hours at 50ºC for brine with SR (a) 20, (b) 30 and (c) 80

4.5 Effect of scale inhibitor on surface growth

The use of scale inhibitors is the most effective method used in preventing the formation of nucleation and subsequent growth of crystals [26]. The effect of three different scale inhibitors (VS-Co, PPCA and DETPMP) on subsequent growth of crystal was studied. The experiment was carried out using scaling brine with SR=80 at 50ºC and a constant flow rate of 20 ml min^{-1}.

In order to evaluate this effect, prior to adding of scale inhibitors the stainless steel surface was pre-scaled for a period of 1 hour. Figure 4-12 presents a schematic diagram illustrating the possible effect of adding scale inhibitor after 1 hour. The images of stainless steel samples were captured and analysed as explained previously. Also, SEM and XRD analyses were carried out on the scale deposited on the steel surface at the end of the test. Measurement of the turbidity with the influence of scale inhibitors is not required since it has been shown previously that during the uninhibited condition there was no bulk precipitation in this experimental conditions.

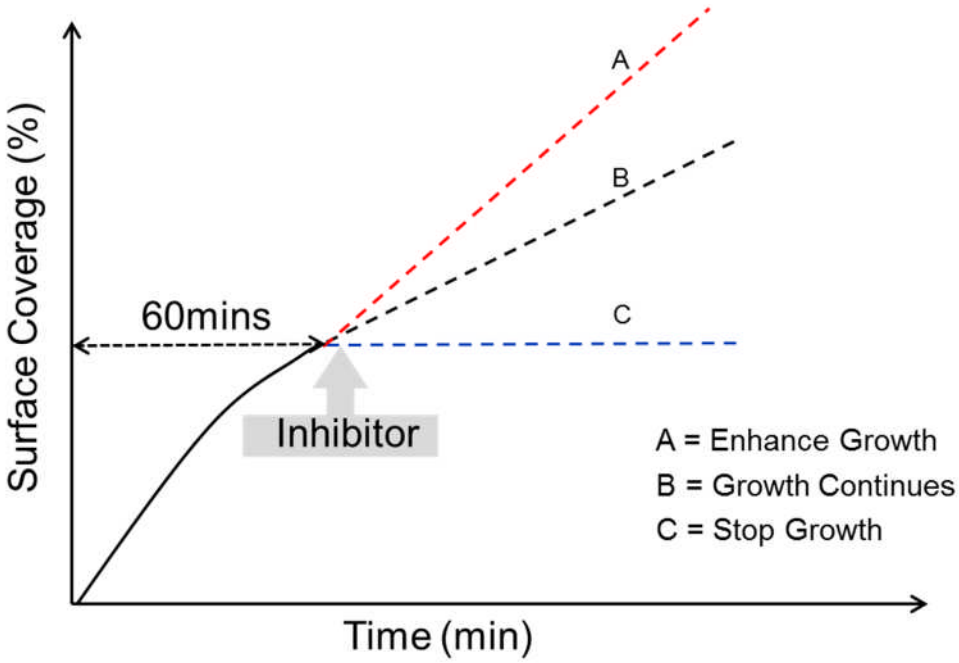

Figure 4-12: Schematic diagram showing the possible effects of inhibitor on surface growth of crystals.

4.5.1 Effect of PPCA on surface scaling

Figure 4-13 shows the effect of scale inhibitor concentration (1ppm and 4ppm) on the surface scaling of barium sulphate at SR=80. At 1ppm, the result shows that surface growth continued for about 60 minutes before it stopped; reducing the final surface coverage of barium sulphate crystals from 22 % to 21 %. However, when the concentration of the PPCA was increased to 4ppm the surface growth of crystals stopped immediately after injection. In this case, the surface coverage and average size of crystals were reduced by 45 % and 48 % respectively.

Figure 4-15 shows the images of scale deposited on the metal surface when 1 ppm and 4 ppm of PPCA were used. The image indicates that the addition of PPCA (1 ppm and 4 ppm) did not change the morphology of the crystals. The crystals formed on the metal surface were rhombic as expected. The XRD pattern provided in Figure 4-14 also confirmed that the addition of PPCA (1 and 4 ppm) affected the growth of crystals. At 1 ppm of PPCA, it was observed that all the crystal faces were suppressed by the inhibitor. This inhibition effect was more noticeable at a concentration of 4 ppm. In this case, most of the dominant faces were totally inhibited, except for (200), (021) and (210) faces; with them having low intensity when compared to the uninhibited case.

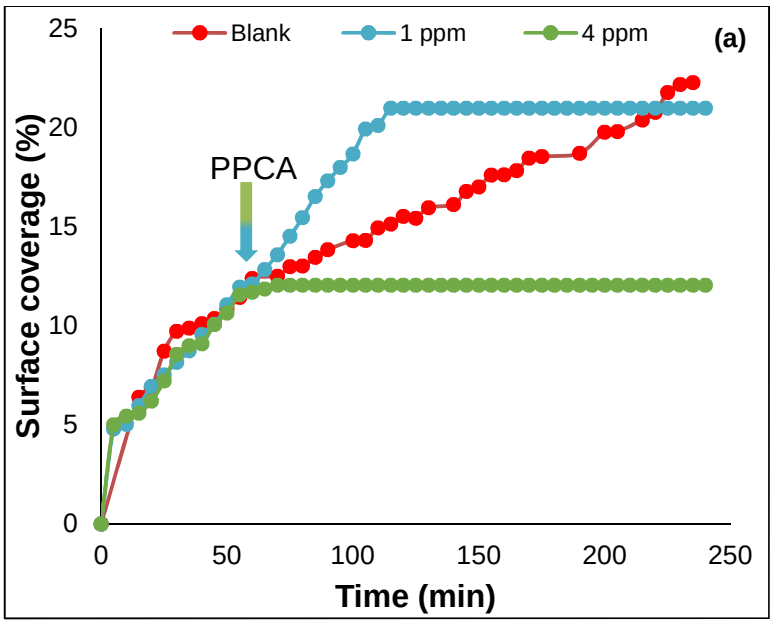

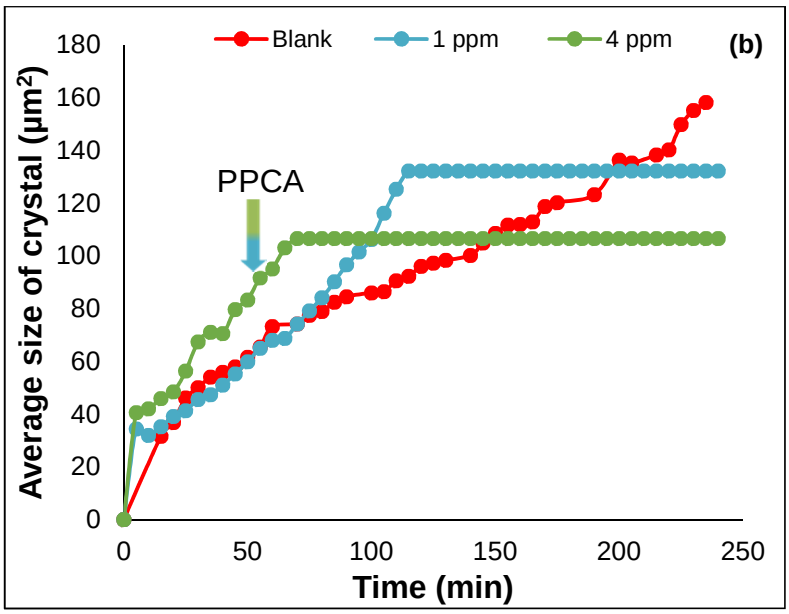

Figure 4-13: Effect of PPCA on crystal growth of $BaSO_4$ (a) Surface coverage and (b) Average size of crystals for SR = 80 at 50°C

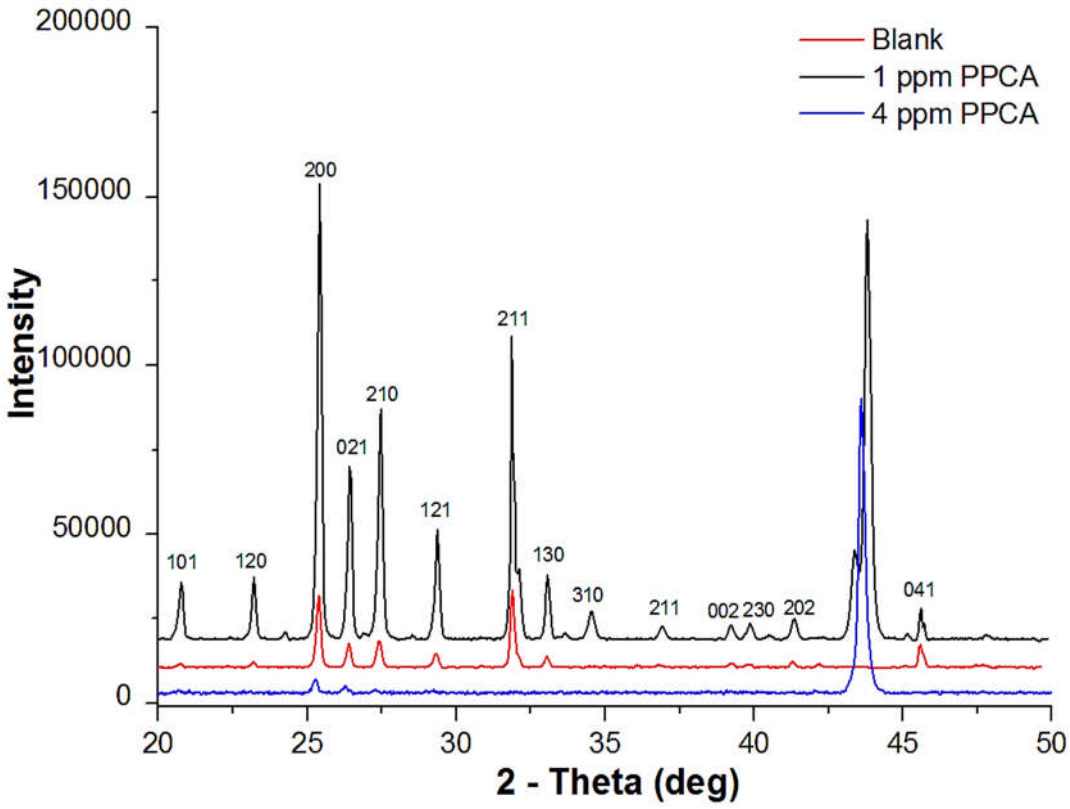

Figure 4-14: XRD diffraction pattern of $BaSO_4$ on stainless steel in the presence of PPCA

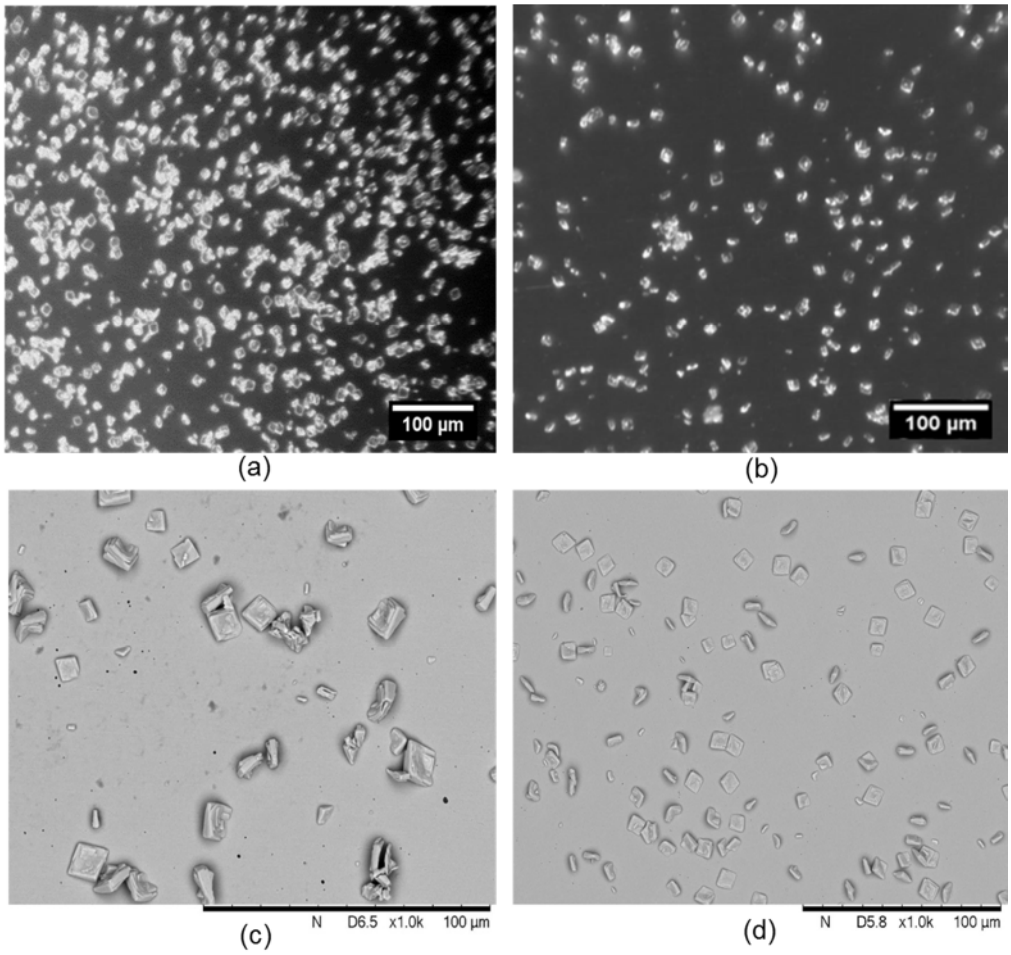

Figure 4-15: Image of $BaSO_4$ crystals captured using the camera at (a) 1 ppm (b) 4 ppm of PPCA; and SEM images of $BaSO_4$ crystals formed on the stainless steel surface at (c) 1 ppm (d) 4 ppm of PPCA

4.5.2 Effect of VS-Co on surface scaling

The effect of VS-Co (1 and 4 ppm) on the subsequent growth of barium sulphate is shown in Figure 4-16. According to the results, the addition of 1 ppm of VS-Co does not have any impact on the growth of barium sulphate crystals. The growth of crystals has a similar kinetics trend as the uninhibited case, and a final surface coverage and average crystals size of 19 % and 121 μm^2.

On the other hand, the surface growth of crystals remains constant from the point of injection to the end of the experiment when 4 ppm of VS-Co was injected. Again, it clear that higher concentration of scale inhibitor is needed to stop the crystal growth.

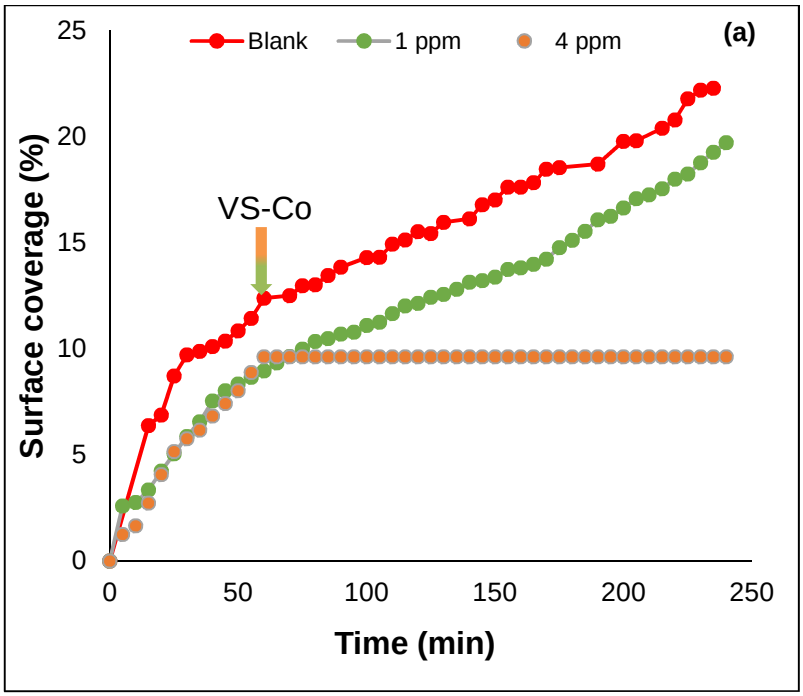

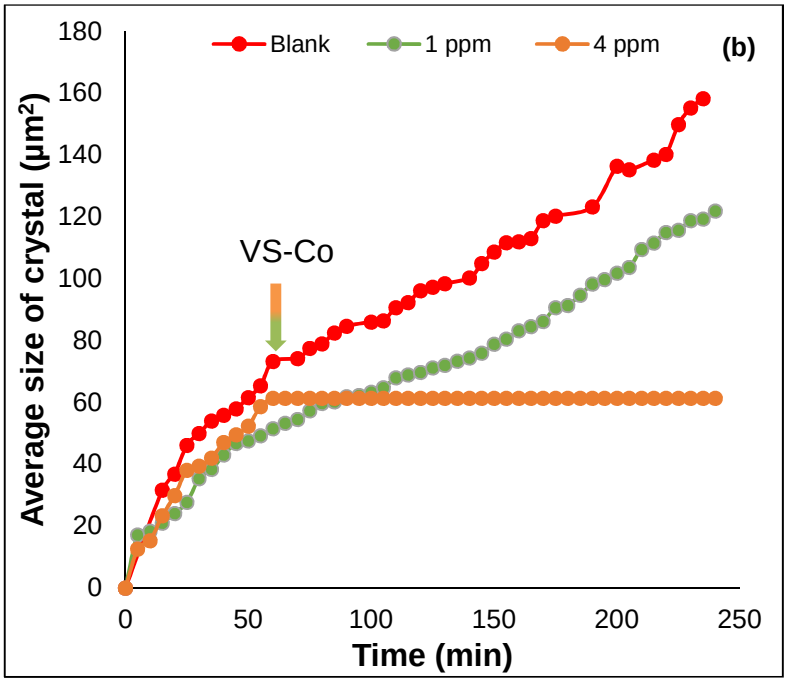

Figure 4-16: Effect of VS-Co on crystal growth of $BaSO_4$ (a) Surface coverage and (b) Average size of crystals for SR = 80 at 50°C

The SEM images of crystals formed on the stainless steel surface after adding VS-CO (1 and 4 ppm) are presented in Figure 4-17. From the images, it is obvious that there was no change in the geometry of the crystals formed in the presence of VS-Co at 1 ppm and 4 ppm. The morphology of crystals formed on the surface was similar to the uninhibited case.

The inhibition effect of VS-Co (1 and 4ppm) on the barium sulphate crystals was also confirmed using a XRD as shown in Figure 4-18. It could be observed from the results that at 1 ppm of VS-Co, the crystals faces do not seem to be influenced. The intensity of most crystal faces presented on the pattern shows no changes when 1 ppm was used. When the concentration of VS-Co was increased to 4 ppm, the result shows that the dominant face of barium sulphate crystal faces were all inhibited.

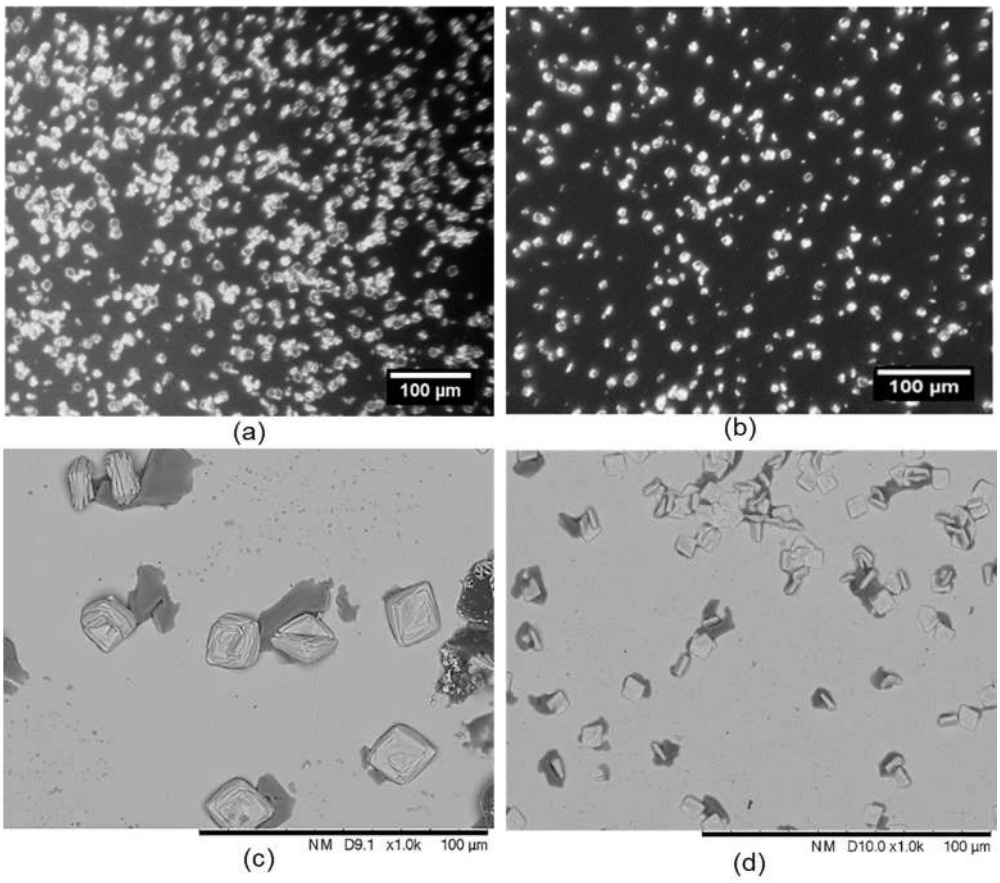

Figure 4-17: Image of $BaSO_4$ crystals captured using the camera at (a) 1 ppm (b) 4 ppm of VS-Co; and SEM images of $BaSO_4$ crystals formed on the stainless steel surface at (c) 1 ppm (d) 4 ppm of VS-Co

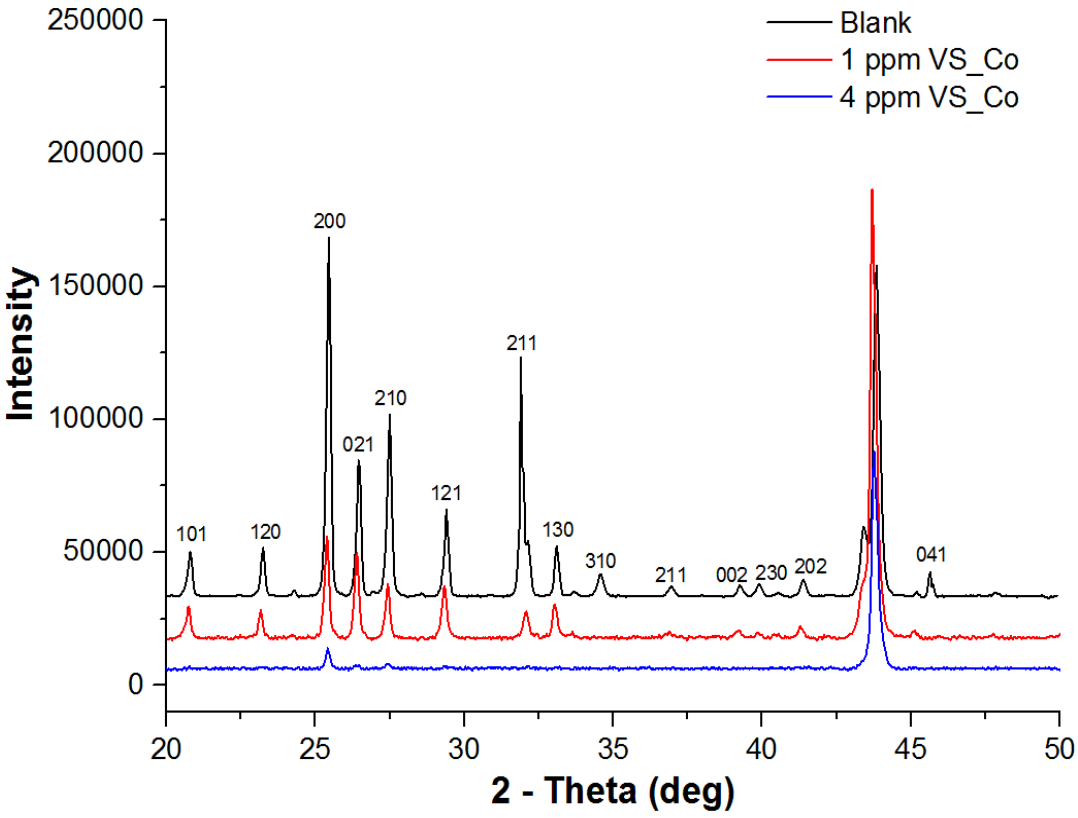

Figure 4-18: XRD diffraction pattern of $BaSO_4$ on stainless steel in the presence of VS-Co

4.5.3 Effect of DETPMP on surface scaling

The surface coverage and the average size of crystals of barium sulphate on the metal surface in the presence of 1 ppm of DETPMP is shown in Figure 4-19. From the result, it was interesting to see that the growth of crystals promotes the formation of barium sulphate rather than reducing it. The surface coverage and average size were increased by 14 % and 33 % respectively. Whereas, the addition of 4 ppm of DETPMP instantly stopped the growth of crystals. Reducing the surface coverage and average size of crystal on the metal surface by 40 % and 35 % respectively.

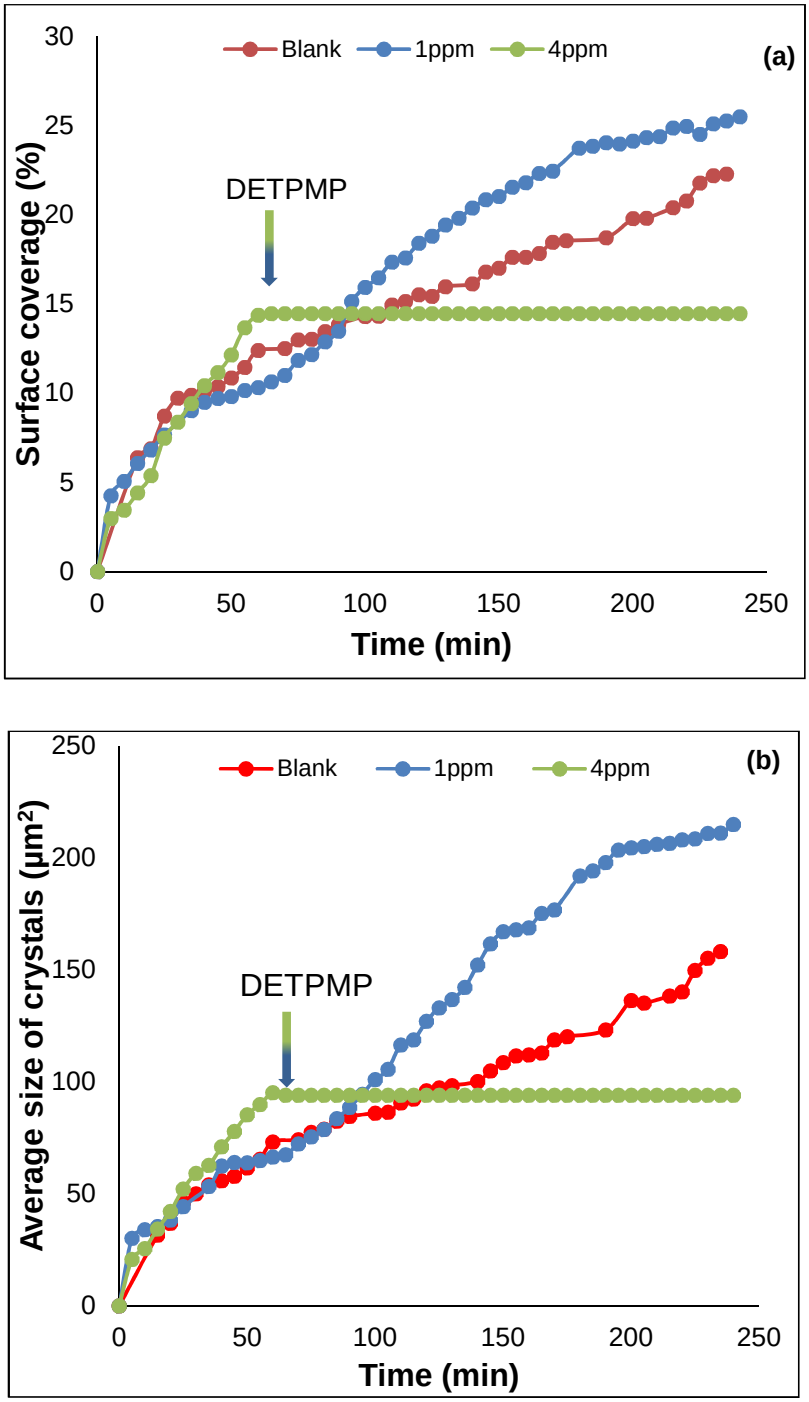

Figure 4-19: Effect of DETPMP on crystal growth of $BaSO_4$ (a) Surface coverage and (b) Average size of crystals for SR = 80 at 50°C

Figure 4-20 shows the images captured and SEM images of the crystals formed when DETPMP (1 and 4 ppm) was used. It was observed that the crystals formed on the surface when 1 ppm of DETPMP were different from crystal formed in the uninhibited test. The crystals formed seems to have different geometry and the crystals edges were feathery, which is clearly

shown at a higher magnification in Figure 4-21. However, when 4 ppm of DETPMP was used the morphology of the crystals formed were rhombic as expected. It was obvious from the image that the surface coverage was greatly reduced when 4 ppm was applied. The XRD pattern is shown in Figure 4-22 also illustrates the effect of DETPMP (1 and 4 ppm) on barium sulphate crystallography. From the results, it is observed that 1 ppm of DETPMP did not affect any of the crystal faces. However, the intensity of the dominant crystal faces were similar to the uninhibited case. At 4 ppm, all the dominant faces were very low, which reveal at this concentration the inhibitor suppresses the subsequent growth of the dominant faces.

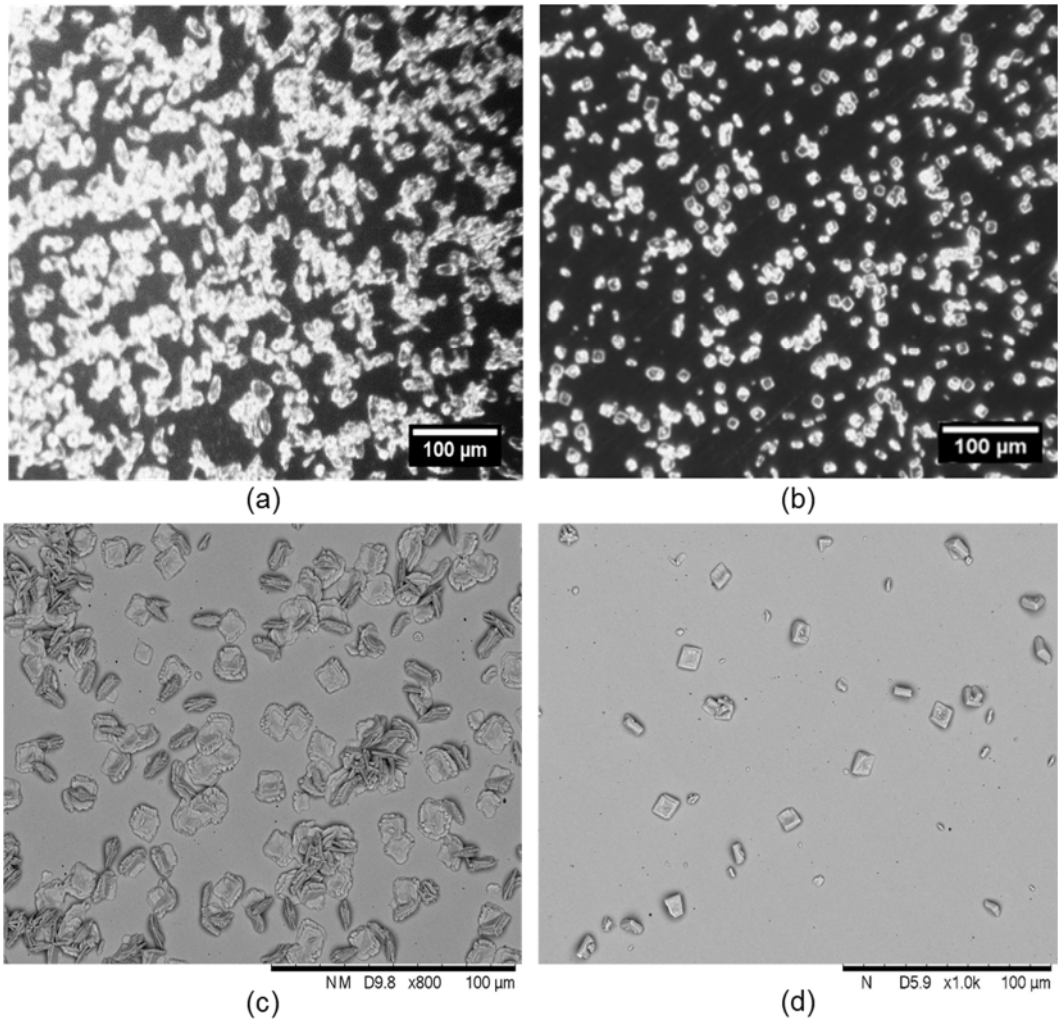

Figure 4-20: Image of $BaSO_4$ crystals captured using the camera at (a) 1 ppm (b) 4 ppm of DETPMP; and SEM images of $BaSO_4$ crystals formed on the stainless steel surface at (c) 1 ppm (d) 4 ppm of DETPMP

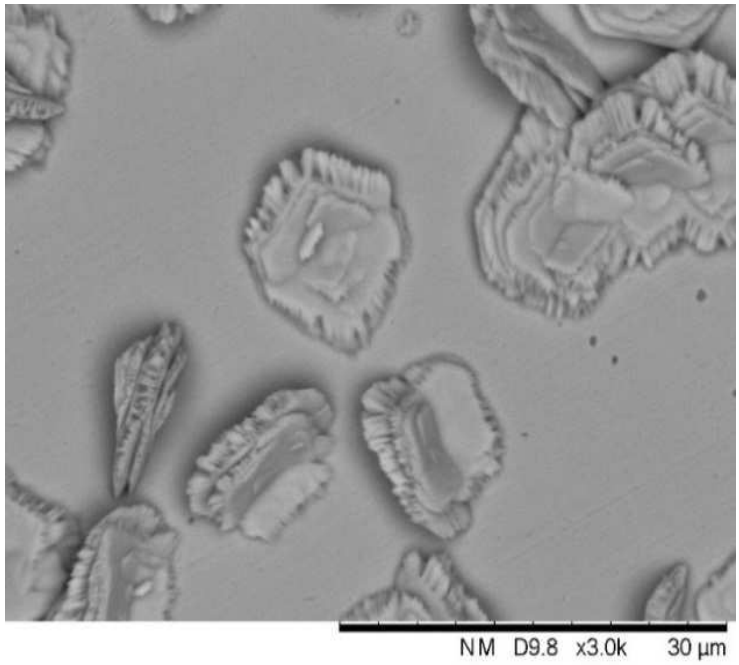

Figure 4-21: Higher magnification of SEM image with 1 ppm of DETPMP

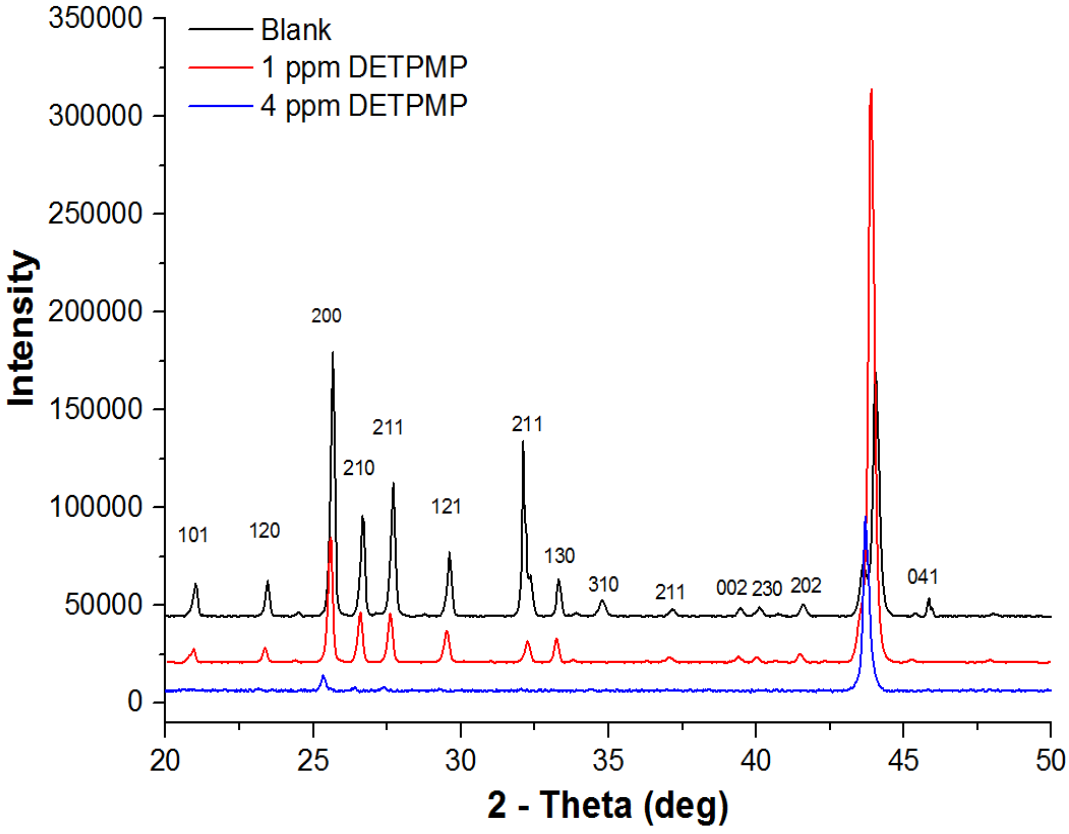

Figure 4-22: XRD diffraction pattern of $BaSO_4$ on stainless steel in the presence of DETPMP

4.6 Summary

The novel flow cell used allows experiments to be carried out under constant thermodynamic conditions which provide a more realistic scaling environment than conventional bulk jar tests. Also, the results show a valuable insight in the crystallization process of barium sulphate. The major key findings are:

- The results show that despite the absence of bulk precipitation of barium sulphate, surface scaling can occur.
- Temperature and saturation ratio not only affect the kinetics of surface deposition of nucleation and growth, it also affects the mechanism of barium sulphate deposition on surfaces.
- The results show that PPCA was effective to stop the growth of $BaSO_4$ even at low concentration (1 ppm).
- DETEMP was seen to enhance surface scaling at 1 ppm, and it also changes the morphology of the $BaSO_4$ crystals formed.
- VS-Co was not effective to stop the growth of barium sulphate at 1 ppm.
- All scale inhibitors instantly stopped the growth of crystals at high concentration of 4 ppm.

The results have shown that the three scale inhibitors performed differently at a low concentration. Also, it was shown that PPCA was seen to have a better surface inhibition at a lower concentration to stop the subsequent growth of crystals. The next chapter present factors that could affect the surface inhibition of mineral scale using PPCA.

Chapter 5 Factors affecting barium sulphate surface growth inhibition

5.1 Introduction

The performance of scale inhibitors in oilfield operations is the main concern of field operators. Data is needed to enable them to make efficient decisions that ensure the control and prevention of scale. These decisions are based on assessing the performance of scale inhibitors under various operating conditions such as pressure, temperature, hydrodynamic conditions and brine composition. In terms of evaluating the effectiveness of these conditions on scale inhibitor efficiency, extensive studies have been conducted to understand the kinetics of scale bulk precipitation [24-26]. In spite of the research conducted on bulk precipitation, there is still a lack of understanding of surface deposition and growth of crystals on equipment surfaces. Moreover, studies have shown that the kinetics of bulk and surface deposition are different [29, 30].

In this chapter, the *in-situ* flow cell was used to study factors that could affect the performance of Polyphosphinocarboxylic acid (PPCA) scale inhibitor in preventing surface fouling of $BaSO_4$ on stainless steel. The experiment examined distinct conditions, such as saturation ratio, pre-scaled surfaces, flow rate, and interval injection of scale inhibitor. The structure of the experimental results presented in this chapter is shown in Figure 5-1.

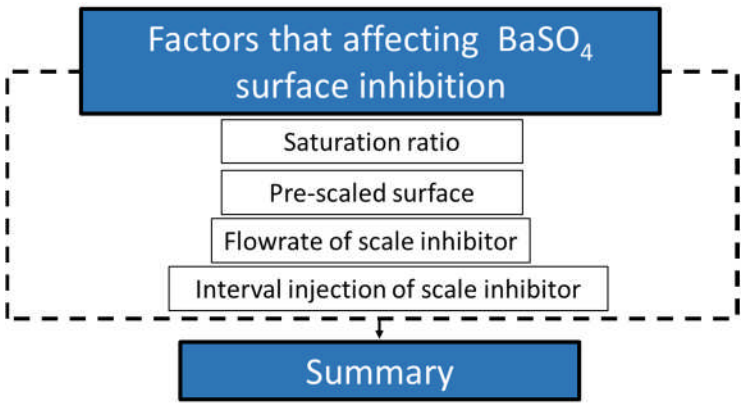

Figure 5-1: Outline of chapter 5

5.2 Brine composition

The supersaturation conditions required for the formation of barium sulphate scale were achieved by mixing two incompatible brines as mentioned in chapter 3. North sea seawater (NSSW) provided the source of anions (SO_4^2) while Formation Water (FW) the source of cations (Ba^{2+}). In this chapter, three different brines with SR = 30, 60 and 80 were used. The composition of the brines used is presented in Table 5-1 and Table 5-2; the brines were mixed 50:50 at a temperature of 50°C

Table 5-1: Composition of brine solution

Ion	Formula	Conc./ppm (NSSW)	Conc./ppm(FW)
Na	NaCl	10890	31275
Ca^{2+}	$CaCl_2.6H_2O$	428	2000
Mg^{2+}	$MgCl_2.6H_2O$	1366	739
K	KCl	460	654
Ba^{2+}	$BaCl_2.2H_2O$	0	See table 5-2
Sr^{2+}	$SrCl_2.6H_2O$	0	771
SO_4^{2-}	Na_2SO_4	See table 5-2	0

Table 5-2: SO_4^{2-} and Ba^{2+} in ppm

Temp	50°C	
SR	**SO_4^{2-}**	**Ba^{2+}**
30	500	65
60	700	80
80	800	110

5.3 Bulk precipitation

The inhibition efficiency test of 1 ppm of PPCA on bulk precipitation was determined for the three different brine solutions at 2 and 22 hours using the bulk jar test. For the three brines used, the inhibition efficiency values were above 95 % (*i.e.* above the MIC) for both 2 and 22 hours as shown in Figure 5-2.

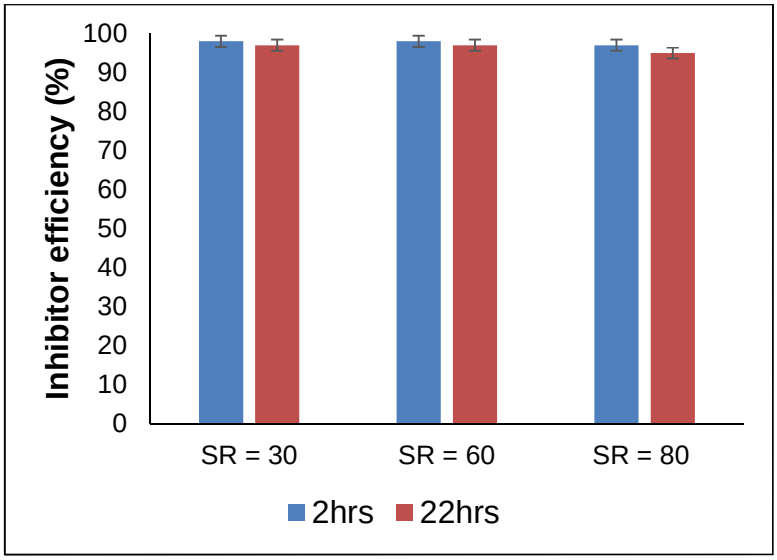

Figure 5-2: $BaSO_4$ Inhibition Efficiency test of brine solutions (SR 30, 60 and 80) using 1 ppm of PPCA

5.4 Effect of saturation ratio on surface inhibition efficiency of PPCA

The effect of saturation ratio has been shown in chapter 4 to greatly influence the surface fouling of barium sulphate on metallic surfaces. In this section, the effect of saturation ratio (30, 60 and 80) on surface inhibition using 1 ppm of PPCA scale inhibitor was examined. The flow rate used for this study was 20 $mlmin^{-1}$ and test duration was 4 hours. In all three scenarios, prior to the injection of scale inhibitor, the metallic surface was pre-scaled for a period of 1 hour during which no inhibitors were present.

Figure 5-3 shows the effect of continuous injection of 1 ppm PPCA on surface fouling at SR = 30. From the results, it is clear that surface growth of crystals

stopped almost immediately after injecting the inhibitor, with a surface coverage and an average crystal size of 3 % and 53 μm^2 respectively. PPCA is known to have good adsorption properties on minerals [26, 105, 116]. Hence, the instantaneous inhibition indicates that the active sites were completely blocked after injecting the inhibitor. When 1 ppm of PPCA was injected at SR = 60, the growth of crystals continued for about 15 minutes before it stopped as shown in Figure 5-4. In this case, the surface coverage and average size of crystals were 6 % and 55 % respectively.

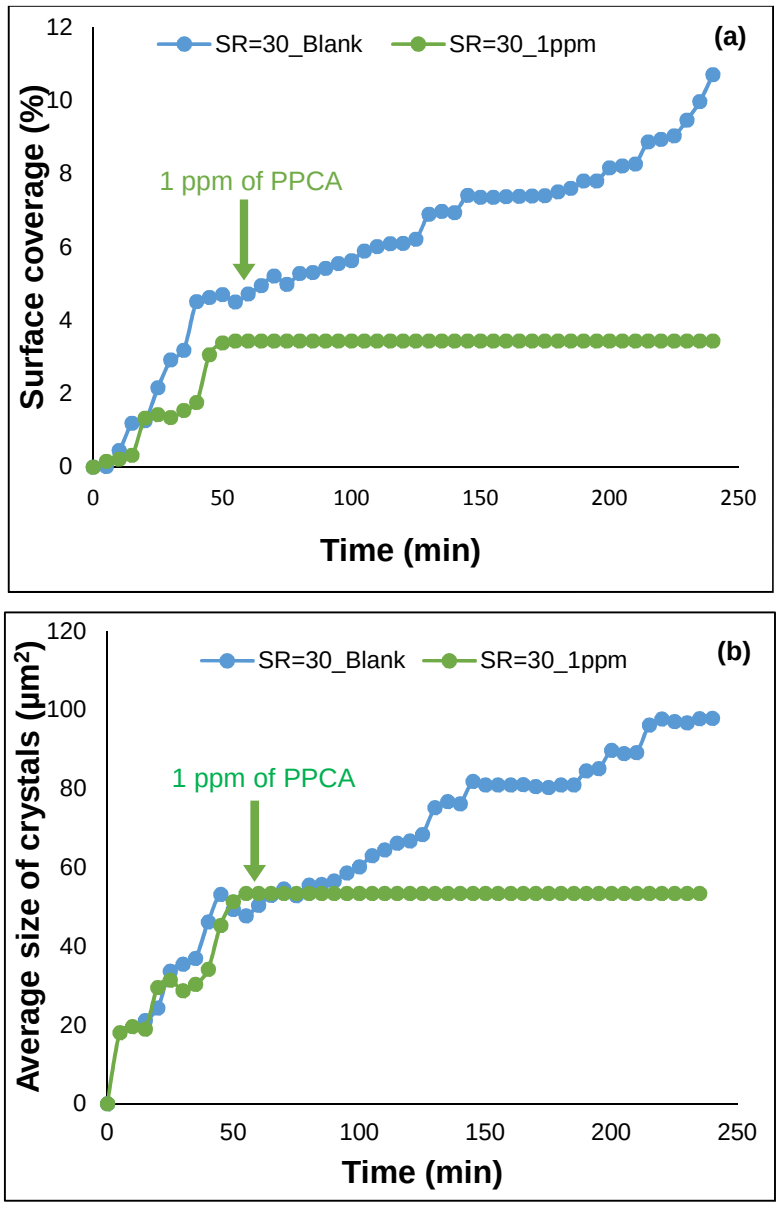

Figure 5-3: Effect of PPCA (1 ppm) on crystal growth of $BaSO_4$ (a) Surface coverage and (b) Average size of crystals at SR = 30 and 50°C

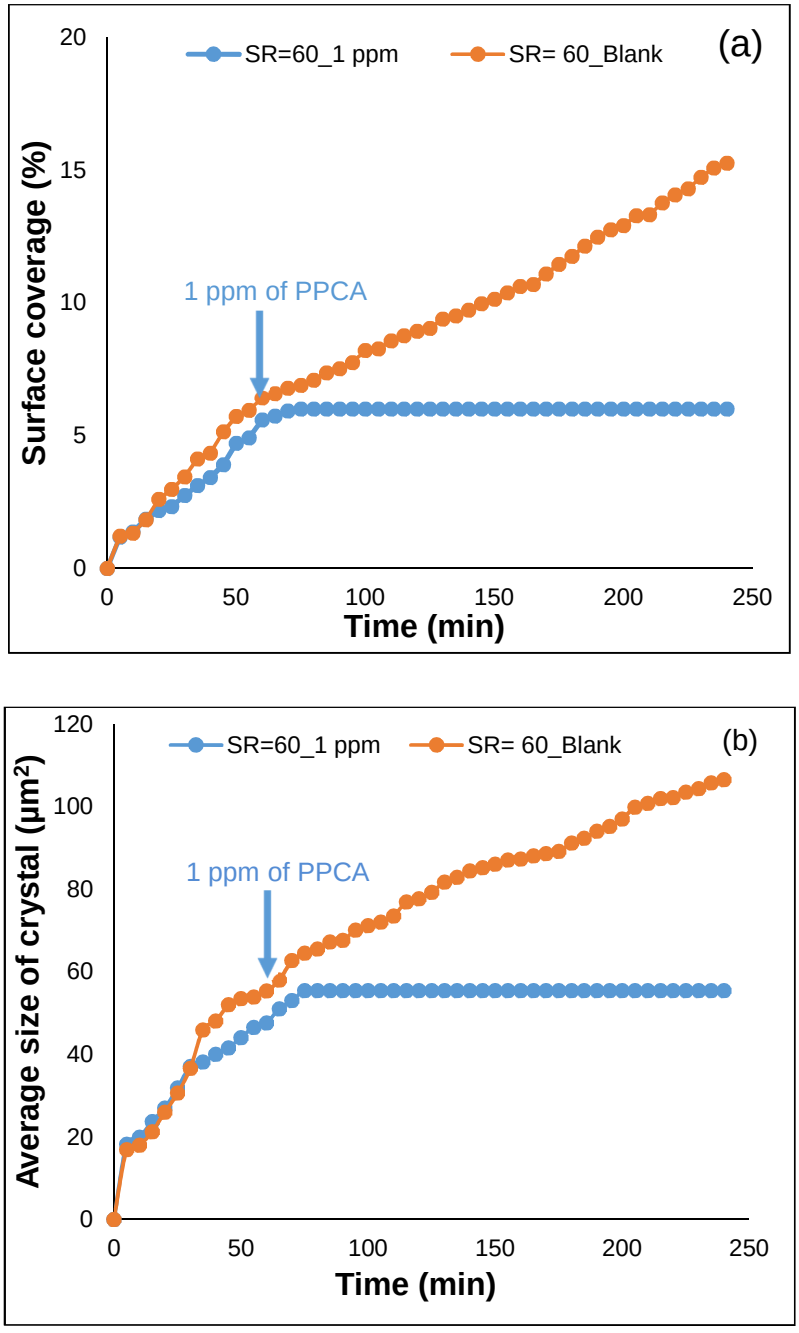

Figure 5-4: Effect of PPCA (1 ppm) on crystal growth of $BaSO_4$ (a) Surface coverage and (b) Average size of crystals at SR = 60 and 50°C

However, when PPCA is injected at higher saturation ratio (SR = 80), surface growth continued for 60 minutes before reaching a plateau as shown in Figure 5-5. In this case, there was only a slight impact of the scale inhibitor on the surface growth of crystals. The surface coverage and average size of crystals were 20 % and 132 % respectively. From these results, it can be observed

that the inhibition of surface scaling by PPCA was significantly affected by the increase of saturation ratio. The time required to stop crystal growth increased as the SR was increased. This is not as expected since 1 ppm of PPCA showed similar performance in preventing bulk precipitation for all brines.

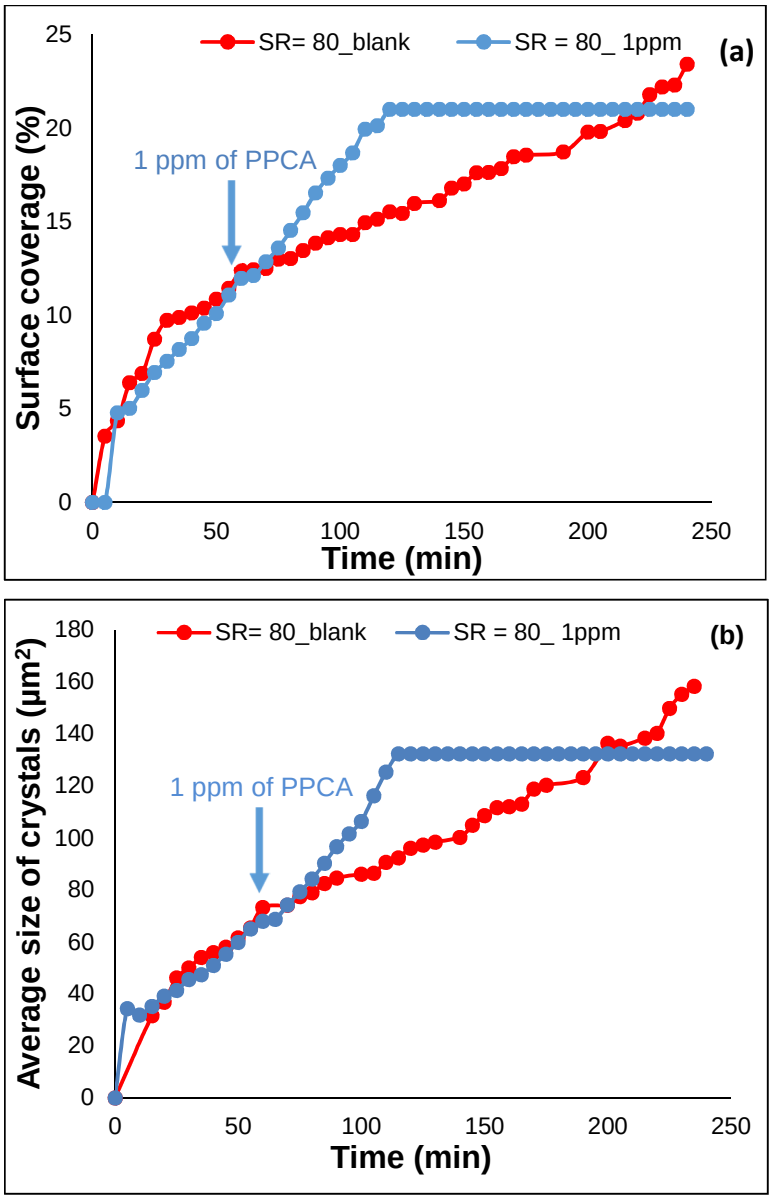

Figure 5-5: Effect of PPCA (1 ppm) on crystal growth of $BaSO_4$ (a) Surface coverage and (b) Average size of crystals at SR = 80 and 50°C

In terms of the effect of PPCA (1 ppm) on the morphology of the scale formed, the crystals formed for the three brines with SR (30, 60 and 80) are presented in Figure 5-6. From the images captured, it was observed that there was no

change in morphology of the crystals on the stainless steel surface for the three brines used; the crystals formed were all rhombic as expected. However, the size of crystals formed on the stainless steel surface increase as the saturation ratio was increased. This can be ascribed to the increase in thermodynamic driving force, which promotes the nucleation and growth of crystals.

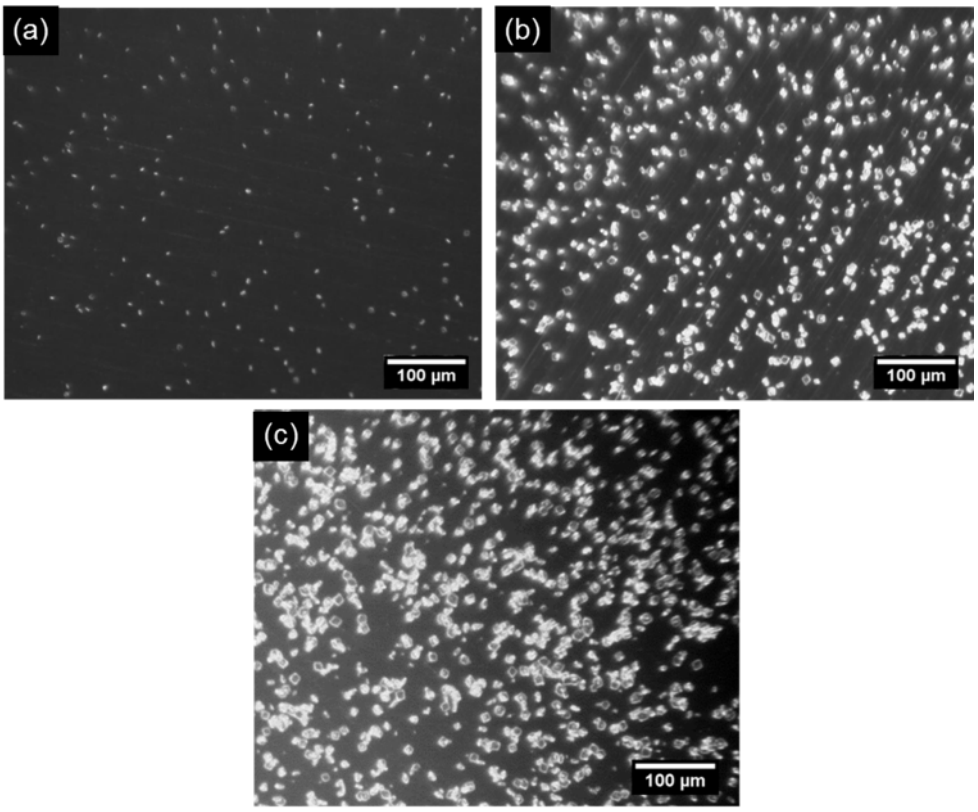

Figure 5-6: Image of $BaSO_4$ crystals formed on a metal surface at (a) SR=30 (b) SR=60 and (C) SR=80

5.5 Effect of flow rate on surface inhibition efficiency of PPCA

It is well understood that flow rate plays a vital role on the scale precipitation and surface deposition processes [120]. It is also important to understand the effect of flow rate on surface inhibition, since the transport of scale inhibitor molecules to the active sites of the crystal is often controlled by mass transport. The surface inhibition studies were conducted using three flow rates (20 $mlmin^{-1}$, 40 $mlmin^{-1}$ and 60 $mlmin^{-1}$). All flow rates used during the test

were laminar as discussed in chapter 3. A brine with SR=80 and 1 ppm of PPCA was used during the experiment. Prior to injection of the scale inhibitor at different flow rates, the stainless steel surface was pre-scaled for 1 hour at a flow rate of 20 mlmin^{-1}. Figure 5-7 presents the effect of surface fouling at different flow rates.

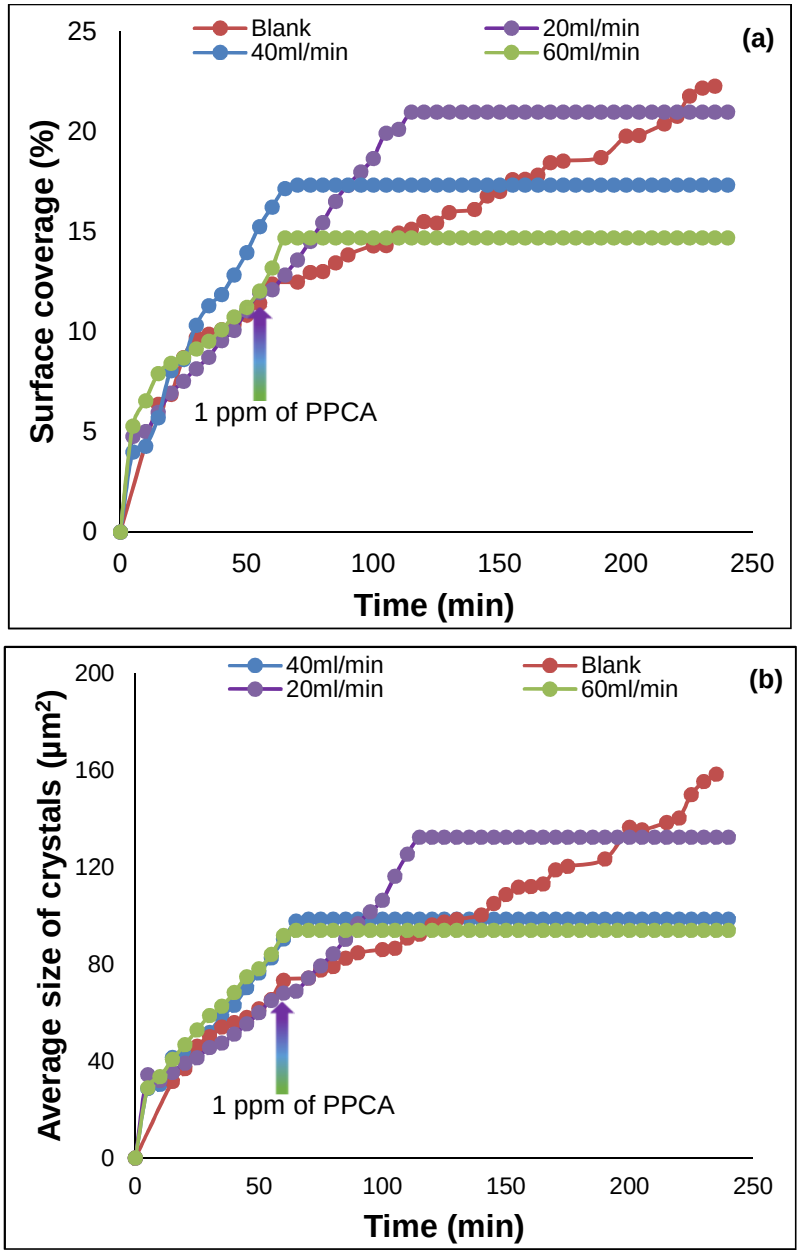

Figure 5-7: Effect of flow rate on crystal growth of $BaSO_4$ (a) Surface coverage and (b) Average size of crystals

From the results presented, it is obvious that increase in flow rate reduces the surface growth of $BaSO_4$. For instance, at a flow rate of 60 ml/min^{-1} it took

about 5 minutes for the surface growth of crystals to stop, whereas when the flow rate was reduced to 20 $mlmin^{-1}$, it took about 1 hour for surface growth of crystals to stop. The image of $BaSO_4$ formed on the stainless steel in the presence of PPCA at different flow rates at the end of each test are presented in Figure 5-8. From the figure, it is evident that the performance of PPCA was favoured by increasing the flow rate.

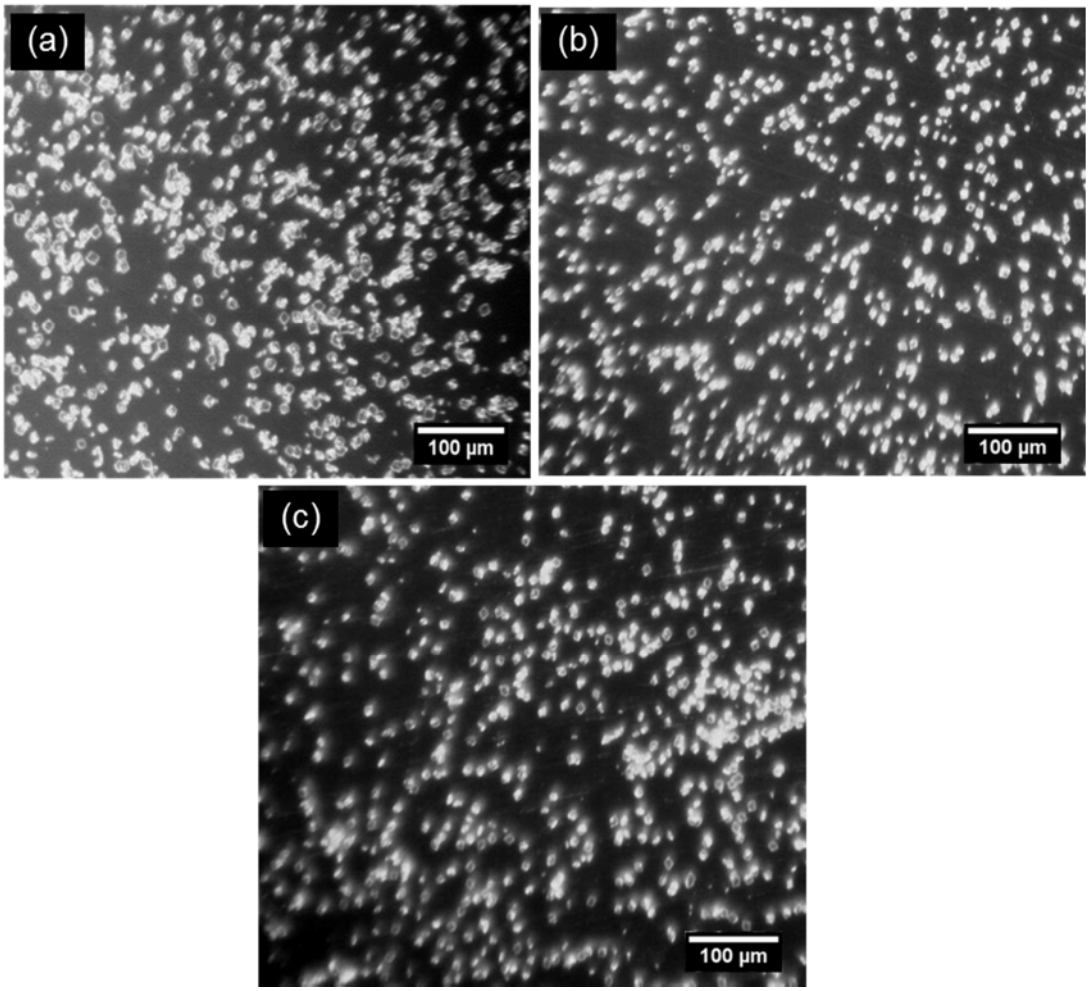

Figure 5-8: BaSO4 deposited on the stainless steel at a flow rate of (a) 20 $mlmin^{-1}$ (b) 40 $mlmin^{-1}$ and (c) 60 $mlmin^{-1}$ after 4 hours

5.6 Effect of a pre-scaled surface on surface inhibition efficiency of PPCA

In oilfield operations, pipelines are often used for several years before inhibitors are required. Hence, prior to the injection of inhibitors, the pipelines

would have been covered with different scale products such as iron carbonate, calcium carbonate, and barium sulphate scale. These products might significantly affect the performance of the scale inhibitors. Thus, there is a need to investigate the problem associated with pre-scaled product on the performance of scale inhibitor. In order to determine the effect of pre-scaled surfaces on surface inhibition efficiency, surfaces were subjected to scaling with a brine of SR=80 for a different period of time (15, 30 and 60 minutes); before 1 ppm of PPCA was injected. The different time of pre-scaling increases the amount of scale formed on the metal sample before injecting the scale inhibitor as shown in Figure 5-9.

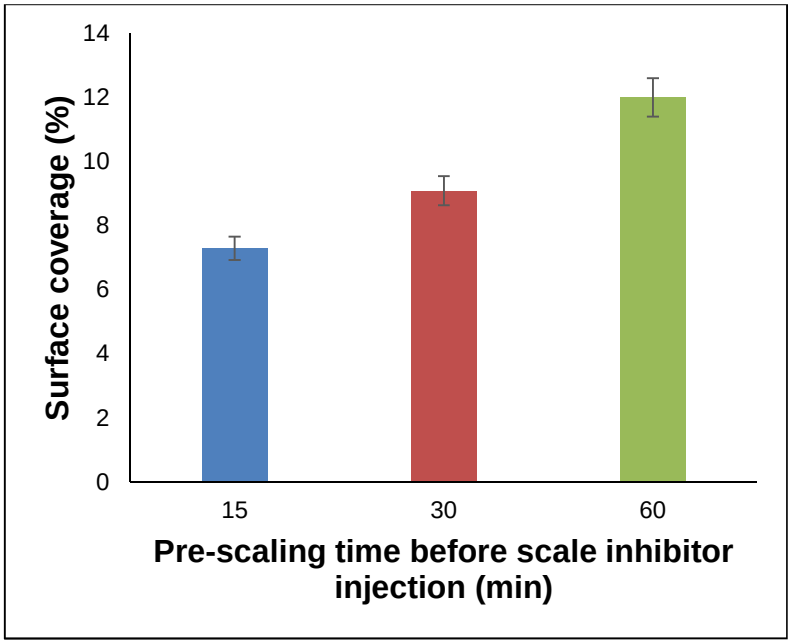

Figure 5-9: Surface coverage of $BaSO_4$ at different pre-scaling time (15, 30 and 60 minutes)

Figure 5-10 presents the effect of a pre-scaled surface on the surface coverage and average size of crystals formed when 1 ppm of PPCA was injected. The results show that the time necessary to fully stop crystal growth increased with increase in injection time. For example, the percentage surface coverage of crystals at 15 minutes and 60 minutes of injection were 7% and 12% respectively. From Figure 5-11, it is obvious that the performance of PPCA was favoured as the amount of pre-scaled surface decreases.

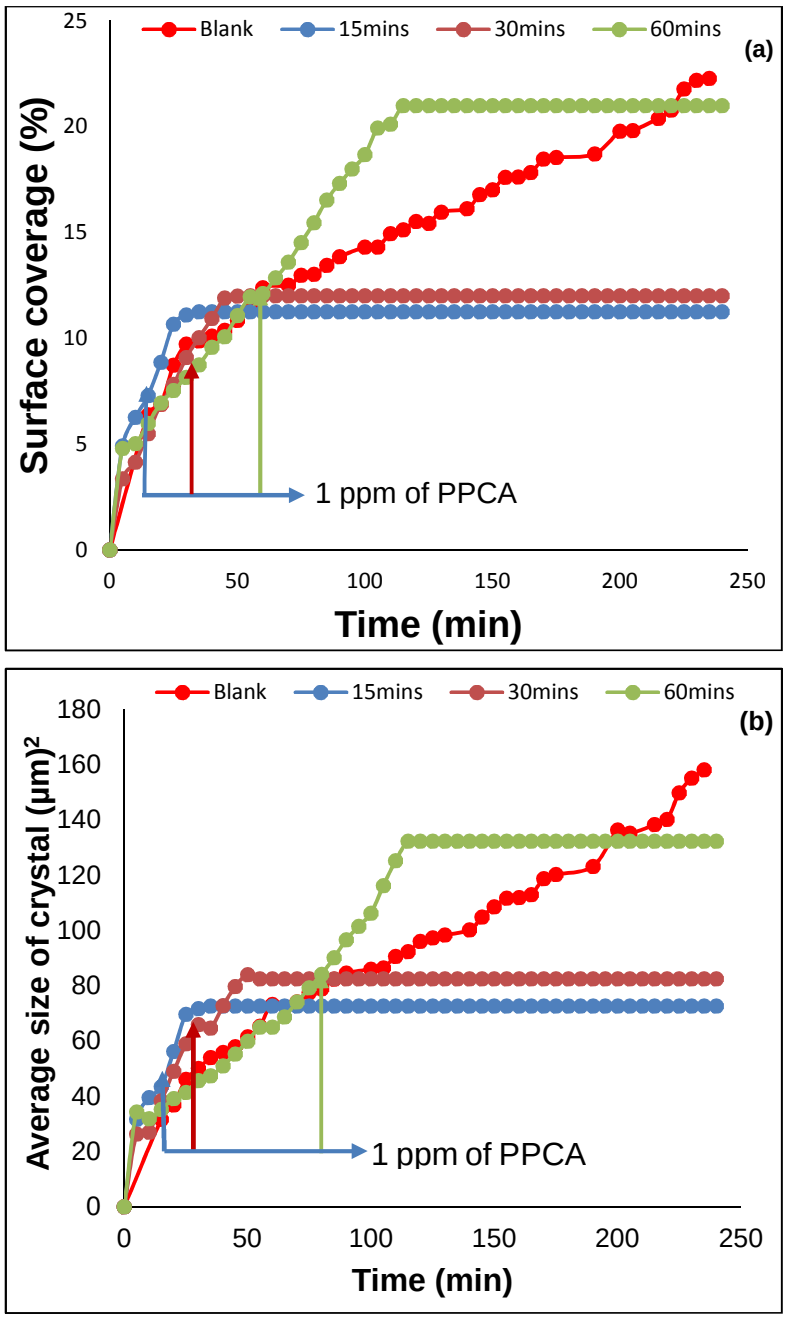

Figure 5-10: Effect of pre-scaled surface on crystal growth of $BaSO_4$ (a) Surface coverage and (b) Average size of crystals

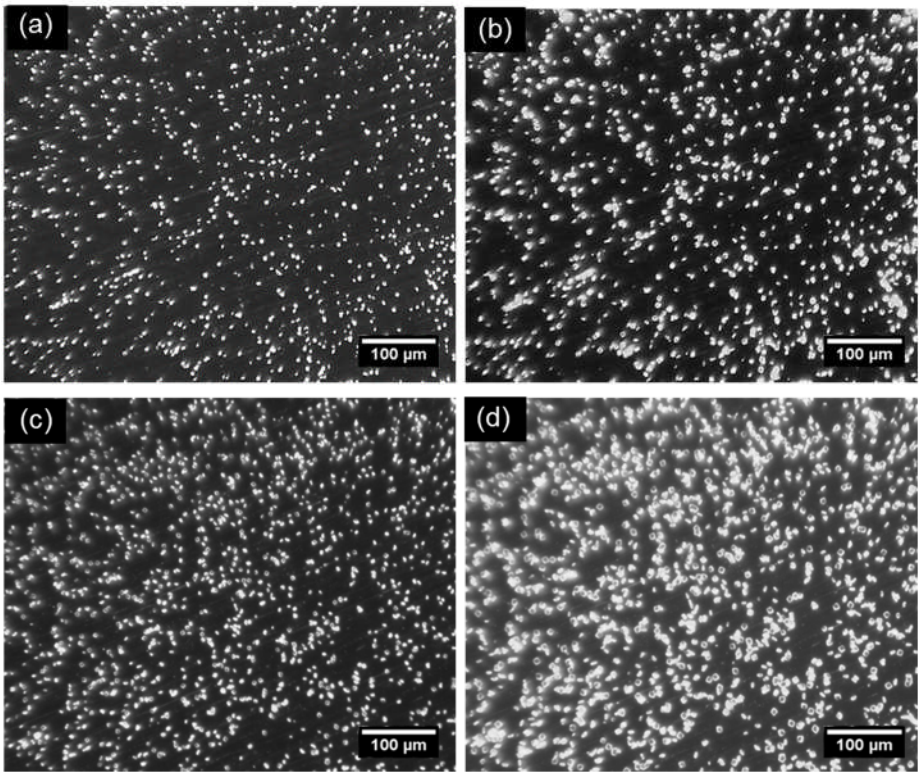

Figure 5-11: Image captured of $BaSO_4$ scale deposited on stainless steel (a) pre-scaled for 15 minutes, (b) and 4 hours after injecting scale inhibitor, (c) pre-scaled for 30 minutes, and (d) 4 hours after injecting scale inhibitor

5.7 Effect of inhibitor interval injection

In previous sections, experiments were carried out by injecting the scale inhibitors continuously. However, when scale inhibitors are injected downhole, it faces some challenges, many of which are associated with the efficiency of injection valves [123, 124]. One of the functions of injection valves is to prevent fluid from entering the injection line. The valve closes when the wellbore pressure is higher than the crack pressure; thus preventing wellbore fluids from flowing into the injection line. The valve remains closed until the pressure in the injection line increases to start the flow. This change in pressure implies that the injection of the chemical inhibitor into the wellbore would not be constant as required but fluctuate due to the periodic opening and closing of the check valve [125]. Hence, the application of scale inhibitor during down-

hole continuous injection may not be continuous; chemicals are sometimes injected into the wellbore intermittently.

The question is how does this periodical injection of scale inhibitor affect the scale inhibition efficiency? In order to evaluate this effect, 1 and 4 ppm of PPCA were injected periodically (15 and 30 minutes) using SR=80 at 50ºC. For simplicity, Figure 5-12 give a graphical illustration of the experiment procedure. Figure 5-13 presents the surface coverage and crystal size as PPCA is injected at 30 minute intervals. From the results, it was observed that after injecting the scale inhibitor the growth of crystals stopped after some minutes. However, it continued to grow when the system was uninhibited. This process continued until the end of the experiment. The final surface coverage and the average size of crystals were 19 % and 113 μm^2 respectively, which is higher when compared to continuous injection of scale inhibitor. This is expected as a higher volume of scale inhibitor was used during continuous injection when compared to interval injection of scale inhibitor as shown in Figure 5-15.

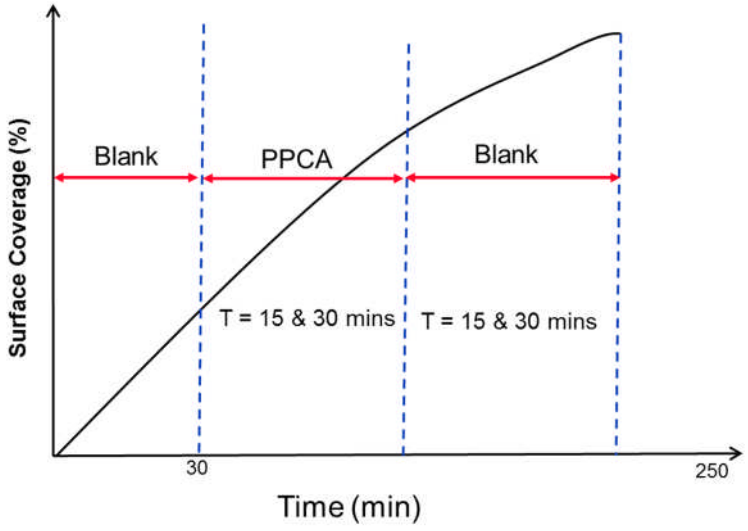

Figure 5-12: Schematic diagram illustrating the periodic injection of scale inhibitor for 15 and 30 minutes.

Nevertheless, when the inhibitor concentration was increased to 4 ppm there was little change in scale inhibitor performance. The surface coverage and average were 18 % and 107 μm^2 respectively. With such a similar surface

coverage and average size of crystals, it shows that there is no benefit of increasing the concentration of PPCA. Figure 5-14 shows the SEM image of scale formed at 30 minutes interval of PPCA. It was observed that the scale formed on the metallic sample was different from when scale formed when the inhibitor was injected continuously. In the case of the interval injection barite scale was formed layer by layer.

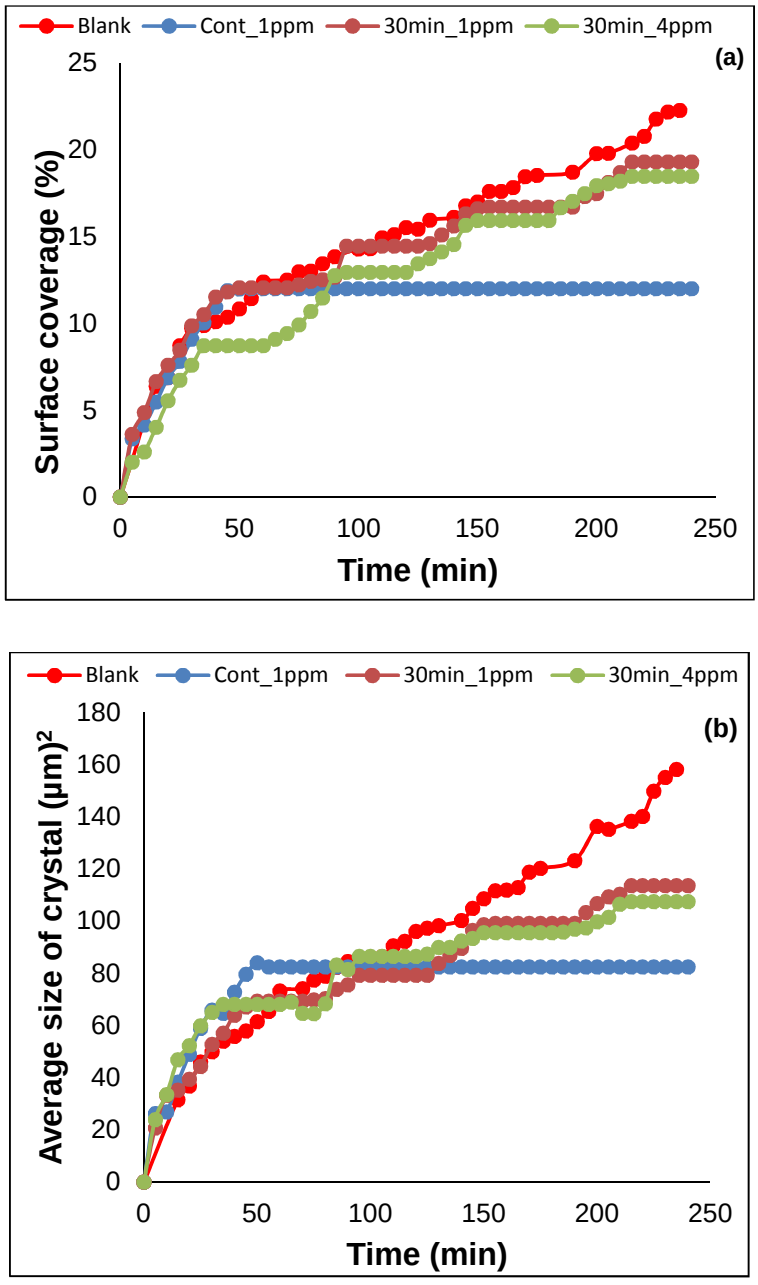

Figure 5-13: Effect of 30 minutes interval injection of PPCA (1 and 4 ppm) on crystal growth of $BaSO_4$ (a) Surface coverage and (b) Average size of crystals

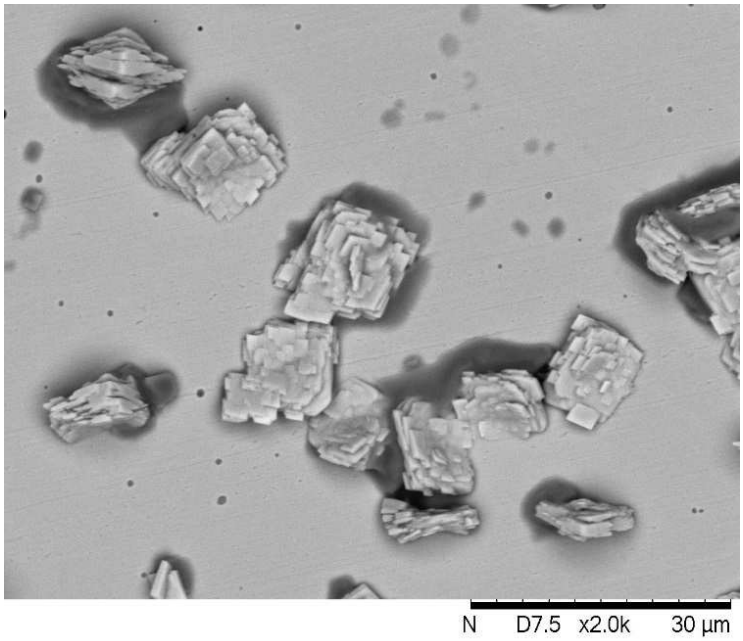

Figure 5-14: SEM image of $BaSO_4$ formed on the metal surface during 30 minutes interval injection after 4 hours

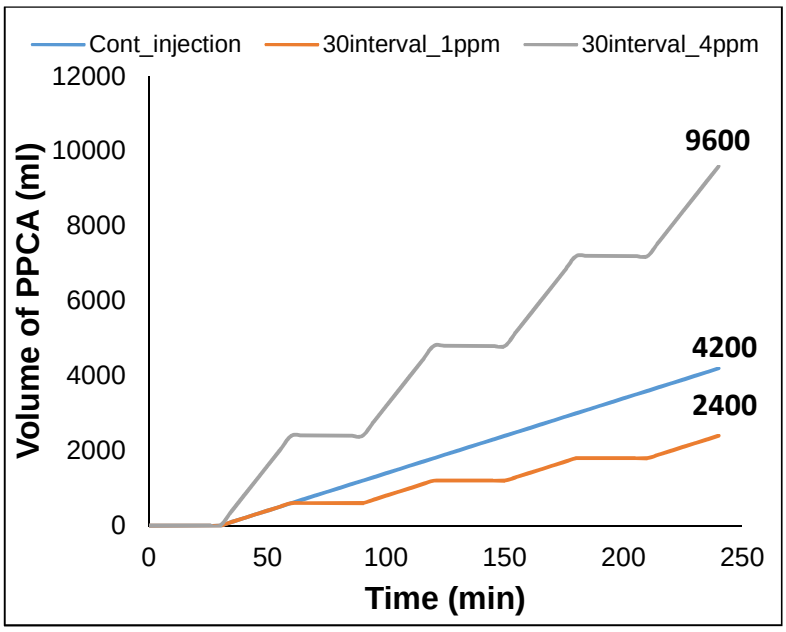

Figure 5-15: Volume of scale inhibitor used

Figure 5-16 shows the surface coverage and average size of crystals when PPCA (1 and 4 ppm) was injected for 15 minutes periodically. The surface coverage and average size of crystals show a similar trend when compared to 30 minutes interval injection of PPCA. However, the results show a better

surface inhibition when compared to 30 minutes interval injection. Also, it can be observed that the crystals formed on the stainless steel surface were different from that of 30 minutes interval injection. In this cases, smaller crystals were formed on the steel surface as shown in Figure 5-17.

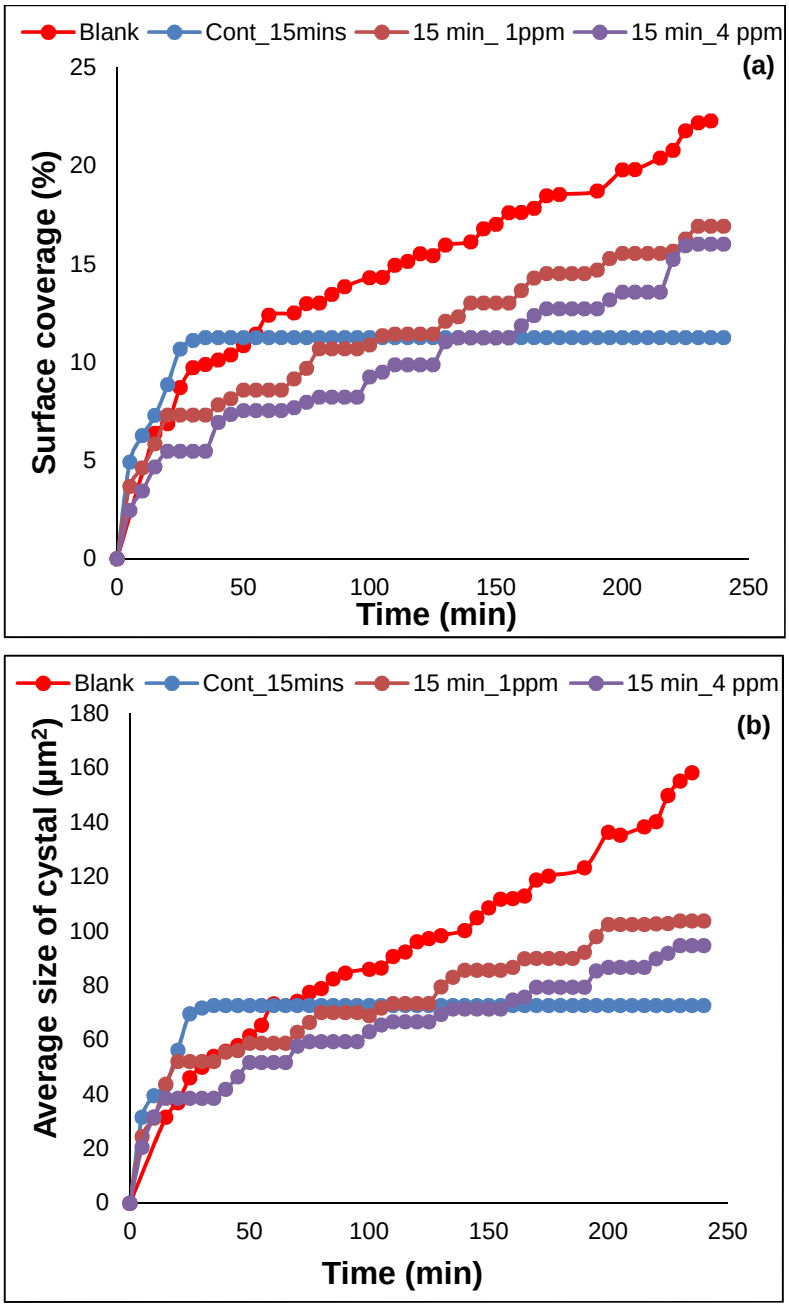

Figure 5-16: Effect of 15 minutes interval injection of PPCA (1 and 4 ppm) on crystal growth of $BaSO_4$ on (a) Surface coverage and (b) Average size of crystals

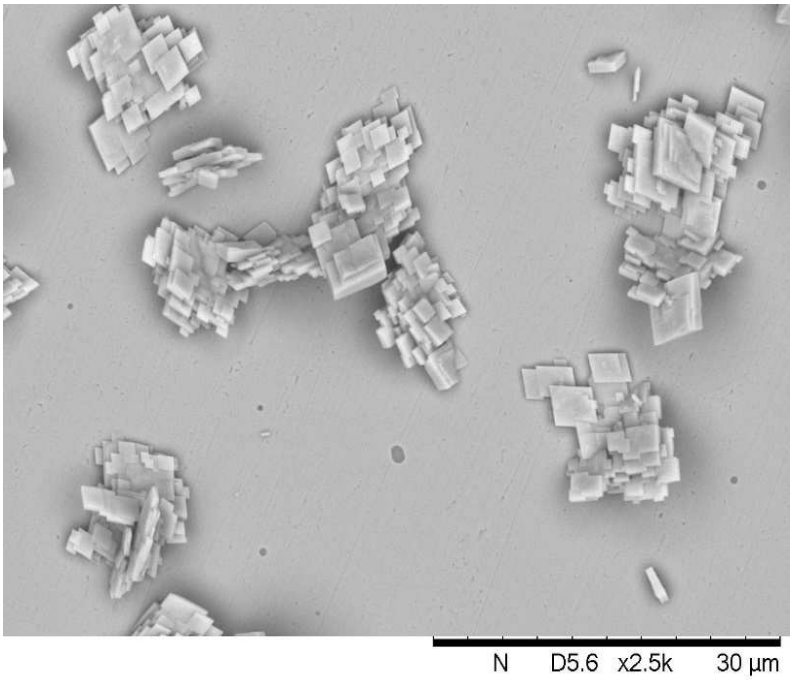

Figure 5-17: SEM image of $BaSO_4$ formed on the metal surface during 15 minutes interval injection after 4 hours

5.7.1 Evaluating the optimum time required to prevent nucleation and growth of crystals

From section 5.7, it was observed that the periodic injection of chemical scale injector reduces the efficiency of scale inhibitors. The surface growth of crystals continues when the injection of scale inhibitor was stopped. However, it can be seen that the scale performance was better when the time of interval injection was reduced from 30 minutes to 15 minutes. This implies that an optimum time (*i.e*. time required for the system to be inhibitor-free, without observing nucleation and subsequent growth of crystals) can be evaluated during the interval injection of scale inhibitor.

In order to investigate the optimum time, the same condition used in section 5.7 was used. However, 1 ppm of PPCA is injected periodically for 30 minutes in the first 1 hour, afterwards the system is left uninhibited (5 and 10 minutes) before re-injecting the scale inhibitor for another 30 minutes. This process is repeated till the end of the experiment. For simplicity, Figure 5-18 gives a schematic illustration of the experimental procedure.

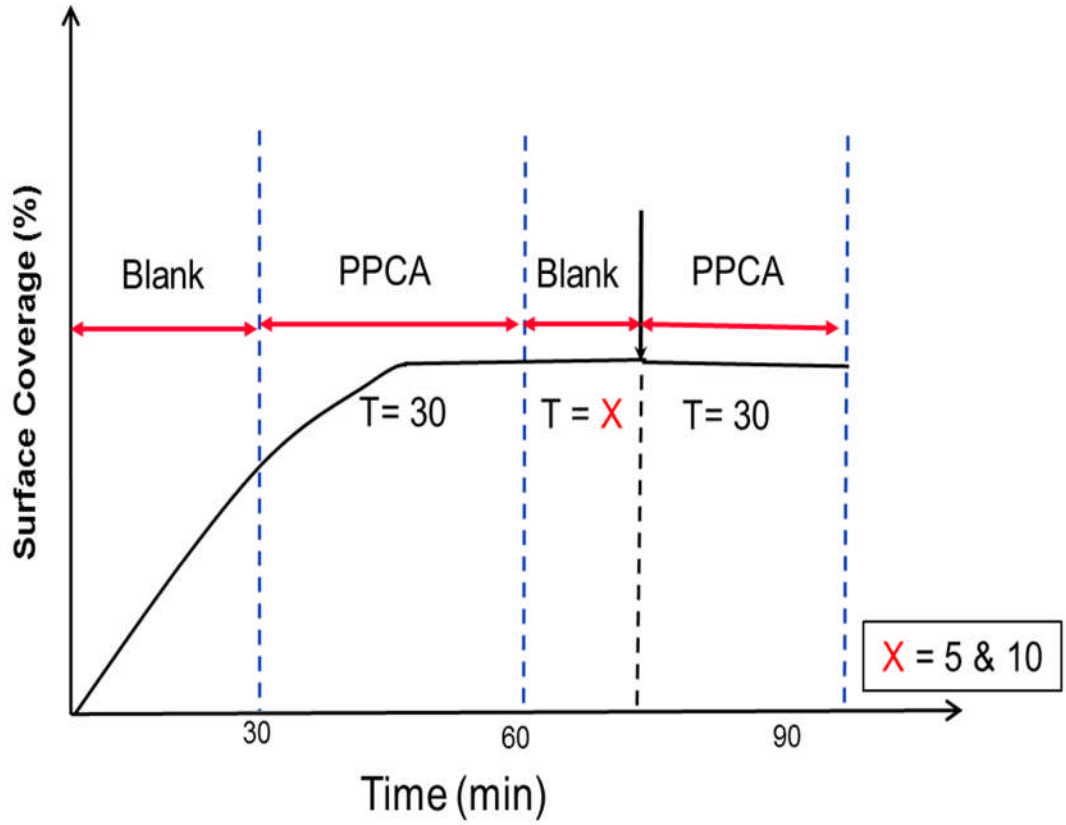

Figure 5-18: Schematic diagram simulating optimum time required to prevent surface growth during periodic injection of scale inhibitor

Figure 5-19 shows the surface coverage of scale deposited on the stainless steel surface when the system was left uninhibited for 10 minutes. It was observed from the results that the surface growth of crystal stopped when the scale inhibitor was injected, but slightly increased when the system was left uninhibited. The surface coverage was reduced to 14 % at the end of the experiment. The SEM image shown in Figure 5-20 shows little crystals growth on edges of crystals already formed on the metal surface. This suggests that the shorter the system is left uninhibited, the lesser scale deposit on the stainless steel surface.

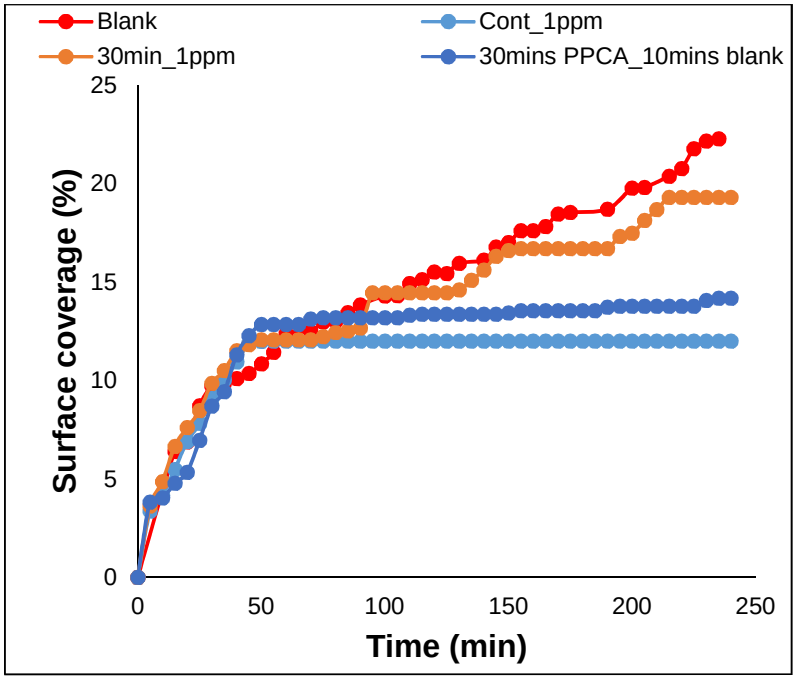

Figure 5-19: Surface coverage of $BaSO_4$ deposited on stainless steel surface when the system was uninhibited for 10 minutes and inhibited for 30 minutes for 4 hours

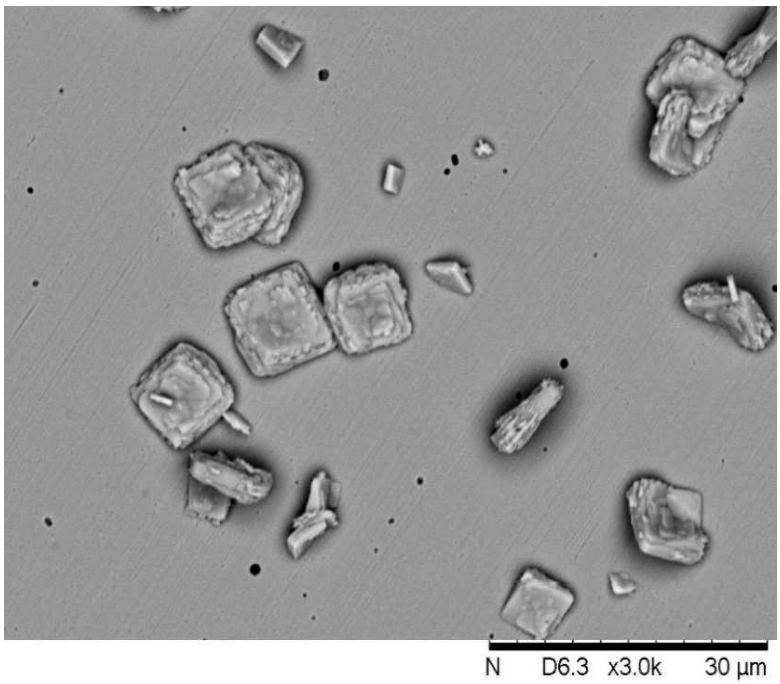

Figure 5-20: SEM image of $BaSO_4$ formed on the stainless steel surface leaving the system uninhibited every 10 minutes for 4 hours

Figure 5-21 shows the surface coverage of scale deposited on the stainless steel surface when the system was left uninhibited for 5 minutes. The results show that there was no increase in the percentage of surface coverage of the crystal on the stainless steel surface. The SEM image presented in Figure 5-22 also revealed that no crystals formed on the pre-existing crystals as previously shown in Figure 5-20. This result suggests that 5 minutes interval is the optimum time the system could be left uninhibited to prevent nucleation and subsequent growth of crystals on the stainless steel surface.

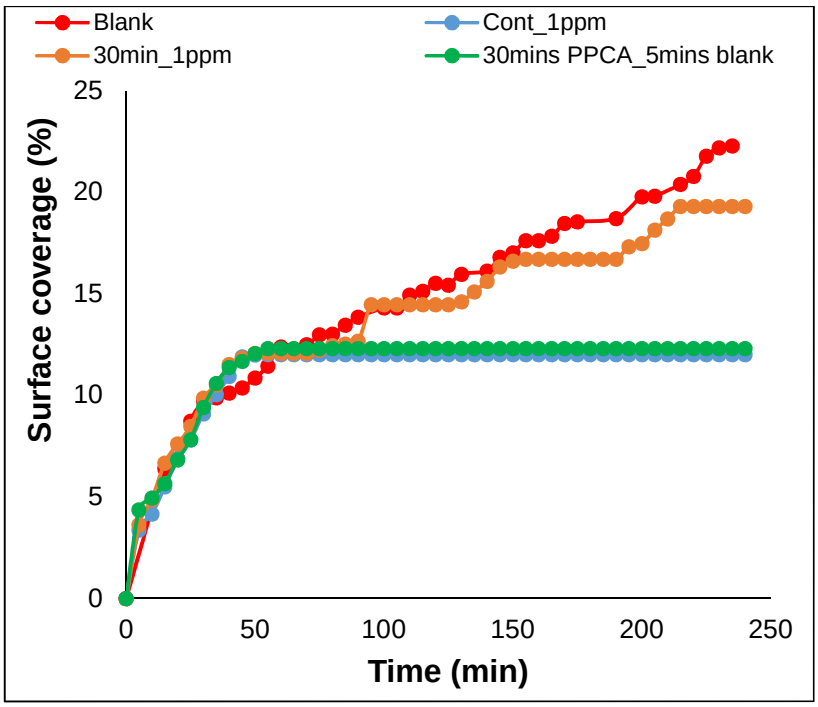

Figure 5-21: Surface coverage of $BaSO_4$ deposited on stainless steel surface when the system was uninhibited for 5 minutes and inhibited for 30 minutes for 4 hours

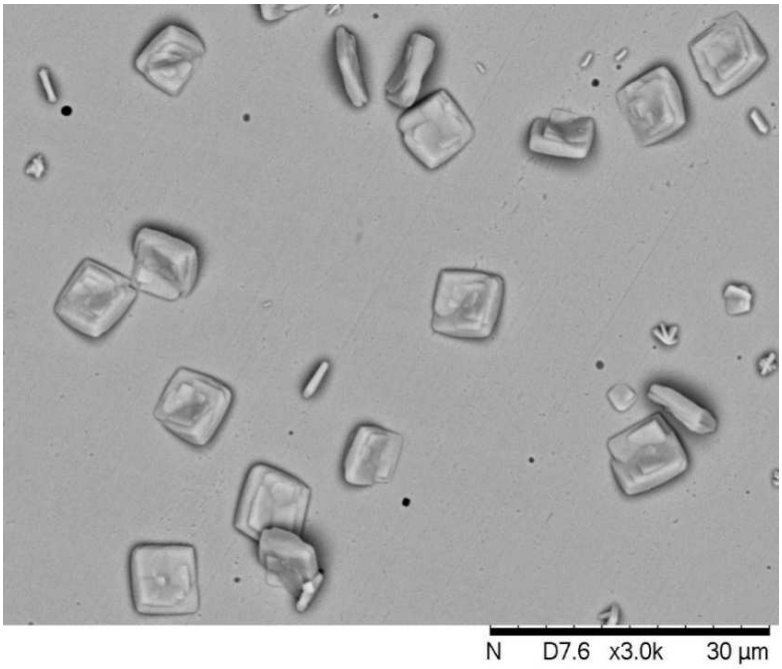

Figure 5-22: SEM image of $BaSO_4$ formed on the metal surface leaving the system uninhibited every 5 minutes for 4 hours

5.8 Summary

The results from this chapter have demonstrated that various factors that can contribute to the failure of scale inhibitor in preventing surface scaling in oilfield applications. Some of the key points are mentioned below:

- The effect of PPCA on the growth of crystal appears to be strongly dependent on the brine chemistry of the solution. The higher the saturation ratio, the longer it takes to stop the surface growth of crystals on the metallic surface.

- The inhibition efficiency of PPCA was reduced as the pre-scaled surface increases. It shows that the effect of pre-scaled surface should be given more consideration when inhibitors are been tested.

- The results show that it is not always the case that an increase in flow rate will reduce the performance of scale inhibitor. Also, it gives insight on an efficient scale inhibition strategies to be developed where the

flow rate can be adjusted in time *i.e.* initially a high flow rate of inhibitor is used to instantly block the active sites on any pre-scaled surface and is later reduced to an optimal level that prevents precipitation.

- The system was able to simulate the injection of scale inhibitors through a control valve. Hence, the system can be used to improve the scale treatment strategies by optimising the injection time interval of scale inhibitors injection.

The study in this chapter reveals some factors that could affect the surface inhibition using PPCA. This study was conducted in a single phase, but in the oil and gas industry operation surface scaling could also occur in the multiphase environment. The next chapter shows results of surface scaling in the multiphase environment.

Chapter 6 Surface scaling in multiphase conditions

6.1 Introduction

Scale formation is recognized as one of the major problems affecting production in the oil and gas industry and is an extensively studied phenomenon. The use of organic scale inhibitor is the most popular strategy used in mitigating the formation of mineral scale in the oil and gas industry [126]. However, in order to select the best scale inhibitor for a specific oil field condition, extensive laboratory tests are needed which include scale inhibitor compatibility, scale inhibitor performance, temperature and pressure tests just to mention a few [26, 126]. Regardless of these efforts to select the best chemicals, the efficiency of scale inhibitor in the oil field and laboratory is quite different. In order to overcome these inconsistencies, a laboratory test matrix is needed to be designed to replicate more accurately the real conditions in an oil field environment. Mineral scaling work has typically been conducted in an aqueous environment to represent a worst case scenario. However, in this study the effect of oil phase is evaluated.

In this chapter, mineral bulk precipitation and surface fouling of barium sulphate were evaluated in a single phase and multiphase environment. Firstly, static bulk jar tests were carried out to evaluate the effect of the scale inhibitor on bulk precipitation. Secondly, in order to examine the effect of multiphase environment on barium sulphate surface fouling, two different surfaces (stainless steel 316L and fluoropolymer coating) were used and the concentration of the oil phase was varied from 5% to 50%. Lastly, the effect of two commercial scale inhibitors (DETPMP and PPCA) on surface scaling in multiphase environments were studied. The outline of this chapter is shown in Figure 6-1.

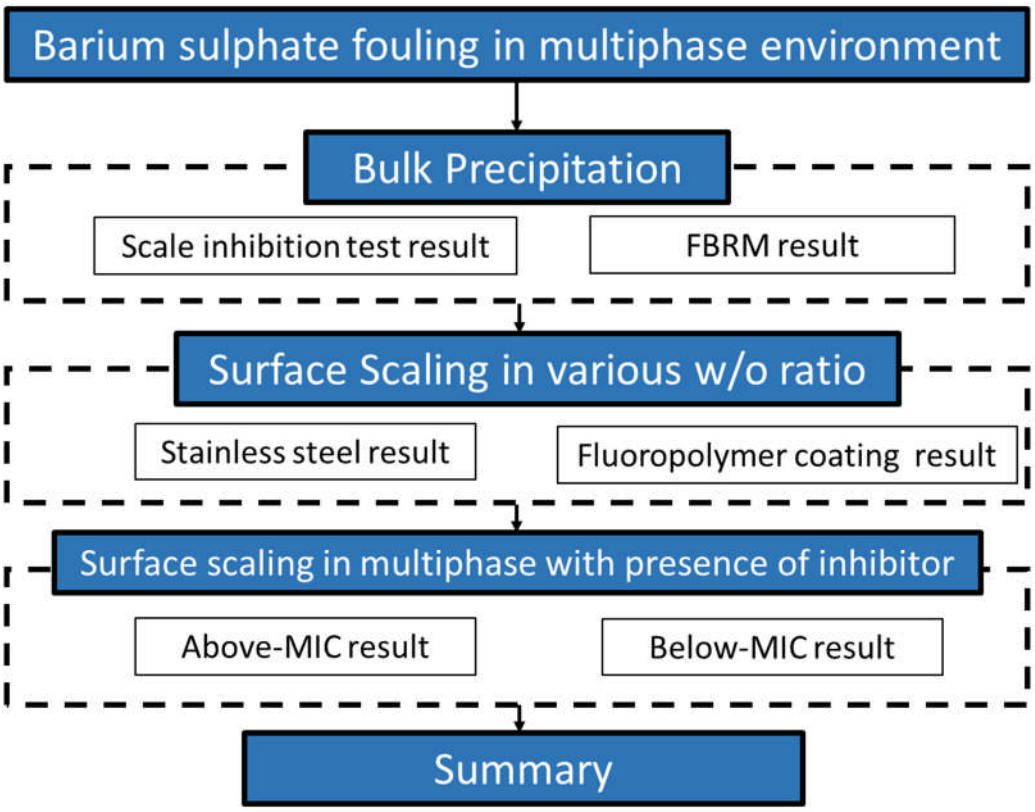

Figure 6-1: Outline of chapter 6

6.2 Experimental details

6.2.1 Surface characterization

Stainless steel 316L was used as the reference material since it is commonly used in the oilfield industry (i.e. valve components and surface piping). Some of the AISI 316L samples were coated with a hydrophobic coating (fluoropolymer). This coating was selected based on its industrial relevance to examine the effect of low surface energy on surface scaling. The roughness and surface energy of AISI 316L and fluoropolymer which was analysed by light interferometry and contact goniometry are presented in Table 6-1. The contact angle measurements for the stainless steel 316L and fluoropolymer are presented in Table 6-2.

Table 6-1: Surface energy and roughness of AISI 316L and fluoropolymer

Surface	Surface energy ($mJ.m^{-2}$)	Surface roughness S_a(µm)
Stainless steel 316L	41.3	0.216
Fluoropolymer	14.2	0.943

Table 6-2: Water and isopar M contact angle values measured on AISI 316L and fluoropolymer

Surface	Water contact angle (θ)	Isopar M contact angle (θ)
Stainless steel 316L	55.5	87.4
Fluoropolymer	101.3	57.1

6.2.2 Multiphase conditions

As explained in chapter 3 Isopar M, an isoparaffinic hydrocarbon with a carbon number ranging from C11 to C16 was used during the experiment. The multiphase conditions were achieved using an overhead dissolver stirrer, which was set at 500 rpm throughout the test to keep the emulsion. The multiphase scaling test was carried out using four different oil-to-water ratios (50:50, 20:80, 5:95 and 0:100).

6.2.3 Brine composition

Scaling tests were carried out at 80°C and at atmospheric pressure. The formation water (FW) and North Sea seawater (NSSW) composition which are presented in Table 6-3 were based on brine compositions found in the North Sea. Barium sulphate was precipitated spontaneously by mixing 900ml of FW and 100 ml of SW. The initial value of saturation ratio was calculated from the Multiscale prediction software was approximatively 114. The compositions of the brine are shown in Table 6-3.

Table 6-3: Composition of brine

Ions	NSSW (ppm)	FW (ppm)
Na^+	10890	31275
Ca^{2+}	428	2000
Mg^{2+}	1366	739
K^+	460	654
Ba^{2+}	-	269
Sr^{2+}	-	771
SO_4^{2-}	2960	-

6.3 Bulk precipitation

6.3.1 Static barium sulphate performance test

The static barium sulphate inhibition efficiency tests were conducted to evaluate the above-MIC and below-MIC concentration of the scale inhibitor (DETPMP and PPCA) under the test conditions. The benchmarks for below-MIC and above-MIC are:

Below-MIC = 40-50% efficiency after 2 and 22 hours and;

Above-MIC = 95-100% efficiency after 2 and 22 hours.

Different inhibitor active concentrations of both inhibitors were tested (1, 2, 3, 4 and 5ppm). The results show that inhibitor efficiency increase as the concentration of inhibitors was increased as expected. However, further increase of scale inhibitor concentration above 4 ppm for both scale inhibitors has a negligible effect on the inhibition efficiency. Based on the benchmarked listed above, it is shown in Figure 6-2 and Figure 6-3 that above-MIC is 4 ppm for PPCA and DETPMP, whereas below-MIC concentration is 1 ppm for both scale inhibitors.

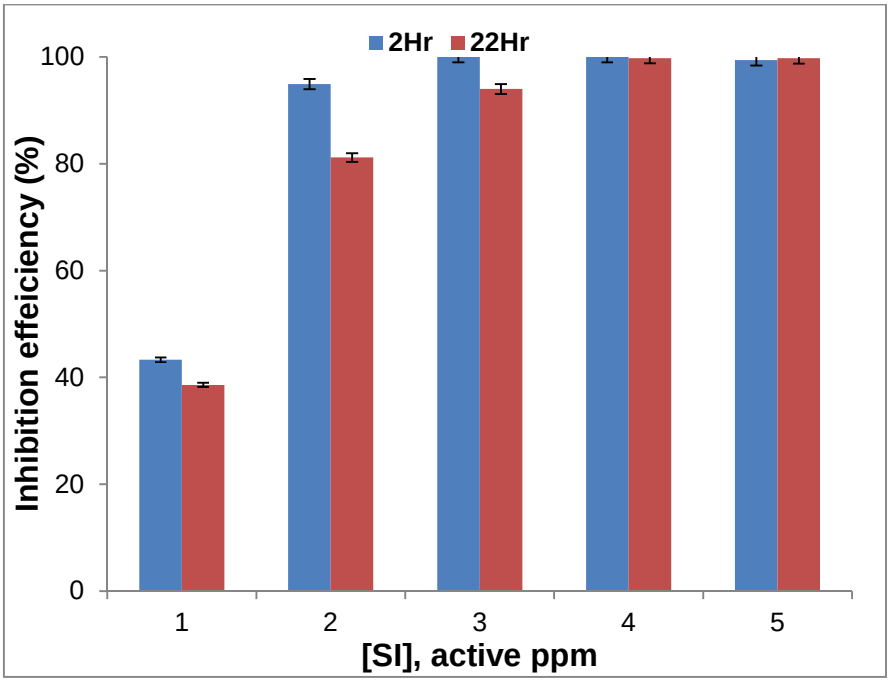

Figure 6-2: Static barium sulphate efficiency test for DETPMP of brine at 80ºC

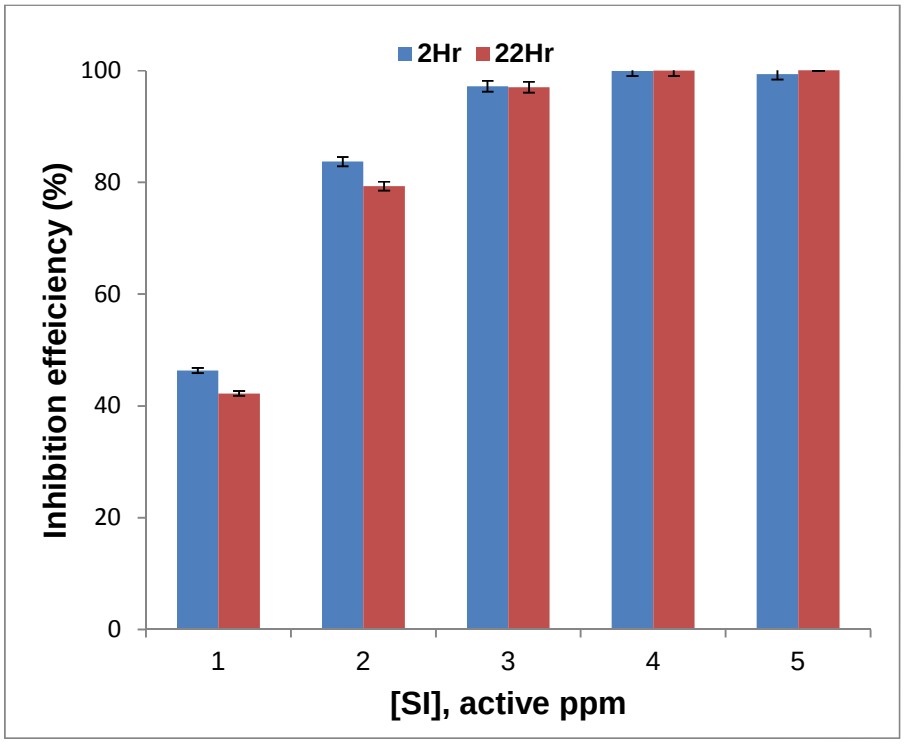

Figure 6-3: Static barium sulphate efficiency test for PPCA of brine at 80ºC

6.4 Surface scaling at various water: oil ratios

In this experiments, stainless steel and fluoropolymer coatings were exposed a barium sulphate scaling environment (single and multiphase). In both cases, the concentration of oil phase was 5 vol.%, 20 vol.% and 50 vol.%. Figure 6-4 and Figure 6-7 shows the amount of barium sulphate deposited on the stainless steel with and without oil phase. The results show that the presence of paraffin oil leads to a decrease in barium sulphate deposition on the stainless steel from 37 ppm in the single phase down to 21 ppm at 5:95 o/w ratio. Although the presence of a low quantity of paraffin oil (5%) significantly reduces the surface scaling by 43%, further addition of oil only has a minor effect on the surface deposition. The barium content reduced by 51 % and 56 % when the o/w ratio were 20:80 and 50:50 respectively. This effect of oil phase on surface deposition was clearly observed in the SEM image shown in Figure 6-5 and Figure 6-6. The amount barium sulphate in multiphase condition was less when compared to single phase condition.

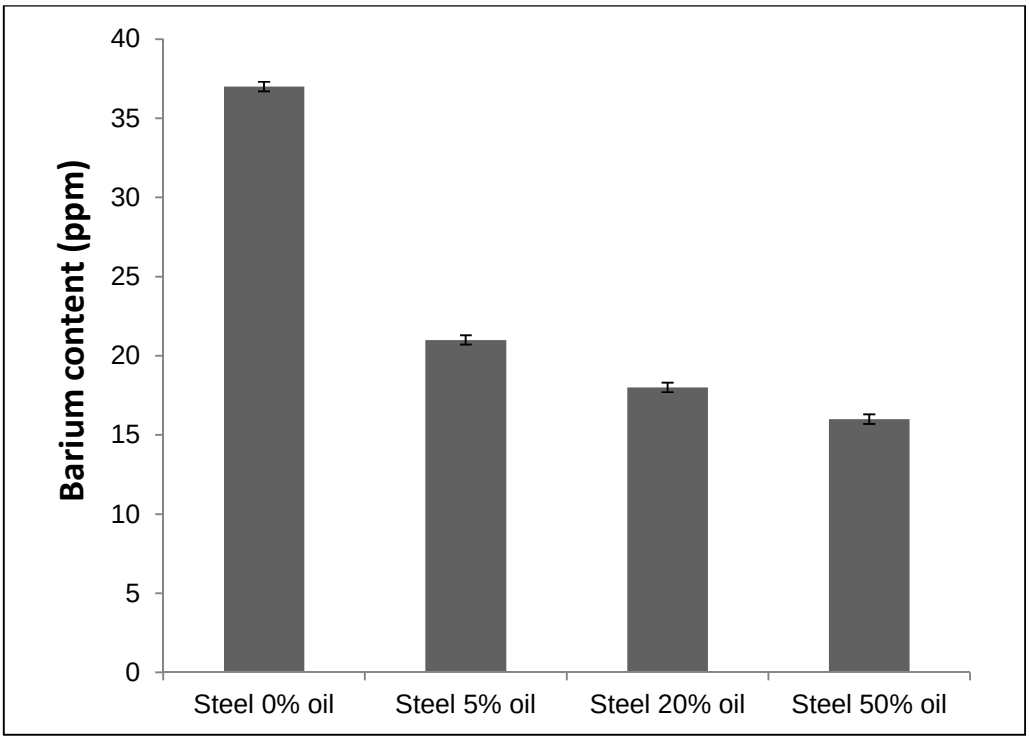

Figure 6-4: Surface barium content at various o/w system on AISI 316L

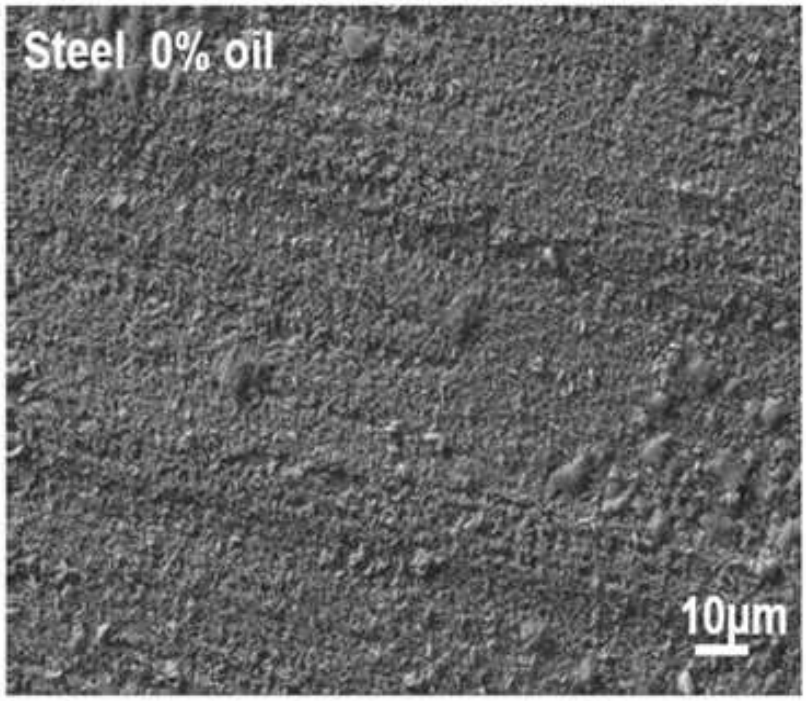

Figure 6-5: SEM micrographs of alloy AISL 316L subjected to barium sulphate scaling environment single phase

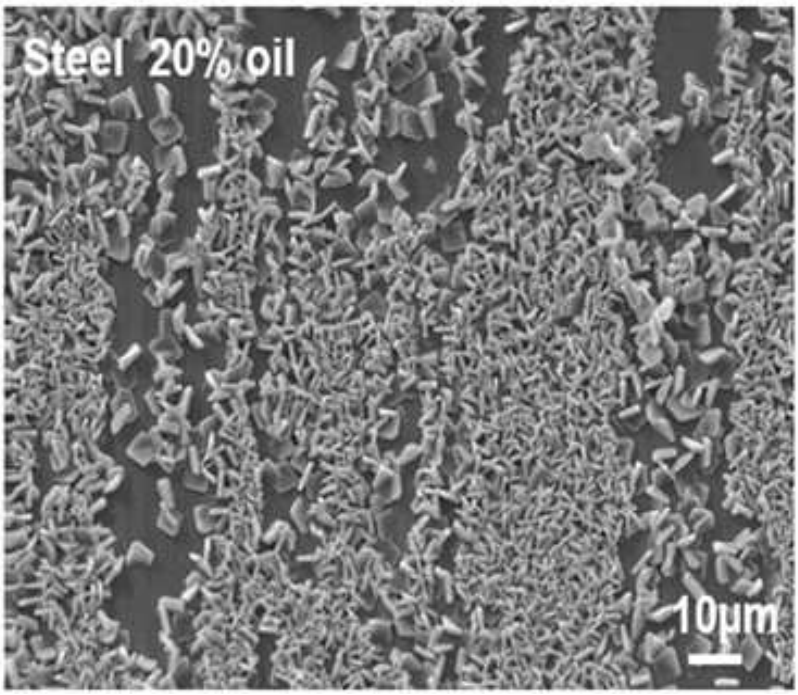

Figure 6-6: SEM micrographs of AISL 316L subjected to barium sulphate scaling environment multiphase (20% oil)

In a single phase scaling environment, the amount of barium sulphate deposited on the fluoropolymer coating was similar to that of stainless steel as presented in Figure 6-7. Having such similar mass gain the benefit of using antifouling coating such as the fluoropolymer was unclear. Nevertheless, when the fluoropolymer was used in a multiphase environment the amount of barium content was drastically reduced when compared with that of stainless steel. At o/w of 5:95 the barium content was reduced to 2 ppm which represents a significant reduction of nearly 95%. At a higher volume of oil, the barium content dropped to 1 ppm at o/w of 20:80 and 50:50. Figure 6-8 and Figure 6-9 shows the SEM micrographs of the fluoropolymer coating sample in single and multiphase conditions. It could be seen that the no barium sulphate scale was deposited on the surface in the multiphase environment.

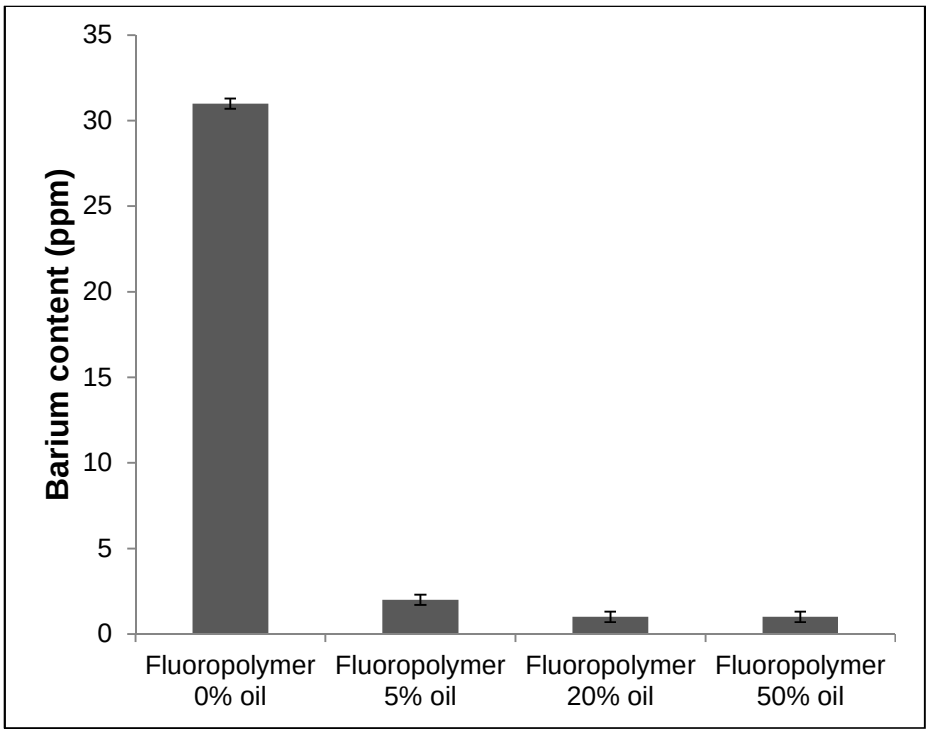

Figure 6-7: Surface barium content at various o/w on fluoropolymer coating

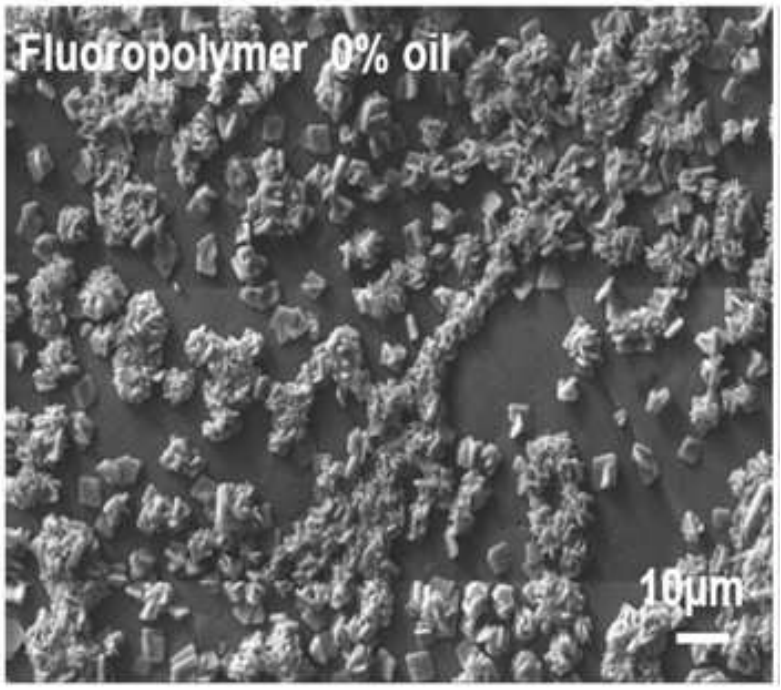

Figure 6-8: SEM micrographs of fluoropolymer coating subjected to single phase barium sulphate scaling environment

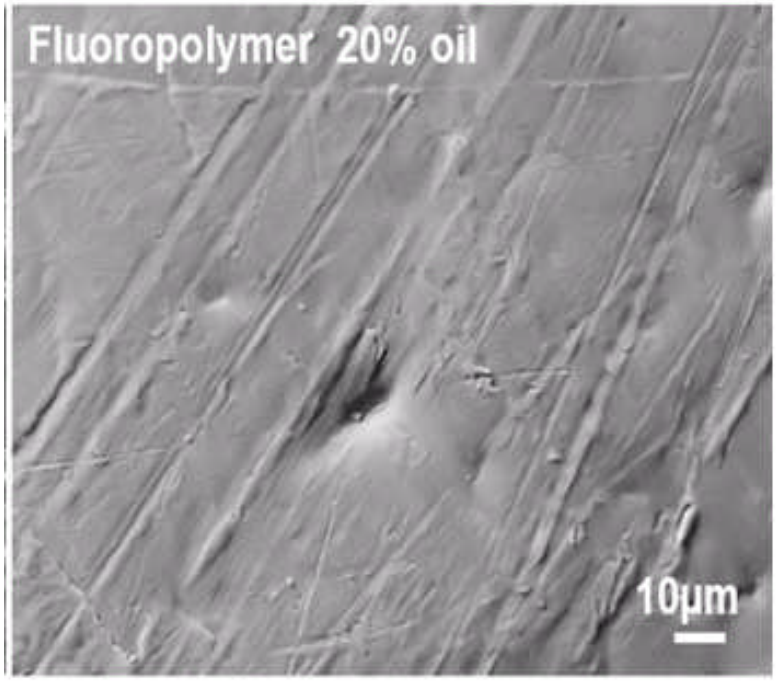

Figure 6-9: SEM micrographs of Fluoropolymer coating subjected to barium sulphate scaling environment multiphase (20% oil content)

6.5 Surface scaling in multiphase environment in presence of scale inhibitors

As shown in previous results the presence of an oil phase leads to a decrease in barium sulphate fouling on the stainless surface. The addition of scale inhibitor above MIC concentration also significantly reduces the amount of scale content measured on the surface. As shown in Figure 6-10, at 4 ppm of PPCA the amount of barium content decreases to 1 ppm and 0.6 ppm in single and multiphase environment respectively. A similar trend was observed when 4 ppm of DETPMP was used, the amount of barium content reduces to 2 ppm and 1 ppm in single and multiphase condition respectively.

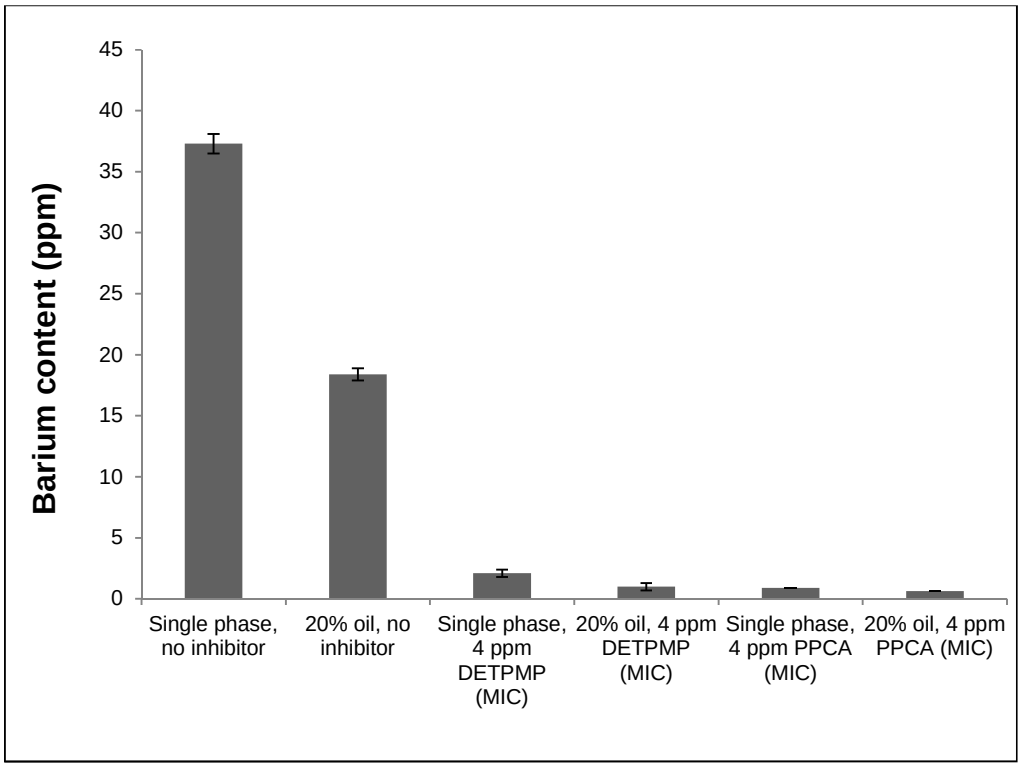

Figure 6-10: Barium content measured on surface single and multiphase condition with the influence of scale inhibitor (DETPMP and PPCA) below MIC.

On the other hand, when the concentration of the inhibitor was below MIC concentration (1 ppm), the results exhibited an opposite trend as shown in Figure 6-11. In the single phase, the amount of barium content increased to 59 ppm and 117 ppm for DETPMP and PPCA respectively. In addition, when

the same concentration was used in the multiphase condition it further promoted the deposition of barium sulphate on the stainless steel surface, which was more prominent for PPCA scale inhibitor. The barium content increased the surface scale build-up to 117 ppm and 162 ppm in single and multiphase conditions respectively.

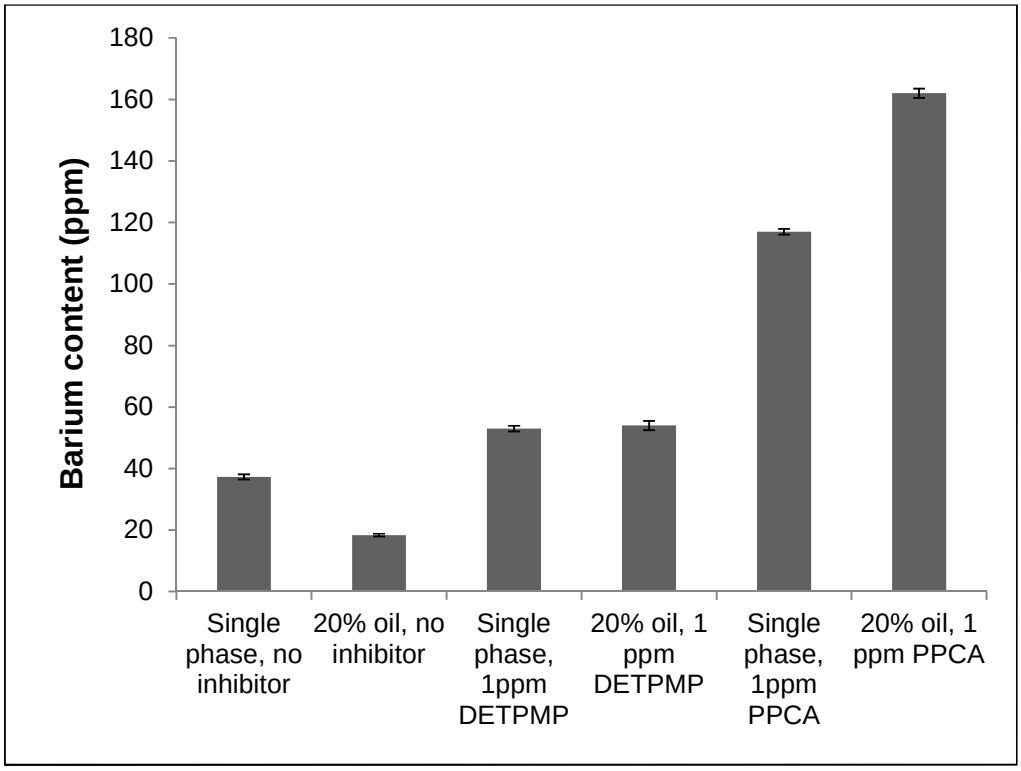

Figure 6-11: Barium content measured on surface single and multiphase condition with the influence of scale inhibitor (DETPMP and PPCA) above MIC.

6.6 Summary

This chapter has shown the effect of oil phase on surface deposition of barium sulphate surface. The summary of findings from these results are as follows:

- Low surface energy coating (such as fluoropolymer) does not show great antifouling properties in single phase scaling tests and amount of barium sulphate deposited were similar to that of stainless steel. However, the efficiency of the fluoropolymer was greatly improved in multiphase condition.

- Applying scale inhibitor below-MIC enhanced surface fouling in single, which was further increased in the multiphase environment; this increase was clearly shown by PPCA scale inhibitor.

- At a concentration above MIC, surface fouling reduces both in multiphase and single phase environment.

The results from this chapter have revealed that the presence of oil droplet can affect the surface scaling of barium sulphate. The next chapter of this thesis gives detailed analysis and discussion of the results presented in the three result chapters (chapter 4, chapter 5 and chapter 6).

Chapter 7 Discussion

7.1 Introduction

The formation of barium sulphate is a persistent problem affecting the oil and gas industry. Due to its high insolubility/resistance to chemical and mechanical treatment, it is difficult to remove when formed. Barium sulphate formation can be predicted using thermodynamic models; nevertheless, it is vital to understand the kinetics of barium sulphate in order to accurately predict the rate at which these scales are being formed. Several research works have been conducted on the kinetics of barium sulphate both in bulk precipitation and on surface deposition; however, these studies were often conducted in a closed system. The limitation of this is the changing saturation ratio as a function of time. In this work, the experimental set-up was designed to study both processes using a once-through flowing system.

In this chapter, the results presented in chapter 4, chapter 5 and chapter 6 are examined and discussed. A complete explanation of the findings from the results is presented and an appraisal of how these findings relate to current literature is given. The chapter is organised into five (5) different sections. The first section compares the kinetics of bulk precipitation and deposition on metallic surfaces. Then the nucleation mechanism of barium sulphate formation on a metallic surface is discussed in the second section. The third section deals with the effect of three scale inhibitors (PPCA, DETPMP, and VS-Co) on the growth of barium sulphate are discussed. The fourth section deals with factors (such as flow rate, pre-scaled surface and interval injection of scale inhibitor) that affect surface scale inhibition. The last part relates to one area of research which has not received any attention in the literature thus far; surface scaling in multiphase environments is discussed.

7.2 Bulk precipitation and surface deposition

The results presented in chapter 4 showed that despite the absence of bulk precipitation, surface fouling occurs which is also apparent from the images shown in Figure 4.3. This implies that induction time for surface fouling is shorter than bulk precipitation for the range of saturation ratios considered. Comparable study has been reported by Sanni *et al.* [127], where the surface induction time of calcium carbonate surface fouling was less than the induction time of bulk precipitation for SR< 60 as shown in Figure 7-1. These results are in agreement with the classical nucleation theory which predicts a lower energy barrier for heterogeneous nucleation (surface fouling) than homogeneous nucleation (bulk precipitation) [31, 50, 51, 121].

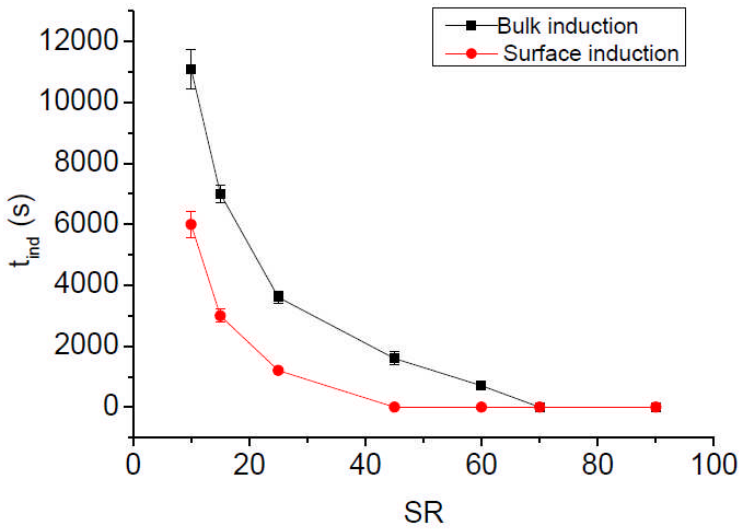

Figure 7-1: Surface and bulk induction time [127]

These results suggest that surface deposition could occur as a result of heterogeneous nucleation and subsequent growth; and not solely by particles migrating from the bulk solution to the surface as previously assumed. In addition, the results demonstrate that heterogeneous nucleation (surface scaling) encourage crystal growth when compared to homogeneous nucleation. Research by Chen *et al.* [29] also confirm these findings. In their study, they found that crystals formed on metallic surfaces were larger than crystals formed in the bulk solution.

The findings from this section demonstrate that barium sulphate scale can form on oilfield equipment when there is no scale formation in the bulk solution. Hence, it is recommended that surface scaling on surfaces should be taken into consideration when designing scale management system.

7.3 Mechanism of barium sulphate deposition on metallic surface

As mentioned in chapter 2, nucleation represents the first step in the crystallization process. Therefore, it is crucial to understand the nucleation mechanism, in order to effectively control the formation of scale on the metallic surface. In this study as stated in chapter 3, a model developed by Beaunier *et al.* [121], which was modified by Euvrard *et al.* [122] was used to study the crystallization process. The model assumes that diffusion controls the crystallization process and that the number of active nucleation sites for a unit area of the substrate is fixed; all nucleation events are independent of each other. Hence, the probability of nucleation at certain times depends on the number of free sites.

According to the literature [128-131], there are two types of nucleation mechanism, namely: instantaneous and progressive. Figure 7-2 gives a schematic diagram illustrating the types of nucleation mechanism. The model proposed that for instantaneous nucleation, S_{ext} (%) coverage has a linear relationship with time. On the other hand, progressive nucleation S_{ext} (%) has a parabolic relationship with time. The experimental data presented in chapter 4 (Figure 4-9 and Figure 4-10) were fitted to evaluate the type of nucleation at each condition. Figure 7-3 to Figure 7-5 shows the plot of S_{ext} (%) versus time for SR = 15, SR = 20, and SR = 80 at 50°C. The results show that S_{ext} (t) was linear with time for SR=80, while it follows a parabolic trend at lower SR=15 and SR =20. Thus, according to the model developed by Beaunier *et al.* [121], nucleation can be considered as instantaneous when SR = 80, while at SR 15 and 20 nuclei were formed on the metallic surface progressively.

Table 7-1 gives a summary of the mechanism of nucleation for each of the experimental conditions used. From the Table 7-1, it is observed that the

mechanism of nucleation tends to slowly change from progressive to instantaneous nucleation when the saturation ratio was increased. This indicates that the nucleation rate increases with increase in the concentration of scaling ions [132]. Similar findings were reported by Beaunier *et al*. [121] when they investigated the influence of calcium ion concentration on formation of calcium carbonate. Scaling solution with a high concentration of calcium ions (200 $mg.l^{-1}$) exhibits instantaneous nucleation mechanism. At lower concentration of calcium ions (40 $mg.l^{-1}$), the mechanism was purely progressive nucleation.

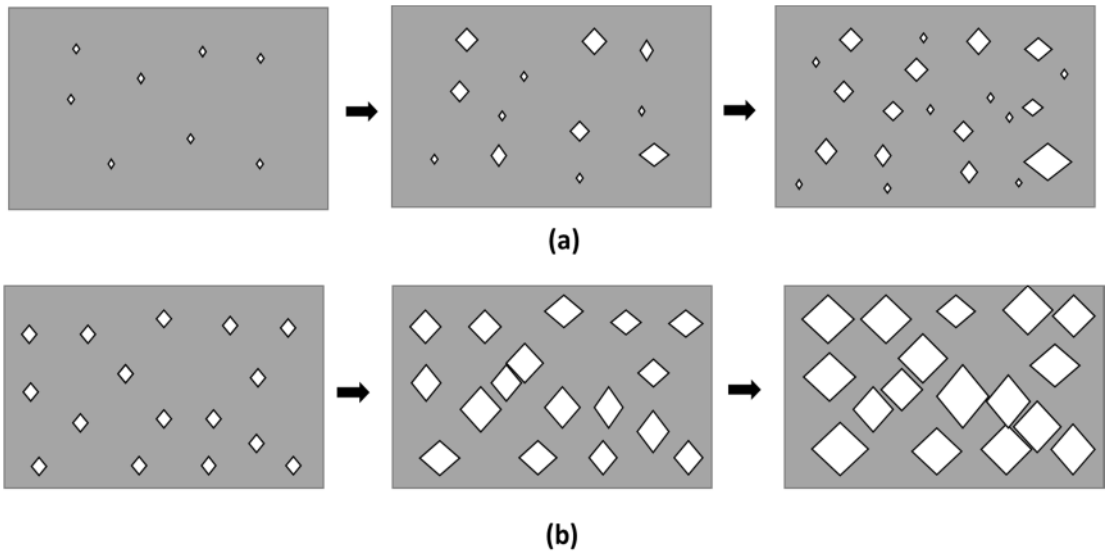

Figure 7-2. (a) Progressive nucleation corresponds to the continuous formation of new nuclei coupled with the growth of nuclei, and (b) Instantaneous nucleation corresponds to a constant number of nuclei, while the growth of nuclei continues.

The model has shown that the type of barium sulphate surface nucleation can be obtained from experimental results. Also, as discussed in section 2.10, scale inhibitors exhibit several mechanisms, however, one of the mechanism is predominant for a specific inhibitor. Hence, combining information from this model and that of the mechanism of scale inhibitor will be very relevant in enhancing the scale treatment strategies and implementation.

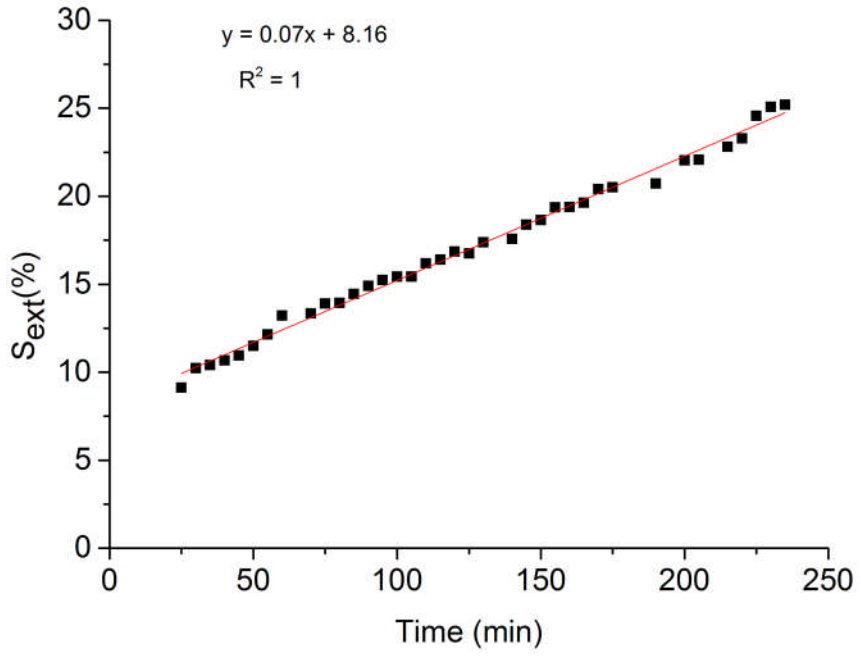

Figure 7-3. Extended surface area as a function of time for experiment brine with SR = 80 at 50°C

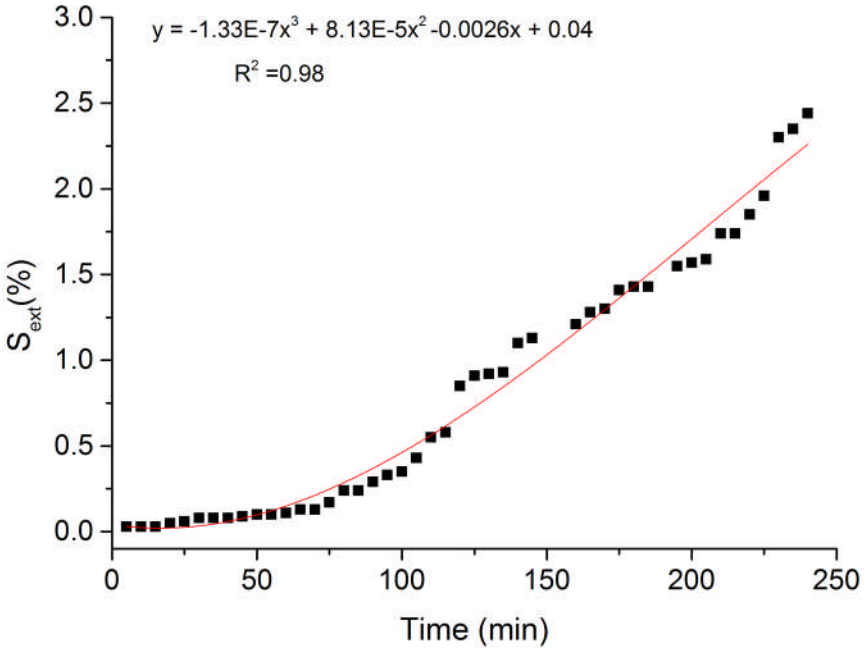

Figure 7-4: Extended surface area as a function of time for experiment brine with SR = 20 at 50°C

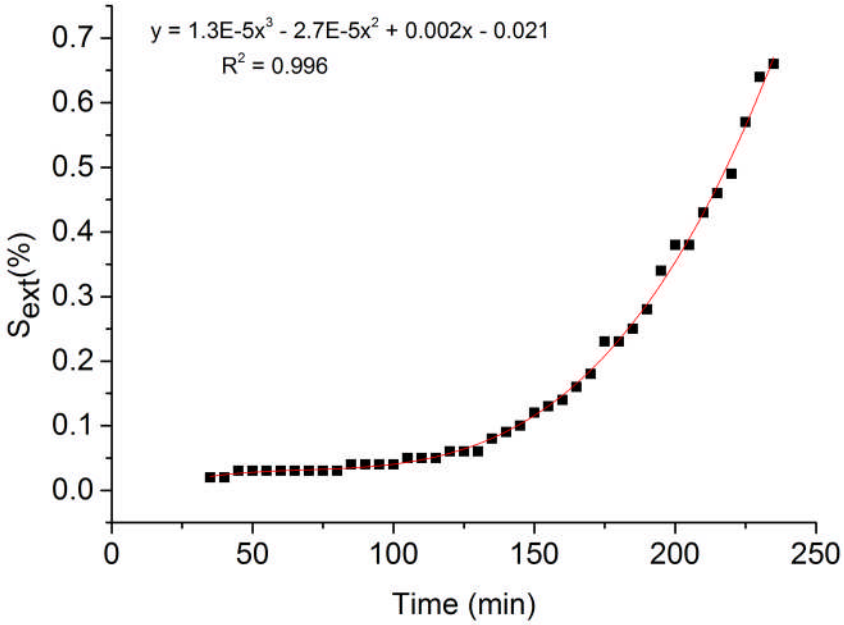

Figure 7-5: Extended surface area as a function of time for experiment brine with SR = 15 at 50°C

Table 7-1: Summary of nucleation mechanism suggested for each experimental condition

SR	Nucleation Mechanism	
	25°C	50°C
15	Progressive	Progressive
20	Progressive	Progressive
30	Progressive	Instantaneous
80	Instantaneous	Instantaneous

7.4 Kinetics of barium sulphate on a metallic surface

In order to determine the crystal growth rate of barium sulphate, the slopes of the linear part of the average size of crystals curve were used. As demonstrated in a study conducted by Hasson *et al*. [133]. Table 7-2 presents the equations fitted on the linear growth of the average size of barium sulphate

crystals and the slopes which represent the rate of crystallization of barium sulphate deposited on the metallic surface.

Table 7-2: Growth rate barium sulphate deposition at different conditions

SR	Temperature	Linear Equation	Rate (μm²/min)
15	25°C	-	-
	50°C	y = 0.01x + 11.32	0.01
20	25°C	-	-
	50°C	y = 0.12x + 18.11	0.12
30	25°C	y = 0.001x + 11.15	0.001
	50°C	y = 0.27x + 34.9	0.27
80	25°C	y = 0.16x + 40.32	0.16
	50°C	y = 0.50x + 31.62	0.50

From Table 7-2, at 50°C, the increase in saturation ratio promoted the crystal growth rate of barium sulphate on the metallic surface, which is in agreement with findings made by other authors [132, 134-136]. However, there was slow growth of crystals at low saturation ratio (SR =15). This was attributed to the formation of new nuclei on the metallic surface rather than the growth of pre-existing nuclei as explained in section 4.4.1. At low saturation ratio, the diffusion of scaling ion will be restricted and it would affect the nucleation and growth process [137]. However, the nucleation process is less affected, since nuclei are smaller than the crystals and cause less depletion of the components in the bulk solution. Hence, the low scaling tendency was less energetic to promote the growth of crystals as compared to the high scaling tendency. These findings are in agreement with an investigation conducted by Beaunier *et al*. [121]. The authors found out that when the surface was pre-treated, nuclei appeared at the first instants however they grew very slowly. According to the authors, the fast deposition rate was used to generate new

nuclei on the scaling surface rather than growing the nuclei already formed on the surface.

When the temperature was reduced to 25°C, no growth rate was observed at saturation ratio (15 and 20). This is to be expected since reducing the temperature would reduce the diffusion of scaling ions to the crystal-water interface [138]. In addition, the average size of crystal deposited on the metallic steel surface at the different saturation was nearly the same for three SR 15 and 20. However, when the saturation ratio was increased to 80, the growth rate of crystals was increased as shown in Table 7-2. In summary, at low saturation ratio crystals growth is at minimum and nucleation dominate. However, as the saturation ratio increase, crystal growth becomes the dominating effect.

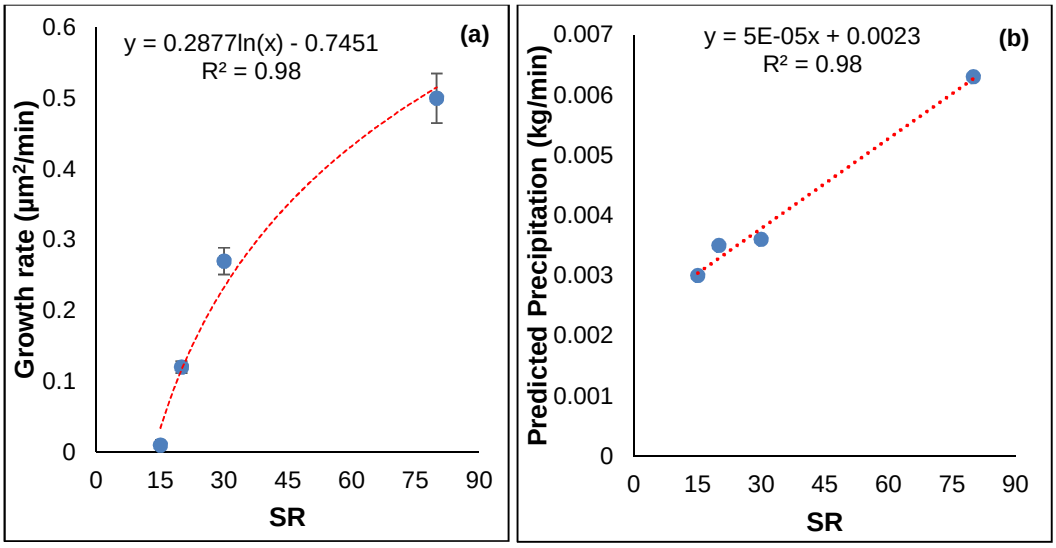

Figure 7-6: (a) Surface growth verse saturation ratio and (b) Bulk precipitation growth rate versus saturation ratio at 50°C

Figure 7-6(a) and Figure 7-6(b) shows the plot of surface growth rate and bulk precipitate growth rate (predicted from multiscale software) as a function of saturation ratio at 50°C. It is interesting to see that different relationships between growth rate and saturation ratio were observed in both cases. Surface growth rate gives a logarithmic relationship with saturation ratio, while bulk precipitation growth rate has a linear relationship with saturation ratio. This indicates that bulk precipitation growth rate cannot be used to predict the

rate of surface scaling. Hence, studying both surface scaling and bulk precipitation is needed to fully understand oilfield scaling processes.

7.4.1 Effect of scale inhibitor on the kinetics and morphology of barium sulphate scale formation

As discussed previously scaling processes comprise both nucleation (birth of new crystals) and subsequent growth of the crystals. In this part of the discussion, the effect of three scale inhibitors (DETPMP, VS_Co and PPCA) on the subsequent growth of barium sulphate crystals were examined. The mechanism by which each of scale inhibitor hinders the growth of barium sulphate were discussed.

In order to evaluate the growth rate of crystals, the slope of the average size of crystal from 60th and 240th minutes was taken as illustrated in Figure 7-7. Table 7-3 gives a summary of the growth rate when the three inhibitors were used.

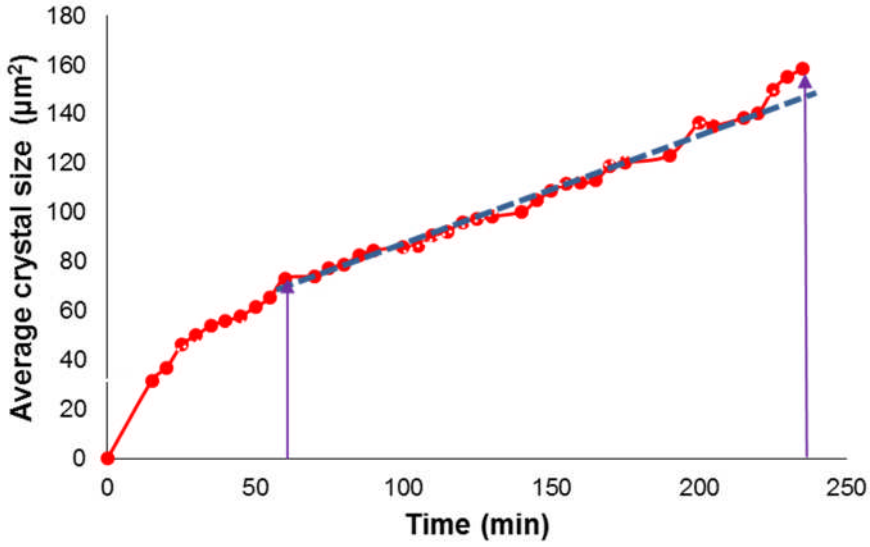

Figure 7-7: Schematic diagram illustrating the growth rate of barium sulphate

Table 7-3: Growth rate evaluated from the change in the average size of crystal (μm.min^{-1}) from 60 minutes to the end of the experiment

Condition	Rate (μm^{2}min^{-1})	
	1 ppm	4 ppm
Blank	0.5	-
PPCA	-	-
DETPMP	1.8	-
VS-Co	0.48	-

7.4.1.1 Effect of DETPMP on barium sulphate formation

The results from Table 7-3 shows that the growth rate of barium sulphate at 1 ppm of DETPMP is higher than that of the uninhibited test. This indicates that at this concentration, surface growth of barium sulphate was enhanced. The enhancement of surface scaling has been previously reported by Graham *et al.* [101] and Baynton *et al.* [139] for barium sulphate scale formation study in the presence of phosphate scale inhibitor. From the study by Baynton *et al.* [139], the authors suggested that the promotion of surface growth was attributed to the weak interaction between the organic anion and barium ions. On the other hand, Graham *et al.* [101] suggested that at low concentration (below MIC) of scale inhibitor, the low surface coverage of the scale inhibitor on the metallic surface resulted in the enhanced growth. The results presented are in agreement with the theory proposed by Graham *et al.* [101].

As seen in Figure 4-20 the crystal morphology observed when 1ppm of DETPMP scale inhibitor was used was different from the uninhibited case. The crystals formed were not rhombic as in the case of the blank test; instead, the shape of the crystal was hexagonal. This change may be due to the inhibition of the growth of (001) face by the scale inhibitor (DETPMP) but lead to the formation of (011) face. Further growth of the (011) face along the horizontal axis led to the elongation of the (001) face, resulting in the hexagonal shape of the crystal formed as shown in Figure 7-8.

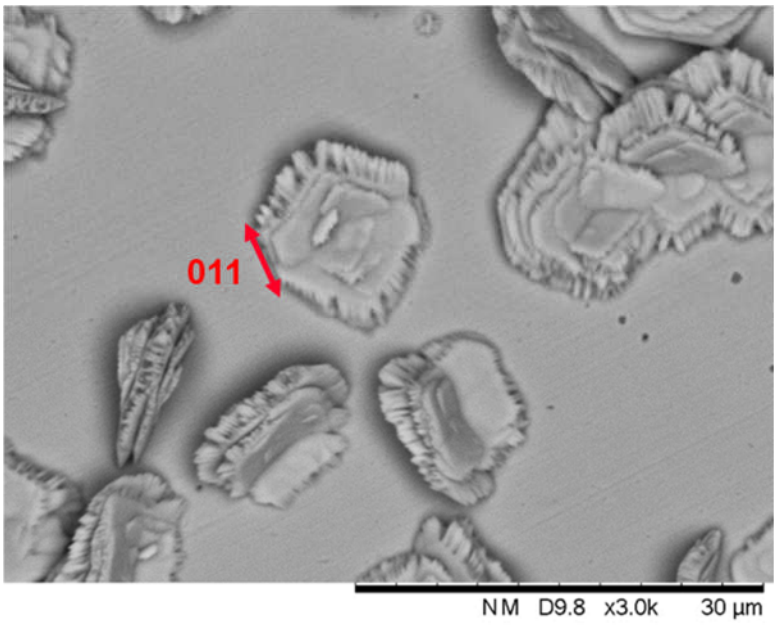

Figure 7-8. SEM image with 1 ppm of DETPMP

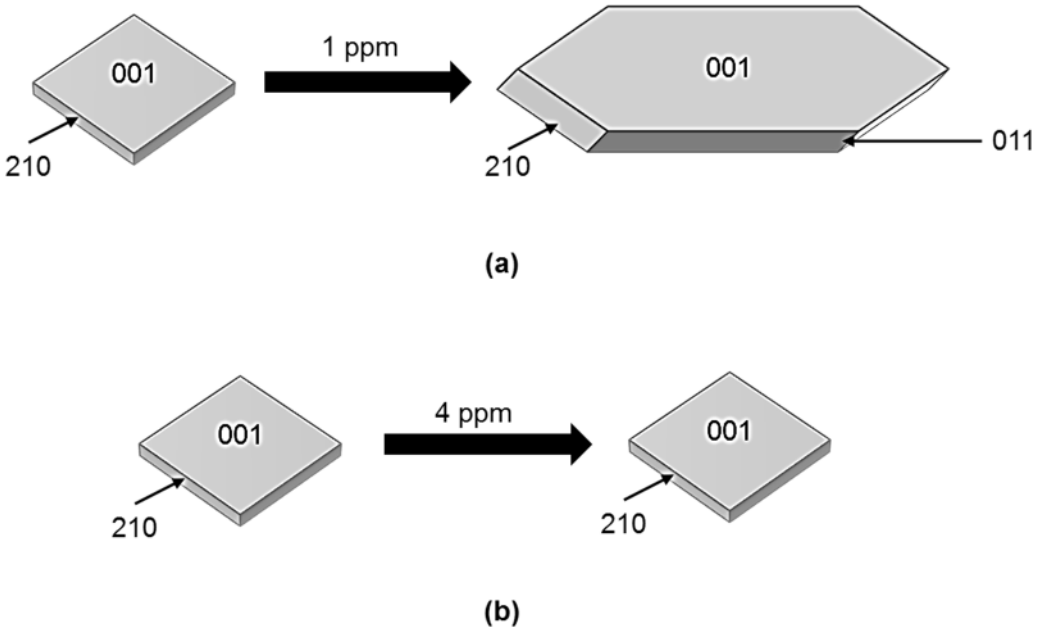

Figure 7-9: Crystal formed on metallic surface when (a) 1 ppm, and (b) 4 ppm of DETPMP was injected

In addition, the formation of (011) face may account for the enhancement of surface coverage when 1 ppm of DETPMP was applied, since the surface area of the crystals increases with the fast growth of (011) face. At high concentration of DETPMP (4ppm), the morphology of the crystal was rhombic.

Hence, at this concentration, it can be assumed that the inhibitors were completely absorbed on the entire growth site ((001) & (210) face); thus the subsequent growth of crystals was stopped. This indicates that the (011) face appear and fades as the concentration of the inhibitor increases as shown in Figure 7-9. This result is consistence with the study reported by Black *et al.* [140], where they found that change in concentration of additives (diphosphonate) affect the formation of (011) face of barite.

7.4.1.2 Effect of PPCA on barium sulphate formation

The results presented in Figure 4-13 showed that when 1 ppm of PPCA was injected, the growth rate was enhanced but attained a plateau until the end of the experiment. As explained in previous section, the enhanced growth rate of crystals was due to the low film coverage of the scale inhibitor after injection. However, PPCA are known to have good adsorption properties on minerals/metals [126] and with the constant supply of PPCA into the flow cell; growth stopped once all active sites were blocked. This indicates that the presence of PPCA hinders surface growth by adsorbing on the distinct step emerging from screw dislocation on the barium sulphate surface [126, 141].

These results demonstrate that PPCA can impede the subsequent growth of crystals even at a low concentration, despite being polymeric scale inhibitors which are primarily known to work through a nucleation inhibition mechanism [26, 98]. This finding is supported by the study reported by Sorbie and Laing [67], where they investigated the mechanism of three different scale inhibitors (DETPMP, PVS, and PPCA). In their study, DETPMP was observed to perform through the crystal growth mechanism, while PVS function through nucleation inhibition mechanism. In the case of PPCA, it showed a performance that is in-between that of DETPMP and PVS. This implies that PPCA exhibits both mechanisms (nucleation inhibition and crystal growth retardation).

Figure 4-15 shows the precipitate formed on the surface of the stainless steel at the end of the experiment. In the case of the uninhibited test the precipitate formed on the steel had a rhombic morphology as expected; having two

dominant faces as shown in Figure 7-10. When PPCA was applied for both concentrations (1 and 4 ppm) same rhombic morphology was observed. This illustrates that the PPCA inhibited the growth of two dominant faces of barium sulphate as illustrated in Figure 7-11. The XRD analysis also confirmed that PPCA inhibitor suppresses the growth of the dominant faces of barium sulphate.

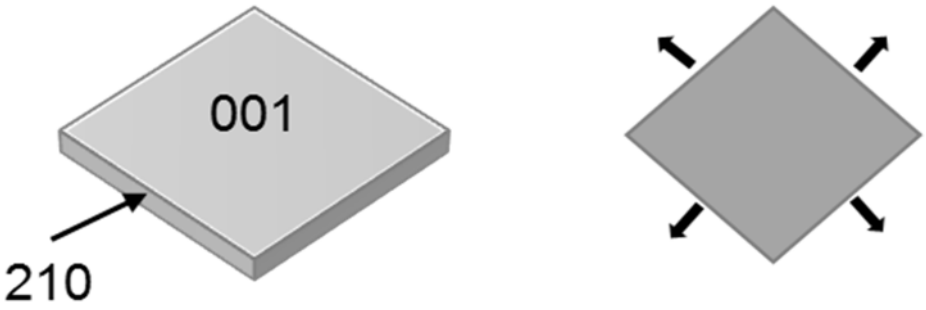

Figure 7-10: Morphology of $BaSO_4$ in the absence of scale inhibitor showing the dominant faces ((210) and (001)).

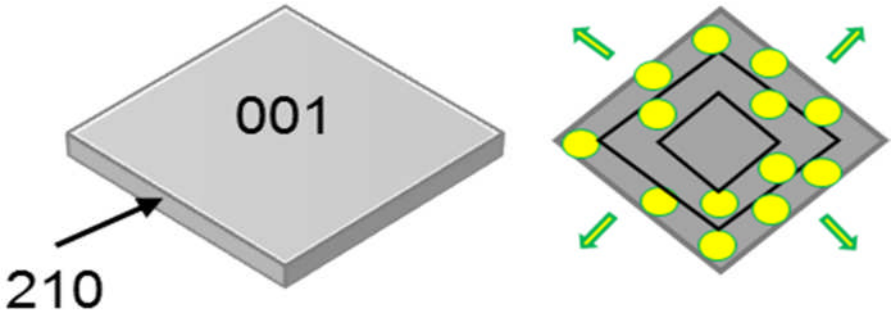

Figure 7-11: Morphology of $BaSO_4$ deposited on stainless steel sample in the presence of PPCA scale inhibitor. PPCA binds to (210) and (001) faces to stop the growth.

7.4.1.3 Effect of VS_Co on barium sulphate formation

From Table 7-3 when 1 ppm of VS-Co was applied, the growth rate was similar to the uninhibited case. This suggests that at this concentration VS-Co was unable to prevent the subsequent growth of crystals. This result is in agreement with literature [67, 139, 142], that postulates polymeric scale

inhibitor (such as VS-Co) functions primarily by nucleation inhibitor mechanism. In a study by Baynton *et al.* [139], it was shown that at a low concentration of sulphated scale inhibitor (benzene-1,3,5-trisulfpnic acid (BTS)), it was effective to impede nucleation process but was less efficient to stop further growth of crystals. Furthermore, when the concentration of the BTS was increased crystals growth stopped.

The results presented in this work are in agreement with the study by Baynton *et al.* [139] since similar trend occurred when the concentration of VS-Co was increased. The further growth of crystals stopped instantly when the 4 ppm of VS-Co was injected. The SEM image presented in Figure 4-17 revealed the morphology of the barium sulphate crystals at 1 ppm of VS_Co was similar to the uninhibited case and that the spiral growth of the crystals continued until the end of the experiment. Also, XRD pattern indicates that at 1 ppm the presence of VS_Co does not have any effect of the dominant faces of barium sulphate.

From the results discussed in this section, the three scale inhibitors performed differently at a lower concentration. The results also demonstrated that scale inhibitor could enhance crystallization process rather than impeding crystal growth. This shows that, if the accurate concentration of scale inhibitor is not applied during production, it might promote the build-up of mineral scale deposit on the surface of oilfield equipment. This recommends that, in evaluating the performance of scale inhibitor to control or prevent the deposition of scale during production, test procedures should take into account the surface which scale is likely to occur. In the next section, some factors that could affect the surface inhibition using PPCA will be discussed.

7.5 Factors that affect surface scale inhibition

7.5.1 Effect of saturation ratio on $BaSO_4$ surface inhibition

The results presented in chapter 5 showed that bulk precipitation inhibition efficiency for the three brines was above 95 % (above MIC). With the high

inhibition efficiency in the bulk, it is expected that the surface fouling will significantly reduce the surface growth of crystal on the metallic surface.

From Figure 5.4, at SR= 30 the surface growth of crystals stopped almost immediately after injecting the inhibitor. PPCA is known to have good adsorption properties on minerals [143-145] and the instantaneous inhibition of surface scaling observed was attributed to the inhibitor molecules being adsorbed and blocking all the active sites of the crystal lattice [21, 126]. However, when 1 ppm of PPCA was injected at SR = 60 and SR = 80, surface growth continued for 15 and 60 minutes before reaching a plateau as shown in Figure 5-4 and Figure 5-5.

The affinity of PPCA molecules for barium sulphate crystals is unlikely to have changed and this suggests that after the scale inhibitor is injected, both processes of adsorption of inhibitor molecules on the active growth sites and incorporation of the scaling ions on the crystal lattice occur simultaneously. The occurrence of these 2 competitive processes, therefore, delay the time necessary for the PPCA molecules to be adsorbed and fully block the active growth sites; but ultimately once all the sites have been blocked, growth stops.

As discussed in section 7.2, the surface scaling barium sulphate on the metallic surface occurs due to heterogeneous nucleation and growth. The scaling kinetics is influenced by two determining steps: diffusion of scaling species to the crystal-water interface, and surface reaction whereby the scaling ions are incorporated into the barium sulphate crystals lattice [106, 133]. With the presence of scale inhibitor, the rate of the latter process would be hindered due to the adsorption of the scale inhibitor molecule on the active growth sites (such as kinks site). On the contrary, increasing the saturation ratio will increase the diffusion of scaling species to the crystal-water interface. Hence, the inhibitory action of the scale inhibitor will be reduced as the saturation ratio is increased. This explains the poor performance of the scale inhibitor when the saturation ratio was increased.

The findings from this sections suggest that saturation ratio apparently have a greater effect on surface inhibition than on bulk precipitation inhibition. In addition, previous studies have shown that scale inhibitor performs differently

in preventing bulk precipitation and surface deposition [31, 146]. In agreement with these findings, the results strengthen the need to differentiate the MIC for bulk precipitation and for surface fouling. The next section addresses the effect of the pre-scaled surface on surface inhibition efficiency.

7.5.2 Effect of pre-scaled surface on $BaSO_4$ surface inhibition

The results presented in Figure 5-10 revealed that the surface inhibition efficiency reduces when the pre-scaled surface was increased. As reported in several literatures, scale inhibitor hinders the crystal growth by adsorbing on the crystallizing surface [141, 142, 147]. In contrast, adsorption process is a surface phenomenon and, as such, the extent of adsorption is proportional to the surface area of the adsorbent (barium sulphate crystals). This suggests that increasing the pre-scaled surface (without increasing the concentration of the inhibitor) will reduce the surface coverage of inhibitor molecules on the active site of the crystals. Thus, delaying the time required for the inhibitor molecule to completely hinder crystals growth; nevertheless, growth stopped once all the active sites were entirely blocked. Figure 7-12 shows a schematic diagram explaining the effect of the pre-scaled surface on the surface inhibition.

This suggests that the adsorption of PPCA seems to be affected when the pre-scaled surface was increased. A research by Martinod *et al*. [148] showed that the performance of scale inhibitor was linked to the rate of adsorption of scale inhibitor at the crystal surface. In this study, the effect of two scale inhibitors (polyaspartate (PASP) and polymaleic (PMA)) on the formation of calcium carbonate on the metallic surface was investigated. It was found that PMA (with higher adsorption rate) instantly blocked the growth of calcium carbonate crystals. However, PMA did not totally stop the growth of crystal due to its low adsorption rate on crystals surface. In another study by Amjad *et al.* [149], they investigated the effect of iron oxide (Fe_2O_3) impurities on calcium carbonate inhibition. It was shown from the study that small amount of Fe_2O_3 particles reduces the scale inhibitors performance. Also, it was

revealed that the negative impact of the particles could only be overcome by increasing the inhibitor concentration.

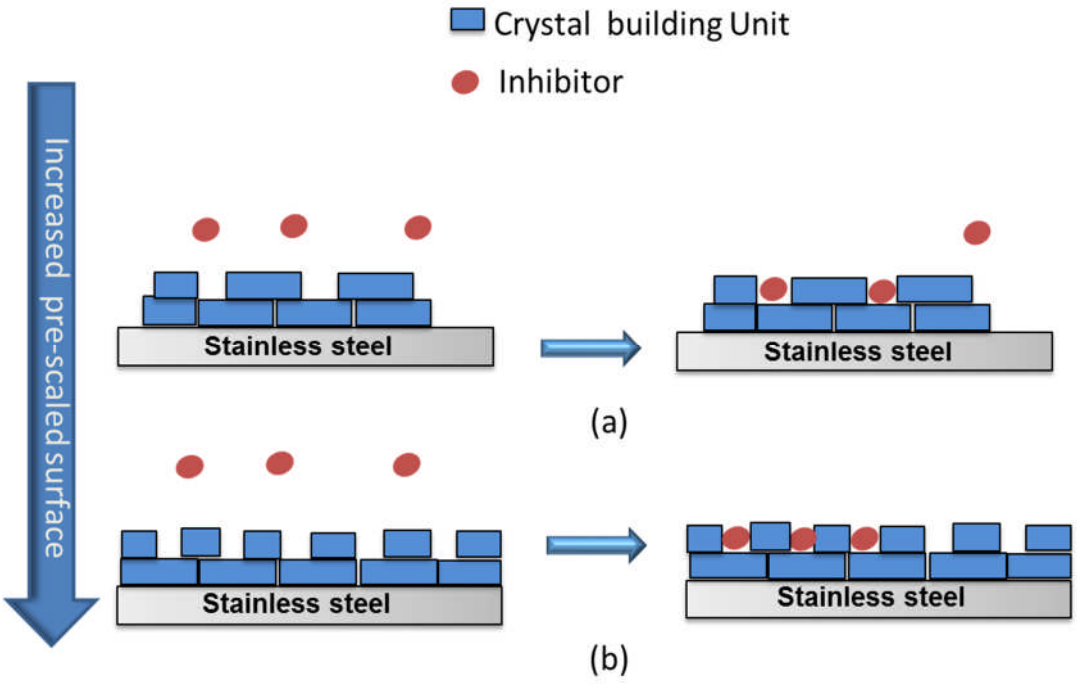

Figure 7-12: Schematic of step growth inhibition by blocking the active site using same concentration at (a) low pre-scaled surface and (b) High pre-scaled surface

In agreement with the findings from Amjad *et al.* [149], this study clearly showed that once a thin layer of scale or any other impurities are formed on the surfaces it reduces the scale inhibitor efficiency, due to the large surface area of adsorption provided by the impurities. The next section discusses the effect of flow rate on surface inhibition.

7.5.3 Effect of flow rate on $BaSO_4$ surface inhibition

The results presented in Figure 5-7 showed the effect of different flow rate on surface inhibition using PPCA. It was observed that when the flow rate was increased from 20 ml/mins to 60 ml/min, the surface coverage and average size of reduced by 42 % to 41 %, respectively. It is interesting to realise this

could occur since increasing the flow rate, means more scaling species and the inhibitor molecules will be present on the surface of the $BaSO_4$ crystals.

As mentioned in section 7.5.1, the kinetics of scale formation involves two determining steps: the first is the diffusion of scaling species to the crystal-water interface, the other is the surface reaction in which the scaling ions are incorporated into the scale crystals lattice [106]. The presence of scale inhibitor cannot influence the diffusion of the scaling ions but exert their action by impeding the latter process (surface reaction of scaling ions) [150, 151]. This indicates that when the flow rate is increased the adsorption of scale inhibitor on the crystals has a more dominant effect than the incorporation of the scaling species at the surface of the growing crystals. Hence, the increase in the mass transfer of the scale inhibitor molecules on the crystals, as well as, the strong effect of the scale inhibitor on the growing crystals account for the high surface inhibition at high flow rate.

This result agrees with previous findings reported by Yang *et al.* [152] when they investigated the effect of flow velocity on inhibition of calcium carbonate. From their research, it was found that the inhibition effect increases with increasing fluid velocity. Also, a positive effect of flow rate was reported by Graham *et al.* [12], where research was conducted on the effectiveness of PPCA scale inhibitor on preventing the barium sulphate adherence and growth at the metal surface under both laminar and turbulent conditions. It was shown that the level of surface adherence is more severe under the laminar condition when compared to test conducted under turbulent conditions.

7.5.4 Intermittent injection of scale inhibitors

In previous sections, scale inhibitors were injected continuously. However, due to some number of challenges encountered during downhole chemical injection, the continuous flow of scale inhibitor maybe disrupt; resulting in periodic injection of scale inhibitor into the wellbore. In this section, the effect of injecting scale inhibitor intermittently is discussed. Figure 5-13 and Figure 5-16 presents the surface growth of crystals on the metallic surface when the

scale inhibitor was injected at periodically at different time interval. From the results, it was observed that the longer the system was left free of scale inhibitor, the more it would reduce the performance of the scale inhibitor.

Also, it is interesting to note that when the system was scale inhibitor-free for an interval of 5 minutes (as shown in Figure 5-21) nucleation or subsequent growth of crystals was not observed. This proposes that the presence of scale inhibitor layer on the surface of the crystals/metallic surface prevented nucleation and crystal growth. This result is similar to the findings reported by Ruiz-Agudo *et al.* [109] and Eroini *et al.* [78] where they studied the effect of scale inhibitor on preventing scale formation on surfaces.

From the research by Eroini *et al.* [78], it was observed that stainless steel surface pretreated with PPCA had less amount of scale deposit when compared with an untreated stainless steel surface. It was postulated that when the stainless steel surface was treated with PPCA it appears to be uncharged, which means no direct interaction of the surface with the scaling ions resulting to the low scale formation on the surface. However, untreated stainless steel exhibits partial charges (both positive and negative), which would lead to direct interaction with the scaling ion; hence promotes surface scaling as illustrated in the schematic diagram presented in Figure 7-13.

The SEM image presented in Figure 7-14 clearly revealed that the crystals formed on the metallic surface during continuous injection were different from crystal formed when the inhibitor was injected periodically. For continuous injection as previously explained in section 7.4.1.2, the presence of scale inhibitor hinders surface growth by adsorbing on the distinct step emerging from screw dislocation on the barium sulphate surface as shown in Figure 7-14a [153]. However, the crystals formed during periodic injection presented in Figure 7-14b, indicates that the growth of subsequent crystals originated from the already existing crystals (epitaxial growth). These crystals appear to be growing at favoured nucleation site available on the earlier deposited scale layers.

Figure 7-15 gives a schematic diagram illustrating the growth steps involved in the formation of crystals during periodic injection. The continuous nucleation

and subsequent growth of the crystals during periodic injection explains the low performance of the scale inhibitor. This result simulates real oilfield scale formation in oilfield pipeline since it demonstrates what really occurs on the surfaces when inhibitor are not injected continuously. Also, it shows how existing crystals layer can function as an active centre for surface nucleation (*i.e.* secondary nucleation) and subsequent growth of crystal.

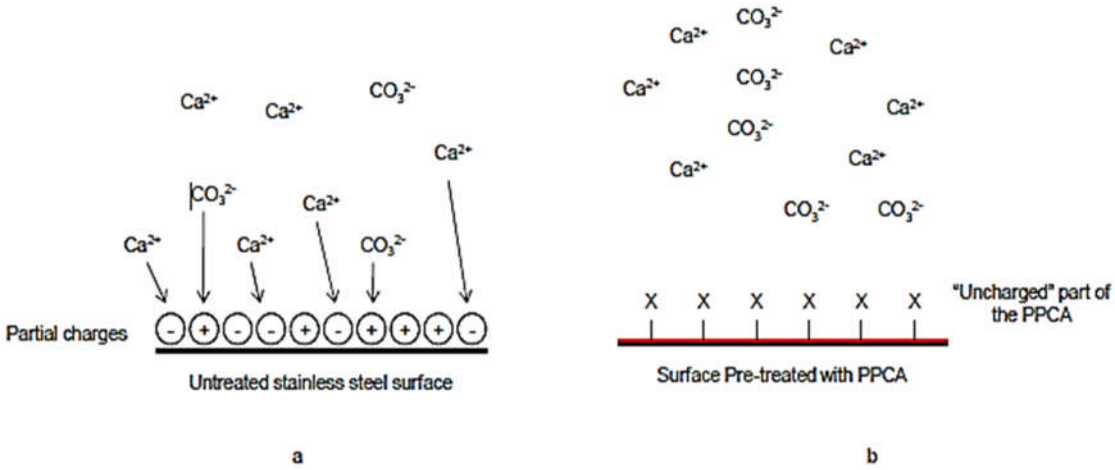

Figure 7-13: Comparison between (a) Untreated stainless steel surface and (b) treated stainless steel (with PPCA) in a solution of calcium carbonate brine solution

The findings from this section clearly elucidate that the intermittent injection of scale inhibitor reduces the performance of the inhibitor due to the continuous nature of scaling process. Hence, for a reliable surface inhibition, appropriate measures should be set in place to ensure scale inhibitors are injected continuously in any location where crystallization starts to occur. In previous discussions, surface inhibition tests were conducted in an aqueous environment. In the next section, surface scaling tests conducted both in an aqueous and oil environment will be discussed.

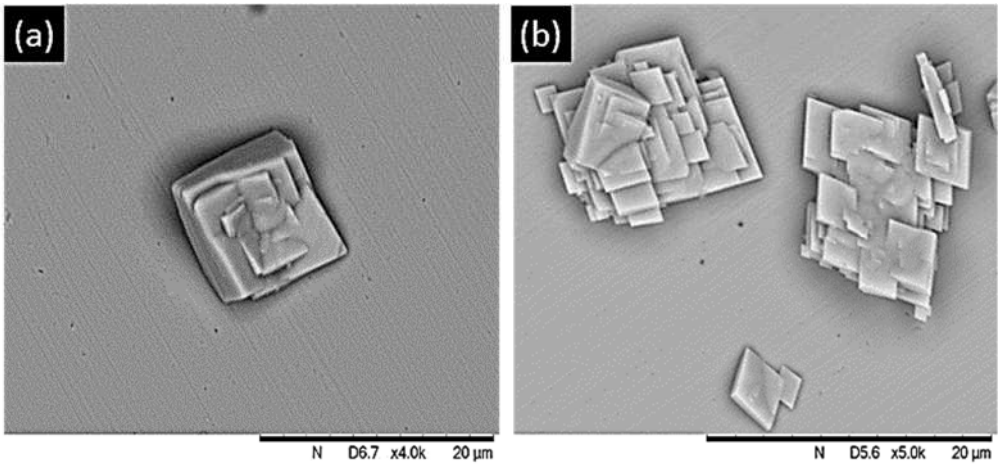

Figure 7-14: Barium sulphate crystal formed on the metallic surface when the scale inhibitor was injected (a) Continuously, and (b) periodically

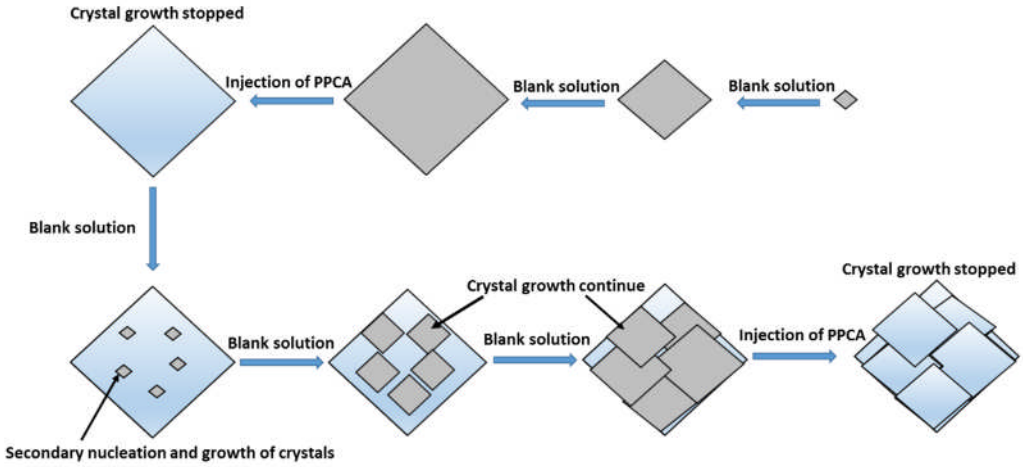

Figure 7-15: Crystal growth of barium sulphate when scale inhibitor is injected periodically

7.6 Scaling in multiphase conditions

7.6.1 Effect of surfaces in multiphase condition

In scaling, various studies have been reported on using surface engineering (chemical and modified coating) in controlling mineral scaling in a single phase environment [6, 16, 20]. However, no study has been reported on how these

coatings performs in a multiphase environment. The aim of this section is to discuss the influence of surfaces in multiphase scaling environment.

From results presented in chapter 6, both surfaces (fluoropolymer and Stainless steel) showed a similar amount of barium sulphate deposition in the single phase environment. With fluoropolymer having a lower surface energy, it is expected that the amount of scale deposited should greatly reduce [154]; but the result exhibited an opposite trend. Comparable findings have been reported in several literatures [16, 61, 155], illustrating no correlation between surface energy and scale deposition. A recent study by Charpentier *et al.* [155], examined the ability to use different modified coating in reducing the mineral surface fouling in subsea safety control valve component. From their study, they reached a conclusion that there was no strong relationship between surface energy and surface fouling. In agreement with the findings reported by Charpentier *et al*. [155], it shows that other parameters (such as surface roughness) would have resulted in the high surface scaling of fluoropolymer, despite having a low surface energy.

Figure 7-16 shows the surfaces of stainless steel and fluoropolymer using light interferometry. From the Figure 7-16, it could be seen that fluoropolymer surface is covered with a micro-scale texture, which is designed to reduce wetting on the surface; thus preventing surface scaling as shown in Figure 7-17a. In contrast, the texture could have a detrimental effect by creating numerous nucleation spot; promoting heterogeneous nucleation and growth of crystals on the surface as illustrated in the schematic diagram presented in Figure 7-17c. The high surface roughness of the fluoropolymer increased the nucleation spot; thus increasing the surface induction time and growth of crystals. This reveals that the poor performance of fluoropolymer on preventing scaling in the single phase environment could be attributed to the surface roughness.

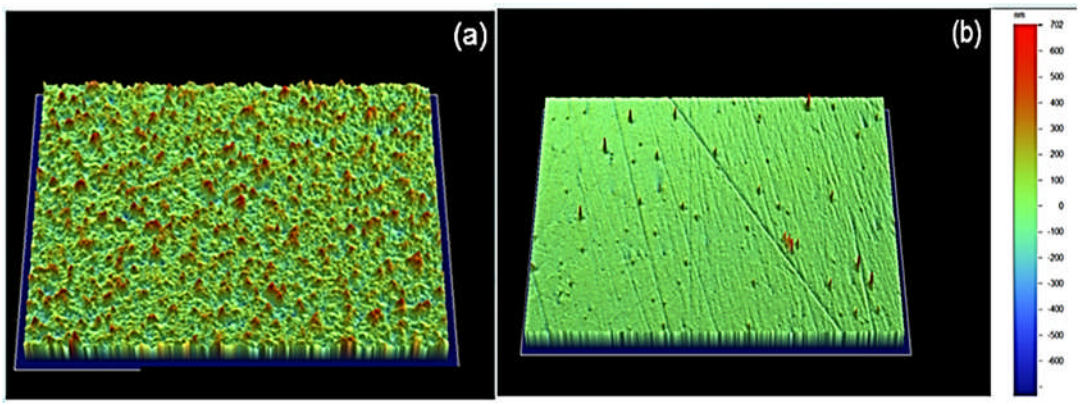

Figure 7-16: Light interferometry 3D scheme of surface of (a) fluoropolymer and (b) Stainless steel

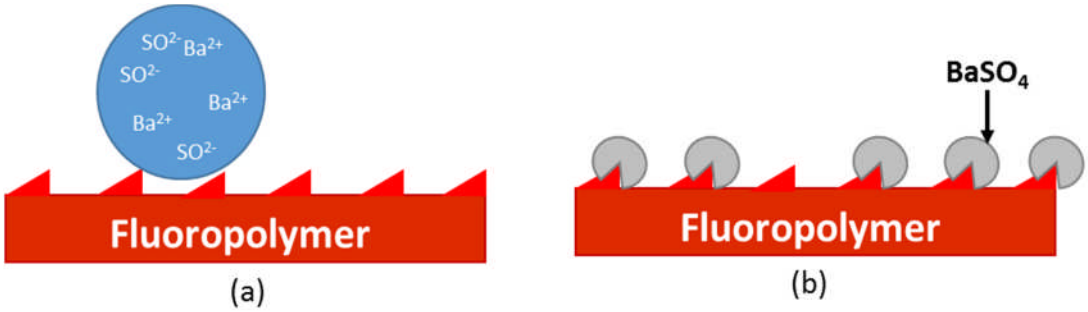

Figure 7-17: (a) Formation of contact angle of a drop on a rough surface (b) Rough surface promoting nucleation and growth of $BaSO_4$ crystal

In a multiphase environment, the results show that the surface fouling reduces with increase in oil concentration in both surfaces. However, the fluoropolymer performed better when compared to the stainless steel. The surface did not reveal any barite crystals on the surface as shown in Figure 6-11. Several explanations can be found to describe more precisely the reduction of mass gain observed in the multiphase environment.

The first reason is the film-forming capability of the emulsion on the substrates. In a single phase environment, only a solid-water interface can exist; however, by introducing oil into the system, the organic phase will displace some of the water molecules from that interface thus reducing surface scaling. The probability of having oil droplets in contact with a solid

surface correlate with a different factors such as the nature of the emulsions or the oil content which explain why surface scaling tends to decrease as the oil content increases [156, 157]. However, the likelihood of a film of paraffin oil wetting the surface does not depend solely on the oil content otherwise both alloys (stainless steel and the fluoropolymer coating) would exhibit similar amounts of barium sulphate. It is suggested that the probability of forming a stable oil film protecting the surface from mineral fouling is associated with the Displacement Energy (DE) – a thermodynamic measure of the ability of a surface to favour oil wetting by displacing water molecules from the interface. DE is defined as:

$$DE = \gamma_{WA} \times Cos\,\theta_{WS} - \gamma_{OA} \times Cos\,\theta_{OS} \qquad 7\text{-}1\ [157]$$

Where γ_{WA} and γ_{OA} denote the water/air and oil/air surface tension respectively while θ_{WS} and θ_{OS} denote the contact angle of water and oil on the surface of interest. Equation 7-1 [157] shows that the DE is simply the difference between the work of adhesion of oil and water, respectively, on the solid surface. An o/w emulsion with an optimal tendency for oil to wet the surface should have a negative DE and the more negative the value of DE is, the more readily such displacement takes place. Using the experimental data presented in Table 6.3, DE was evaluated at 40 and -28 for AISI 316L and the fluoropolymer coating respectively. Such displacement energy values show that clean metal surfaces such as AISI 316L samples used in the current study are polar and thus have an affinity for water. Therefore the latter will have a low contact angle and will be prone to surface scaling as presented in Figure 7-18. The fluoropolymer, however, is highly hydrophobic and favours the displacement of water and the formation of a stable oil layer that prevents scale forming at the surface of the sample.

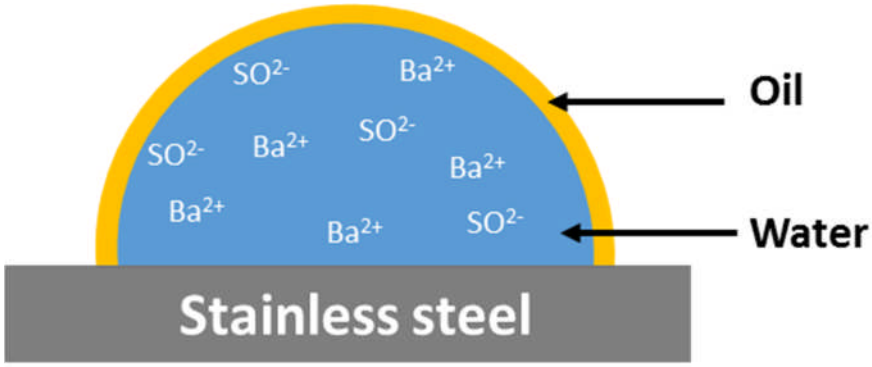

Figure 7-18: High affinity of stainless steel to water exposing the surface to scaling ions

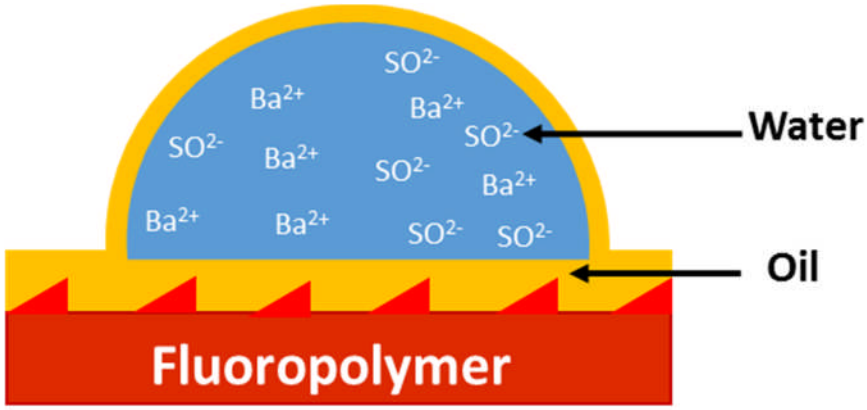

Figure 7-19: Stable oil film formed on the substrate preventing contact of the water phase

Lastly, the adhesion of pre-precipitated crystals from the bulk solution to the surface. In a single phase environment, when the scale is formed in the bulk it could be adhered to the surface due to intermolecular force. Nevertheless, in a multiphase environment, they are two competing processes taking place in the bulk solution. Firstly, the adhesion of crystal from the bulk solution to the surface. The second process is when the crystals are been absorbed strongly on the oil-water interface [158]. Figure 7-20 presents a graphical illustration of barium sulphate absorbed on the o/w emulsion. With the occurrence of this latter process, it implies that the amount of crystal that will be readily available for adhesion process will greatly reduce. Hence, this

process may have also accounted for the reduction of surface scaling in the multiphase environment.

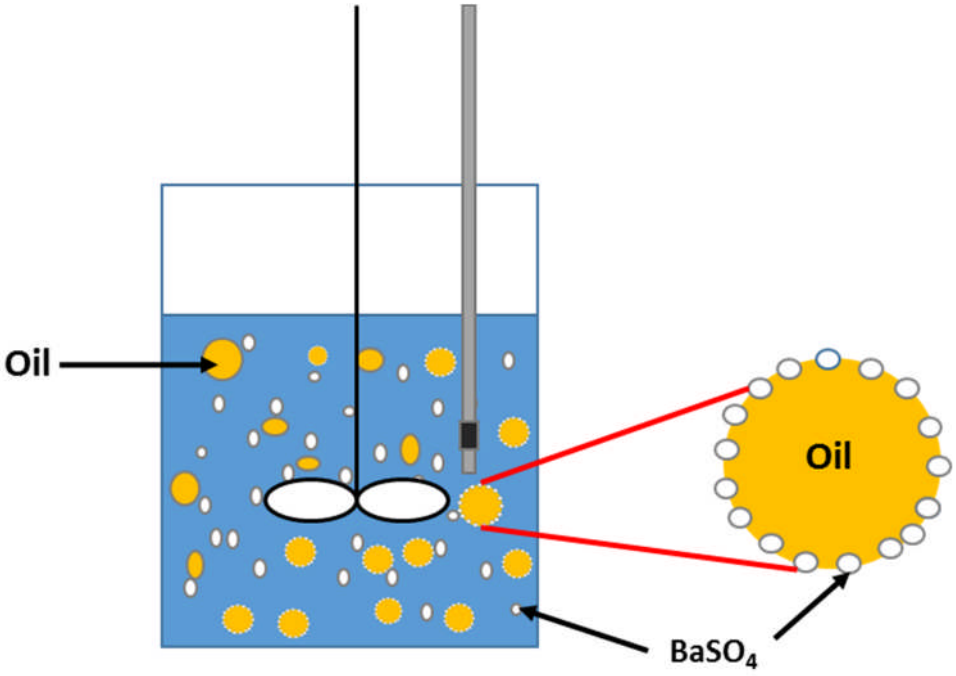

Figure 7-20: Schematic diagram illustrating the absorption of BaSO4 crystals on the o/w emulsion

7.6.2 Effect of scale inhibitors on multiphase condition

The performance of scale inhibitors on preventing surface growth has been reported in many literatures. However, these studies were based on evaluating the efficiency of surface inhibition in a single phase environment. In real oilfield operation, scaling often happens in a multiphase environment. This section is aimed at understanding surface scale inhibition both in single phase and the multiphase environment.

The result presented in Figure 6-10 showed that at a concentration of above the MIC for both scale inhibitor (PPCA and DETPMP), surface fouling was significantly reduced in the single phase and multiphase conditions. In this case, the metallic surface was fully covered by the scale inhibitor; thus preventing the surface from scaling [159, 160]. However, at a concentration below the MIC for both scale Inhibitors (PPCA and DETPMP), surface fouling

in the single phase and multiphase condition was enhanced. However, the behaviour in single phase has already been shown in a study reported by Graham *et.al*. [34, 101]. In their study, the enhancement of surface growth was explained to occur due to the absence of inhibitor film at the metal surface as well as the lower nucleation energy barrier of the surface compared to the bulk solution.

In multiphase conditions, it is believed that there are 2 processes taking place and opposing each other. The first one is the presence of an organic phase wetting the surface which contributes to reducing surface scaling as previously explained. The second effect, however, is the partitioning of the scale inhibitor between the aqueous phase and the organic phase. The second process can be detrimental for surface scaling if the initial concentration of scale is already low. The partitioning coefficient (P) is defined as the ratio of concentrations of a compound in a mixture of two immiscible phases at equilibrium. P is often measured in a water/octanol system and is a direct measure of the difference in solubility of a chemical in two phases. It is often used in its logarithm form as shown in Equation 7-2:

$$\mathbf{Log\ P_{oct/water}} = \mathbf{Log}\left(\frac{\mathbf{[solute]octanol}}{\mathbf{[solute]water}}\right) \qquad 7\text{-}2$$

DETPMP has a very low partition coefficient (log P ≈ -3.4) [161] which indicates the inhibitor will mostly remain in the aqueous phase and therefore remain effective. Such low affinity with the organic phase explains why the scaling tests at 1 ppm of DETPMP in single and multiphase exhibit very similar surface barium content. PPCA, however, has an affinity for organic solvents and values of log P around 0 [162] have been reported depending on the molecular weight of the polymer and the pH of the aqueous phase. Such compatibility with oil is likely to explain the increase of barium content deposited on the surface in multiphase condition when PPCA is present at a concentration below MIC.

The results obtained in this section revealed that the presence of oil droplet could influence the deposition of barium sulphate on surfaces. Anti-scaling surface with low surface energy was shown not to performed impressively in

the aqueous phase, but the performance was greatly increased in the presence of oil phase. On the contrary, the presence of multiphase was revealed to have a negative impact on the performance of scale inhibitor. These findings suggest that, in choosing a scale inhibitor and anti-scaling surfaces in preventing or reducing barium sulphate formation, a good knowledge of how these surfaces/inhibitors perform in both single phase and multiphase environment is vital. Hence, the test should be conducted to evaluating the performance of the surfaces both in an aqueous environment and multiphase environment.

Chapter 8 Conclusions

This study has concentrated on understanding the bulk precipitation and surface scaling of barium sulphate in the absence and presence of scale inhibitors. This chapter gives a summary of the main outcomes obtained from this work. The chapter is divided into three sections based on the study objectives.

8.1 Kinetics of barium sulphate bulk precipitation and surface deposition with and without the presence of scale inhibitor

- The results confirmed that the deposition of scale on surfaces can occur solely by heterogeneous nucleation and subsequent growth; rather than the adhesion of scale from the bulk solution. Therefore, it implies that surface fouling as result of heterogeneous nucleation and growth on surfaces should be taken into consideration when designing a scale treatment strategy.

- The study shows the strong effect of saturation ratios on nucleation and growth mechanisms of barium sulphate on stainless steel surfaces. A distinct two-step mechanism with instantaneous nucleation followed by growth of crystals was observed at high saturation ratios, whilst at lower saturation ratios, progressive nucleation was observed with the formation of new nuclei and growth of existing crystals occurring simultaneously throughout the experiments.

- The temperature was seen to plays an important role in the rate of nucleation and the nucleation mechanism of surface crystallization of barium sulphate.

- At high concentration of scale inhibitors (DETPMP, PPCA and VS-Co), the further growth of crystals on the metallic surface was stopped

instantly. However, a different trend was observed for the each scale inhibitors at low concentration.

- The results showed that PPCA completely stopped the subsequent growth of crystals at a low concentration (1 ppm), by adsorbing on the dominant faces of the crystals.

- At lower concentration of DETPMP, crystal growth of barium sulphate on the metallic surface was enhanced. Furthermore, it resulted to change in morphology of the crystals formed on the metallic surface (*i.e.* crystal had a hexagonal shape due to the appearance of (011) crystal face). The (011) crystal face disappears when the concentration of DETPMP was increased. This results clearly indicated that at high concentration, the molecule of the DETPMP was likely absorbed on the dominant faces of barium sulphate.

- Low concentration of VS-Co was not effective to stop the crystal growth of barium sulphate on the metallic surface.

8.2 Factors influencing surface inhibition of barium sulphate

- The study revealed that the performance of scale inhibitor on hindering bulk precipitation is different from surface inhibition. Also, it shows that the efficiency of scale inhibitor on preventing surface growth reduces as the saturation ratio is increased.

- This work highlight the limitations of current procedures used to evaluate the minimum inhibitor concentration (MIC) required to stop bulk precipitation but disregard surface fouling aspects.

- The results showed that increase in flow rate increases the surface efficiency of scale inhibitor (PPCA). Furthermore, these findings give insight on an efficient scale inhibition strategies to be developed where the dose rate can be adjusted in time *i.e.* initially a high flow rate of

inhibitor is used to instantly block the active sites on any pre-scaled surface and is later reduced to an optimal level that prevents precipitation.

- The study showed that the presence of pre-existing barium sulphate crystal reduces the scale inhibition efficient. This was attributed to the large surface area provided by the pre-existing crystals for adsorption of scale inhibitors.

- This study revealed the negative outcome of under-injecting scale inhibitor during continuous injection of scale inhibitor. Also, it demonstrates how pre-existing crystals layer can act as a nucleation site for subsequent crystal growth.

8.3 Surface scaling in multiphase environment

- The results presented shows that surface fouling of barium sulphate on metallic steel surfaces was reduced as the concentration of oil phase was increased.

- Low surface energy coatings such as the fluoropolymer used in this study do not show great antifouling properties in aqueous phase scaling tests and the barium sulphate mass gain was similar to the one observed on stainless steel.

- In multiphase conditions, the use of fluoropolymer hugely reduced the deposition of barium sulphate on the metallic surface. The performance of the fluoropolymer coating tested was attributed to its propensity to favour an oil wetting state, which prevented the surface of fluoropolymer not to be in contact with the aqueous phase where scaling occurs.

- The work shows that in the presence of scale inhibitors, the ability of the inhibitor to migrate into the organic phase is of paramount importance especially when concentration falls below MIC levels. The dosage of scale inhibitors below the optimum (MIC) concentration can result in a dramatic increase of surface scaling.

Chapter 9 Future work

This work conducted in this study have demonstrated to meet the set objectives of this study. Nevertheless, there are some other factors and conditions which are encountered in the oilfield operations that were not considered in this study. Therefore in this chapter, the following recommendations are suggested in order to further understand the bulk precipitation and surface deposition of barium sulphate in the oil and gas facilities.

9.1 Improving the *in-situ* flow rig design

The *in-situ* flow rig has revealed to be suitable for studying both bulk precipitation and surface scaling of barium sulphate in a flowing system. In this work, the set-up was designed to operate under laminar flow regime, atmospheric pressure and at moderate temperatures. However, in oil and gas operations, they are sometimes faced with more severe physical conditions (e.g. turbulent flow regime, high temperature and pressure). Hence, further development and modification of the *in-situ* flow rig is suggested to be able to simulate more severe oilfield conditions.

9.2 The influence of other chemicals on surface scale formation and inhibitor

Extensive information of different scale inhibitors on the subsequent growth on barium sulphate has been obtained from this study. However, these experiments were carried out using just scale inhibitors. In real oilfield operations, they are other flow assurance problems been faced and it requires the continuous injection of various chemicals to prevent their occurrences (such as corrosion inhibitors, gas hydrate inhibitors and wax inhibitors). Hence, further studies should be conducted to investigate the interactions between scale inhibitor and other inhibitors, as well as, evaluating the effect

(synergistic or antagonistic) on scale formation inhibitors both in the bulk solution and on surfaces.

9.3 Effect of impurities on the barium sulphate surface inhibition

The study has shown that the presence of pre-existing crystal layer affects the surface inhibition efficiency of PPCA scale inhibitors. However, they are various insoluble material (metal oxides, metal carbonate and clay) found in production water used during seawater injected. Future work should investigate how these insoluble materials affect the inhibition of barium sulphate scale.

9.4 Scaling in multiphase environment

The result has shown that the presence of the oil phase affects the surface scaling barium sulphate. Nevertheless, it will be interesting to evaluate the influence of other experimental parameters (such as the effect of scale on the stability of emulsions, the effect of emulsion size on the kinetic of scale precipitation and wetting properties) in a multiphase scaling environment. This will further expand the understanding of scale formation in oil and gas industry.

References

[1] U. S. E. I. Administration, "EIA, International Energy Outlook," Washington, DC2001.

[2] K. D. Demadis, E. Mavredaki, A. Stathoulopoulou, E. Neofotistou, and C. Mantzaridis, " Industrial water systems: problems, challenges and solutions for the process industries," *Desalination,* vol. 213, pp. 38-46, 2007.

[3] L. C. Uren, *Petroleum Production Engineering; Oil field Exploitation*: M.-H.B. Company, 1953.

[4] A. I. Levorsen and F. A. Berry, *Geology of petroleum* vol. 8: WH Freeman San Francisco, 1967.

[5] W. A. England, "Secondary migration and accumulation of hydrocarbons, In the petroleum system from source to trap," *Amer. Assoc. Petrol,* vol. 60, pp. 211-217, 1994.

[6] T. Geddert, I. Bialuch, W. Augustin, and S. Scholl, "Extending the Induction Period of Crystallization Fouling Through Surface Coating," *Heat Transfer Engineering,* vol. 30, pp. 868-875, 2009/10/01 2009.

[7] B. Olliver and M. Magot, *Petroleum Microbiology*. Washington DC: ASM press, 1995.

[8] R. A. Betty Simkins, *Energy Finance: Analysis and Valuation, Risk Management and Future of Energy*. New Jersey: John Wiley & Sons, Inc., 2013.

[9] A. Badr, "Inhibition of barium sulphate at high-barium formation water," *Petroleum Science and Engineering,* pp. 90-97, 2012.

[10] S. Foroutan and J. Moghadasi, "A neural network approach to predict formation damage due to calcium sulphate precipitation," in *SPE European Formation Damage Conference & Exhibition*, 2013.

[11] S. J. Dyer and G. M. Graham, "The effect of temperature and pressure on oilfield scale formation," *Journal of Petroleum Science and Engineering,* vol. 35, pp. 95-107, 7// 2002.

[12] A. C. Todd and M. Yuan, "Barium and Strontium Sulfate Solid Solution Formation in Relation to North Sea Scaling Problems," *SPE Production Engineering,* vol. 5, pp. 279-285, 08/01/1990 1990.

[13] J. Moghadasi, H. Müller-Steinhagen, M. Jamialahmadi, and A. Sharif, "Model study on the kinetics of oil field formation damage due to salt precipitation from injection," *Journal of Petroleum Science and Engineering,* vol. 43, pp. 201-217, 8// 2004.

[14] W. W. Frenier and M. Ziauddin, *Formation, removal, and inhibition of inorganic scale in the oilfield environment*: Society of Petroleum Engineers Richardson, TX, 2008.

[15] W. C. Cheong, P. H. Gaskell, and A. Neville, "Substrate effect on surface adhesion/crystallisation of calcium carbonate," *Journal of Crystal Growth,* vol. 363, pp. 7-21, 1/15/ 2013.

[16] M. M. Vazirian, T. V. J. Charpentier, M. de Oliveira Penna, and A. Neville, "Surface inorganic scale formation in oil and gas industry: As adhesion and deposition processes," *Journal of Petroleum Science and Engineering,* vol. 137, pp. 22-32, 1// 2016.

[17] H. Nam, C. Bai, J. Shim, and Y. I. Cho, "A study on the reduction of CaCO3 fouling in hot-water storage tank by short pulse plasma application (rev 1 yc)," *Applied Thermal Engineering,* vol. 102, pp. 108-114, 6/5/ 2016.

[18] C. J. Hinrichsen, "Preventing scale deposition in oil production facilities: An industry review," in *CORROSION 98*, 1998.

[19] G. M. Graham, E. J. Mackay, S. J. Dyer, and H. Bourne, "The Challenges for Scale Control in Deepwater Production Systems: Chemical Inhibition and Placement," in *CORROSION 2002*, 2002.

[20] T. V. J. Charpentier, A. Neville, S. Baudin, M. J. Smith, M. Euvrard, A. Bell*, et al.*, "Liquid infused porous surfaces for mineral fouling mitigation," *Journal of Colloid and Interface Science,* vol. 444, pp. 81-86, 4/15/ 2015.

[21] G. M. Graham, L. S. Boak, and K. S. Sorbie, "The Influence of Formation Calcium and Magnesium on the Effectiveness of Generically

Different Barium Sulphate Oilfield Scale Inhibitors," *SPE Production & Operations,* vol. 18, pp. 28-44, 02/01/2003 2003.

[22] K. S. Sorbie, R. M. S. Wat, and A. C. Todd, "Interpretation and Theoretical Modeling of Scale-Inhibitor/Tracer Corefloods," *Society of Petroleum Engineers,* 1992/8/1/ 1992.

[23] K. Sorbie, M. Yuan, and M. Jordan, "Application of a scale inhibitor squeeze model to improve field squeeze treatment design," in *European Petroleum Conference*, 1994.

[24] S. Shaw and K. Sorbie, "Structure, Stoichiometry, and Modelling of Calcium Phosphonate Scale Inhibitor Complexes for Application in Precipitation Squeeze Processes," presented at the 2013 SPE International Symposium on Oilfield Chemistry, The Woodlands, TX, USA, 2013.

[25] S. S. Shaw, "Investigation into the mechanism of formation and prevention of Barium sulphate oilfied scale," PhD, Petroleum Engineering, University of Heriot Watt, 2012.

[26] L. S. Boak, G. M. Graham, and K. S. Sorbie, "The Influence of Divalent Cations on the Performance of BaSO Scale Inhibitor Species," presented at the SPE International Symposium on Oilfield Chemistry, Houston, Texas, 1999.

[27] M. B. Tomson, A. T. Kan, and G. Fu, "Inhibition Of Barite Scale In The Presence Of Hydrate Inhibitors," *Society of Petroleum Engineers,* 2005/9/1/ 2005.

[28] Z. Amjad, "Inhibition of barium sulfate precipitation: Effects of additives, solution pH, and supersaturation," *Water Treatment,* vol. 9, pp. 47-56, // 1994.

[29] T. Chen, A. Neville, and M. Yuan, "Calcium carbonate scale formation—assessing the initial stages of precipitation and deposition," *Journal of Petroleum Science and Engineering,* vol. 46, pp. 185-194, 3/15/ 2005.

[30] E. Mavredaki, "Barium Sulphate Formation Kinetics and Inhibition at Surfaces," Doctor of Philosophy, School of Mechanical Engineering, The University of Leeds, Leeds, 2009.

[31] F.-A. Setta and A. Neville, "Efficiency assessment of inhibitors on CaCO3 precipitation kinetics in the bulk and deposition on a stainless steel surface (316 L)," *Desalination,* vol. 281, pp. 340-347, 10/17/ 2011.

[32] G. M. Graham, L. S. Boak, and C. M. Hobden, "Examination of the Effect of Generically Different Scale Inhibitor Species (PPCA and DETPMP) on the Adherence and Growth of Barium Sulphate Scale on Metal Surfaces," presented at the International Symposium on Oilfield Scale, Aberdeen, United Kingdom, 2001.

[33] O. Bukuaghangin, A. Neville, and T. V. Charpentier, "Scale Formation in Multiphase Conditions," presented at the Oil Field Chemistry Symposium, Gielo, 2015.

[34] A. Graham, E. Vieille, A. Neville, L. Boak, and K. Sorbie, "Inhibition of BaSO4 at a Hastelloy metal surface and in solution: The Consequences of falling below the Minimum Inhibitor Concentration (MIC)," in *SPE International Symposium on Oilfield Scale*, 2004.

[35] A. Morizot and A. Neville, "A study of inhibitor film formation using an electrochemical technique," in *CORROSION 2000*, 2000.

[36] J. Moghadasi, M. Jamialahmadi, H. Müller-Steinhagen, and A. Sharif, "Formation Damage Due to Scale Formation in Porous Media Resulting From Water Injection," presented at the SPE International Symposium and Exhibition on Formation Damage Control, Lafayette, Louisiana, 2004.

[37] J. Moghadasi, M. Jamialahmadi, H. Müller-Steinhagen, A. Sharif, M. R. Izadpanah, E. Motaei*, et al.*, "Formation Damage in Iranian Oil Fields," presented at the International Symposium and Exhibition on Formation Damage Control, Lafayette, Louisiana, 2002.

[38] T. Chen, "New insights into the mechanisms of calcium carbonate mineral scale formation and inhibition," School of Engineering and Physical Sciences, Heriot-Watt University, Edinburgh, UK, Edinburgh, 2005.

[39] J. Moghadasi, M. Jamialahmadi, H. Müller-Steinhagen, A. Sharif, A. Ghalambor, M. R. Izadpanah*, et al.*, "Scale Formation in Iranian Oil Reservoir and Production Equipment During Water Injection,"

presented at the International Symposium on Oilfield Scale, Aberdeen, United Kingdom, 2003.

[40] E. J. Mackay, "Scale Inhibitor Application in Injection Wells to Protect Against Damage to Production Wells: When Does It Work?," presented at the SPE European Formation Damage Conference, Sheveningen, The Netherlands, 2005.

[41] M. M. Jordan and E. J. Mackay, "Intergated Field Development For Effective Scale Control Throughout the Water Cycle in Deep Water Subsea Fields," presented at the SPE Europec/EAGE Annual Conference, Madrid, Spain, 2005.

[42] M. S. H. Bader, "Sulfate removal technologies for oil fields seawater injection operations," *Journal of Petroleum Science and Engineering,* vol. 55, pp. 93-110, 1// 2007.

[43] S. Otakar and G. John, *Precipitation: Basic Priciple and Inustrial Application*. Boston: Butterworth Heinemann, 1992.

[44] A. Antony, J. H. Low, S. Gray, A. E. Childress, P. Le-Clech, and G. Leslie, "Scale formation and control in high pressure membrane water treatment systems: A review," *Journal of Membrane Science,* vol. 383, pp. 1-16, 11/1/ 2011.

[45] W.-Y. Shih, A. Rahardianto, R.-W. Lee, and Y. Cohen, "Morphometric characterization of calcium sulfate dihydrate (gypsum) scale on reverse osmosis membranes," *Journal of Membrane Science,* vol. 252, pp. 253-263, 4/15/ 2005.

[46] J. R. Luft and G. T. DeTitta, "A method to produce microseed stock for use in the crystallization of biological macromolecules," *Acta Crystallogr D Biol Crystallogr,* vol. 55, pp. 988-93, May 1999.

[47] O. Söhnel and J. W. Mullin, "Interpretation of crystallization induction periods," *Journal of Colloid and Interface Science,* vol. 123, pp. 43-50, 5// 1988.

[48] M. Crabtree, D. Eslinger, P. Fletcher, A. Johson, and G. King, "Fighting Scale- Removal and prevention," *Oilfield review,* pp. 30-45, 1999.

[49] C. H. L. Goodman, *Crystal growth : theory and techniques*. London ; New York Plenum Press, 1974.

[50] J. W. Mullin, *Crystallization*: Elsevier Butterworth-Heinemann, 2001.

[51] A. S. Myerson, *Handbook of Industrial Crystallization*: Butterworth-Heinemann, 2001.

[52] A. Chianese, F. Di Berardino, and A. G. Jones, "On the effect of secondary nucleation on the crystal size distribution from a seeded batch crystallizer," *Chemical Engineering Science,* vol. 48, pp. 551-560, 2// 1993.

[53] P. J. Daudey, G. M. van Rosmalen, and E. J. de Jong, "Secondary nucleation kinetcs of ammonium sulfate in a CMSMPR crystallizer," *Journal of Crystal Growth,* vol. 99, pp. 1076-1081, 1// 1990.

[54] A. E. D. M. Van der Heijden, J. P. Van der Eerden, and G. M. Van Rosmalen, "The secondary nucleation rate: a physical model," *Chemical Engineering Science,* vol. 49, pp. 3103-3113, 9// 1994.

[55] A. W. Vere, *Crystal Growth: Principles and Progress*. New York: Plenum, 1987.

[56] D. Packham, "Theories of Fundamental Adhesion," in *Handbook of Adhesion Technology*, L. M. da Silva, A. Öchsner, and R. Adams, Eds., ed: Springer Berlin Heidelberg, 2011, pp. 9-38.

[57] S. Ebnesajjad, "1 - Introduction and Adhesion Theories," in *Handbook of Adhesives and Surface Preparation*, S. Ebnesajjad, Ed., ed Oxford: William Andrew Publishing, 2011, pp. 3-13.

[58] V. Eroini, "Kinetic study of calcium carbonate formation and inhibition by using an in-situ flow cell," Doctor of Philosophy, School of Mechanical Engineering, The University of Leeds, 2011.

[59] E. J. W. Verwey, J. T. G. Overbeek, and J. T. G. Overbeek, *Theory of the Stability of Lyophobic Colloids*: Dover Publications, 1999.

[60] R. Oliveira, "Understanding adhesion: A means for preventing fouling," *Experimental Thermal and Fluid Science,* vol. 14, pp. 316-322, 5// 1997.

[61] M. Förster, W. Augustin, and M. Bohnet, "Influence of the adhesion force crystal/heat exchanger surface on fouling mitigation," *Chemical Engineering and Processing: Process Intensification,* vol. 38, pp. 449-461, 9// 1999.

[62] B. Yong and B. Qiang, *Subsea Engineering Handbook*. Waltham: Elsevier Inc, 2012.

[63] A. B. BinMerdhah, "Inhibition of barium sulfate scale at high-barium formation water," *Journal of Petroleum Science and Engineering,* vol. 90–91, pp. 124-130, 7// 2012.

[64] V. Tantayakom, T. Sreethawong, H. S. Fogler, F. F. de Moraes, and S. Chavadej, "Scale inhibition study by turbidity measurement," *Journal of Colloid and Interface Science,* vol. 284, pp. 57-65, 4/1/ 2005.

[65] M. o. Environment, "Requirements for determining barite sites," M. o. Environment, Ed., ed. British Columbia: Protocol 14, 2009.

[66] K. Peyvandi, A. Haghtalab, and M. R. Omidkhah, "Using an electrochemical technique to study the effective variables on morphology and deposition of CaCO3 and BaSO4 at the metal surface," *Journal of Crystal Growth,* vol. 354, pp. 109-118, 9/1/ 2012.

[67] K. S. Sorbie and N. Laing, "How Scale Inhibitors Work: Mechanisms of Selected Barium Sulphate Scale inhibitors Across a Wide Temperature Range," presented at the SPE International Symposium on Oilfield Scale, Aberdeen, United Kingdom, 2004.

[68] A. J. B. Hennessy and G. M. Graham, "The effect of additives on the co-crystallisation of calcium with barium sulphate," *Journal of Crystal Growth,* vol. 237–239, Part 3, pp. 2153-2159, 4// 2002.

[69] F. Jones, A. Oliviera, G. M. Parkinson, A. L. Rohl, A. Stanley, and T. Upson, "The effect of calcium ions on the precipitation of barium sulphate 1: calcium ions in the absence of organic additives," *Journal of Crystal Growth,* vol. 262, pp. 572-580, 2/15/ 2004.

[70] G. G. A. Hennessy, J. Hastings, D.P. Siddons, Z. Zhong, "New pressure flow cell to monitor BaSO4 precipitation using synchrotron in situ angle-dispersive X-ray diffraction," *Journal of Synchrotron Radiation,* pp. 323-324, 2002.

[71] M. F. Brigatti, E. Galli, and L. Medici, "Ba-rich celestite: new data and crystal structure refinement," *Mineralogical Society,* pp. 447–451, 1997.

[72] E. Mavredaki, A. Neville, and K. Sorbie, "Assessment of barium sulphate formation and inhibition at surfaces with synchrotron X-ray diffraction (SXRD)," *Applied Surface Science,* vol. 257, pp. 4264-4271, 2/15/ 2011.

[73] M. I. El-Hattab, "Scale Deposition in Surface and Subsurface Production Equipment in the Gulf of Suez," *Journal of Petroleum Technology,* vol. 37, pp. 1640-1652, 09/01/1985 1985.

[74] O. J. G. Vetter, "How Barium Sulfate Is Formed: An Interpretation," *Journal of Petroleum Technology,* vol. 27, pp. 1515-1524, 12/01/1975 1975.

[75] M. M. Jordan, K. Sjuraether, I. R. Collins, N. D. Feasey, and D. Emmons, "Life Cycle Management of Scale Control within Subsea Fields and its Impact on Flow Assurance, Gulf of Mexico and the North Sea Basin," presented at the SPE Annual Technical Conference and Exhibition, New Orleans, Louisiana, 2001.

[76] V. Khoi Vu, C. Hurtevent, and K. A. Davis, "Eliminating the Need for Scale Inhibition Treatments for Elf Exploration Angola's Girassol Field," presented at the International Symposium on Oilfield Scale, Aberdeen, United Kingdom, 2000.

[77] M. Förster and M. Bohnet, "Influence of the interfacial free energy crystal/heat transfer surface on the induction period during fouling," *International Journal of Thermal Sciences,* vol. 38, pp. 944-954, 12// 1999.

[78] V. Eroini, N. Kapur, A. Neville, and M. Euvrard, "Preventing scale formation using modified surfaces," in *CORROSION 2011*, 2011.

[79] H. Müller-Steinhagen and Q. Zhao, "Investigation of low fouling surface alloys made by ion implantation technology," *Chemical Engineering Science,* vol. 52, pp. 3321-3332, 10// 1997.

[80] R. Jaouhari, A. Benbachir, A. Guenbour, C. Gabrielli, J. Garcia-Jareno, and G. Maurin, "Influence of water composition and substrate on

electrochemical scaling," *Journal of The Electrochemical Society,* vol. 147, pp. 2151-2161, 2000.

[81] T. Charpentier, A. Neville, S. Baraka-Lokmane, C. Hurtevent, J. Ordonez-Varela, and F. M. Nielsen, "Evaluation of anti-fouling surfaces for prevention of mineral scaling in sub-surface safety valves," in *SPE International Oilfield Scale Conference and Exhibition*, 2014.

[82] S. A. Parsons and J. MacAdam, "Scaling On Heat Transfer Surfaces: Chemical Versus Non-chemical Control," in *CORROSION 2004*, 2004.

[83] M. M. Jordan, K. Sjursaether, M. C. Edgerton, and R. Bruce, "Inhibition of Lead and Zinc Sulphide Scale Deposits Formed during Production from High Temperature Oil and Condensate Reservoirs," presented at the SPE Asia Pacific Oil and Gas Conference and Exhibition, Brisbane, Australia, 2000.

[84] O. J. Vetter, "Oilfield Scale---Can We Handle It?," *Journal of Petroleum Technology,* vol. 28, pp. 1402-1408, 12/01/1976 1976.

[85] K. S. Sorbie, P. Jiang, M. D. Yuan, P. Chen, M. M. Jordan, and A. C. Todd, "The Effect of pH, Calcium, and Temperature on the Adsorption of Phosphonate Inhibitor Onto Consolidated and Crushed Sandstone," presented at the SPE Annual Technical Conference and Exhibition, Houston, Texas, 1993.

[86] L. S. Boak, "Factors that impact scale inhibitor mechanisms," Heriot-Watt University, 2013.

[87] W. J. Benton, I. R. Collins, I. M. Grimsey, G. M. Parkinson, and S. A. Rodger, "Nucleation, growth and inhibition of barium sulfate-controlled modification with organic and inorganic additives," *Faraday Discussions,* vol. 95, pp. 281-297, 1993.

[88] S. Taj, S. Papavinasam, and R. W. Revie, "Development of green inhibitors for oil and gas applications," in *CORROSION 2006*, 2006.

[89] M. Jordan, K. Sjursaether, M. Edgerton, and R. Bruce, "Inhibition of Lead and Zinc Sulphide Scale Deposits Formed during Production from High Temperature Oil and Condensate Reservoirs," in *SPE Asia Pacific Oil and Gas Conference and Exhibition*, 2000.

[90] Z. Amjad and P. G. Koutsoukos, "Evaluation of maleic acid based polymers as scale inhibitors and dispersants for industrial water applications," *Desalination,* vol. 335, pp. 55-63, 2/17/ 2014.

[91] G. Graham, K. Sorbie, and M. Jordan, "How scale inhibitors work and how this affects test methodology," in *IBC, 3rd International Conference on Solving Oilfield Scaling, Aberdeen, UK*, 1997, pp. 22-23.

[92] M. C. Van der Leeden and G. M. Van Rosmalen, "Development of Inhibitors for Barium Sulphate Depositiom," *3rd International Symposium on Chemicals in the Oil Industr,* pp. 65-85, , 1988.

[93] M. C. Van der Leeden and G. M. Van Rosmalen, "Inhibition of Barium Sulfate Deposition by Polycarboxylates of Various Molecular Structures," *SPE Production Engineering,* vol. 5, pp. 70-76, 02/01/1990 1990.

[94] M. C. Van der Leeden, Reediji, J. and Van Rosmalen, G.M., "The Influence of Various Phosphonates on the Growth Rate of Barium Sulphate Crystals in Suspension," *Estudios Geol.,* pp. 279-287, 1982.

[95] M. Andrei and F. Gagliardi, "Redissolution studies in bulk and in coreflood for PPCA scales inhibitor," *Journal of Petroleum Science and Engineering,* vol. 43, pp. 35-55, 6// 2004.

[96] L. A. Bromley, D. Cottier, R. J. Davey, B. Dobbs, S. Smith, and B. R. Heywood, "Interactions at the organic/inorganic interface: molecular design of crystallization inhibitors for barite," *Langmuir,* vol. 9, pp. 3594-3599, 1993/12/01 1993.

[97] S. S. Shaw, K. S. Sorbie, and L. S. Boak, "The Effects of Barium Sulphate Saturation Ratio, Calcium and Magnesium on the Inhibition Efficiency: I Phosphonate Scale Inhibitors," presented at the SPE International Conference on Oilfield Scale, Aberdeen, UK, 2010.

[98] S. S. Shaw, K. Sorbie, and L. S. Boak, "The Effects of Barium Sulfate Saturation Ratio, Calcium, and Magnesium on the Inhibition Efficiency: Part II Polymeric Scale Inhibitors," *SPE Production & Operations,* vol. 27, pp. pp. 390-403, 11/01/2012 2012.

[99] M. Yuan, "Barium Sulfate Scale Inhibition in the Deepwater Cold Temperature Environment," presented at the International Symposium on Oilfield Scale, Aberdeen, United Kingdom, 2001.

[100] N. Laing, G. M. Graham, and S. J. Dyer, "Barium Sulphate Inhibition in Subsea Systems - The Impact of Cold Seabed Temperatures on the Performance of Generically Different Scale Inhibitor Species," presented at the International Symposium on Oilfield Chemistry, Houston, Texas, 2003.

[101] A. L. Graham, L. S. Boak, K. S. Sorbie, and A. Neville, "How Minimum Inhibitor Concentration (MIC) and Sub-MIC Concentrations Affect Bulk Precipitation and Surface Scaling Rates," *SPE Production & Operations,* vol. 21, pp. pp. 19-25, 02/01/2006 2006.

[102] A. L. Graham, L. S. Boak, A. Neville, and K. S. Sorbie, "How Minimum Inhibitor Concentration (MIC) and Sub-MIC Concentrations Affect Bulk Precipitation and Surface Scaling Rates," presented at the SPE International Symposium on Oilfield Chemistry, The Woodlands, Texas, 2005.

[103] B. Tolaieb, R. Bingham, and A. Neville, "Barium Sulfate Kinetics on Steel Surfaces at Different Supersaturation Ratios," in *CORROSION 2013*, 2013.

[104] F. Jones, P. Jones, M. I. Ogden, W. R. Richmond, A. L. Rohl, and M. Saunders, "The interaction of EDTA with barium sulfate," *Journal of Colloid and Interface Science,* vol. 316, pp. 553-561, 12/15/ 2007.

[105] A. Duchene, A. Neville, and M. Euvrard, "An In-Situ Flow Cell To Highlight Different Mechanisms Of CaCO3 Inhibition By Green And Non Green Polymers," in *OTC Brasil*, 2011.

[106] D. Hasson, D. Bramson, B. Limoni-Relis, and R. Semiat, "Influence of the flow system on the inhibitory action of CaCO3 scale prevention additives," *Desalination,* vol. 108, pp. 67-79, 2// 1997.

[107] C. M. Pina, C. V. Putnis, U. Becker, S. Biswas, E. C. Carroll, and D. Bosbach, "An atomic force microscopy and molecular simulations study of the inhibition of barite growth by phosphonates," *Surface Science,* vol. 553, pp. 61-74, 3/20/ 2004.

[108] H. H. Teng, P. M. Dove, and J. J. De Yoreo, "Kinetics of calcite growth: surface processes and relationships to macroscopic rate laws," *Geochimica et Cosmochimica Acta,* vol. 64, pp. 2255-2266, 7// 2000.

[109] C. Ruiz-Agudo, C. V. Putnis, and A. Putnis, "The effect of a copolymer inhibitor on baryte precipitation," *Mineralogical Magazine,* vol. 78, pp. 1423-1430, 2014.

[110] N. Abdel-Aal, K. Satoh, and K. Sawada, "Study of the adhesion mechanism of $CaCO_3$ using a combined bulk chemistry/QCM technique," *Journal of Crystal Growth,* vol. 245, pp. 87-100, 11// 2002.

[111] C. Garcia, G. Courbin, C. Noilc, F. Ropital, and C. Fiaud, "Development of the electrochemical quartz crystal microbalance to control carbonate scale deposit," NACE International, Houston, TX (United States)1999.

[112] T. Chen, A. Neville, K. Sorbie, and Z. Zhong, "In-situ monitoring the inhibiting effect of polyphosphinocarboxylic acid on CaCO3 scale formation by synchrotron X-ray diffraction," *Chemical Engineering Science,* vol. 64, pp. 912-918, 3// 2009.

[113] A. Quddus and I. M. Allam, "BaSO4 scale deposition on stainless steel," *Desalination,* vol. 127, pp. 219-224, 2/20/ 2000.

[114] M. Euvrard, C. Filiatre, and E. Crausaz, "A cell to study in situ electrocrystallization of calcium carbonate," *Journal of Crystal Growth,* vol. 216, pp. 466-474, 6/15/ 2000.

[115] A. Quddus and L. M. Al-Hadhrami, "Hydrodynamically deposited CaCO3 and CaSO4 scales," *Desalination,* vol. 246, pp. 526-533, 9/30/ 2009.

[116] S. Labille, A. Neville, G. Graham, and L. Boak, "An Assessment of Adhesion of Scale and Electrochemical Pre-treatment for the Prevention of Scale Deposition on Metal Surfaces," in *International Symposium on Oilfield Scale*, 2002.

[117] A. C. Martinod, "An Integrated Study of CaCO3 Formation and Inhibition," Doctor of Philosophy, School of Mechanical Engineering, The University of Leeds, Leeds, 2008.

[118] J. R. Davis and A. I. H. Committee, *Metals Handbook Desk Edition 2nd Edition*: Taylor & Francis, 1998.

[119] N. International, "Laboratory Screening Test to Determine the Ability of Scale Inhibitors to Prevent the Precipitation of Barium Sulfate or Strontium Sulfate, or Both, from Solution (for Oil and Gas Production Systems)," ed: NACE International.

[120] O. Sanni, T. Charpentier, N. Kapur, and A. Neville, "Study of surface deposition and bulk scaling kinetics in oilfield conditions using an in-situ flow rig," in *NACE-International Corrosion Conference Series*, 2015.

[121] L. Beaunier, C. Gabrielli, G. Poindessous, G. Maurin, and R. Rosset, "Investigation of electrochemical calcareous scaling: Nuclei counting and morphology," *Journal of Electroanalytical Chemistry,* vol. 501, pp. 41-53, 3/23/ 2001.

[122] M. Euvrard, F. Membrey, C. Filiatre, C. Pignolet, and A. Foissy, "Kinetic study of the electrocrystallization of calcium carbonate on metallic substrates," *Journal of Crystal Growth,* vol. 291, pp. 428-435, 6/1/ 2006.

[123] J. H. Olsen, "Statoil Experiences and Consequences related to Continuous Chemical Injection," in *SPE Annual Technical Conference and Exhibition*, 2011.

[124] N. Goodwin, O. G. Svela, J. H. Olsen, B. M. Hustad, T. Tjomsland, and G. M. Graham, "Qualification Procedure For Continuous Injection Of Chemicals In The Well-Method Development," in *SPE International Conference on Oilfield Scale*, 2012.

[125] C. Stewart-Liddon, N. J. Goodwin, G. M. Graham, T. Tjomsland, B. M. Hustad, O. G. Svela*, et al.*, "Qualification of Downhole Valves Used in Continuous Injection Systems," in *SPE International Oilfield Scale Conference and Exhibition*, 2014.

[126] G. M. Graham, K. S. Sorbie, and M. M. Jordan, "How scale inhibitors works and How this affects test methodology," presented at the IBC LTD Conference, Aberdeen, 1997.

[127] O. Sanni, "Calcium carbonate surface/bulk scaling mechanisms and kinetics in a once-through in-situ flow visualization rig," Ph.D., Mechanical Engineering University of Leeds, 2016.

[128] B. J. Hwang, R. Santhanam, and Y. L. Lin, "Nucleation and Growth Mechanism of Electropolymerization of Polypyrrole on Gold/Highly Oriented Pyrolytic Graphite Electrode," *Journal of The Electrochemical Society,* vol. 147, pp. 2252-2257, June 1, 2000 2000.

[129] B.-J. Hwang, R. Santhanam, C.-R. Wu, and Y.-W. Tsai, "Nucleation and Growth Mechanism of Electropolymerization of Aniline on Highly Oriented Pyrolytic Graphite at a Low Potential," *Electroanalysis,* vol. 13, pp. 37-44, 2001.

[130] J. Simitzis, D. Triantou, and S. Soulis, "Synthesis and characterization of electrically conducting copolymers based on biphenyl and thiophene," *Journal of Applied Polymer Science,* vol. 118, pp. 1494-1506, 2010.

[131] D. Triantou, S. Soulis, D. Perivoliotis, and C. Charitidis, "Influence of electrochemical copolymerization conditions of 3-methylthiophene and biphenyl on the morphology and nanomechanical properties of the films," *Journal of Applied Polymer Science,* vol. 132, 2015.

[132] Ś. F. E. Boerlage, M. D. Kennedy, I. Bremere, G. J. Witkamp, J. P. van der Hoek, and J. C. Schippers, "Stable barium sulphate supersaturation in reverse osmosis," *Journal of Membrane Science,* vol. 179, pp. 53-68, 11/15/ 2000.

[133] D. Hasson, M. Avriel, W. Resnick, T. Rozenman, and S. Windreich, "Mechanism of Calcium Carbonate Scale Deposition on Heat-Transfer Surfaces," *Industrial & Engineering Chemistry Fundamentals,* vol. 7, pp. 59-65, 1968/02/01 1968.

[134] J. F. Wu, C. Y. Tai, W. K. Yang, and L. P. Leu, "Temperature effects on the crystallization kinetics of size-dependent systems in a continuous mixed-suspension mixed-product removal crystallizer," *Industrial & Engineering Chemistry Research,* vol. 30, pp. 2226-2233, 1991/09/01 1991.

[135] O. Bukuaghangin, O. Sanni, N. Kapur, M. Huggan, A. Neville, and T. Charpentier, "Kinetics study of barium sulphate surface scaling and inhibition with a once-through flow system," *Journal of Petroleum Science and Engineering,* vol. 147, pp. 699-706, 11// 2016.

[136] S. Rosa and H. E. Lundager Madsen, "Kinetics of mass crystallization of calcium carbonate at 25, 30 and 37 °C," *Journal of Crystal Growth,* vol. 318, pp. 99-102, 3/1/ 2011.

[137] X. Bogdanović and W. Hinrichs, "Influence of temperature during crystallization setup on precipitate formation and crystal shape of a metalloendopeptidase," *Acta Crystallographica Section F: Structural Biology and Crystallization Communications,* vol. 67, pp. 421-423, 2011.

[138] R. A. Judge, R. S. Jacobs, T. Frazier, E. H. Snell, and M. L. Pusey, "The effect of temperature and solution pH on the nucleation of tetragonal lysozyme crystals," *Biophysical Journal,* vol. 77, pp. 1585-1593, 1999.

[139] A. Baynton, B. D. Chandler, F. Jones, G. Nealon, M. I. Ogden, T. Radomirovic*, et al.*, "Phosphonate additives do not always inhibit crystallization," *CrystEngComm,* vol. 13, pp. 1090-1095, 2011.

[140] S. N. Black, L. A. Bromley, D. Cottier, R. J. Davey, B. Dobbs, and J. E. Rout, "Interactions at the organic/inorganic interface: binding motifs for phosphonates at the surface of barite crystals," *Journal of the Chemical Society, Faraday Transactions,* vol. 87, pp. 3409-3414, 1991.

[141] M. C. Van der Leeden and G. M. Van Rosmalen, "Adsorption Behaviour of Polyelectrolytes in Relation to the Crystal Growth Kinetics of Barium Sulfate," in *Mineral Scale Formation and Inhibition*, Z. Amjad, Ed., ed Boston, MA: Springer US, 1995, pp. 99-110.

[142] C. E. Inches, K. El Doueiri, and K. S. Sorbie, "Green inhibitors: Mechanisms in the control of barium sulfate scale," in *CORROSION 2006*, 2006.

[143] W. H. Leung and G. H. Nancollas, "Nitrilotri (methylenephosphonic acid) adsorption on barium sulfate crystals and its influence on crystal

growth," *Journal of Crystal Growth,* vol. 44, pp. 163-167, 1978/09/01 1978.

[144] L. Dupont, A. Foissy, R. Mercier, and B. Mottet, "Effect of Calcium Ions on the Adsorption of Polyacrylic Acid onto Alumina," *Journal of Colloid and Interface Science,* vol. 161, pp. 455-464, 12// 1993.

[145] S.-T. Liu and D. W. Griffiths, "Adsorption Of Aminomethylphosphonic Acids On The Calcium Sulfate Dihydrate Crystal Surface," in *SPE Oilfield and Geothermal Chemistry Symposium*, 1979.

[146] T. Chen, A. Neville and M. Yuan, " Assessing the effect of Mg^{2+} on $CaCO_3$ scale formation-bulk precipitation and surface deposition.," *Journal of Crystal Growth,* vol. 275, pp. 1341-1347, 2005.

[147] T. Chen, P. Chen, H. Montgomerie, T. Hagen, R. Benvie, Q. Guo*, et al.*, "Do We Need Higher Dose Scale Inhibitors to Inhibit Scale under Turbulent Conditions? Insight into Mechanisms and New Test Methodology," in *SPE International Oilfield Scale Conference and Exhibition*, 2014.

[148] A. Martinod, A. Neville, and M. Euvrard, "Experimental investigation of scaling control by a non-phosphorous polymer: polyaspartic acid," *Desalination and Water Treatment,* vol. 7, pp. 86-92, 2009/07/01 2009.

[149] Z. Amjad, "Influence of Iron Oxide (rust) on the Performance of Phosphonates as Calcium Carbonate Inhibitors," in *CORROSION 2016*, 2016.

[150] S. Kırboga and M. Öner, "The inhibitory effects of carboxymethyl inulin on the seeded growth of calcium carbonate," *Colloids and Surfaces B: Biointerfaces,* vol. 91, pp. 18-25, 3/1/ 2012.

[151] J. Chung, I. Granja, M. G. Taylor, G. Mpourmpakis, J. R. Asplin, and J. D. Rimer, "Molecular modifiers reveal a mechanism of pathological crystal growth inhibition," *Nature,* vol. 536, pp. 446-450, 08/25/print 2016.

[152] Q. Yang, Y. Liu, A. Gu, J. Ding, and Z. Shen, "Investigation of Calcium Carbonate Scaling Inhibition and Scale Morphology by AFM," *Journal of Colloid and Interface Science,* vol. 240, pp. 608-621, 2001/08/15 2001.

[153] S. Farmanesh, S. Ramamoorthy, J. Chung, J. R. Asplin, P. Karande, and J. D. Rimer, "Specificity of Growth Inhibitors and their Cooperative Effects in Calcium Oxalate Monohydrate Crystallization," *Journal of the American Chemical Society,* vol. 136, pp. 367-376, 2014/01/08 2014.

[154] S. Bargir, S. Dunn, B. Jefferson, J. Macadam, and S. Parsons, "The use of contact angle measurements to estimate the adhesion propensity of calcium carbonate to solid substrates in water," *Applied Surface Science,* vol. 255, pp. 4873-4879, 2/15/ 2009.

[155] J. T. V. Charpentier, S. Baraka-Lokmane, A. Neville, C. Hurtevent, J. R. Ordonez-Varela, F. Moeller Nielsen*, et al.*, "Comparison of characteristic of anti-scaling coating for subsurface safety valve for use in oil and gas industry," in *International Petroleum Technology Conference*, 2014.

[156] H. Liang, D. Guo, L. Ma, and J. Luo, "Investigation of film formation mechanism of oil-in-water (O/W) emulsions at high speeds," *Tribology International,* vol. 109, pp. 428-434, 5// 2017.

[157] M. Ratoi-Salagean, H. A. Spikes, and H. L. Rieffe, "Optimizing Film Formation by Oil-in-Water Emulsions," *Tribology Transactions,* vol. 40, pp. 569-578, 1997/01/01 1997.

[158] X. Wang, W. Zhou, J. Cao, W. Liu, and S. Zhu, "Preparation of core–shell CaCO3 capsules via Pickering emulsion templates," *Journal of Colloid and Interface Science,* vol. 372, pp. 24-31, 4/15/ 2012.

[159] A. Martinod, M. Euvrard, A. Foissy, and A. Neville, "European Desalination Society and Center for Research and Technology Hellas (CERTH), Sani Resort 22 –25 April 2007, Halkidiki, GreeceProgressing the understanding of chemical inhibition of mineral scale by green inhibitors," *Desalination,* vol. 220, pp. 345-352, 2008/03/01 2008.

[160] A. Martinod, A. Neville, M. Euvrad, and K. Sorbie, "Electrodeposition of a calcareous layer: Effects of green inhibitors," *Chemical Engineering Science,* vol. 64, pp. 2413-2421, 5/15/ 2009.

[161] EPIWIN, "Software for estimating physical/chemical properties ", ed. United State: Environmental Protection Agency, 2000.

[162] CCC, "Material Safety Data Sheet," Canada2015.

A